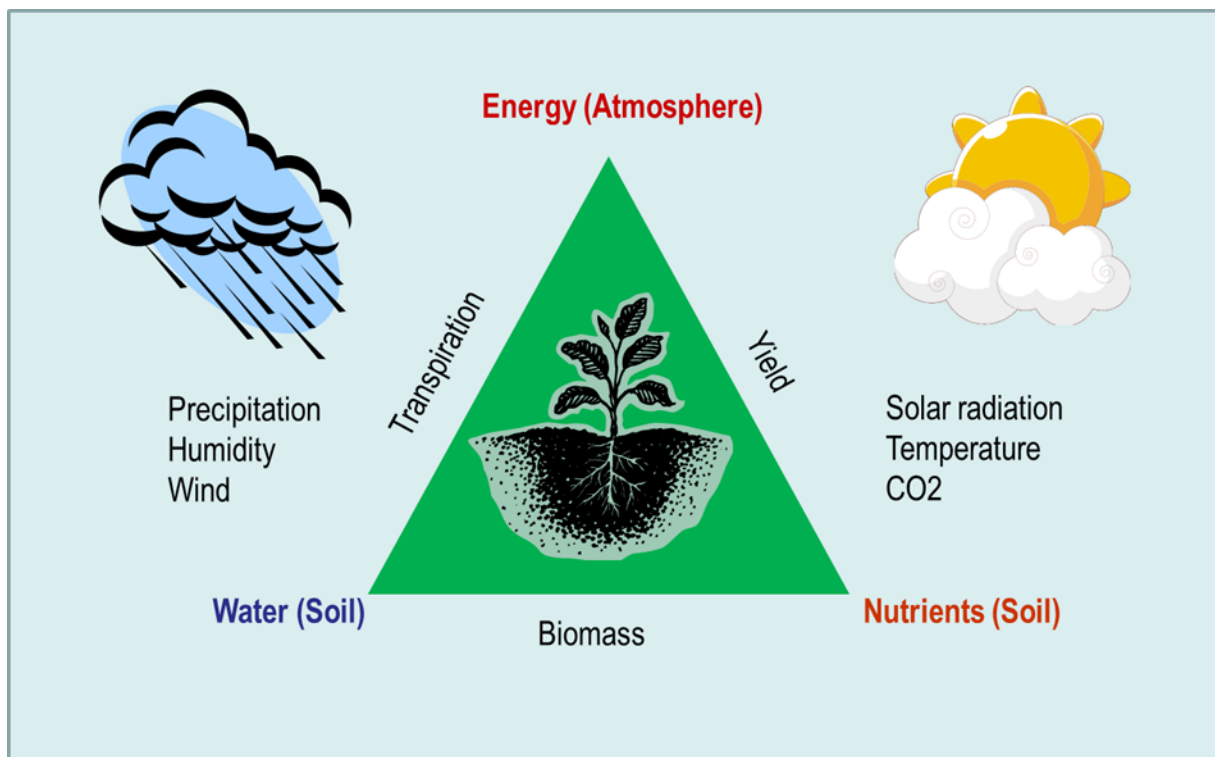


RECLAMATION

Managing Water in the West

Plant Physiological Responses to Atmospheric Forcings Affecting Crop Water Use and Yields: Literature Review and Model Comparisons

Research and Development Office
Science and Technology Program
Final Report ST-2018-1858-01



Mission Statements

Protecting America's Great Outdoors and Powering Our Future

The Department of the Interior protects and manages the Nation's natural resources and cultural heritage; provides scientific and other information about those resources; and honors its trust responsibilities or special commitments to American Indians, Alaska Natives, and affiliated island communities.

The following form is a Standard form 298, Report Documentation Page. This report was sponsored by the Bureau of Reclamations Research and Development office. For more detailed information about this Report documentation page please contact Michael Tansey at 916-978-5197. THIS TEXT WILL BE INVISIBLE. IT IS FOR 508 COMPLIANCE OF THE NEXT PAGE.

Disclaimer:

This document has been reviewed under the Research and Development Office Discretionary peer review process https://www.usbr.gov/research/peer_review.pdf consistent with Reclamation's Peer Review Policy CMP P14. It does not represent and should not be construed to represent Reclamation's determination, concurrence, or policy.

REPORT DOCUMENTATION PAGE		<i>Form Approved</i> <i>OMB No. 0704-0188</i>
T1. REPORT DATE: SEPTEMBER 2018	T2. REPORT TYPE: RESEARCH	T3. DATES COVERED
T4. TITLE AND SUBTITLE Plant Physiological Responses to Atmospheric Forcings Affecting Crop Water Use and Yields: Literature Review and Model Comparisons		5a. CONTRACT NUMBER
		5b. GRANT NUMBER
		5c. PROGRAM ELEMENT NUMBER 1541 (S&T)
6. AUTHOR(S) Michael Tansey, mtansey@usbr.gov , 916-978-5197		5d. PROJECT NUMBER ST-2018-1858-01
		5e. TASK NUMBER
		5f. WORK UNIT NUMBER MP 740
7. PERFORMING ORGANIZATION NAME(S) AND ADDRESS(ES) Bureau of Reclamation, Mid Pacific Region, 2800 Cottage Way, Sacramento, CA 95825		8. PERFORMING ORGANIZATION REPORT NUMBER
9. SPONSORING / MONITORING AGENCY NAME(S) AND ADDRESS(ES) Research and Development Office U.S. Department of the Interior, Bureau of Reclamation, PO Box 25007, Denver CO 80225-0007		10. SPONSOR/MONITOR'S ACRONYM(S) R&D: Research and Development Office BOR/USBR: Bureau of Reclamation DOI: Department of the Interior
		11. SPONSOR/MONITOR'S REPORT NUMBER(S) ST-2018-1858-01
12. DISTRIBUTION / AVAILABILITY STATEMENT Final report can be downloaded from Reclamation's website: https://www.usbr.gov/research/		
13. SUPPLEMENTARY NOTES		
14. ABSTRACT <i>(Maximum 200 words)</i> Crop water requirements and crop yields are important considerations that are necessary for managing current demands as well as planning for future water needs. They are commonly employed in the hydrologic and economic models that Reclamation along with many other water management agencies routinely use to make operational and infrastructure investments decisions. In this study, the physiological responses of plants to environmental conditions are reviewed in detail at scales ranging from molecular to global to in order to describe how transpiration, biomass and yield interact with atmospheric forcings. The literature review also describes experimental and modeling studies which have been performed to understand and quantify the effects of changes in atmospheric forcings on crop responses. Finally, a modeling study based on six atmospheric scenarios representing a wide range of potential conditions is performed to elucidate relationships between the atmospheric conditions and the transpiration, biomass and yield responses of six major crops commonly grown in the Reclamation service areas in the western United States.		

15. SUBJECT TERMS crop transpiration, biomass and yield and model comparisons					
16. SECURITY CLASSIFICATION OF:			17. LIMITATION OF ABSTRACT U	18. NUMBER OF PAGES 183	19a. NAME OF RESPONSIBLE PERSON Michael Tansey
a. REPORT U	b. ABSTRACT U	c. THIS PAGE U			19b. TELEPHONE NUMBER 916-978-5197

S Standard Form 298 (Rev. 8/98)
P Prescribed by ANSI Std. Z39-18

BUREAU OF RECLAMATION

Research and Development Office Science and Technology Program

Division of Planning, Mid Pacific Region, Decision Support
Analysis Branch, MP-740
(Final Report) ST-2018-1858-01

Plant Physiological Responses to Atmospheric Forcings Affecting Crop Water Use and Yields: Literature Review and Model Comparisons

Prepared by: Michael Tansey, Ph.D.
Regional Climate Change Coordinator, Mid-Pacific Region, MP-740

Francisco Flores-Lopez

Peer Review: Francisco Flores-Lopez, Ph.D.
Water Resources Engineer, California Department of Water Resources, Sacramento, CA

For Reclamation disseminated reports, a disclaimer is required for final reports and other research products, this language can be found in the peer review policy:

This document has been reviewed under the Research and Development Office Discretionary peer review process https://www.usbr.gov/research/peer_review.pdf consistent with Reclamation's Peer Review Policy CMP P14. It does not represent and should not be construed to represent Reclamation's determination, concurrence, or policy.

Acknowledgements

This study was made possible by a long and productive collaboration with my colleagues at the Stockholm Environment Institute in Davis, California. I would especially like to thank Dr. Charles Young and Dr. Francisco Flores-Lopez for their efforts in developing and applying the modeling tools used in this study along with extra thanks to Francisco for his peer review of this study. Funding support for this study was provided by the Reclamation Office of Science and Technology, Office of Policy and Administration and my supervisor, Dr. Jobaid Kabir. I would also like to thank my colleague, Arlan Nickel, whose support for my work in the Basin Study Program made this study feasible and Geoffery McDonald, the Mid Pacific Region's librarian, who provided valuable assistance in organizing the Mendeley bibliography. Finally, I would like to thank my wife, Dr. Marcia Scavone-Tansey, for her help in performing the statistical analyses and proof reading of this document. The responsibility for any errors or omissions remain solely with this author.

Acronyms and Abbreviations

⁰ C	degrees centigrade	MJ/m ²	mega joules per square meter
Apr	April	NoCC	historic climate scenario
Aug	August	Nov	November
C3	photosynthetic pathway	O ₂	oxygen
C4	photosynthetic pathway	Oct	October
CEN	central tendency climate scenario	PM	Penman - Monthieth
CO ₂	carbon	R ²	coefficient of determination
Dec	December	Rs	solar radiation (MJ/m ²)
Delta	change in variable or factor	RUE	radiation use efficiency (kg/ha per MJ/m ²)
DOI	United States Department of the Interior	SC	stomatal conductance
ea	atmospheric vapor pressure	Sep	September
es	saturation vapor pressure	T	temperature
ET	evapotranspiration	Tbase	basal growth temperature
ETc	crop evapotranspiration	Tdew	dew point temperature
ETo	reference crop evapotranspiration	Tmax	maximum daily temperature
Feb	February	Tmin	minimum daily temperature
GCM	global climate model	Topt	optimal growth temperature
HD	hot dry climate scenario	TUE	transpiration use efficiency
HW	hot wet climate sceanrio	USDA	United States Department of Agriculture
Jan	January	VPD	vapor pressure deficit (kPa)
Jul	July	WD	warm dry climate scenario
Jun	June	WW	warm wet climate scenario
kPa	kilo Pascals		
LAI	leaf area index		
Mar	March		

Executive Summary

Crop water requirements and crop yields are important considerations that are necessary for managing current demands as well as planning for future water needs. They are commonly employed in the hydrologic and economic models that Reclamation along with many other water management agencies routinely use to make operational and infrastructure investments decisions.

Reclamation performs these evaluations by applying a variety of modeling tools including several methods of estimating crop evapotranspiration from reference evapotranspiration at an agro-meteorology stations such as those in Reclamation's AgroMET network. At these stations, a standardized reference evapotranspiration is computed from measurements of a variety of atmospheric forcings including precipitation, temperature, solar radiation, humidity, and wind speed. Crop evapotranspiration is computed from a standard reference by the application of empirically determined crop coefficients. This approach has been applied with great success in the management of irrigation water scheduling. However, it relies on the validity of the empirically determined coefficients remaining constant. This study explores how long term changes in atmospheric forcings and changes crop evapotranspiration may challenge this assumption.

In this study, the physiological responses of plants to environmental conditions are reviewed in detail at scales ranging from molecular to global in order to describe how transpiration, biomass and yield interact with atmospheric forcings. The literature review also includes a discussion of experimental and modeling studies which have been performed to understand and quantify the effects of changes in atmospheric forcings on crop responses. Finally, a modeling study based on six atmospheric scenarios representing a wide range of potential conditions is performed to elucidate relationships between the atmospheric conditions and transpiration, biomass and yield responses of six major crops commonly grown in the Reclamation service areas in the western United States.

The atmospheric forcings used in the assessment are based climate scenarios developed by Reclamation for the Sacramento and San Joaquin Basins Study. Six climate scenarios were selected to characterize a wide range of potential atmospheric forcings occurring over an eighty nine year study period. To characterize plant responses four atmospheric forcings were selected including temperature, solar radiation, carbon dioxide and humidity expressed as the vapor pressure deficit. A correlation coefficient analysis was performed to evaluate the relationships between these atmospheric variables so that plant responses to them could be better understood. The correlation analysis was also used as a tool in the assessment of the transpiration, biomass and yield results from modeling study.

Interestingly, the correlations between the some of the atmospheric forcings varied between climate scenarios. For example, the correlation between temperature and carbon dioxide was relatively low in scenarios with only slight warming but increased significantly in hot scenarios. However, the negative correlation between carbon dioxide and solar radiation and positive correlations between temperature and the vapor pressure deficit were high in all scenarios.

The effects of atmospheric forcings also were variable depending on nature of the crop. For example, increasing temperature could result in increased transpiration, biomass production and yield up to the point in which temperature exceeds the optimal growth range of the crop. Further increases would reverse the trend. Crops responses to carbon dioxide also exhibit opposing effects. For example, increasing carbon dioxide may result in increased canopy vegetative growth which contributes to increased transpiration and at the same time increasing carbon dioxide may contribute to reduced transpiration because of its effect on water vapor exchange between the plant's leaves and the atmosphere. Similarly, the effect of increasing vapor pressure deficits may contribute to increased transpiration, biomass production and yield but once it increases passes a crop's threshold tolerance continued increases result in decreases in these responses. Because of these complexities, correlations between crops responses and atmospheric forcings can change from strong positive correlations in one scenario to negative in another one.

These complexities and the dynamically changing responses result in a wide range of crop transpiration, biomass and yield responses. These responses and their relationships with the atmospheric forcings are evaluated and described in detail by this study. These complexities also mean that using the standardized reference evapotranspiration method which depends on maintaining a constant ratio between transpiration of a particular crop and the standard reference is not reliable method to use in long term planning studies in which the atmospheric forcings may be considerably different than those used to determine the crop coefficients.

Finally, it is important to recognize that the results presented in this study are based on the application of single model calibrated for a particular location in the Central Valley of California. Although the model was able to reproduce accepted values of crop evapotranspiration and yield for the six crops studied, there is always uncertainty in crop parameters and the values used in this study would not likely be valid at other locations. Furthermore, it is important to recognize the model used does not simulate the important effects of plant nutrients which significantly affect plant physiological responses. As described in the text, there are many levels of complexities in crop models each one with its own requirements in terms of data inputs, parameters, level of effort and expertise needed to apply successfully. While the results presented in this study provide important insights, the significance of additional refinements should be explored further in future studies.

Contents

1.	Plant Physiology	9
1.1	Introduction.....	9
1.2	Plant Form and Function.....	10
1.3	Cell Structure and Function	12
1.4	Photosynthesis.....	19
1.5	Respiration	25
2.	Atmospheric Factors Influencing Crop Evapotranspiration and Yield.....	29
2.1	Introduction.....	29
2.2	Overview of Temperature Response Effects on Crop Growth and Yields.....	31
2.3	Overview of Carbon Dioxide Response Effects on Crop Growth and Yields.....	33
2.4	Overview of Atmosphere and Carbon Dioxide Response Effects on Crop Evapotranspiration	34
2.5	Simple Assessment of the Combined Effects of Temperature and Carbon Dioxide on Potential Crop ET and Yields.	37
3.	Modeling Crop – Atmosphere Relationships.....	40
3.1	Overview of Modeling Approaches.....	40
3.2	Description of Selected Crop Models.....	43
3.3	Crop Modeling Data	50
4.	Climate – Crop Modeling Studies	52
4.1	Crop Evapotranspiration – Climate Interactions.....	52
4.2	Crop Yield – Climate Interactions	60
5.	Assessment of Plant Physiological Responses to Atmospheric Forcings.....	66
5.1	Background.....	66
5.2	Selection of Representative Crops	66
5.3	Selection of Representative Atmospheric Forcings	67
5.4	Calibration of the WEAP-PGM Crop Model.....	78
5.5	Transpiration Responses to Atmospheric Forcings	96
5.6	Biomass and Yield Responses to Atmospheric Forcings	106
6.	Summary of Results	117
6.1	Atmospheric Forcings.....	117
6.2	Transpiration Responses to Atmospheric Forcings	118
6.3	Biomass and Yield Responses to Atmospheric Forcings	120
	References.....	122
	Appendix A – WEAP-PGM Algorithms	1
	Appendix B – Development of Atmospheric Forcings for WEAP-PGM.....	42

Tables

Table 2.2.1 Temperature (⁰ C) Dependence of various Life Cycles Phases for some Major Agriculture Crops.....	33
Table 2.3.1. Percent change in Yield due to Increasing CO ₂ from 330 to 660 ppm under Ideal Growth Conditions.....	34

Table 2.4.1. Sensitivity of the ASCE Hourly PM Equation to Weather and Plant Variables	36
Table 2.5.1. Simplified Assessment of Combined Temperature and CO ₂ Changes on Major Agricultural Crops.....	38
Table 4.1.1 Temperature and Precipitation Changes on the Central Valley Basins	56
Table 4.1.2 Applied Water Demands and Changes in the Central Valley Basins	59
Table 4.2.1. Selected Crop Yields (Tons/Acre dry weight) in the Central Valley Basins.....	64
Table 5.3.1. Correlation Coefficients of Atmospheric Forcings with CO ₂	77
Table 5.3.2 Correlation Coefficients of Atmospheric Forcings with Tmax	78
Table 5.3.3 Correlation Coefficients of Atmospheric Forcings with Rs	78
Table 5.4.1 Seasonal ET totals from the CUP and PGM models at Firebaugh	80
Table 5.4.2 Crop Yields from the SWAP and WEAP-PGM models at Firebaugh	81
Table 5.5.1 Correlations of Alfalfa & Winter Wheat Transpiration with Atmospheric Forcings.....	98
Table 5.5.2 Correlations of Corn and Safflower Transpiration with Atmospheric Forcings	102
Table 5.5.3 Correlations of Citrus and Vine Transpiration with Atmospheric Forcings.....	105
Table 5.6.1 Correlations of Alfalfa and Winter Wheat (W_Wheat) Yield with Atmospheric Forcings by Scenario	109
Table 5.6.2 Correlations of Corn and Safflower Yield with Atmospheric Forcings by Scenario.....	112
Table 5.6.3 Correlations of Citrus and Vine Yield with Atmospheric Forcings by Scenario.....	115

Figures

Figure 1.1.1 Interactions of Plants with Environmental Factors	9
Figure 1.2.1 Plant Form and Functions.....	10
Figure 1.3.1 Generalized Plant Cell.....	12
Figure 1.3.2 Generalized Plant Leaf Cells in the C3 Photosynthetic Pathway.....	13
Figure 1.3.3 Comparison of Leaf Cell Structure in C3 and C4 Plants.....	14
Figure 1.3.4 Transport of Sugars and Water in the Vascular Tissue	15
Figure 1.3.5 Movement of Water Solutes in Root Cells.....	16
Figure 1.3.6 Transport of Water from Roots to Leaves	17
Figure 1.3.7 Function of Guard Cells in Plant Leaves.....	18
Figure 1.4.1 The Two Stages of Photosynthesis.....	19
Figure 1.4.2 Light Dependent Reactions in the Thylakoid Membranes	20
Figure 1.4.3 Three Phases of the Calvin Cycle.....	22
Figure 1.4.4 Photorespiration.....	23
Figure 1.4.5 C4 Photosynthesis	24
Figure 1.5.1. The Three Stages of Respiration	25
Figure 1.5.3 Mitochondrion Electron Transport Chain	27
Figure 1.5.4 Summary of Photosynthesis and Aerobic Respiration	27
Figure 2.1.1. Major Global Climate and Vegetation Zones.....	29
Figure 2.1.2 Relationship between major vegetation types, temperature and precipitation	30

Figure 4.1.1 Period Averaged Maximum Temperature (Tmax), Solar Radiation (Rs), Carbon Dioxide (CO2) and Vapor Pressure Deficit (VPD) in the Central Valley.	58
Figure 5.3.1 Total Annual Precipitation and Changes from the NoCC Reference by Scenario during the Study Period (2011 – 2099).....	68
Figure 5.3.2 Period Mean Total Precipitation by Month and Changes from the NoCC Reference by Scenario	69
Figure 5.3.3 Boxplots of the Total Annual Precipitation by Scenario.....	69
Figure 5.3.4 Mean Annual Tmax and Changes from the NoCC Reference by Scenario during the Study Period (2011 – 2099).....	70
Figure 5.3.5 Period Mean Tmax by Month and Changes from the NoCC Reference by Scenario.....	70
Figure 5.3.6 Boxplots of the Mean Annual Tmax by Scenario	71
Figure 5.3.7 Mean Annual Rs and Changes from the NoCC Reference by Scenario during the Study Period (2011 – 2099)	71
Figure 5.3.8 Period Mean Rs by Month and Changes from the NoCC Reference by Scenario.....	72
Figure 5.3.9 Boxplots of the Mean Annual Rs by Scenario	72
Figure 5.3.10 Mean Annual CO2 and Changes from the NoCC Reference by Scenario during the Study Period (2011 – 2099).....	73
Figure 5.3.11 Period Mean CO2 by Month and Changes from the NoCC Reference by Scenario.....	73
Figure 5.3.12 Boxplots of the Mean Annual CO2 by Scenario	74
Figure 5.3.13 Mean Annual VPD and Changes from the NoCC Reference by Scenario during the Study Period (2011 – 2099).....	74
Figure 5.3.14 Period Mean VPD by Month and Changes from the NoCC Reference by Scenario.....	75
Figure 5.3.15 Boxplots of the Mean Annual VPD by Scenario.....	76
Figure 5.3.16 Correlations between Tmax and CO ₂ in the WD and HW Scenarios	76
Figure 5.3.17 Correlations between Rs and CO ₂ in the WD and HW Scenarios	77
Figure 5.3.18 Correlations between VPD and CO ₂ in the WD and HW Scenarios.....	77
Figure 5.4.1 Illustration of Crop LAI Development as a Function of HUI	79
Figure 5.4.2 Comparison of the WEAP-PGM and CUP Simulated ETC.....	81
Figure 5.4.3 Plant Growth Parameters – Alfalfa & Winter Wheat - Leaf Area Index (LAI), Canopy Development & Harvest.....	83
Figure 5.4.4 Plant Growth Parameters – Corn & Safflower - Leaf Area Index (LAI), Canopy Development & Harvest	85
Figure 5.4.5 Plant Growth Parameters – Citrus & Vine - Leaf Area Index (LAI), Canopy Development & Harvest	87
Figure 5.4.6 Plant Growth Parameters – Alfalfa & Winter Wheat - Radiation Use Efficiency (RUE) and Temperature Effects on Growth	89
Figure 5.4.7 Plant Growth Parameters – Corn & Safflower - Radiation Use Efficiency (RUE) and Temperature Effects on Growth	91
Figure 5.4.8 Plant Growth Parameters – Citrus & Vine - Radiation Use Efficiency (RUE) and Temperature Effects on Growth.....	93
Figure 5.4.9 Plant Growth Parameters – Alfalfa & Winter Wheat - Stomatal Conductance Effects on Transpiration.....	94

Figure 5.4.10 Plant Growth Parameters – Corn & Safflower - Stomatal Conductance Effects on Transpiration.....	95
Figure 5.4.11 Plant Growth Parameters – Citrus & Vine - Stomatal Conductance Effects on Transpiration	96
Figure 5.5.1 Transpiration – Alfalfa and Winter Wheat (W_Wheat) by Scenario	97
Figure 5.5.2 Changes in Transpiration - Alfalfa & Winter Wheat with Changes in CO2 and VPD by Scenario.....	99
Figure 5.5.3 Period Mean Monthly Changes in Transpiration and VPD by Scenario.....	100
Figure 5.5.3 Transpiration – Corn and Safflower (Safldr) by Scenario.....	101
Figure 5.5.4 Changes in Corn and Safflower Transpiration and Changes in Tmax by Scenario.....	102
Figure 5.5.5 Period Mean Monthly Changes in Transpiration and Tmax by Scenario	103
Figure 5.5.6 Transpiration – Citrus and Vine by Scenario	104
Figure 5.5.7 Changes in Citrus and Vine Transpiration and Changes in CO2 and VPD by Scenario.....	106
Figure 5.6.1 Biomass and Yield – Alfalfa and Winter Wheat (W_Wheat) by Scenario	108
Figure 5.6.2 Changes in Biomass and Yield - Alfalfa and Winter Wheat (W_Wheat) and Changes in CO2 by Scenario	110
Figure 5.6.3 Biomass and Yield – Corn and Safflower (Safldr) by Scenario.....	111
Figure 5.6.4 Changes in Yield – Corn and Safflower (Safldr) and Changes in Tmax, Rs and CO2 by Scenario	113
Figure 5.6.5 Biomass and Yield – Citrus and Vine by Scenario	114
Figure 5.6.6 Changes in Yield – Citrus and Vine and Changes in Tmax, Rs and CO2 by Scenario.....	116
Figure 6.2.1 Comparison of Alfalfa and Corn Transpiration by Scenario.....	120

1. Plant Physiology

1.1 Introduction

In this section, the basic characteristics of plants that affect their water use, growth and yield are described at the whole plant and cellular scales. This background information is intended to provide the reader with a general overview of how plants interact with their surroundings. In this regard, it should be noted that this report is focused on terrestrial plants which are of interest in Reclamation's mission of providing water for irrigated crops in the western United States.

Figure 1.1.1 is a generalized representation of plant interactions with various environmental factors.

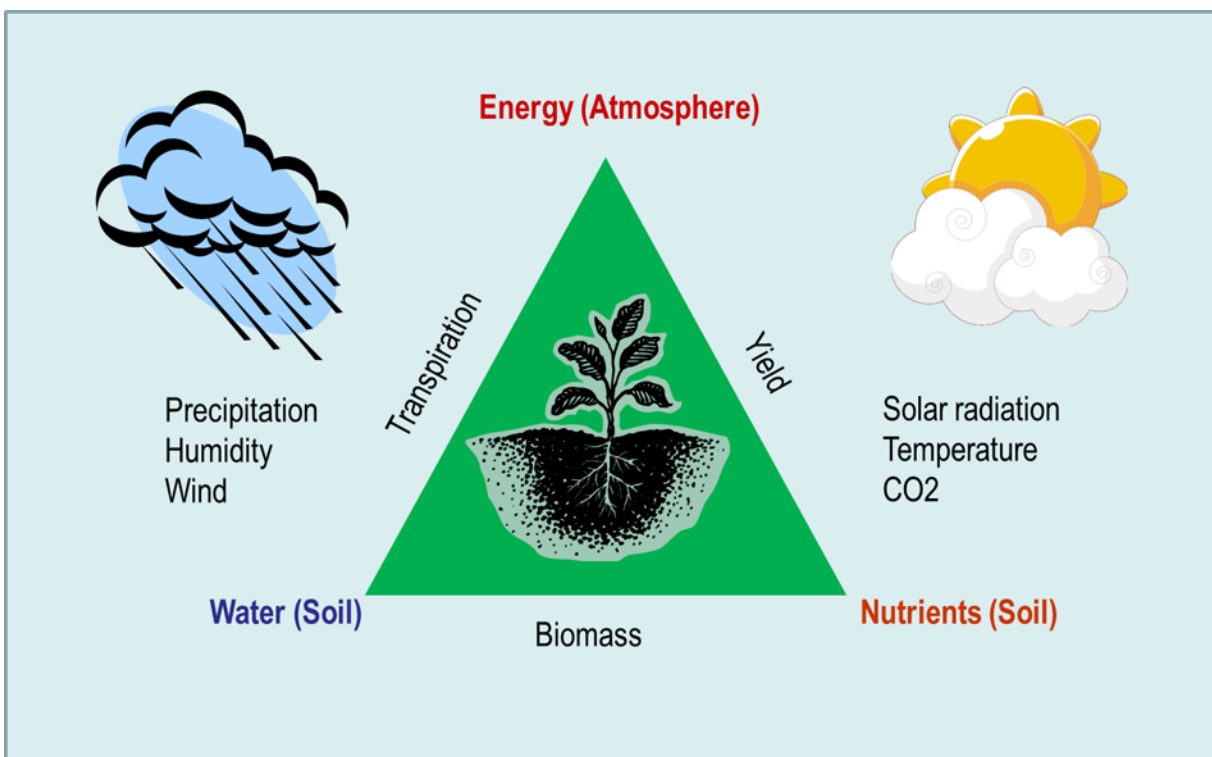


Figure 1.1.1 Interactions of Plants with Environmental Factors

The atmospheric forcings affecting plant water use (transpiration), growth (biomass) and yield include precipitation, temperature, humidity, solar radiation, wind and carbon dioxide (CO₂). However, it must be noted that soil characteristics both physical and chemical are other important factors. In this report, the role of atmospheric factors is the primary emphasis. There are also other factors which are equally important such as disease, insect predators and ozone that are not considered in the discussion.

1.2 Plant Form and Function

All living organism require energy to survive. Plants are classified as autotrophic organisms because they can capture the energy of sunlight by photosynthesis to produce sugars and other metabolic molecules. Flowering plants are classified into two broad groups based on the type of seeds they produce. The monocot group characterized by a single embryonic seed leaf includes many agriculturally important plants. Examples are grasses, corn, wheat, rice, potatoes, sugar cane, bananas, garlic and onions as well as many ornamental flowers such as orchids and lilies. The dicot group which has two embryonic seed leaves includes deciduous trees such as olives, almonds, apples, peaches and pears; vegetables crops including tomatoes, peppers, sweet potatoes, squash, cauliflower, broccoli and beans; and pasture crops such as alfalfa and clover.

On Figure 1.2.1, the plant is divided into above and below ground regions.

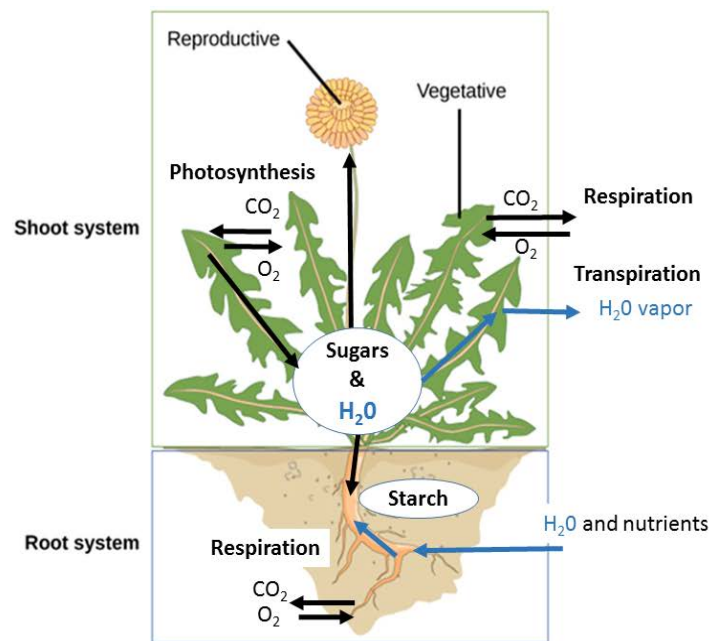


Figure 1.2.1 Plant Form and Functions

Credit: Modified by Michael Tansey for this report from Figure 1 Chapter 14.1 of Biology: Mixed Majors, Part 11 by OpenStax College

Source: <https://cnx.org/contents/45PurvSQ@14B:LvReeTUD@1/The-Plant-Body>

License: Creative Commons Attribution license 4.0

The shoot system is the above ground portion of the plant. It consists of a stem on which leaves, flowers and fruits are located. In dicots, leaves are typically oval or palmate with netlike veins while in monocots they tend to be narrow with parallel veins.

Photosynthesis occurs primarily in the leaves and young portions of the stem where CO_2 and water are combined to form the energy rich sugars ($\text{C}_6\text{H}_{12}\text{O}_6$) which can be stored as starches. During photosynthesis, water vapor and oxygen escape into the atmosphere as CO_2 enters into the leaves. The sugars produced by photosynthesis may be stored in a various plant organs which develop as the plant matures during the growing season. Like photosynthesis, respiration also occurs in the shoot system. It is the process by which plants obtain the chemical energy necessary for growth by breaking down sugar in a process which consumes oxygen and produces CO_2 and water. In this regard, it is the opposite of photosynthesis.

In addition to supporting the above ground portion of the plant, the stem connects the shoot system with the below ground root system. It transports sugars, water and other compounds such as growth regulating hormones between them. Water is transported upward from the roots to the leaves while sugars may be transported be either upwards or downwards to actively growing regions or stored as starch. In dicots, the vascular tissue is arranged in a ring within the stem while in monocots it is scattered throughout the stem.

Located below ground, the root system anchors the plant in place. It absorbs water and obtains minerals from the surrounding soil. In dicots, there is typically a large taproot with smaller secondary branching roots while in monocots the root system is a fibrous network with many equal sized roots.

Sugars transported downward from the shoot system may be stored throughout root system and in some cases in specialized organs such as tubers like the one shown on Figure 1.2.1. While photosynthesis does not occur in roots, respiration does. Thus, oxygen enters and CO_2 is released from the roots into the soil. The very fine root “hairs” which exist on the roots greatly increase the amount of contact between the soil pores and plant roots. This enhances water absorption and mineral uptake. Furthermore, the roots are in contact with soil organisms such as fungi which increases water absorption. In some plants such as legumes there are symbiotic bacteria which inhabit root nodules where they transform nitrogen gas into inorganic forms of nitrogen which plants need to synthesize amino acids and other biologically important molecules.

1.3 Cell Structure and Function

Plant cells like those of animals are classified as eukaryotic because their genetic material is contained within a nuclear envelope. Figure 1.3.1 is a generalized representation of a plant cell.

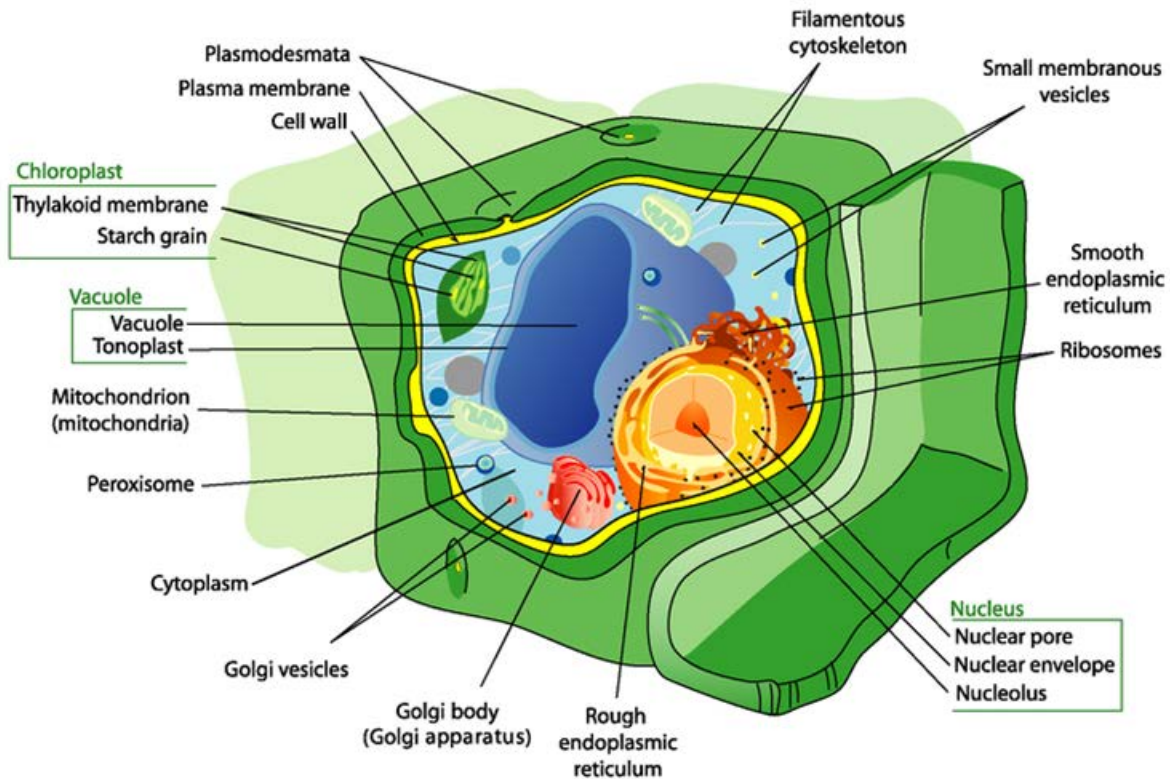


Figure 2.3.1 Generalized Plant Cell

Credit: Mariana Ruiz Villarreal (User:LadyofHats/Wikimedia Commons)

Source: http://commons.wikimedia.org/wiki/File:Plant_cell_structure_svg.svg

License: Public Domain

However, plant cells differ from those of animals because they have cell walls which support the plant's structure. Within the cell, plants also have several structures not found in animal cells. These include chloroplasts in which photosynthesis occurs and vacuoles which contain water and wastes. Their presence increases the cell's internal pressure which provides additional support from within the cell.

Leaves are the primary plant structure in which photosynthesis occurs. Figure 1.3.2 shows the cellular organization of a typical plant leaf using the C₃ photosynthetic pathway (discussed in Section 1.4). Most plants both monocots and dicots have this type of cellular structures. The outer waxy cuticle which helps prevent water loss overlies both the upper and lower epidermal cells. Within the lower epidermis, the guard cells which open and close in response to

environmental and metabolic signals form the edges of the stomatal opening where water vapor, CO_2 and O_2 may diffuse into or out of the leaf. The ground tissue, also called the mesophyll, contains palisade and spongy parenchyma cells consisting of numerous plastids of which chloroplasts are one type. The chloroplasts are surrounded by a double membrane which encloses a semifluid material called stroma. Within the stroma are grana which are stacks of interconnected cells called thylakoids whose membranes contain the green pigment chlorophyll. Other plastids present in the stroma function as storage containers where sugars produced by photosynthesis can be converted to starch.

The vascular tissue within the leaf contains both xylem cells which transport water and dissolved mineral solutes upward from the roots to the leaves and phloem cells which transport dissolved sugars and other metabolites throughout the plant. Bundle sheath cells surround the vascular tissue.

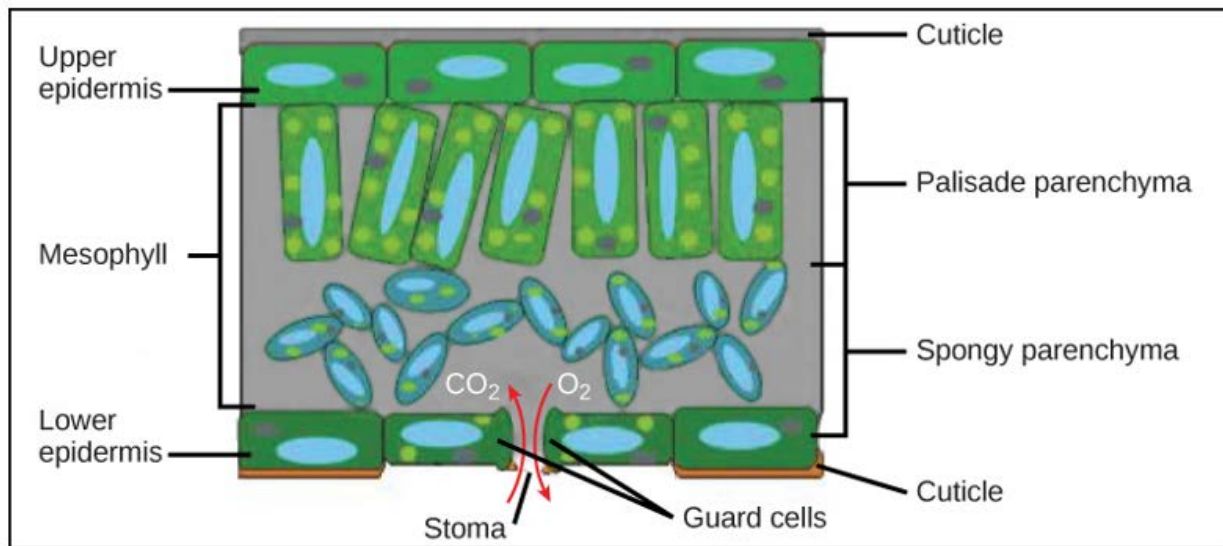


Figure 3.3.2 Generalized Plant Leaf Cells in the C3 Photosynthetic Pathway

Credit: Derived from Figure 6, Chapter 14.4 of General Biology Part II: Mixed Majors by OpenStax College.

Source: <https://cnx.org/contents/45PurvSQ@14.1:jIV8Em9p@1/Leaves>

License: Creative Commons Attribution license 4.0

The internal structure of plants using the C4 photosynthetic pathway is somewhat different as shown on Figure 1.3.3. In this case, the mesophyll cells have a circular arrangement around the bundle sheath cells creating more direct contact with the chloroplasts.

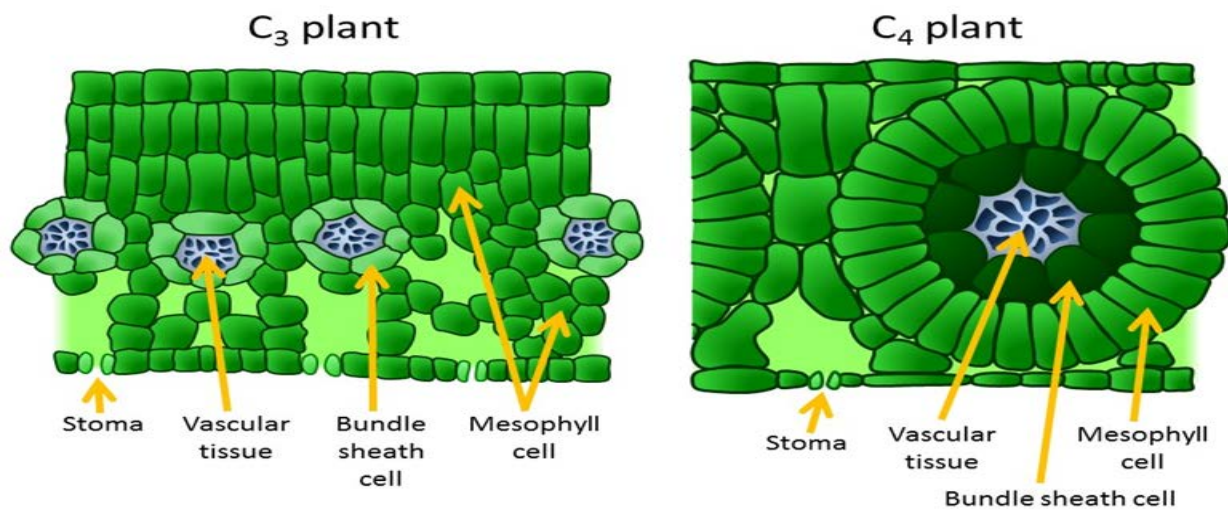


Figure 4.3.3 Comparison of Leaf Cell Structure in C₃ and C₄ Plants

Credit: Figure 2, Chapter 24, Principles of Biology

Source: <https://cnx.org/contents/24nI-KJ8@26.8:0LbfPSK3@9/Photosynthetic-Pathways>

License: Creative Commons Attribution license 4.0

The phloem cells of vascular system transport sugars from sources in the leaves to sinks where growth is occurring such as buds, flowers, fruits and roots. This process requires moving sugars from lower concentrations in the leaves to high concentrations in the phloem cells. This transport process is mediated by the companion cells which consume energy to move the sugars across the cell walls. Because of the high concentration of sugars in the phloem, water moves through the permeable walls of the xylem by osmosis into the phloem increasing the turgor pressure. As shown on Figure 1.3.4, sugars can be converted into insoluble starches in the sink cells thus lowering their concentration causing sugars to be transported in the phloem into lower concentration sink cells by diffusion. This diffusion also increases the water concentration in the phloem relative to the xylem which promotes osmotic transport of water from the phloem into high solute concentration bearing fluid in the xylem.

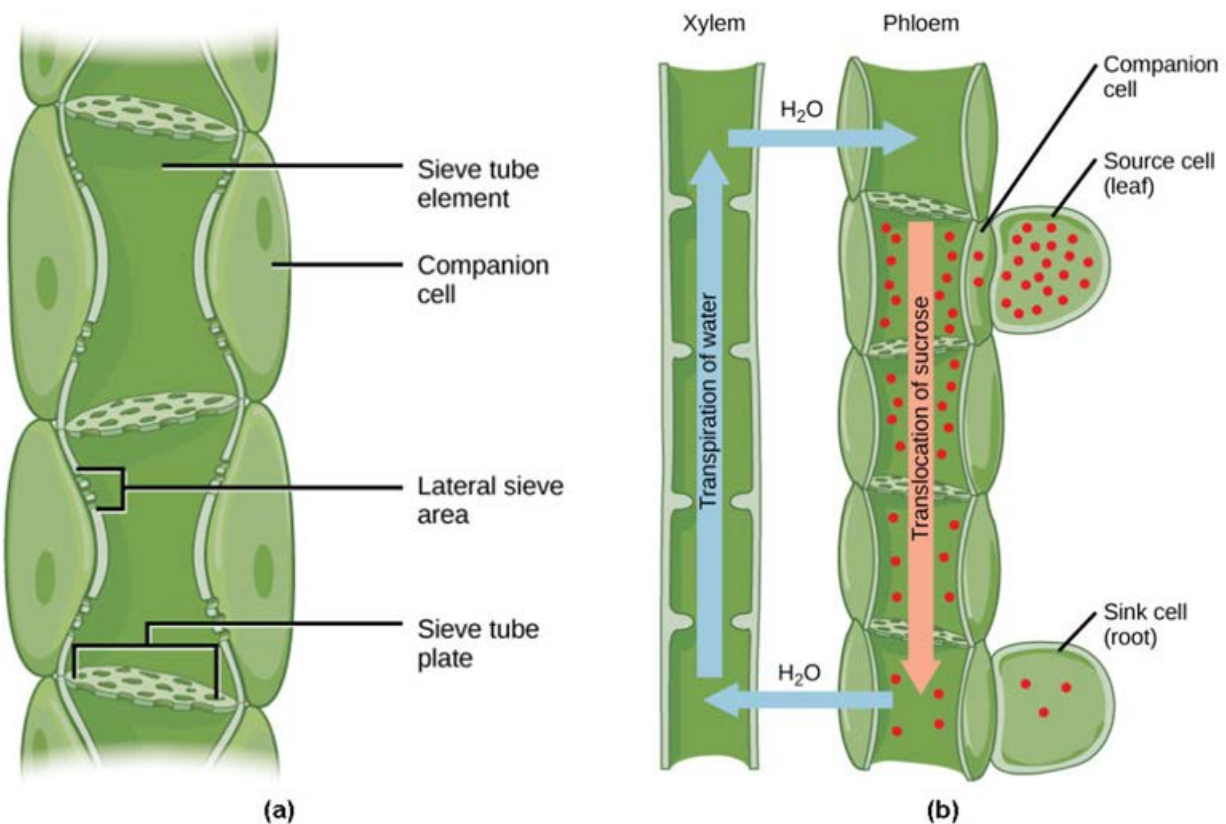


Figure 5.3.4 Transport of Sugars and Water in the Vascular Tissue

Credit: Figures 6 and Figure 7, Chapter 30.5 Biology by OpenStax College

Source: https://cnx.org/contents/GFy_h8cu@11.5:5aq8b3HZ@5/Transport-of-Water-and-Solutes-in-Plants

License: Creative Commons Attribution license 4.0

The movement of water from the roots to the leaves occurs in the xylem from high pressure to lower pressure in the mesophyll cells of the leaves. Water enters the root cells by diffusion across the permeable root cell walls either within the cell walls (apoplastic) or through the cells (symplastic). To promote this diffusion, root cells must actively transport dissolved mineral solutes from relatively low concentrations in the soil water to higher concentrations within the cells. This transport requires the expenditure of energy that comes from downward transport of sugars in the phloem. This movement causes an increase of water pressure within the root cells which tends to push water upwards.

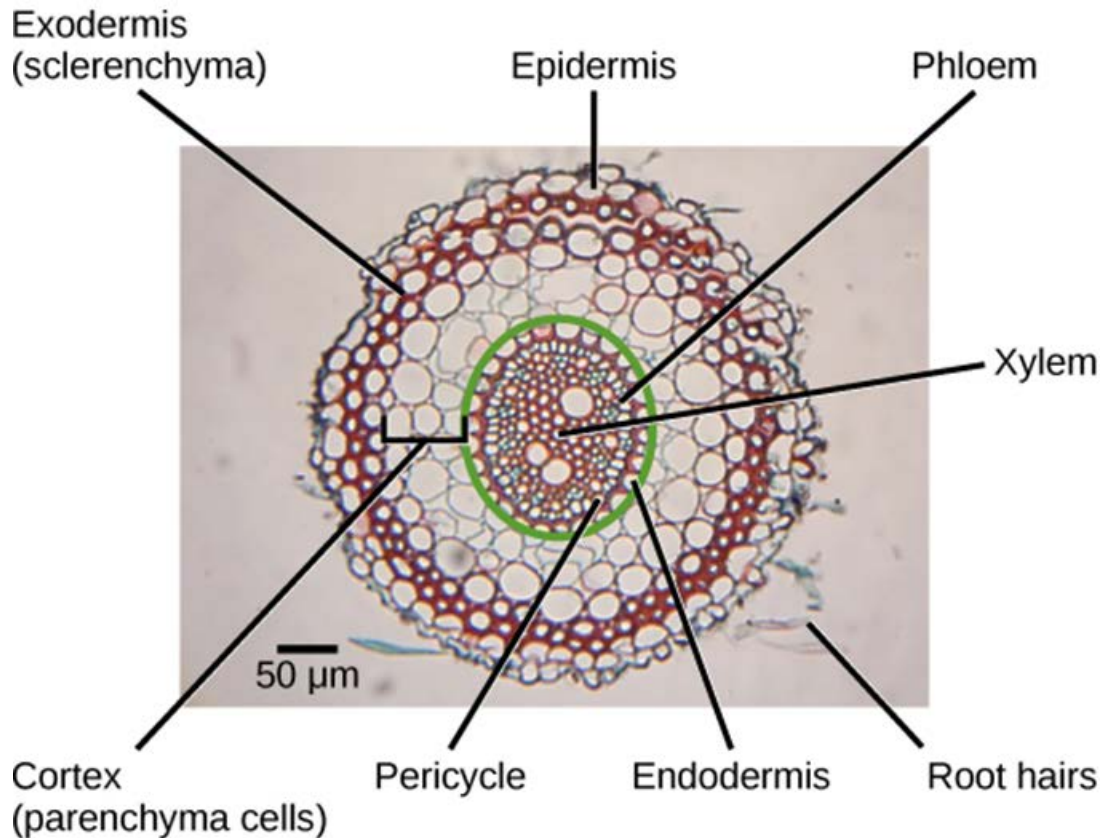


Figure 6.3.5 Movement of Water Solutes in Root Cells

Credit: Figure 3, Chapter 14, General Biology Part II: Mixed Majors by OpenStax College

Source: <https://cnx.org/contents/45PurvSQ@14.1:dIZkXWkq@1/Roots>

License: Creative Commons Attribution license 4.0

However, this pressure alone would be insufficient to move water large vertical distances. As shown on Figure 1.3.6, it is evaporation of water within plant leaves (transpiration) that creates a large negative difference in water pressure between the roots and leaves. Because water molecules are cohesive and also adhere to the xylem's cell walls, they can maintain a continuous flow of water from the roots to the leaves over large vertical distances.

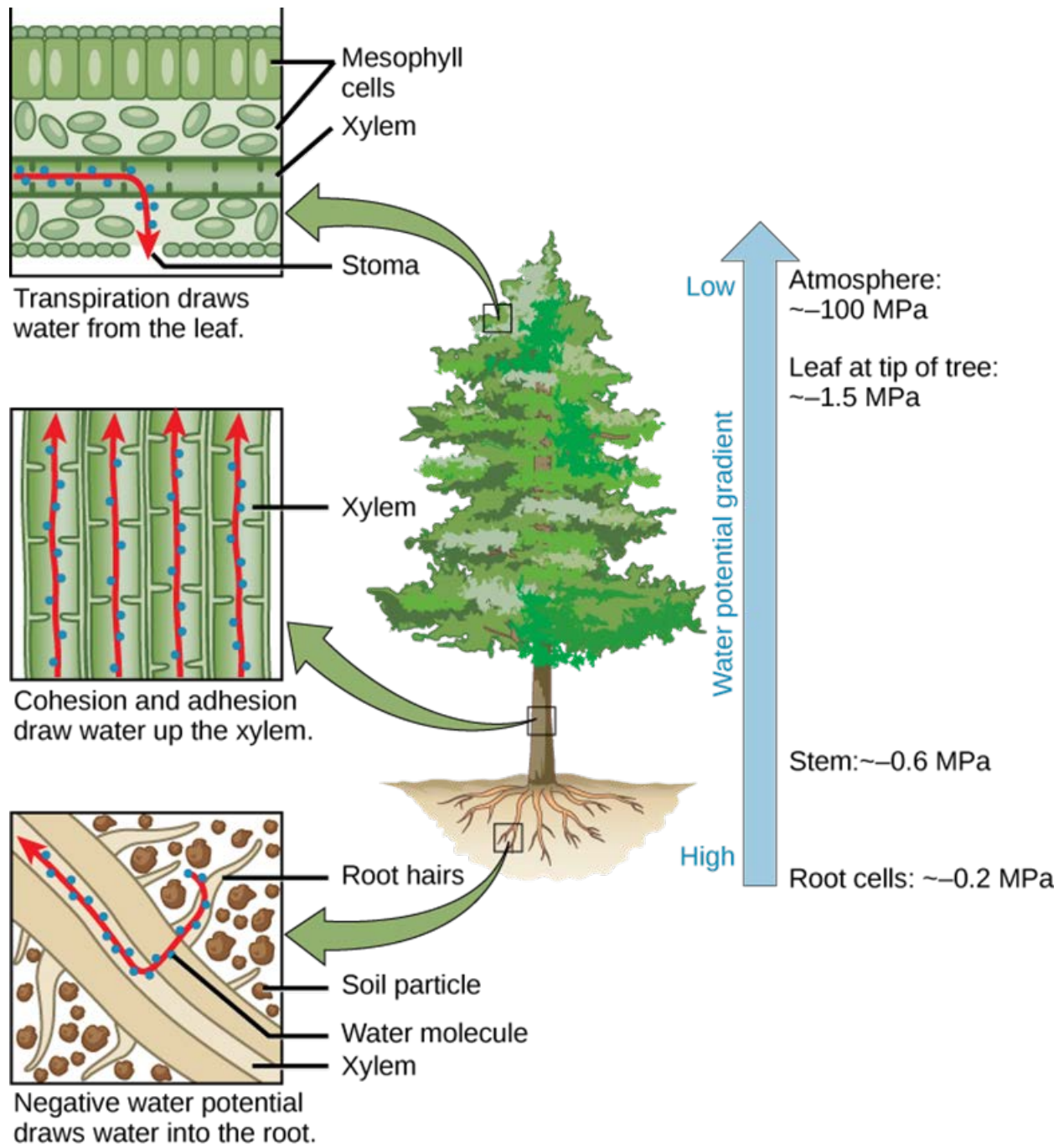


Figure 7.3.6 Transport of Water from Roots to Leaves

Credit: Figure 4, Chapter 30.5, Biology by OpenStax College

Source: https://cnx.org/contents/GFy_h8cu@11.5:5aq8b3HZ@5/Transport-of-Water-and-Solutes-in-Plants

License: Creative Commons Attribution license 4.0

As shown on Figure 1.3.6, the rate of evaporation from the stoma depends in part on the atmospheric conditions represented by the atmospheric water potential (ψ). As the difference

Plant Physiological Responses to Atmospheric Forcings

between the saturated vapor pressure of the water film adhering to the stomatal cell wall and the surrounding atmospheric vapor pressure (referred to as the vapor pressure deficit) increases, the rate of transpiration increases.

When the rate of transpiration exceeds the plants ability to transport water from the roots to the leaves, plants have evolved mechanisms to reduce the rate transpiration by closing the stoma's guard cells shown on Figure 1.3.7 (b). When water is abundant, it diffuses into the guard cells because of a high concentration of potassium ions in the guard cells.

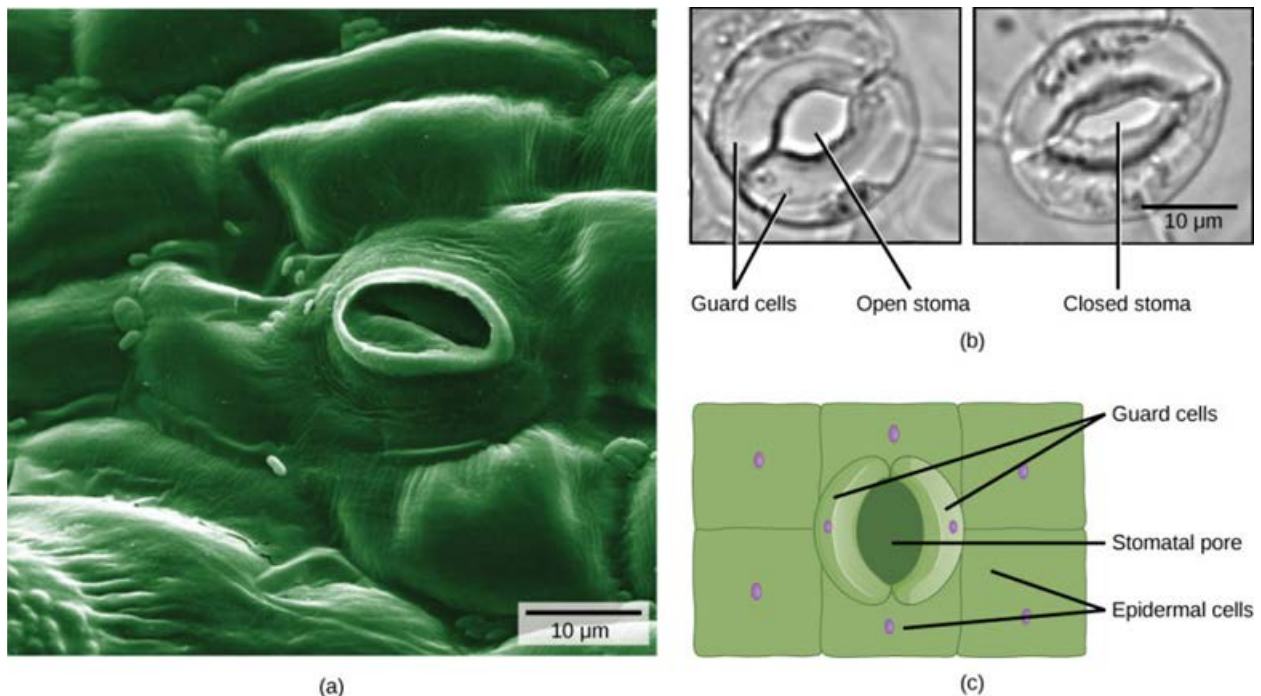


Figure 8.3.7 Function of Guard Cells in Plant Leaves

Credit: Figure 8, Chapter 22, Principles of Biology by OpenStax College

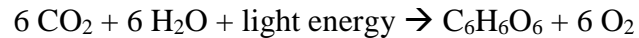
Source: <https://cnx.org/contents/24nI-KJ8@26.8:L83J5z9V@4/The-Plant-Body>

License: Creative Commons Attribution license 4.0

This increase in turgor pressure causes the guard cells to open and allows CO_2 to enter as water vapor and O_2 escape into the atmospheric. When water is lacking, the potassium ion gradient is reversed and water diffuses out of the guard cells and they close. However, when the guard cells close, CO_2 can no longer enter and O_2 builds up within the mesophyll causing photosynthesis to shut down and photorespiration to increase. Besides water availability, plants can control the extent to which their stoma are open based on a variety of other environmental factors including light, atmospheric humidity and CO_2 concentration.

1.4 Photosynthesis

Plants use the energy of sunlight to combine CO_2 and water to make the sugar molecule glucose ($\text{C}_6\text{H}_{12}\text{O}_6$) and O_2 . The overall chemical reaction is:



This reaction occurs in the chloroplasts of the mesophyll cells in two stages. The first stage includes light dependent reactions which occur in the thylakoid membranes while the second stage occurs in the stromal fluid. These two stages are shown conceptually on Figure 1.4.1.

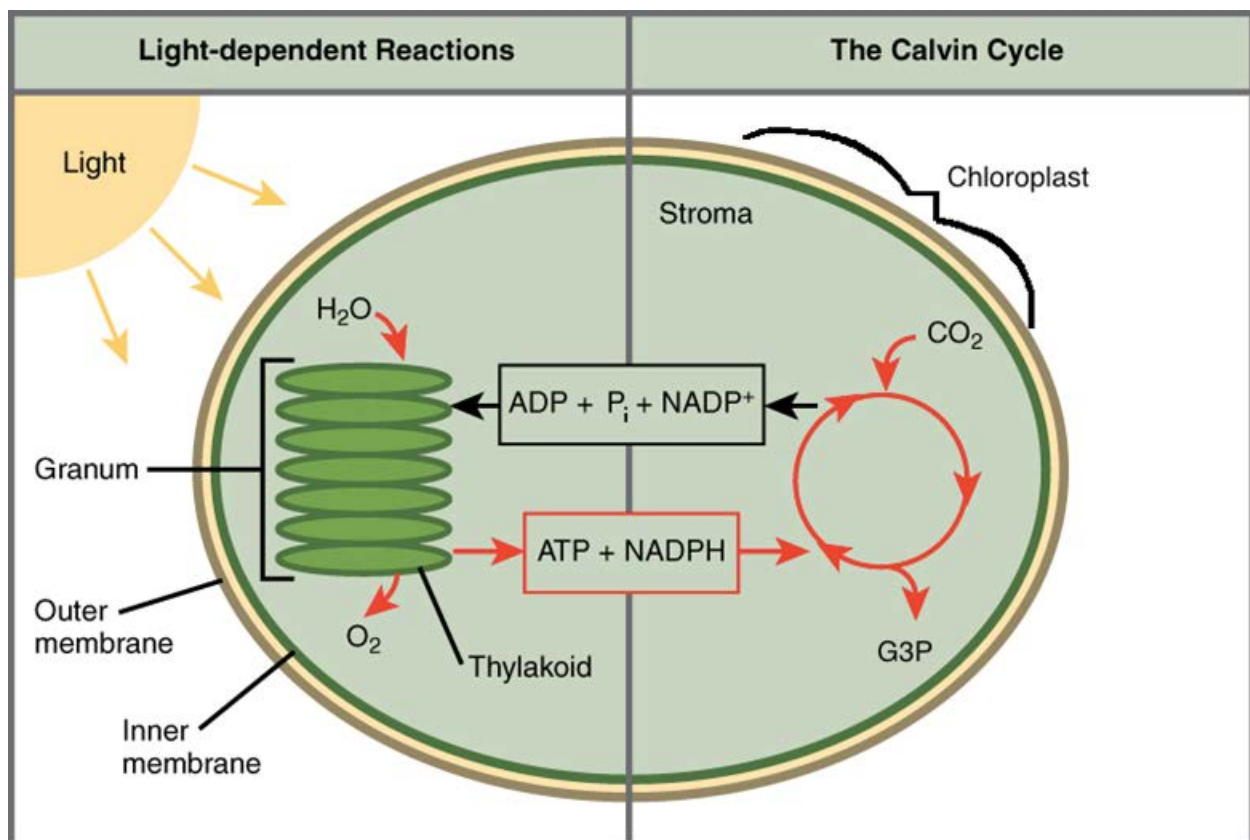


Figure 9.4.1 The Two Stages of Photosynthesis

Credit: Figure 6, Chapter 8.1, Biology by OpenStax College

Source: https://cnx.org/contents/GFy_h8cu@11.5:W7ctJeSI@8/Overview-of-Photosynthesis

License: Creative Commons Attribution license 4.0

The reactants in light dependent reactions are water molecules which are split using energy derived from light to produce oxygen and hydrogen ions and two energy carrying molecules, ATP and NADPH which are made from ADP, NADP^+ and ionic phosphorus (P_i). In the second stage called the Calvin Cycle, the energy contained in these molecules is used to combine CO_2 and water to produce the glyceraldehyde 3 phosphate (G3P) molecules along with ionic

phosphorous and energy depleted ADP and NADP⁺ molecules which are subsequently recycled in Stage 1. Glucose as well as other substances can be synthesized by combining G3P molecules.

In the thylakoid membrane of the chloroplasts shown on Figure 1.4.2, there are two distinct light energy harvesting complexes called photosystems I and II.

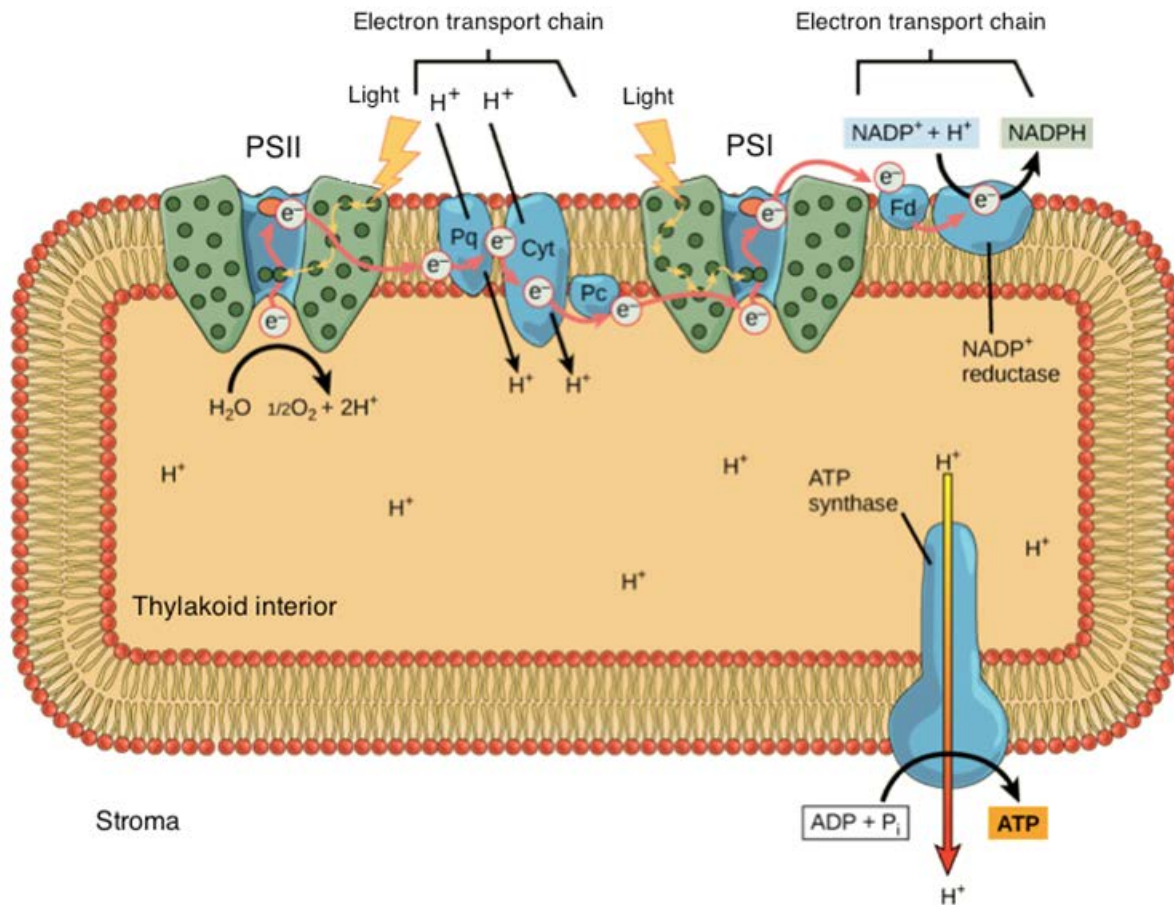


Figure 10.4.2 Light Dependent Reactions in the Thylakoid Membranes

Credit: Figure 8, Chapter The Light-Dependent Reactions of Photosynthesis by Open Stax College

Source: <https://cnx.org/contents/-CmzvUct@13/The-Light-Dependent-Reactions-of-Photosynthesis>

License: Creative Commons Attribution license 4.0

Each has a reaction center labelled PSI and PSII on Figure 1.4.2 has several types of pigment molecules including chlorophyll which absorb energy at various wavelengths. The light energy absorbed by these molecules is transmitted to the reaction center which causes an electron to be energized. In photosystem II, a water molecule is split into oxygen and hydrogen ions yielding an electron which balances the loss of the energized electron. This energized electron is passed to the cytochrome complex where some of its energy is used to pump hydrogen ions (H⁺) into the

thylakoid space. Now depleted, the electron enters photosystem I where it is re-energized by light energy absorbed by the pigment molecules. This electron is used in a reaction catalyzed by NADP⁺ reductase to create the energy carrier molecule, NADPH. In addition, the H⁺ concentration gradient between the inner thylakoid space and the stroma fluid causes H⁺ to pass through the membrane into the stroma which drives ATP synthase to catalyze the production of energy carrier ATP from ADP and Pi.

The energy carrier molecules ATP and NADPH produced in stage 1 provide chemical energy for the stage 2 Calvin Cycle. This chemical energy is used to combine CO₂ and water to produce the sugar precursor molecule G3P. The Calvin Cycle occurs in three phases as shown on Figure 1.4.3. In the first phase (Carbon Fixation), the enzyme Rubisco catalyzes the reaction of 3 CO₂ and 3 water molecules with 3 molecules of ribulose biphosphate (RuBP) which produces in 6 molecules of 3-Phosphoglycerate. In Phase 2 (Reduction), energy from 6 ATP and 6 NADPH is used to produce 6 molecules of G3P also known as PGAL. In Phase 3 (Regeneration), 5 of G3P molecules are used to regenerate 3 RuBP molecules by consuming energy from 3 additional ATP molecules while the 6th G3P molecule forms ½ of a glucose which means the process must cycle twice to produce a full glucose molecule. Therefore, it's the energy carrier molecules produced in the light dependent reactions that make the production of glucose possible. As long as sufficient ATP molecules are being produced by the light dependent reactions, increasing the CO₂ concentration results in the production of glucose molecules.

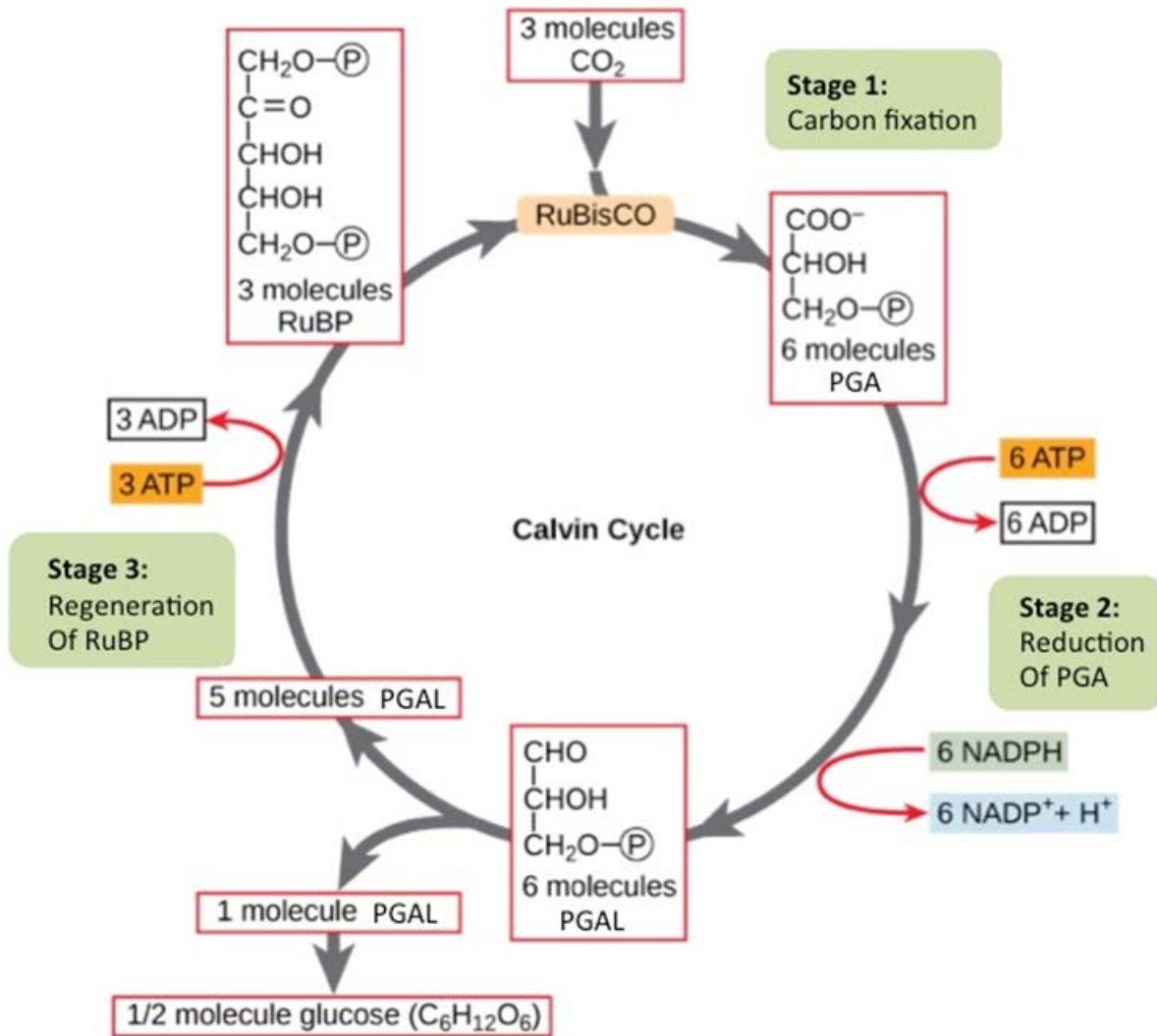


Figure 11.4.3 Three Phases of the Calvin Cycle

Credit: Figure 2, Chapter 18.2, Principles of Biology by OpenStax College
 Source: <https://cnx.org/contents/24nI-KJ8@26.8:Yc-9hZ70@9/Calvin-Cycle>
 License: Creative Commons Attribution license 4.0

However, when the stomata's guard cells close, CO_2 becomes depleted in the mesophyll tissue and the concentration of O_2 produced by the light dependent reactions increases. This affects the functioning of the Rubisco enzyme. As shown on Figure 1.4.4, as CO_2 decreases and O_2 increases, Rubisco starts using O_2 to produce 2-phosphoglerate (PGA) with the release of CO_2 but no production of glucose. This process is called photorespiration but unlike respiration (described in the next section) it does not produce energy carrier molecules like ATP.

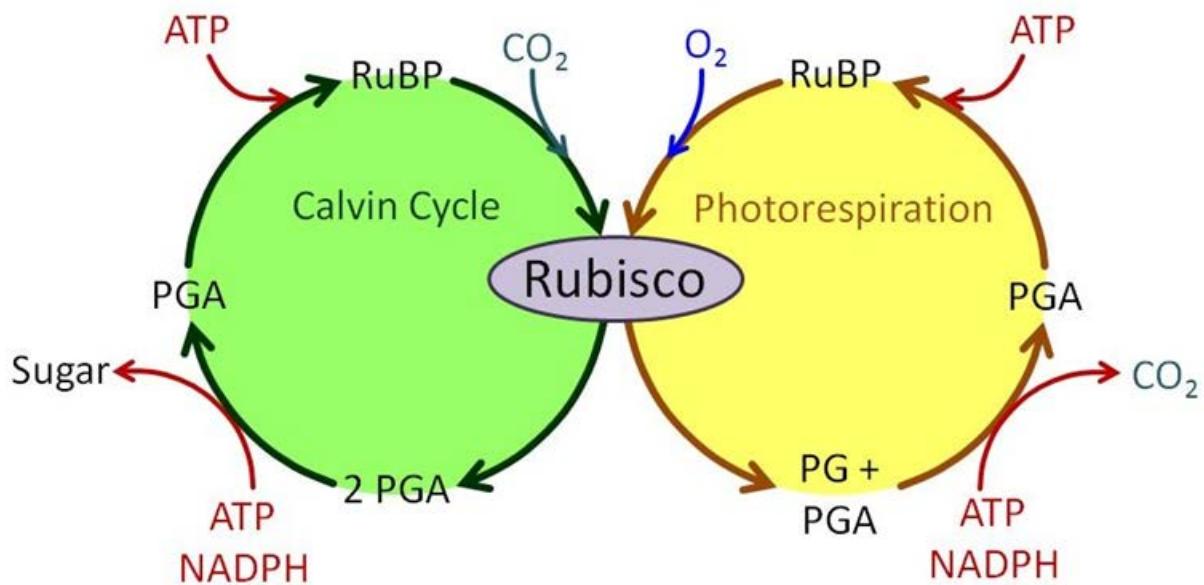


Figure 12.4.4 Photorespiration

Credit: Figure 1, Chapter 24, Principles of Biology by OpenStax College

Source: <https://cnx.org/contents/24nI-KJ8@26.8:0LbfPSK3@9/Photosynthetic-Pathways>

License: Creative Commons Attribution license 4.0

As indicated in Section 1.2, the C₃ photosynthetic pathway is the most common but not all plants follow it. In C₄ plants, both the mesophyll and bundle sheath cell contain chloroplasts (see Figure 1.3.3). The mesophyll cells of C₄ plants contain the enzyme PEP carboxylase. This enzyme catalyzes a reaction between phosphoenolpyruvic acid (PEP) and CO₂ to produce the 4 carbon oxaloacetate molecule. The presence of oxygen does not affect this reaction thereby avoiding the occurrence of photorespiration. This makes C₄ photosynthesis more efficient under low CO₂ conditions and less responsive to high concentrations. Oxaloacetate is then transformed into malate as shown on Figure 1.4.5 from which CO₂ is released and pyruvate generated in the bundle sheath cells. The released CO₂ is subsequently combined with RuBP in the Calvin Cycle leading to the production of glucose. In the mesophyll cells, PEP is also regenerated using ATP produced in the light dependent reactions.

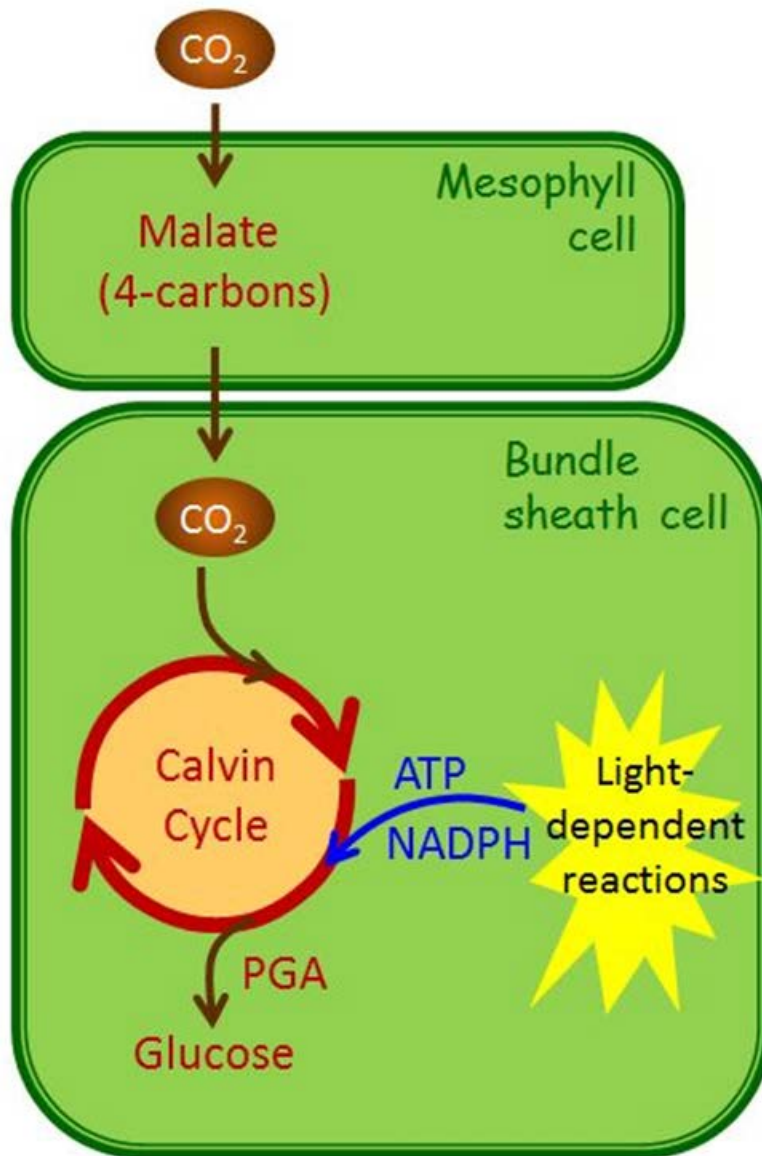


Figure 13.4.5 C4 Photosynthesis

Credit: Figure 3, Chapter 24, Principles of Biology by OpenStax College

Source: <https://cnx.org/contents/24nI-KJ8@26.8:0LbfPSK3@9/Photosynthetic-Pathways>

License: Creative Commons Attribution license 4.0

Some plants mostly succulents growing in hot, dry climates use a variant of the C4 photosynthetic pathway called CAM. These plants only open their stomata at night allowing CO₂ to enter while avoiding the excessive loss of water vapor. Like C4 plants, the CO₂ is accumulated organic acid molecules and later during daylight hours when the stoma are closed used to produce glucose by photosynthesis similar to C3 plants.

1.5 Respiration

Plants use the chemical energy stored in the bonds of glucose to obtain energy needed to perform other metabolic functions. The process can be expressed by the overall equation:



This reaction is essentially the opposite of photosynthesis except that energy is produced. During respiration, the chemical energy of the glucose molecule is transformed into chemical energy stored in the ATP molecule while CO_2 and water are produced. The high energy bonds of the ATP molecule are the primary source of energy used support other plant growth metabolic functions.

The complete metabolism of glucose occurs in three major stages including glycolysis, the Cycle Krebs also known as the citric acid cycle and oxidative phosphorylation. The overall process of respiration is shown on Figure 1.5.1.

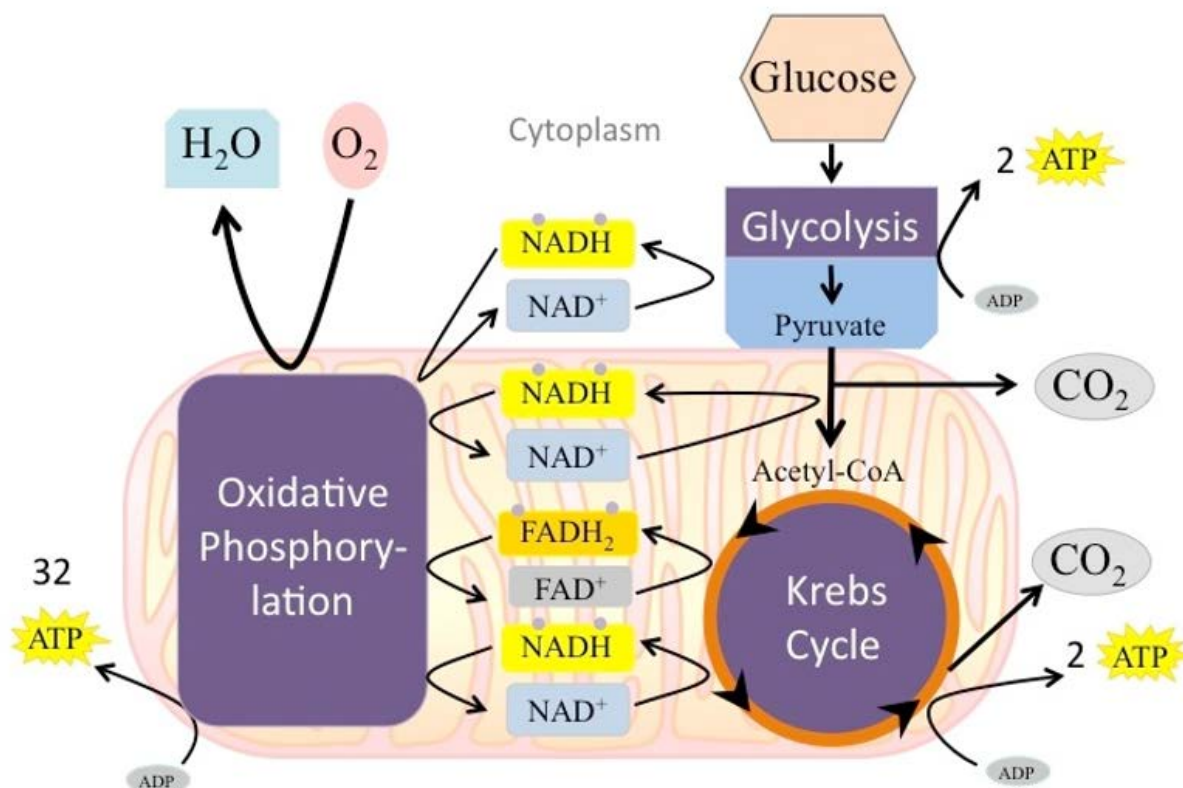


Figure 14.5.1. The Three Stages of Respiration

Credit: Figure 5, Chapter 19.3, Principles of Biology by OpenStax College

Source: <https://cnx.org/contents/24nI-KJ8@26.8:nH1AyC1-@9/Oxidative-Phosphorylation>

License: Creative Commons Attribution license 4.0

In glycolysis, each molecule of glucose is initially broken down into two molecules pyruvate. This reaction which occurs in the cell's cytoplasm produces a net of one ATP molecule as well as two electron carrier NADH molecules. Under anaerobic conditions, the pyruvate molecules undergo fermentation to either lactate or ethanol releasing CO_2 . These reactions occur in the cytoplasm. In the presence of oxygen, pyruvate is instead transported into the mitochondrion where it is combined with Coenzyme A (CoA) to form the compound Acetyl CoA. This reaction releases one molecule of CO_2 and produces two molecules of the electron carrier NADH.

In the second stage of respiration, Acetyl CoA enters the Krebs Cycle. In this eight step cycle each Acetyl CoA first combines with a molecule of oxaloacetate to form citrate as CoA is released for recycling. Mitochondrial enzymes process the citrate through additional rearrangements until oxaloacetate is regenerated. As shown on Figure 1.5.2, these steps produce two molecules of ATP along with 3 molecules of NADH, one molecule of FADH_2 (another electron carrier) while two additional molecules of CO_2 are released.

The third stage of respiration occurs in the inner membrane space of the mitochondrion. Similar to the membranes of the thylakoids within the chloroplasts, the inner membrane of the mitochondria contain specialized proteins that form an electron transport chain (ETC). As shown on Figure 1.5.3, these ETC proteins (shown in blue) obtain electrons from NADH and FADH_2 and use them to catalyze a reaction between oxygen and hydrogen ions to produce water. This is the opposite to the splitting of water that occurs at the reaction center of photosystem II.

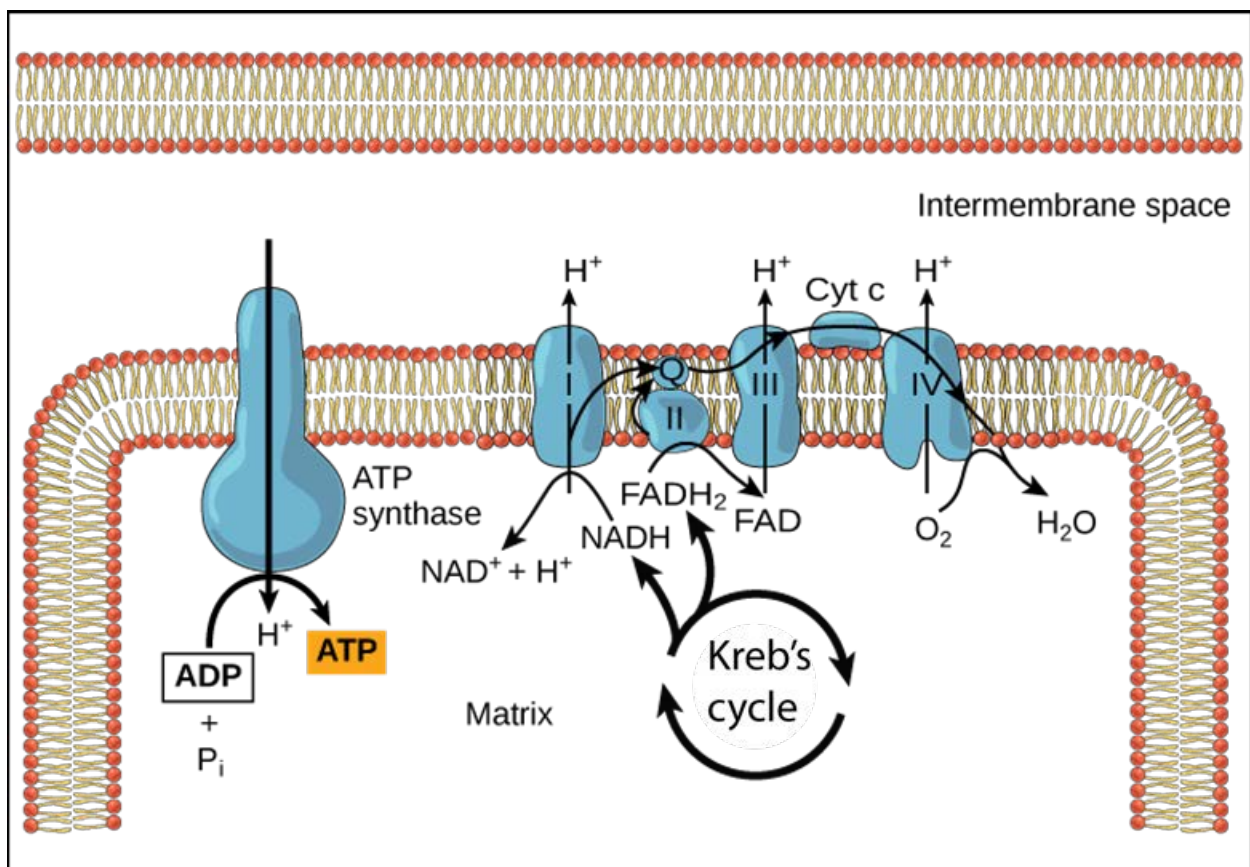


Figure 15.5.3 Mitochondrion Electron Transport Chain

Credit: Figure 3, Chapter 19.3, Principles of Biology by OpenStax College

Source: <https://cnx.org/contents/24nI-KJ8@26.8:nH1AyC1-@9/Oxidative-Phosphorylation>

License: Creative Commons Attribution license 4.0

At the same time this reaction is occurring, these proteins use the energy of the electrons to pump hydrogen ions against the concentration gradient into the intermembrane space. In the same way as the production of ATP in photosynthesis occurred, these hydrogen ions discharge through the ATP synthase enzyme driving the production of ATP. Figure 1.5.4 shows a summary of photosynthesis and ATP production during each stage of respiration. Depending on plant type, respiration produces 30 or 32 ATP molecules per molecule of glucose when it is completely metabolized.

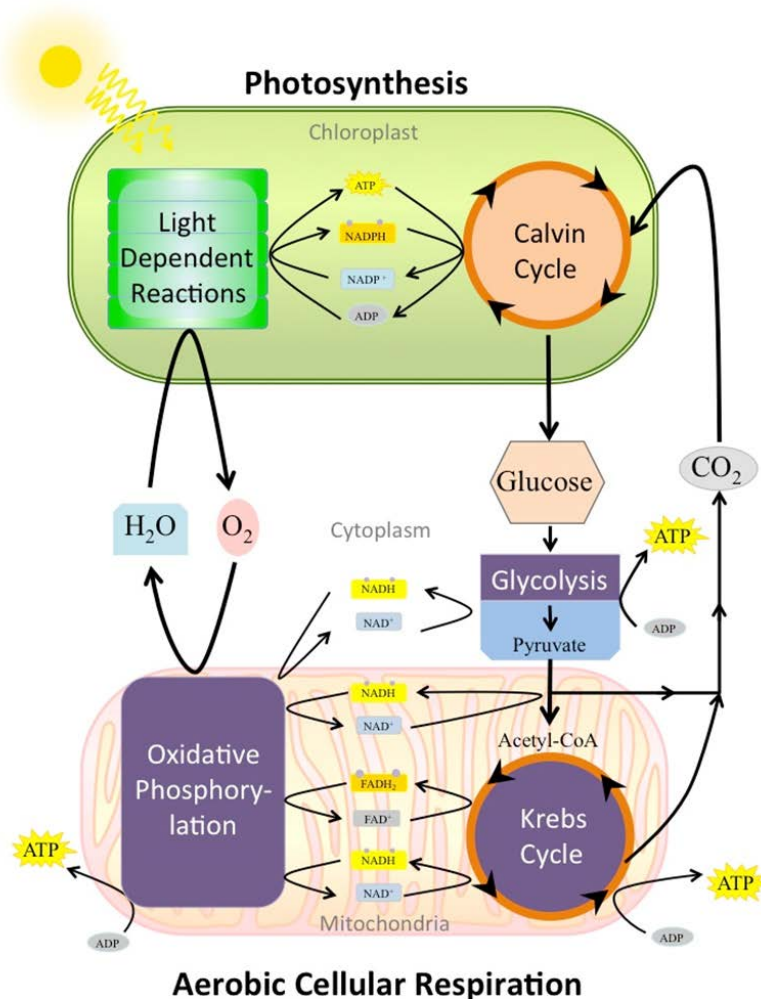


Figure 16.5.4 Summary of Photosynthesis and Aerobic Respiration

Credit: Figure 6, Chapter 19.3, Principles of Biology by OpenStax College

Plant Physiological Responses to Atmospheric Forcings

Source: <https://cnx.org/contents/24nI-KJ8@26.8:nH1AyC1-@9/Oxidative-Phosphorylation>
License: Creative Commons Attribution license 4.0

2. Atmospheric Factors Influencing Crop Evapotranspiration and Yield

2.1 Introduction

An overview of interactions between atmospheric factors and crop responses is presented in this section. The focus of this study is on irrigated crops assuming that adequate water is supplied to meet the crop's consumptive use requirements. Other important conditions effecting ET and yield including nutrients, plant disease and weed competition; soil physical and chemical properties; cultural and irrigation management practices are also assumed to be non-limiting factors.

As shown on Figure 2.1.1, a strong relationship between major climate and vegetation zones exists at the global scale.

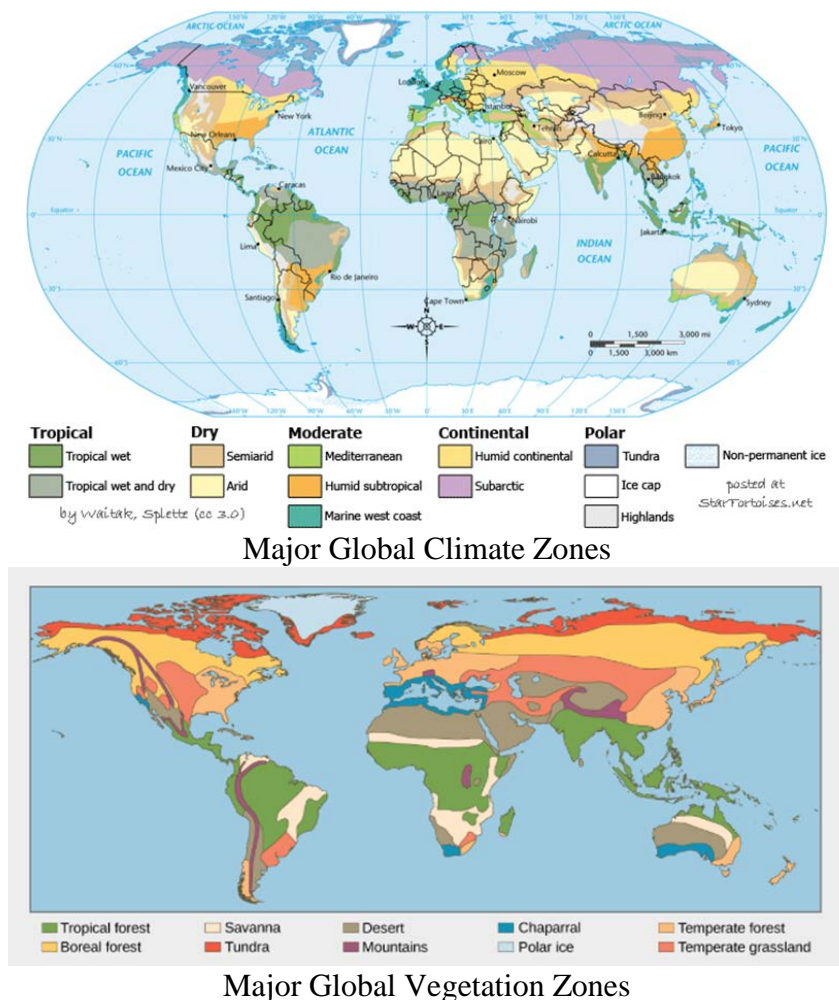


Figure 2.1.1. Major Global Climate and Vegetation Zones

Plant Physiological Responses to Atmospheric Forcings

Note: Composite Figure 2.1.1 was developed by Michael Tansey for this report from the following two sources.

Credit: ClimateMap World.png

Source: https://commons.wikimedia.org/wiki/File:ClimateMap_World.png

License: [GNU Free Documentation License](https://creativecommons.org/licenses/by-sa/4.0/).

Credit: Figure 2, Chapter 5.6, Principles of Biology by OpenStax College

Source: https://cnx.org/contents/24nI-KJ8@26.8:ehB-Hyi7@8/Biomes#fig-ch44_03_01

License: [Creative Commons Attribution license 4.0](https://creativecommons.org/licenses/by-sa/4.0/)

Figure 2.1.2 shows the Holdridge Life Zone relationships between major vegetation types and climate characteristics at global and regional scales. However, other meteorological conditions including solar radiation, humidity and wind are well known to exert important influences on the types and distribution of plant species. Like native vegetation, agricultural crops have been adapted over long periods of time to grow well under a wide range of climate conditions.

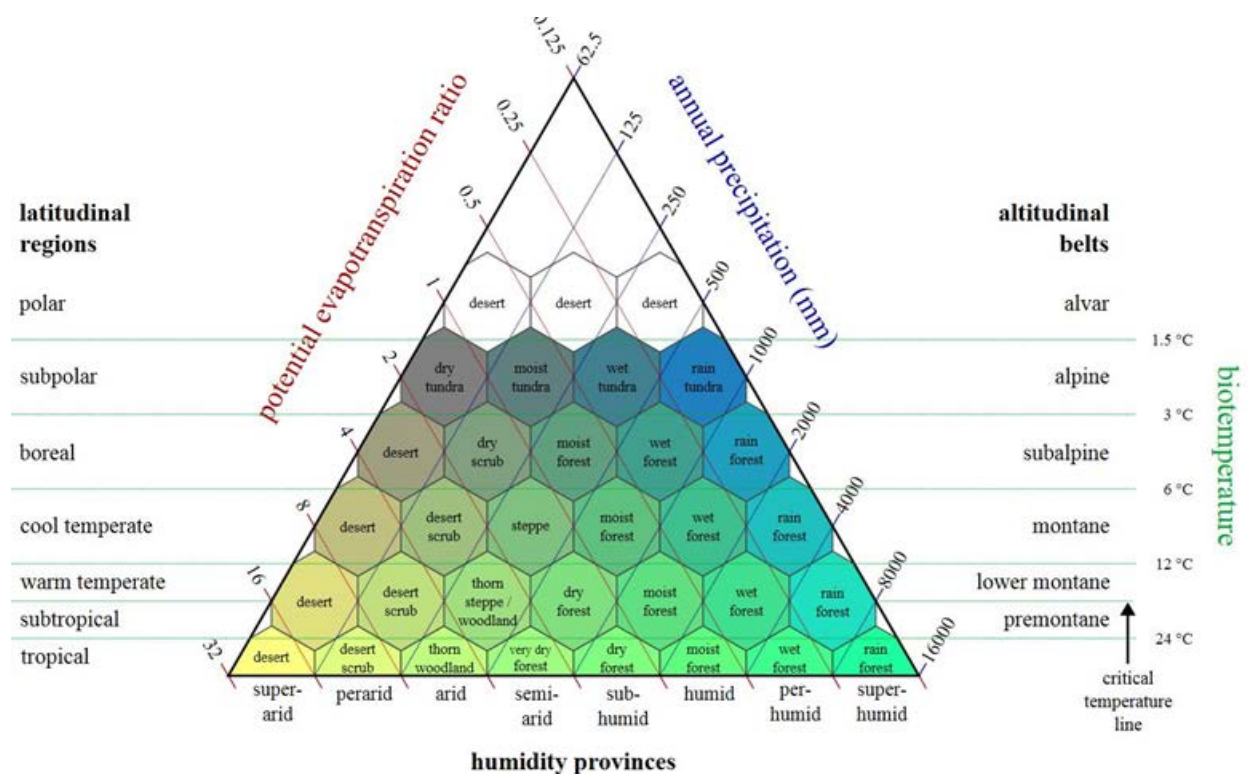


Figure 2.1.2 Relationship between major vegetation types, temperature and precipitation

Credit: Lifezones Pengo.svg

Source: <https://commons.wikimedia.org/w/index.php?curid=1737503>

License: [Creative Commons BY SA \(any version\)](https://creativecommons.org/licenses/by-sa/4.0/)

2.2 Overview of Temperature Response Effects on Crop Growth and Yields

It is well known that various plant species respond to temperature differently. Although plants are also adapted to other conditions (soil and nutrients), there exists an optimum temperature range in which plant specific biological processes such as photosynthesis and respiration are maximized. Outside of this range (either above or below), these processes decrease until mortality occurs. Depending on the balance of responses to these processes, higher temperatures can lead to either increased or decreased plant growth. Furthermore, biological responses to temperature are nonlinear, resulting in plant effects becoming increasing larger as temperature increases.

An important effect of temperature is how it affects photosynthetic efficiency which is defined as the net amount of CO₂ fixed into sugar per unit of light energy received. In C3 plant, increasing temperature results in a decline in photosynthetic efficiency. This is the result of several factors. First, the solubility of CO₂ in water decreases more with increasing temperature than the solubility of O₂ which increases its concentration causes the Rubisco enzyme to favor photorespiration which produces no sugar (Figure 1.4.4). Second, the Rubisco enzyme itself undergoes changes in its properties that stimulate its reaction with O₂ over CO₂. This temperature effect does not occur on C4 plants which first convert CO₂ into 4 carbon acids by reaction in O₂ concentration has no affect. Subsequently in the bundle sheath cells, CO₂ is enzymatically released and C3 photosynthesis proceeds without interference from O₂.

For vegetative development, there is a base temperature (T_b) at which growth commences. As temperature increases, a plant's life cycle (phenological) phases occur more quickly. However, beyond the optimum temperature range, development (node and leaf appearance rate) slows. For non-perennial crops, faster development is not necessarily ideal because a shorter life cycle results in smaller plants, shorter reproductive phase duration, and lower yield potential. Consequently, the optimum temperature for yield is nearly always lower than the optimum temperature for vegetative growth. During the reproductive stage, higher temperatures affect pollen viability, fertilization, as well as grain and fruit formation. Although there is considerable genotypic variation among fruit and nut crops, winter temperatures can affect their ability to survive specific low temperature extremes (winter hardiness) and the dormancy period needed for optimum flowering and fruit set in the spring and summer (vernalization).

As temperature increases, the basal temperature required to initiate plant growth occurs earlier in the year. For perennial crops, this earlier spring growth combined with a corresponding extension of warmer temperatures in the fall may increase the length of the growing season. The U.S. Global Change Research Program (USGCRP, 2008) estimated that the growing season in the Northern Hemisphere has already lengthened by about 1 to 4 days per decade in the last 40 years, especially at high latitudes. This lengthening may also expose plants to other changes in climatic conditions. For many plant species, day-length (photoperiod) also affects their life cycles. However, the intensity of solar radiation is less during spring and fall. Thus, warming may not result in the corresponding growth increases that temperature alone might seem to imply.

Plant Physiological Responses to Atmospheric Forcings

Temperature is a major forcing of atmospheric humidity. As temperature increases, the rate of evaporation from the oceans results in higher atmospheric humidity. Increased atmospheric humidity also reduces the intensity of solar radiation (R_s) reaching the earth's surface. Although this reduction is not large, it reduces the energy available for photosynthesis as well as ET. Changes in atmospheric humidity may also affect the ability of plants to produce biomass and yield by changing the vapor pressure deficit (VPD) which is defined as the difference between the stomatal vapor pressure (e_s) and vapor pressure of the surrounding atmosphere (e_a). Because the saturation vapor pressure is a strongly nonlinear function of temperature, e_s typically increases more rapidly than e_a especially as the ambient temperature increases. Thus, increasing temperature typically causes an increase in VPD. If the increase in VPD remains below plant specific thresholds, an increase in VPD results in increased ET. However, when the threshold is exceeded, ET may decrease in relation to the VPD increase. For some crops, growth may also be affected because increasing VPD may decrease the crop's radiation use efficiency (RUE) resulting in less growth.

Table 2.2.1 summarizes information about temperature dependence of various life cycles phases for some major agriculture crops grown in the Reclamation project areas.

Table 2.2.1 Temperature (°C) Dependence of various Life Cycles Phases for some Major Agriculture Crops

Crop	Base ¹ Temp Veg Prod	Opt ² Temp Veg Prod	Base ³ Temp Reprod	Opt ⁴ Temp Reprod	Opt Temp Range Reprod Yield	Failure Temp Reprod Yield	% Yield ⁵ Change Per °C increase
Corn	8	34	8	34	18-22	35	-3.3
Cotton	14	37	14	28-30	25-26	35	-4.8
Rice	8	36	8	33	23-26	35-36	-10
Wheat	0	26	1	26	15	34	-5.4

Footnotes:

1. Base Temp Veg Prod = Base temperature for vegetative production
2. Opt Temp Veg Prod = Optimum temperature for vegetative production
3. Base Temp Reprod = Base temperature for reproductive phase
4. Opt Temp Reprod = Optimum temperature for reproductive phase
5. Estimated yield changes in North America relative to beginning of 21st century

Source: Synthesis and Assessment Product 4.3, Tables 2.2 and 2.6 (USGCRP, 2008)

2.3 Overview of Carbon Dioxide Response Effects on Crop Growth and Yields

The effects of carbon dioxide (CO₂) vary among various plant species. Most agricultural crops use the C3 photosynthetic pathway. Early studies of C3 plants conducted in enclosures under ideal growth conditions indicated a 33 percent increase in average yield occurred when CO₂ was increased from 330 to 660 (Kimball, 1983). Under similar conditions, the yield response of C4 plants such as corn increased by only about 10%. More recently, new “free-air CO₂ enrichment” (FACE) experiments have allowed evaluations of responses under experimental conditions that more closely simulate field conditions. Although some FACE results suggest yield responses that are less than previously reported (Long et al., 2006), the FACE experiments generally corroborate the previous enclosure studies (Ziska and Bunce, 2007). Table 2.3.1 presents a summary of various plant responses to an increase of CO₂ from 330 to 660 ppm for selected major agriculture crops grown in the Reclamation project areas.

Bloom (2010) summarized multiple studies of changes in aboveground biomass when CO₂ concentrations were increased from 366 to 567 ppm. For both C3 and C4 grasses, average increases of approximately 10% occurred. Substantially larger increases were reported for legumes (75%) and trees (50%).

Table 2.3.1. Percent change in Yield due to Increasing CO₂ from 330 to 660 ppm under Ideal Growth Conditions

Crop	Carbon Fixation Pathway	Leaf Photosynthesis	Total Biomass	Grain Yield
Corn	C4	3	4	4
Cotton	C3	0 - 33	0 - 46	0 - 44
Rice	C3	0 - 36	0 - 30	0 - 30
Sorghum	C4	0 - 9	0 - 3	0 - 8
Wheat	C3	0 - 35	0 - 27	0 - 31

Modified from: Synthesis and Assessment Product 4.3, Tables 2.7 (USGCRP, 2008)

The combined effects of increasing temperature and CO₂ can be beneficial to yields of certain leaf crops such as lettuce and spinach because increasing both CO₂ and temperature speeds the early growth phase in which these crops are harvested. However, for crops such as cotton, rice, sorghum and wheat no reported increases in yield occurred. For such closed canopy crops, increasing CO₂ at elevated temperatures caused additional increases in canopy temperatures typically ranging from 1 - 2 °C. This increased canopy temperature occurs especially in C3 plants because elevated CO₂ allows reductions in leaf stomatal aperture which in turn reduces evaporative cooling of the leaves. Because the optimum temperature for yield is typically less than for vegetative growth (see Table 2.2.1 above), the combined effects of increased CO₂ and temperature may offset some the potential of increased CO₂ on yields. Therefore, even though the effects of CO₂ may be large they are also dependent on temperature as well as other atmospheric forcings.

2.4 Overview of Atmosphere and Carbon Dioxide Response Effects on Crop Evapotranspiration

The potential effects of climate change on plant water use can be examined by an analysis of well known Penman-Monteith (PM) equation (Monteith, 1981).

$$\mathbf{ET} = \left\{ \frac{\Delta(\mathbf{R}_n - \mathbf{G}) + \mathbf{K}_t \rho_a \mathbf{C}_p \frac{(\mathbf{e}_s - \mathbf{e}_a)}{r_a}}{\Delta + \gamma \left(1 + \frac{\mathbf{r}_s}{r_a}\right)} \right\} / \lambda \rho_w \quad (\text{Eqn 1})$$

Where in SI units the terms of the equation are given by:

ET = Crop evapotranspiration [mm d⁻¹]

R_n = Net solar radiation [MJ m⁻² d⁻¹]

G = Soil heat flux [MJ m⁻² d⁻¹]

e_s = Saturation vapor pressure of the canopy [kPa]

e_a = Actual vapor pressure of the surrounding atmosphere [kPa]

r_a = Aerodynamic resistance [$s\ m^{-1}$]

r_s = Canopy resistance [$s\ m^{-1}$]

Δ = Slope of the saturation vapor pressure-temperature curve [$kPa\ ^\circ C^{-1}$]

C_p = Specific heat capacity of moist air [$MJ\ kg^{-1}\ ^\circ C^{-1}$]

ρ_a & ρ_w = Mean air and water density respectively [$kg\ m^{-3}$]

γ = Psychrometric constant ($kPa\ ^\circ C^{-1}$)

λ = Latent heat of vaporization ($MJ\ kg^{-1}$)

K_t = 86,400 $s\ d^{-1}$

The terms in Eqn. 1 depend on both biological and meteorological conditions. It is worth noting that air temperature does not appear directly in the PM equation. The ASCE PM method (Allen et al., 2005) describes relationships between several variables in Eqn. 1 and daily or hourly temperatures. Temperature dependent variables include the latent heat of vaporization λ , the mean air density, ρ_a , slope of the saturation vapor pressure-temperature curve, Δ , and the psychrometric constant, γ . The net radiation term, R_n , also depends on temperature through the effect of surface temperature on outgoing long-wave radiation.

The saturation vapor pressure, e_s , is a function of air temperature and affects the stomatal vapor pressure which drives the diffusion of water vapor from leaves but, as discussed above, may decrease stomatal conductance caused by elevated CO_2 can increase leaf temperature which in turn increases e_s . Therefore, the vapor pressure deficit (VPD) defined as the difference between e_s and e_a may increase because of the combined effects CO_2 and increased air temperature.

In the PM equation, an increase in the VPD results in an increase in ET. However, it is important to recognize that plant response to increased VPD is not as simple as represented in the PM equation. Initially, increasing VPD produces increased plant transpiration. However, when VPD increases beyond certain plant type specific thresholds, some plants respond reducing their transpiration to prevent excessive loss of cell fluids. Streck (2003) provides a comprehensive review of published research on plant responses to VPD. Although the exact mechanisms by which plants respond to VPD (Addington et al 2004) is still an area of research and it is known that not all plants exhibit the response (Ocheltree et al 2014), it is sufficiently well established and potentially significant enough that this response referred to as “apparent feedforward” is included in the WEAP-CV PGM used in this study as well as other models simulating the dynamics of plant growth processes.

Other meteorological influences on crop ET include the effects of the canopy albedo on the reflection of incoming short-wave radiation, the influence of wind speed and crop height on aerodynamic resistance, r_a , and the effects of stomatal conductance and canopy development typically expressed in terms of the leaf area index (LAI) [m^2 leaf area per m^2 soil surface] on canopy resistance, r_s .

Kimball (2007) performed a temperature sensitivity analysis on some of the meteorological and plant variables used in the ASCE hourly PM equation (Allen et al, 2005) using data obtained from a weather station in Maricopa, AZ during the year 1987. Results from this study are presented in Table 2.4.1.

Table 2.4.1. Sensitivity of the ASCE Hourly PM Equation to Weather and Plant Variables

Weather or Plant Variable	ET Sensitivity (% Change in ET)	
	Summer Day	Whole Year
Temperature effect per $\Delta^\circ\text{C}$ at constant absolute humidity	2.39	3.44
Solar Radiation effect per $\Delta\%$ R_s	0.58	0.40
Atmospheric vapor pressure effect per $\Delta\%$ e_a	-0.16	-0.40
Wind effect per $\Delta\%$ U	0.29	0.38
Stomatal conductance effect per $\Delta\%$ g_s	0.08	0.16
LAI effect per $\Delta\%$ LAI	0.08	0.16

In Table 2.4.1, the sensitivity of ET to temperature is greatest of all the variables considered. As discussed above, temperature affects many of the variables in the PM equation but its effect on the vapor pressure deficit ($e_s - e_a$) is most likely the main cause of its higher significance in the results. However, increasing atmospheric humidity, e_a , reduces ET by decreasing the VPD. Furthermore, it worth noting that temperature effects on growth and LAI of non-reference crops are not really represented in this analysis because reference crops are assumed to have a constant canopy height and LAI throughout the growing season which is not representative of most agricultural crops.

Higher temperatures also have the potential to affect crop phenological characteristics related to crop ET. For perennial crops, increased warming will continue lengthening the growing season which will tend to increase total annual ET. For annuals, earlier warming may cause a shift in the growing season to earlier in the year. These shifts may or may not increase crop water use. As discussed above, more rapid growth due to warming may shorten the actual growth period resulting in reduced water consumption for some crops. However, for those crops (either annual or perennial) exhibiting photoperiod sensitivity, earlier growing season initiation may result in slower growth in the spring when solar radiation in the northern hemisphere is less intense and consequently reduce ET during the early vegetative growth stage. Furthermore, growing season

shifts may result in crops being exposed to other climatic conditions such as increased precipitation and/or humidity or decreased wind speed which would also tend to reduce crop ET.

In addition, the effects of rising CO₂ are likely to exert a significant influence on crop ET. Based on relative gradients in concentration between the stomata and atmosphere, Bloom (2010) estimated that the rate of diffusion of water vapor out of plant is about 40 times faster than the rate of CO₂ diffusion into the leaf. For C3 plants, it was estimated 500 - 1000 water molecules are lost per molecule of CO₂ entering the leaf whereas for C4 plants due their lower internal CO₂ requirements only 200 - 300 molecules of water are lost. Under a doubling of CO₂, plants could potentially assimilate twice as many molecules of CO₂ per molecule of water lost. Plants could respond to increasing CO₂ by either decreasing their stomatal openings to maintain similar CO₂ concentrations or they could keep their stomata open and thereby lose more water while increasing the assimilation of CO₂ and potentially increasing growth.

Bloom (2010) summarizes a large number of experimental studies indicating that plants actually respond using a combination of these strategies. In C3 crops, stomatal conductance was reduced by an average by 22% when CO₂ concentrations increased from 366 to 567 ppm. For C4 crops, the average reduction in stomatal conductance was about 30%. For both C3 and C4 crops, CO₂ assimilation in the leaf cells increased on average by approximately 10%. Other studies have reported similar responses to elevated CO₂ in both C3 and C4 plants. Kimball and Idso (1983) reported a 34% reduction in stomatal conductance when the CO₂ concentration was increased from 340 to 660 ppm. Based on data from FACE experiments, Ainsworth and Long (2005) reported an average reduction in stomatal conductance of between 20 - 22 % when CO₂ concentrations were increased from 360 to 600 ppm.

2.5 Simple Assessment of the Combined Effects of Temperature and Carbon Dioxide on Potential Crop ET and Yields.

A simplistic assessment of combined effects of temperature and CO₂ changes on ET and yield can be made by making assumptions about changes in atmospheric conditions. It is important to recognize that atmospheric forcings are in varying degrees dependent on each other. For example, crop yield should tend to increase with increasing CO₂ and R_s. However, R_s decreases with increasing CO₂ because CO₂ is correlated with increasing temperature which increases atmospheric humidity which decreases R_s. Thus, the simulative effects of CO₂ on yield can be reduced by accompanying decreases in R_s. Therefore, a simple assessment like the one presented here neglects many of the complexities of plant – atmospheric interactions. The reader may ask why present one? The answer is that it's simple and when compared to more complete assessments it can reveal the importance of factors not included.

Reclamation (2011) estimated median temperature changes for each of its 8 major basins for the early, mid and late 21st century step change periods. Using these estimates, a reasonable consensus estimate for temperature change during the period from early to mid to late 21st century is approximately +2 °C. The U.S. Climate Change Science Program's Science Assessment Product 4.2 report (2008) estimated that increasing CO₂ to 700 ppm would likely increase global average surface temperature by between +1.7 and +4.4 °C by 2100. Thus a

Plant Physiological Responses to Atmospheric Forcings

reasonable assumption for a CO₂ concentration corresponding to a +2 °C change in temperature is about 660 ppm. This value is also convenient because considerable research has focused on this value and established that stomatal response remains linear for CO₂ increases up to this value. For this simplistic assessment, only the effects of temperature and CO₂ on ET are evaluated.

In order to estimate temperature effects on ET, average growing season crop coefficients were estimated using crop development periods and corresponding crop coefficients presented in FAO Irrigation and Drainage Paper 56 (Allen et al., 1998). These annual average K_c values for the major crops considered here were corn (0.83), cotton (0.65), rice (1.05), tomato (1.09), and wheat (0.76). These growing season averaged crop coefficients were then used to compute temperature change effects on ET based on the reference crop ET change per °C presented in Table 2.3.1 above. For the simplified assessment, it was also assumed that the 10% increase in CO₂ assimilation observed in both C3 and C4 (Bloom, 2010) crops would be reflected in a corresponding increase in LAI (see Table 2.3.1 above). The results are presented in Table 2.5.1 below.

Table 2.5.1. Simplified Assessment of Combined Temperature and CO₂ Changes on Major Agricultural Crops

Crop	Yield Change (%)			ET Changes (%)			
	Temp (+2°C)	CO ₂ (660 ppm)	Combined ¹ Effects	Temp (+2°C)	LAI (660 ppm)	Stomatal Response (660 ppm)	Combined ¹ Effects
Corn	-6.6	4	-2.6	5.7	1.6	-30 ³	-22.7
Cotton	-9.6	44	34.4	4.5	1.6	-25	-18.9
Rice	-20	30	10	7.2	1.6	-25	-16.2
Tomato	-21	32 ²	11	7.5	1.6	-25	-15.9
Wheat	-10.8	31	20.2	4.5	1.6	-25	-18.9

Footnotes:

1. Assumes that temperature and CO₂ effects are additive.
2. Assumes average yield change for C3 plants.
3. Assumes that corn responds similarly to the C4 crops reported by Bloom (2010) in Figure 5.15.

As can be observed in Table 2.5.1 above, the yield changes are variable ranging from slight decreases to significant increases depending on plant sensitivities. In contrast, ET declines are consistently greater than 15% due the significant increase in CO₂ to 660 ppm and its potentially significant effects on stomatal conductance at this elevated concentration. However, it must be emphasized that these effects do not consider many other factors which also have the potential to exert significant impacts either up or down on ET and yield.

3. Modeling Crop – Atmosphere Relationships

This section provides discussions of various modeling approaches, a description of some of the most commonly used crop models and sources of crop modeling data.

3.1 Overview of Modeling Approaches

Like other types of modeling, crop models range from simple to complex. The simplest are often single purpose models using statistical methods (e.g. regression) to estimate a particular output (e.g. yield) for a specific crop (e.g. corn) using a limited number of variables (e.g. temperature, precipitation, fertilizer application rates etc.). However, for climate related studies, such models have limitations because the included regression variables (e.g. temperature and precipitation) are likely to be correlated with non-stationary climate changes (e.g. CO₂, solar radiation etc.) which were not explicitly represented in model development. Furthermore, transferability to areas outside the region where the input variables (e.g. soil types, water table depth, etc.) have similar characteristics is another problem requiring modifications. However, simple models often have advantages in terms of the level of effort necessary to obtain data for inputs, develop the model and interpret the results. Consequently, these models can provide important information especially for initial assessments at the local to regional scales.

As the objectives of the crop modeling become more multi-purpose, more comprehensive and longer term, modeling approaches that explicitly account for multiple factors are desirable. Typically, these ecophysiological models include to varying degrees representations of meteorological conditions, biogeochemical processes occurring in various plant organs, soil-plant-water interactions and management practices with explicit temporal scales ranging from minutes to days and spatial scales ranging individual plants (m²) to fields (~100 ha). Regional and even global scale crop simulations using these models are typically performed by extrapolation of smaller scale results based on externally developed land use data.

These models are often applied to better understand the effects of a wide range of external factors such as climate, soil conditions and management actions for a variety of applications including agricultural productivity, soil and water conservation, surface and groundwater quantity and quality and ecosystem sustainability and biodiversity. In general, these models represent physical and biological processes deterministically but empirical relationships are also used when scientific knowledge and/or parameterization data are lacking or computational efficiency is necessary to accomplish study objectives. Although these models overcome various limitations of the simpler models, it must be recognized that the data requirements, expertise needed and level of effort to develop and apply them is correspondingly greater.

In ecophysiological models, plant responses to climate are typically simulated by model components that represent to varying extents plant phenology; photosynthesis and respiration; biomass accumulation, partitioning and organ growth; water balance; N-uptake and translocation and other factors (Tubiello and Ewert, 2002). Phenology is generally simulated as a function of accumulated daily temperature and day length. Photosynthetic response to light is often

computed using exponential or rectangular hyperbolic functions along with various methods to determine how much of the incident solar radiation is intercepted by the canopy. Some crop models use more detailed biochemical equations. Simpler models calculate net biomass production by multiplying intercepted light by the radiation use efficiency (RUE) which is usually assumed to be constant throughout the growth period but may change as a function of CO₂ and VPD. In some models, biomass production may also be limited by a transpiration use efficiency (TUE) to account for the influence of low relative humidity. In models that compute maintenance and growth respiration, CO₂ may affect photosynthesis and respiration rates indirectly through changes in growth rates.

The modeling of climate effects on crop transpiration has been simulated using several different approaches. In some simpler models (Richie, 1972), actual crop transpiration is computed based on the minimum of potential evapotranspiration (PET), which may be computed by a variety of methods, and root water uptake which is computed as a function of soil water content and the root abundance. In such models, the effects of elevated CO₂ may be simulated by reducing the stomatal conductance which reduces the PET rate. However, stomatal closure has been observed to elevate leaf temperature which increases water vapor diffusion rate. In simpler models, this effect may be empirically simulated by increasing air temperature which is generally assumed to equal leaf temperature. In more complex models, the simulation of photosynthetic carbon uptake is linked with calculations of stomatal conductance. In these models, the algorithms that optimize carbon fixation and transpiration reduce stomatal conductance under water stress conditions which reduces the diffusion of CO₂ into the leaf. Increasing the atmospheric CO₂ concentration has a similar effect on stomatal conductance. In more complex models, reduced stomatal conductance also directly affects leaf temperature and associated phenological stage development rates. In some models, the effects of elevated CO₂ on increased optimum photosynthetic temperature can be simulated. However, comparisons between simple and more complex models did not show significant differences due to this effect (Tubiello and Ewert, 2002).

Biomass partitioning among roots, stems, leaves, and grain or fruit is simulated in simpler models by using constant allocation fractions that may change with crop phenological stages. More complex models dynamically allocate carbon among organ groups. In these models, elevated CO₂ may dynamically modify partitioning and biomass accumulation through feedbacks between photosynthesis and organ growth known as source-sink relations. In simpler models, harvest yield is computed from final above-ground biomass using a harvest yield index coefficient that may also depend on accumulated water and heat stress. In more complex models, harvest yield is based on the dynamic feedbacks used in computing grain or fruit growth.

Other important factors that can affect crop responses to climate changes include air pollutants especially ozone, soil quality, weeds, pests and diseases. Ozone effects the assimilation of CO₂ by reducing stomatal conductance and/or decreasing biochemical activity due to cell damage (Tubiello and Ewert, 2002). Some or all of these effects are simulated to varying extents in both simple and complex models.

White et al. (2011) described three general modeling approaches that have been implemented in crop models to simulate the effects of climate changes crop water use and yields.

Plant Physiological Responses to Atmospheric Forcings

1. Models that use RUE and/or TUE with various adjustments depending on the model to account for effects of CO₂, temperature, water, nutrients and other environmental or physiological factors affecting daily net productivity.
2. Models that simulate the processes of photosynthesis and respiration at the leaf-level, scaled to canopy level considering losses through respiration and senescence. Plant temperature affects multiple processes and is either assumed equal to air temperature or obtained from simple submodels. CO₂ effects photosynthesis and stomatal conductance. Depending on the model, other environmental and physiological factors affecting growth and yield such as soil nutrients and water availability and management practices are frequently included.
3. Models that explicitly simulate the physiological effect of elevated CO₂ on reduced stomatal conductance and increased in canopy temperature. Processes of photosynthesis and respiration are simulated in ways similar to the second class of models. Other environmental and physiological factors affecting growth and yield are also included.

Typically, these models include sub-modules to represent the effects of meteorology, hydrology, plant physiology and management factors. Brief descriptions of the major data requirements and processes included in these models are provided below. Additional, model specific information is provided for some of the most commonly used models in crop studies is provided in the following section.

Meteorology requirements typically include temperature, precipitation, solar radiation, humidity and wind speed at daily to monthly time scales. Weather data requirements for computing ET by the PM method are greater than for other methods such as Priestly-Taylor, Hargreaves-Samani, Blaney-Criddle and others. Because many weather stations do not collect the required solar radiation, humidity and wind speed data, some models employ estimation procedures that provide the needed weather inputs from temperature, precipitation, elevation, and latitude. For ecophysiological studies, atmospheric CO₂ concentrations are also typically required.

Hydrology modules typically provide the means to represent interactions between soil-plant-climate factors. Input data requirements include soil characteristics affecting soil evaporation (E_s), erosion, surface runoff, soil infiltration, redistribution of soil moisture within the soil profile, actual crop transpiration, and deep percolation from the root zone. Some models have the ability to simulate shallow water table effects on ET. For models that include plant - soil nutrient interactions, soil organic matter, nitrogen and phosphorus mineralization, speciation and volatilization, specific parameters representing relationships between soil concentrations and plant requirements during various life cycle stages are required. Models that include capabilities to simulate nutrients, pesticides, herbicides and bacteria require various types of soil and constituent transport parameters.

Plant modules typically include processes that represent plant growth, biomass production and yield. Plant growth is commonly simulated based on plant specific life cycle stage dependent responses to temperature, radiation, humidity, photoperiod, plant available soil water and nutrients and CO₂. Some models directly simulate the effects of photosynthesis and respiration on carbohydrate and protein contents within various plant organs. In these models, yield is computed based on the availability of these substrates during the specific growth stages and may

include re-translocation of substrates and nutrients between plant organs in response to environmental stresses. In other models, crop yields are computed as a function of a temperature based harvest index. Plant growth is usually partitioned into above and below biomass based on plant specific characteristics. In some models, the vertical distribution of roots includes the effects of layer specific soil water content during the growing season.

Management modules generally include capabilities to represent field operations affecting water use, crop yields, soil erosion, runoff, accumulation and transport of sediment, nutrients, herbicides and pesticides in surface and ground water. Typical management activities include crop specific dates for planting single, multi-crops and crop rotations; tillage; fertilization, herbicide and pesticide applications; plant residue management and irrigation scheduling. Most of these models allow both user defined and automated scheduling of crop management practices based on dynamic temperature and moisture conditions.

3.2 Description of Selected Crop Models

Ecophysiological models have been applied to study the effects of climate conditions on agroecosystems for several decades. Using explicit search and selection criteria to identify climate change crop studies, White et al. (2011) identified 221 journal publications that addressed simulation methods, impacts and adaptations relative to climate change. Of these reviewed studies, their primary focus was impacts (66%), methods (19%) and adaptation (15%). Of the 35 crops explicitly identified, the most studied crops included wheat (35%), maize (25%), rice (11%), soybean (7%) and potato (3%). Taken together, these crops represented 80% of the studies reviewed. Tubiello and Ewert (2002) reported similar results. About 25% of the studies (55) were focused on the United States.

White et al. (2011) indicated that more than 70 models had been applied to study climate change effects on agroecosystems in the 221 studies reviewed. In these studies, the 5 most frequently used models were referenced in more than 50% of the studies. In the order of their prevalence, the top 5 models included CERES (29%), EPIC (11%), APSIM (6%), CropSyst (4%) and DSSAT - CSM+CropGro (4%). In a survey of the crop modeling community, Rivington and Koo (2010) obtained similar results relative to the most commonly used models. Brief descriptions of the most commonly used models are provided below:

1. CERES (Crop Environment Resource Synthesis) models have been developed for a variety of crops including wheat, maize, rice, sorghum, millet, and barley. CERES models were among the earliest crop models developed which probably influenced the prevalence of CERES references in the White's literature review. These ecophysiological models are deterministic but not overly mechanistic. Their primary focus is on how cultivar properties, planting density, climate (including CO₂), soil water, and nitrogen affect crop growth, development, and yield. Their primary purpose is to examine how alternative management practices (fertilization and irrigation) affect yield at the farm and regional scales. They have also been used to study nitrogen leaching and the effects of climate change.

CERES models account for a variety of crop development, growth and yield processes in the following:

Plant Physiological Responses to Atmospheric Forcings

- Phenological development stages
- Growth of leaves, stems, and roots
- Biomass accumulation and partitioning in plant organs
- Soil water balance and crop water use
- Transformations of nitrogen in the soil, uptake by roots, and partitioning between plant organs

Crop biomass accumulation is calculated independently of the plant development. Biomass production is simulated as a function of radiation use efficiency, leaf area index with reductions due to temperature and moisture stresses. Cultivar phenological development stages are computed based primarily on accumulated degree-days. Photosynthesis determines the growth rate of leaves, stems and roots. The root zone soil water content is computed based on soil characteristics affecting runoff, infiltration and drainage. Mineral nitrogen dynamics in the soil profile are also simulated.

Data inputs include:

- Climate variables such as latitude, daily solar radiation, temperature and precipitation and atmospheric CO₂ concentration and
- Management variables such as sowing date, plant density, row spacing, sowing depth, irrigation and fertilizer schedules and
- Crop genetic constants, phenology and growth parameters and
- Soil parameters such as albedo, soil texture and water holding properties and profile characteristics

Many of the original CERES crop models (e.g. CERES-Wheat) have been updated for use in the DSSAT-CSM model described below.

Key references relevant to the CERES models include Jones and Kinery (1986) and Mearns et al. (1999). Additional online information for the CERES models is available at <http://epicapex.brc.tamus.edu/>

2. EPIC (Environmental Policy Integrated Climate) was originally developed during the 1980's to simulate effects of soil erosion on agricultural productivity in the United States. It is a deterministic, field scale, daily time step model designed to simulate drainage areas that are characterized by homogeneous weather, soil characteristics, crops, and management practices including tillage effect on surface residue, soil bulk density and nutrients as well as fertilizer and irrigation effects on crop yield.

EPIC's crop growth model uses approaches that are similar to the CERES models. One significant difference is a simpler representation of phenological stages in crop development. The biophysical processes represented in the model include:

- Solar radiation, saturation vapor pressure, canopy and soil albedo effects on potential evaporation in default method; other PET methods (5) available
- Plant evaporation computed as linear function of potential evaporation and Leaf Area Index (LAI) ; two stage soil evaporation based on soil characteristics

- Biomass production function of photosynthetically active radiation (PAR) and crop specific radiation use efficiency (RUE) with adjustment for water, temperature, nitrogen, phosphorous stresses.
- Daily adjustment of potential biomass into above ground and root growth that reflect water, temperature and nutrient stresses (nitrogen and phosphorous)
- Canopy development and senescence computed as function of biomass and crop specific maximum LAI
- Influence of atmospheric CO₂ on biomass production and canopy resistance in the Penman Monteith ET equation can be simulated
- Crop yields are computed by accumulating growing season weighted daily increments of stress adjusted biomass up to a maximum crop specific yield

EPIC requires more than 400 input data items including about three hundred climatic characteristics and 50 crop parameters (Adejuwon, 2005). However, many of these inputs can be obtained or estimated from existing EPIC databases.

Data inputs include:

- Climate variables including precipitation, solar radiation, relative humidity, minimum and maximum temperature, wind speed and atmospheric CO₂ concentration.
- Management variables such as details of farm operations including scheduling of tillage, type and amounts of fertilizer and pesticides applied, irrigation, density of planting, among others.
- Crop parameters such as radiation use efficiency, crop height, canopy development and senescence, basal and optimal growth temperatures, optimum crop yield, root - shoot biomass production ratio, maximum root depth, maximum LAI.
- Soil parameters such as bulk density, water-holding capacity, wilting point, hydraulic properties and profile characteristics.

The APEX (Agricultural Policy / Environmental eXtender) model enhances the EPIC model capabilities to simulate entire farms and small watersheds. APEX has additional algorithms that route water, sediment, nutrients, and pesticides from farms through watersheds and channels. It also has groundwater and reservoir simulation capabilities. New versions of these models (WinEPIC and WinAPEX) have also been developed recently.

Key references relevant to the EPIC model include Williams et al. (1989) and Williams et al. (2008) and Stockle (1992). Additional online information for EPIC and APEX models is available at <http://epicapex.brc.tamus.edu/>

3. APSIM (Agricultural Production Systems Simulator) is an ecophysiological model designed to simulate growth, development and yield of crops, pastures and forests in relation to climate, plant genotype, soil characteristics and management practices affecting long-term productivity such as loss of soil organic matter, structural degradation, acidification and erosion. APSIM is a deterministic, multi-crop area based, daily time step model with existing capabilities to simulate more than 20 crops including wheat, maize, rice, soybean, potato, sorghum, millet, various grain legumes, safflower, sunflower, cotton, sugarcane, lucerne (alfalfa) and others.

Plant Physiological Responses to Atmospheric Forcings

The APSIM uses a generic crop model template (GCROP) that consists of component sub-modules for crop parameters (CPF); basic plant physiological process (CPL), crop components such as phenology and biomass (GMS) and a standard interface (SCI) to manage interactions with other APSIM modules (e.g. soils, meteorology). The biophysical processes simulated in GCROP include:

- Transpiration – calculated as minimum of water supply (based on soil water content and root distribution) and water demand (based on radiation energy for biomass production)
- Phenology – crop growth stages computed based on accumulated thermal time (degree days) and photoperiod. Development may be reduced by water or nitrogen stress
- Biomass – calculated as minimum of either energy supply (based on intercepted radiation and RUE) or crop growth stage dependent water supply (based on transpiration efficiency and VPD) effects on daily biomass production; computes Harvest Index for yield; and re-translocates carbon between plant parts
- Leaf Area Development – calculated from thermal time effects on daily increase in number of leaves and leaf size; maybe limited by carbon and water supply and senescence
- Senescence – computed as function of age, light competition, water and temperature stresses
- Nitrogen – simulates demand, uptake, fixation and re-translocation in plant

The MICROMET module (Snow and Huth, 2004) was developed to improve capabilities to compute ET using the Penman Monteith equation in multilayer and intermingled canopies such as occur in forested, chaparral and inter-cropped field areas.

APSIM data inputs are dependent on the particular user selected modules included in the simulation. A brief description of data inputs employed by some of the modules relevant to this study is provided below:

- Plant module inputs include basic information about crop canopy and root characteristics such as RUE, canopy light extinction, leaf senescence, max crop height and rooting depth, development stages and associated degree days, plant organ fractionation coefficients, soil water extraction limits, specific root length and others
- Soil module includes inputs for simulating soil water, nitrogen, carbon, phosphorus and temperature; soil management practices such as fertilization, irrigation and erosion.
 - Soil water processes can be simulated by either a cascading bucket approach (SoilWat) similar to the EPIC and CERES models or by a numerical solution of unsaturated flow (SWIM2). Hydrologic processes simulated include runoff, drainage, soil and potential evaporation, unsaturated flow, solute flux and flow
- Meteorology module includes station name, latitude and temperature, precipitation and radiation data at daily, monthly or annual time scales
- Manager module allows user to control APSIM simulations.

Key references relevant to the APSIM model include Wang et al. (2002) and Keating et al. (2003); Additional online information is available from the link <http://www.apsim.info/Wiki/>

4. CropSyst (Cropping Systems Simulation Model) is an ecophysical model developed for the purpose of simulating the effects of the climate, soils, and management practices including crop rotations, cultivar selection, irrigation, nitrogen fertilization, soil and irrigation water salinity, tillage operations, and crop residue on agroecosystems. It is a multi-year, multi-crop, daily time step that simulates a single biophysically homogeneous area managed in a uniform manner. Functionality for simulating multiple land areas is available through ArcGIS.

The CropSyst modules provide algorithms that compute water and nitrogen budgets, phenology, biomass production including the effects of CO₂, canopy development, root growth, crop yield and residue. The methods used to simulate these biophysical processes are briefly described below:

- Water budget – components include precipitation, irrigation, runoff, infiltration, soil evaporation, plant transpiration, redistribution, and deep percolation
 - Redistribution can be simulated by a simple cascading approach similar to APSIM, EPIC and CERES models or a numerical solution of the Richard's equation similar to APSIM
 - Potential crop ET is computed using either a Penman-Monteith or Priestly Taylor based reference crop and crop specific coefficients; actual crop ET is computed based on PET and plant available soil water
- Nitrogen budget – simulated N processes include fixation, mineralization, nitrification, and denitrification; crop N uptake is determined as the minimum of crop nitrogen demand (growth requirements plus its deficiency demand difference between the crop maximum and actual nitrogen concentration) and potential nitrogen uptake
- Phenology - daily accumulation of thermal time (daily average temperature above a base temperature and below a cutoff temperature) during specific growth stages; vernalization and photoperiod requirements need to be considered
- Biomass – uses minimum value based on biomass-temperature-VPD and biomass-PAR-RUE relationships; nitrogen and water stresses may reduce biomass
- Canopy development – LAI is computed a function of biomass accumulated during crop growth stages including senescence
- Root growth - root depth increases to a maximum depth as canopy develops; root density is assumed zero at the current soil depth and increases linearly to a maximum density at a depth near the soil surface
- Yield – computed from total daily accumulated biomass at physiological maturity and stress adjusted Harvest Index (harvestable yield /aboveground biomass)

CropSyst inputs depend on which modules are included in the simulation. Brief descriptions of module inputs are provided below:

- Soil module - layer thickness and texture must be specified; bulk density, volumetric water content and unsaturated water content and water potential relationship parameters may be specified or computed by pedo-transfer functions based on soil texture
- Plant module - Phenology (basal and optimum temperatures, thermal time requirements to reach specific growth stages); Morphology (Maximum LAI, root depth, specific leaf area, leaf area duration, root characteristics and others); Biomass (growth transpiration

biomass coefficient, radiation-use efficiency, nitrogen demand and root uptake parameters water, N and salinity and CO₂ sensitivity parameters); Yield harvest index; Residue decomposition and shading parameters

- Meteorology module - requires temperature, precipitation and radiation for PT method; plus wind, humidity for PM method; weather generation capabilities are included in CropSyst
- Management module – includes scheduled and automatic management events such irrigation application date, amount, and salinity concentration; nitrogen fertilization application date, amount, source, and application mode, tillage operations, and residue management; management events can be scheduled using actual date, relative date (relative to year of planting or synchronized with phenological events).

Key references relevant to the CropSyst model include Stockle et al. (1992) and Stockle et al. (2003); Additional information is available at http://bioearth.wsu.edu/cropsyst_model.html

5. DSSAT-CSM (Decision Support System for Agrotechnology Transfer) was designed to integrate knowledge about soil, climate, crops and management to support better decisions about transferring agricultural production technologies from one location to others. It is a deterministic ecophysiological model that simulates the effects of soil, water and management on the daily growth, development and yield of multiple crops grown in a uniform area over multiple years. The Cropping System Model (CSM) is used to simulate crops using a single soil and a single weather module. As of Version 4.5, over 28 crops are supported by DSSAT-CSM.

DSSAT-CSM simulates various biophysical processes affecting crop growth, development and yield. Methods used include the following:

- Water budget – methods include runoff using SCS approach, infiltration and redistribution using the cascading bucket approach, soil water content including upward unsaturated flow; two stage soil evaporation with actual plant transpiration computed as minimum of potential evaporation and root water uptake based on soil water content and root density, PET can be computed by PM, PT or Richie's method (see APSIM model)
- Carbon and Nitrogen budget – decomposition of soil organic matter computed as function of computed soil temperature and water content; accounts for plant senescence (above ground and subsurface) and transport by soil water
- Phenology – life cycle growth stages computed as function of temperature, photoperiod and sensitivity to N and P availability
- Plant growth – crop photosynthesis computed as function of RUE adjusted for light interception, plant density, CO₂ concentration and N, temperature and water stresses or hourly hedgerow light interception-leaf-level based on canopy development and orientation, CO₂ and temperature; accounts for growth stage dependent plant organ assimilate needs and respiration effects; root growth based on growth stage dependent carbohydrate requirements
- Yield – computed based on plant growth and stresses during growth period

DSSAT-CSM inputs depend on which methods and sub-modules are included in the simulation. Brief descriptions of some of the general types of module inputs are provided below:

- Land Use Module - includes site latitude and longitude; average annual temperature and amplitude, slope and aspect, and others
- Weather - daily solar radiation, maximum and minimum temperature, precipitation and other simulation specific characteristics (e.g. humidity and wind for PM ET)
- Soil - layer thicknesses, upper and lower soil water content limits, bulk density, organic carbon, pH, rooting and drainage factors
- Crop - photosynthesis and respiration coefficients associated with growth stages; plant organ composition parameters; carbon and nitrogen mining parameters; plant growth, senescence and dry matter partitioning parameters; phenology, crop height and width parameters

Key references relevant to the DSSAT-CSM model include Jones et al. (1989a) and Jones et al. (2003); Additional information is available at <http://dssat.net/about>

While not included in the White (2011) study, the WEAP-PGM model is described in this section because it was the model selected for use in this study. Furthermore, it is a model in which Reclamation has employed in several studies of the effects on climate change on California's Central Valley (Reclamation, 2016).

6. WEAP-PGM (Water Evaluation and Planning system – Plant Growth Model)

The Water Evaluation and Planning System (WEAP) is a decision support system for integrated water resources management and policy analysis. WEAP was created in 1988 and continues to be developed and supported by the Stockholm Environment Institute (SEI), a non-profit research institute. The Plant Growth Method (PGM) was added to WEAP in 2015. The result of previous collaborative effort between Reclamation and SEI, PGM simulates daily ET, plant growth, yield as functions of temperature, solar radiation, atmospheric humidity, and wind speed and CO₂, heat unit accumulation, and temperature and water stress. The PGM algorithms are based on the SWAT and EPIC models described above. WEAP-PGM can simulate both the hydrology and management of complex, multi-priority water management systems. Additionally, WEAP-PGM has been calibrated to simulate many types of crops grown in Central Valley of California.

The PGM simulates the infiltration and redistribution of soil moisture differently than SWAT or APEX. Infiltration is simulated using the Phillips equation to account for the effects on unsaturated flow in a multi-layer soil profile. PGM also has the capability to account for the effects of a shallow ground water table on root zone soil moisture.

In order to simulate the effects of climate on crop water use, biomass and yield, PGM algorithms simulate the following processes:

- Effects of temperature on soil evaporation and plant transpiration
- CO₂ effects on radiation use efficiency (RUE).
- CO₂ effects on crop leaf area (LAI).
- CO₂ effects on crop transpiration.
- VPD effects on crop transpiration.
- VPD effects on radiation use efficiency (RUE).
- Plant growth and yield driven by accumulation of daily heat units.

- Effects of temperature and water stress on crop biomass and yield.

WEAP-PGM requires both crop parameters, soil properties and climate variables. Some crop parameters may be estimated from existing WEAP-PGM crop database. However, it is important to recognize that calibration of the crop parameters is typically required.

Data inputs include:

- Climate variables include daily precipitation, maximum and minimum temperature, incoming short wave length solar radiation, relative humidity or dew point temperature, wind speed and atmospheric CO₂ concentration.
- Crop parameters including radiation use efficiency, crop height, canopy development and senescence, basal and optimal growth temperatures, growing season heat units, optimum crop yield, root - shoot biomass production ratio, maximum root depth, maximum LAI as well as parameters describing the effects of VPD and CO₂ on RUE and LAI.
- Soil parameters such as field capacity, wilting point, saturated and unsaturated soil hydraulic properties and profile characteristics.

Key references relevant to the WEAP-PGM model include Reclamation (2016). A detailed description of the WEAP algorithms is presented in Appendix A of this report. Additional information is available at <https://www.weap21.org/index.asp?action=200>.

3.3 Crop Modeling Data

Modeling the effects of climate change on crop ET and yield requires a variety of data types to specify the fundamental interactions between crops and the agroecosystems in which they are grown. The scientific literature provides an extensive source of information about crop modeling and parameters for use in models. In addition, many of the most frequently used models including EPIC, APSIM, CropSyst, DSSAT-CSM as well as WEAP-PGM provide databases with crop parameters, soil properties, and weather information that are available from their websites.

Other sources of agricultural soil and a climate data are also available online. The USDA National Agricultural Statistics Service (NASS) provides downloadable GIS and spreadsheet data on crop types and acreages by county for the entire continental United States. This remotely sensed data is available on annual basis from the late 1990's up to the year previous to the current calendar year. This cropland data information can be obtained from <http://nassgeodata.gmu.edu/CropScape/>. In many instances, crop models require soil data as an input. In addition to data that may be provided with various models, the USDA Natural Resources and Conservation Service (NRCS) provides downloadable geospatial soil survey data that can be used to develop soil characteristics necessary for crop modeling. A link to this data is <https://sdmdataaccess.nrcs.usda.gov/>. Crop models also provide capabilities to either directly specify or develop the weather data necessary for running the model. The types, frequencies and time periods of these data requirements are generally dependent on the simulations to be performed. Most models provide users with the ability to generate daily or even hourly data from monthly averages using user specified site and climate characteristics. Reclamation and others

have developed an archive of bias corrected and spatially downscaled climate (temperature and precipitation) and hydrology (unimpaired flows) projections for the period from 1950-2099 at the monthly and daily time scales based on the IPCC AR4 and AR5 Coupled Model Intercomparison Project (CMIP3 and CIMIP5) GCM simulations. For the continental U.S., bias-corrected, spatially downscaled (BCSD) projections from these studies may be downloaded online from http://gdo-dcp.ucllnl.org/downscaled_cmip3_projections/ . Carbon dioxide data associated with the emissions scenarios and representative concentration pathways may be downloaded from <https://tntcat.iiasa.ac.at/RcpDb/dsd?Action=htmlpage&page=welcome>

4. Climate – Crop Modeling Studies

To address the potential effects of climate on agriculture, crop models have been employed for the past several decades. Many studies have tended to focus on the effects of particular aspects of climate (e.g. temperature) without simultaneously considering the effects of other climatic influences (e.g. humidity). Additional difficulties occur because readily available climate data typically lack the meteorological variables needed for modeling key biophysical processes (e.g. solar radiation, wind, humidity and CO₂). Furthermore, coupling plant growth and yield simulations with crop water use may not be considered or only treated as a simple sensitivity analysis (e.g. effects of CO₂). Finally, due to the computationally intensive nature of crop modeling, climate data are frequently limited to only a few scenarios that may neither capture the central tendency nor a representative range of climate uncertainties (e.g. warmer-drier, warmer-wetter) relative to the central tendency of a large ensemble of climate scenarios.

In the following subsections, the studies described were selected based on the criteria that they combined meteorological conditions based on atmospheric processes with crop model simulations based on dynamic biophysical processes affecting evapotranspiration, growth, and yield including the effects of CO₂. These criteria are important because meteorological variables such as temperature (T), solar radiation (Rs), atmospheric humidity (ea) and CO₂ are not independent. Therefore, meaningful studies of plant - atmospheric interactions require the use climate models to provide realistic atmospheric conditions. Many of these studies involved assessment of the potential climate changes on crop water use and yield. In addition, only studies reporting results involving irrigated crops grown in Reclamation service areas are described below.

4.1 Crop Evapotranspiration – Climate Interactions

In an early study of the sensitivity of crop ET (ET_c) to potential climate changes, Rosenberg et al. (1990) calibrated the Penman Monteith (PM) equation to observations of wheat growing at Mead, NB and tall grass prairie near Manhattan, KS during their summer growth periods. The order of sensitivity of ET_c to changes in climate variables was temperature (T,+), greater than net radiation (R_n,+) greater than absolute humidity (ea,-) greater than canopy resistance (rs,-) greater than leaf area index (LAI,+) and greater than wind speed (U,+), where inputs followed by (+) indicate direct and inverse (-) proportionally respectively. The authors also examined various combinations of changes in these variables on ET_c. Of these combinations, the simulations using values of T +3 °C, R_n +10%, ea +10%, rs +40% (~660 ppm CO₂) and LAI +15% seem to be potentially the most representative of projected changes in conditions in the latter portion of the 21st century [Allen et al. 1991, Kimball (2007), Reclamation (2011)]. For these changes in input variables, the summer wheat ET_c was estimated to increase by +13% and the tall grass prairie by +10%. It is important to note that these changes are estimated for a summer period at the northern hemisphere solar radiation maximum.

Kimball (2007) performed a similar type of sensitivity analysis for alfalfa growing at Maricopa, AZ. For these analyses, a PM model was calibrated to daily ET data using hourly data from nearby AZMET station during the year 1987. The calibrated PM model used to simulate temperature changes ranging from +1.2 to +5.8 °C based on values reported in the IPCC 3rd

Assessment. The ET sensitivity analysis also examined the effects of increasing stomatal resistance by 40% and LAI by 10% such as might be obtained for a crop like alfalfa at an elevated CO₂ concentration around 700 ppm. For annual temperature increases in the range of +2-3.5 °C such as estimated by the end of the 21st century in the western United States (Reclamation, 2011) and making the reasonable assumption that absolute humidity increases (Allen et al, 1991) such that relative humidity remains approximately constant, alfalfa ET during the peak growing season would increase by between 0.6% to 2.9%. Under the same assumptions, changes in annual alfalfa ET would range from -0.3% to +2.7%.

In another early study of climate change effects on crop water requirements in central and southern Great Plains (Nebraska, Kansas, Oklahoma and Texas), Allen et al (1991), employed the Penman Monteith method and unadjusted projections of changes in GCM simulated mean monthly surface air temperature, precipitation, solar radiation, humidity and wind resulting from an assumed doubling of CO₂ from 330 to 660 ppm. The GCM models used for the study were the Geophysical Fluid Dynamics Laboratory (GFDL) (Manabe and Wetherald, 1987) and the Goddard Institute of Space Studies (GISS) (Hansen et al., 1988). Changes in ET and irrigation water requirements (IR) under the doubled CO₂ forcing relative to the historical period from 1951-1980 were examined for alfalfa, corn and winter wheat crops. A delta change ratio method was used to create daily climate inputs based on the forced mean monthly GCM results and daily historical period records from 17 non-agricultural weather stations. Adjustments to account for differences in temperature measurements between agricultural and non-agricultural areas were applied. No adjustments in wind speed or humidity measurements were made. These measurement discrepancies would have a tendency to result in overestimates of ET. In general, both GCM models projected increases in air temperatures during the growing season on the order of +3-5 °C. Although considerable monthly variability was projected by both models, annual precipitation changes over the region averaged about +3-5%. Considerable variation in annual wind speeds ranging -26% to +26% were reported. Humidity changes were projected to range from +32-36% and solar radiation changes during growing season months increased in a range from +1-7%.

The effects of projected temperature and solar radiation changes on the crop growth stages were used to provide estimates of changes in planting dates, acceleration of growth stages and length of the growth period. Interestingly, the authors noted that earlier and/or later growth could result in crops growing during spring and fall seasons when solar radiation was reduced thereby offsetting the effects of increased growing season length. The effects of doubled CO₂ were evaluated by assuming increases in canopy resistances of 0% (no CO₂ effects), 20%, 40%, 60% and 80%. The analyses for corn and wheat also assumed that existing basal crop coefficients (K_{cb}) values could be used with projected alfalfa ET as the reference crop to compute the crop ET (ET_c). Soil evaporation was computed separately based on assumptions about types of irrigation systems and frequency of water applications.

For alfalfa, growing season length increased consistently throughout the region by approximately 40 days. Similarly, annual ET_c increased everywhere. With no CO₂ effects on canopy resistance, the models showed significant but consistent differences with the warmer GFDL model showing greater increases in ET_c (+40-60%) relative to the less warm GISS model (+30-40%). As canopy resistance was increased, a corresponding linear reduction in ET_c occurred. At a 40% increase in canopy resistance similar to what has been commonly observed in many agricultural crops at 660

ppm CO₂, the projected annual ET_c relative to no CO₂ effects was reduced by approximately 15% throughout the region. However, even at an 80% canopy resistance, alfalfa ET_c increased by approximately 5-10% relative to the historic period because of the longer growth period.

For wheat winter, the growth period length was reduced by between 36-48 days throughout the region. These reductions were attributed to later fall planting and earlier spring harvest. The growth period length reductions were accompanied by corresponding reductions in annual ET. With no CO₂ effects on canopy resistance, ET_c reductions ranged from -1% to -11%. At a 40% increase in canopy resistance, ET_c reductions ranged from -12% to -22% (approximately -15% relative to the no CO₂ effects simulations). At an 80% increase in canopy resistance, ET_c reductions ranged from -22% to -28%.

For corn, the growth period length ranged from a decrease of 80 days to an increase of 10 days. A strong latitudinal correlation was observed in the growth period length. Large decreases in the northern Great Plains were attributed to more rapid life cycle stage changes in the summer months eliminating the need for extended fall season development when reduced solar radiation and seasonal temperatures result in slower maturation. In contrast for the central and southern regions, growth period length increased slightly because reduced solar radiation during the early spring resulted in slower life cycle stage changes. These slight changes were more pronounced for the less warm GISS model. The simulated changes in annual ET_c also reflected the latitudinal trends exhibited by growth period length. With no CO₂ effects on canopy resistance, ET_c ranged from a 10% reduction in the northern plains to a 25% increase in the south. At a 40% increase in canopy resistance, ET_c ranged from -20% in the north to +10% in the south. At an 80% increase in canopy resistance, ET_c reductions ranged from -28% in the north to -2% in the south.

In summary, this study by Allen et al. (1991) demonstrates the importance of considering the integrated effects of multiple climatic factors not just temperature and precipitation on crop ET_c. Clearly, seasonal changes in other climate conditions such as solar radiation and humidity that varied with changes in planting and harvest dates exerted significant albeit potentially opposite influences on crop ET_c. Finally, it is important to note that the methods used in this study simulated changes in ET_c through empirical relationships between temperature (degree days) and solar radiation (photoperiod) on canopy development (LAI) without fully simulating crop growth. In the ecophysiological crop models described in the previous section, the effects in temperature, solar radiation, humidity and CO₂ on crop growth (biomass) would be explicitly simulated and could result in either increased or decreased leaf areas and stomatal conductances which in turn would affect ET_c. Furthermore, as discussed above, the effects of CO₂ were arbitrarily imposed without regard its relationships with other climate variables.

Izaurrealde et al. (2003) used the results from the HadCM2 global climate model to assess the impacts of climate changes on agricultural production and irrigation water supplies throughout the United States for 10 year periods centered on 2030 and 2095. Projected temperatures and precipitations from the GCM were used as inputs to the EPIC crop model. However, it was not clear which of the 5 methods available in EPIC was used for estimating reference ET_o. Furthermore, actual crop ET (ET_c) is affected by soil properties and irrigation management which were not described. The assessment was performed at the 4-digit Hydrologic Unit Area (HUA) and only the dominant vegetation within the HUA was simulated. Although the assessments were done for individual HUAs, the reported results were combined into 10

agricultural regions of which only 4 (Pacific, Mountain, Northern Plains and Southern Plains) are located in the western United States. Because latitudinal trends in climate within the Pacific and Mountain regions are significant, the averaged results presented in this study do not reflect these important geographic differences.

The HadCM2 model was chosen because it simulates 21st century temperatures (+2.8 °C) that are intermediate to results from several other GCM models (+1.7-5°C) used for by the National Assessment Synthesis Team (2001). However, it is important to note the HadCM2 model projects significantly wetter conditions in California, Nevada, Utah, Arizona, New Mexico and Texas than the median values of the 112 projections presented in Reclamation's Secure Water Act Report. For example, precipitation increases ranged from 1-21% in 2030 and 12-35% in 2095. In Reclamation's report some of these same areas had decreases in precipitation ranging from 10-15% or more.

In the study, the effects of climate change on ET_c were not explicitly presented. Instead, the effects of climate change on the irrigation requirements (IR) which accounts for effective precipitation were reported. For the climate sensitivity analyses, CO₂ was increased to 560 ppm corresponding to an approximately 30% increase in canopy resistance. For irrigated corn in the western region basins, reported IR changes in 2030 ranged from -16% in the Lower Colorado to +115% in California and from -25% in the Lower Colorado to +97% in California by 2095. For irrigated alfalfa in the western region basins, reported IR changes in 2030 ranged from -3% in the Lower Colorado to +52% in Missouri and from -11% in the Lower Colorado to +71% in California by 2095.

The study also provided assessments of the effects of climate change on basin water yields (essentially runoff) and irrigation requirements. In general, they concluded that elevated CO₂ will reduce watershed transpiration losses and result in increased water yields which combined with decreased crop transpiration will contribute to an improvement in water supply-demand imbalances. However, due to with the dependence of the results on a single GCM that projects consistently wetter conditions throughout the 21st century, their quantitative projections have considerable uncertainty.

Ficklin et al. (2009) performed an assessment of climate changes on water supplies and crop water use in the San Joaquin Valley, CA. For this assessment, the Soil Water Assessment Tool (SWAT) (Gassman et al, 2007) model was used. This model uses methods to simulate plant growth and ET_c that are similar to the EPIC model described in Section 3. For this study, the Penman Monteith method was used to simulate crop ET_c. Because SWAT simulates plant growth (biomass) and based on accumulated degree days, temperature exerts an additional influence on ET_c beyond what is included in the PM method. However, the 2005 version of SWAT used for this study only accounts for the effects of increased CO₂ on reduced stomatal conductance but not on increased canopy LAI. Furthermore, increased canopy temperatures that are related to stomatal closure in response to elevated CO₂ were not simulated. Consequently, the reported ET_c values can be viewed as representing lower values than might actually occur if these processes had been included in the simulations.

Of the total cropland in the study area, several major crop groupings were reported by California Department of Water Resources (2007) including fruit and nuts (38%), field crops (36%), truck

crops (17%) and grains (4%). Model parameters for these crops were obtained from the SWAT model database and used without additional calibration. Soil survey data from the SSURGO database (USDA) was also used to parameterize the model. Two temperature - emission scenarios (A1F1, + 6.4 °C & 970 ppm CO₂) and B1, +1.1 °C & 550 ppm CO₂) were selected to represent upper limits and lower limits of future climate changes. Weather generators were used to create 50 year future daily maximum and minimum temperatures, precipitation, solar radiation and humidity time series based on climate data measured at CIMIS agro-meteorology stations located in the study area.

For the lower limit B1 scenario, overall average crop ET_c ranged from -4.2% to -13.1% as precipitation change varied from +20% to -20% relative to the current period baseline. For the upper limit A1F1 scenario, overall crop average ET_c ranged from -35.7% to -39.7% as precipitation was changed from +20% to -20% relative to the current period baseline. If climate conditions similar to the Reclamation's median projected values of + 2.3 °C and a -8.6 % reduction in precipitation, linear interpolation of these results indicates -27.8% change in the overall crop average ET_c.

Reclamation has also performed several studies in which the effects of potential climate changes on crop ET, water demands and irrigation requirements have been assessed. These studies include Reclamation (2016, 2015, 2014 and 2013). All of these studies except Reclamation (2016) used the CIMIP Phase 3 (CIMIP-3) climate projections. The most geographically extensive assessment, Reclamation (2015) provided estimates of crop ET and irrigation water requirements (IWR) but did not include the effects of VPD and CO₂ on ET_c, biomass or yield. The Sacramento and San Joaquin Basins Study (Reclamation, 2016) was based on the more recent CIMIP-5 projections and employed WEAP-PGM to simulate the effects of potential climate changes including the effects of VPD and CO₂ on crop water demands and yield of crops grown in the Central Valley of California. The simulations were based on sub-regional planning areas with up to 22 different crop types grown in the Central Valley.

In this study, six dynamically changing climate scenarios and three dynamically changing socioeconomic scenarios were developed to characterize a range of potential future uncertainties using results from CIMIP Phase 5 projects for the climate scenarios and assumptions on changes in population and land use based on the California Water Plan to develop three socioeconomic scenarios referred to as Slow Growth (SG), Current Trends (CT) and Expansive Growth (EG). In each of the scenarios, irrigated land area was decreased in the order of EG greater than CT greater than SG. The assumptions and methodology used to develop these socioeconomic-climate scenarios are described in detail in Reclamation (2016).

Table 4.1.1 characterizes the temperature and precipitation for the Reference scenario (RF) and changes for five climate scenarios including Warm-Dry (WD), Hot-Dry (HD), Hot-Wet (HW), Warm-Wet (WW) and Central Tendency (CEN) during three time periods in three major hydrologic regions.

Table 4.1.1 Temperature and Precipitation Changes on the Central Valley Basins

Table 4.1.1a. Mean Annual **Temperature** (in °C) in the RF scenario and Climate Scenarios % Changes in the Sacramento River, San Joaquin River, and Tulare Lake Hydrologic Regions.

	Ensemble-Informed Scenarios					
	RF Average	WD	HD	HW	WW	CEN
Sacramento River Hydrologic Region						
2015-2039	12.6	0.6	1.3	1.3	0.6	1.0
2040-2069	12.3	1.3	2.7	2.9	1.3	2.0
2070-2099	12.6	1.7	4.0	4.3	1.7	2.8
San Joaquin River Hydrologic Region						
2015-2039	13.8	0.6	1.3	1.3	0.6	0.9
2040-2069	13.3	1.3	2.7	2.8	1.2	1.9
2070-2099	13.7	1.7	3.9	4.2	1.7	2.7
Tulare Lake Hydrologic Region						
2015-2039	14.8	0.5	1.3	1.3	0.6	0.9
2040-2069	14.4	1.3	2.6	2.7	1.2	1.9
2070-2099	14.7	1.7	3.9	4.1	1.7	2.7

Table 4.1.1b Annual **Precipitation** (in mm) in the RF scenario and Climate Scenarios % Changes in the Sacramento River, San Joaquin River, and Tulare Lake Hydrologic Regions.

	Climate Scenarios					
	RF Average	WD	HD	HW	WW	CEN
Sacramento Hydrologic Region						
2015-2039	843	-7.9	-7.5	8.0	9.7	0.1
2040-2069	925	-8.4	-8.9	15.0	13.9	2.1
2070-2099	946	-8.2	-8.3	19.4	16.8	3.9
San Joaquin Hydrologic Region						
2015-2039	646	-9.2	-8.9	10.0	9.4	-0.2
2040-2069	681	-11.4	-12.4	12.6	14.3	0.8
2070-2099	695	-10.9	-12.8	19.0	19.7	2.5
Tulare Hydrologic Region						
2015-2039	397	-11.4	-10.5	9.7	11.7	-0.3
2040-2069	406	-14.5	-14.2	12.3	14.5	-0.4
2070-2099	418	-12.4	-14.8	18.9	21.0	1.5

As shown in Table 4.1.1a, temperature steadily increases with time in all the scenarios. There is also a marked increase from north to south with the hottest temperatures occurring in the Tulare Hydrologic Region. In the hottest scenarios (HD & HD), the temperature increase reaches approximately 4 °C by the century's end in all the hydrologic regions. In the scenarios with the least warming (WD & WW), temperature increases by about 2 °C by the end of the century in all regions. The CEN scenario is intermediate between the warm and hot scenarios with approximately 2 °C of warming. In the case of precipitation, there is no steady change over time in the drier scenarios (WD & HD) but the declines generally decrease from north to south in a range from about -8% in the Sacramento Hydrologic Region to about -13% in the Tulare region. For the wetter scenarios (WW & HW), a steady increase over time occurs but lacks a clear

Plant Physiological Responses to Atmospheric Forcings

geographical direction of change with early century changes in the neighborhood of +10% up to about +20% by century's end. The CEN scenario has only minor changes from the RF scenario.

The period average maximum daily temperatures (Tmax), solar radiation (Rs), carbon dioxide (CO₂) and vapor pressure deficit (VPD) were also developed for each climate scenario because these climate inputs are necessary from simulating transpiration, biomass and yield with the WEAP-PGM model. The methods are described in Appendix 4B of Reclamation (2016). Period averaged values for the atmospheric variables in each climate scenario during the 2011-2040, 2041-2070, and 2070-2099 periods are presented in Figure 4.1.1 for the U.C. Davis CIMIS station located in the Sacramento Hydrologic Region.

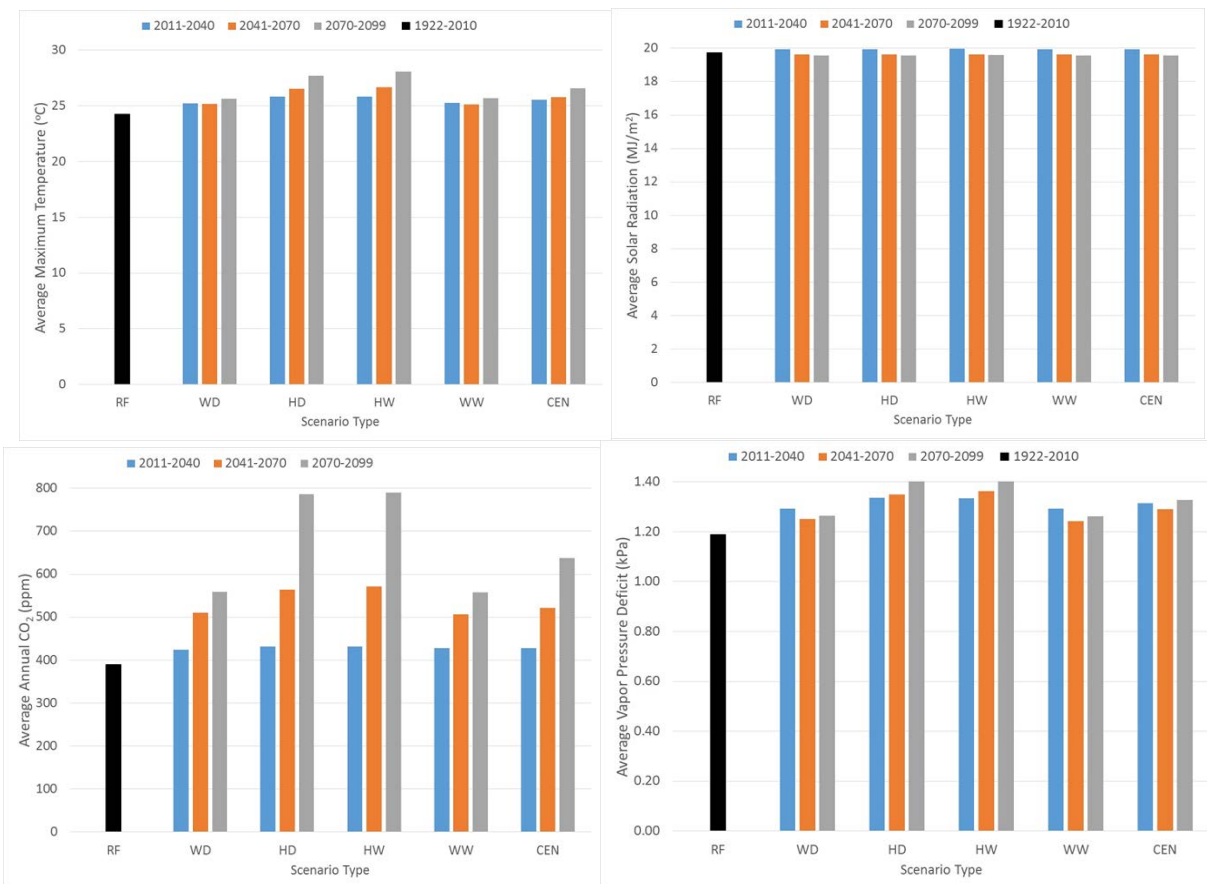


Figure 4.1.1 Period Averaged Maximum Temperature (Tmax), Solar Radiation (Rs), Carbon Dioxide (CO₂) and Vapor Pressure Deficit (VPD) in the Central Valley.

From Figure 4.1.1, it can be observed that there is a directly proportional relationship between CO₂ and Tmax in all the time periods. However, this relationship appears to be weaker in the scenarios with less warming (WW & WD). In contrast, a weak but inversely proportional relationship exists between CO₂ and Rs in all scenarios and time periods. Interestingly, the VPD in scenarios with less warming (WW and WD) increases slightly more in the early century than in the later periods. This also occurs in the CEN scenario. However, in the hotter scenarios (HW & HD), VPD increases throughout the century along with Tmax and CO₂.

Based on the SG socioeconomic scenario, Table 4.1.2 presents the average annual applied irrigation water demands in thousands of acre-feet per year (TAF/year) for the RF climate scenario and percentage change in each other climate scenarios relative to the RF scenario (% Δ RF) in the Sacramento River, San Joaquin River, Tulare Lake and Central Valley Hydrologic Regions for the 2015–2039, 2040–2069, 2070–2099 and the overall 2015–2099 time periods.

Table 4.1.2 Applied Water Demands and Changes in the Central Valley Basins

Location	Time	Climate Scenarios					
		RF	WD	HD	HW	WW	CEN
Location	Period	(TAF/yr)	% Δ RF				
Sacramento Hyd. Region	2015-2039	4,794	1.2	3.2	2.1	-0.5	1.7
	2040-2069	4,440	-0.9	1.4	-0.3	-2.1	0.7
	2070-2099	4,199	-2.0	-12.2	-13.5	-3.2	-4.0
San Joaquin Hyd. Region	2015-2039	4,949	1.2	3.8	1.2	-1.5	1.0
	2040-2069	4,708	-1.4	0.6	-2.9	-4.7	-0.9
	2070-2099	4,481	-3.3	-20.2	-23.0	-7.2	-8.8
Tulare Lake Hyd. Region	2015-2039	10,559	1.0	3.3	0.7	-1.9	0.6
	2040-2069	9,990	-0.9	-0.2	-3.7	-4.0	-1.2
	2070-2099	9,718	-3.0	-16.9	-20.6	-7.1	-7.9
Total Central Valley	2015-2039	21,966	1.1	3.4	1.2	-1.4	1.0
	2040-2069	20,688	-1.1	0.3	-2.8	-3.8	-0.8
	2070-2099	19,887	-3.0	-17.3	-20.2	-6.3	-7.5
	2015-2099	20,781	-1.1	-4.7	-7.4	-3.9	-2.5

Although there are generally slight increases in agricultural water demand during the early century period (2015-2039), the overall decrease in the mid (2040-2069) and especially the late century is downward (2070-2099). In the late 20th century, this decrease in agricultural water demand is especially large in the hotter scenarios (HD & HW) ranging from -12% in the Sacramento Valley to more than -20% in the San Joaquin and Tulare Lake Hydrologic Regions. For the scenarios with less warming (WD & WW), the declines are considerably smaller ranging from about -2% in the Sacramento Valley to -3% to -7% in the San Joaquin and Tulare Lake regions. In the CEN scenario, agricultural water demand decreases in the range of -4% to -9% are intermediate to the warmer and hotter scenarios.

From Table 4.1.1a and Figure 4.1.1 it is clear that temperature is steadily increasing through the century in all scenarios. In the early century, these relatively small increases in temperature are accompanied by relatively small increases in CO₂ and VPD. These slight increases correspond with the slight increases in agricultural water demand during this period. However, by mid-century, the initial increases have moderated and in some cases become declines relative to the RF scenario. The increasing CO₂ and declining Rs at mid-century are atmospheric forcings which would account for this reversal in crop water demands. By late century, the large increases in CO₂ and VPD especially in the HD and HW scenarios result in the corresponding large

declines in crop water use. The lesser increases in CO₂ and VPD in the WD, WW, and CEN correspond with the lesser declines in crop water demands in these scenarios. The decreases in Rs in the mid and late century would also contribute to the declines. Finally, it is likely that the large temperature increases in the HD and HW may have exceeded the optimal temperature range of some crops thus contributing to a reduction in growth which would also result in reduced ET_c.

4.2 Crop Yield – Climate Interactions

In an early study using GCM results to evaluate potential climate change impacts on crop yields in the central and southern Great Plains, Rosenzweig (1990) used the same Geophysical Fluid Dynamics Laboratory (GFDL) and the Goddard Institute of Space Studies (GISS) temperature and precipitation outputs as Allen et al. (1991) (described above) as inputs to the CERES-Wheat and CERES-Maize (corn) models (described above) to evaluate the effects of doubled CO₂ concentrations (660 ppm) on the yields at 14 locations in Nebraska, Kansas, Oklahoma and Texas.

In this study, future climate change was simulated by increasing CO₂ concentrations from a baseline of 330 to 660 ppm and running the models to an equilibrium climate condition. At the elevated CO₂ concentration, the GISS and GFDL simulated mean annual region-wide temperature increases were about +4.5°C and +5°C respectively. Both models projected a latitudinal trend of increased annual temperature changes (ΔT) from south to north (relative to the 1950-1980 baseline). The GISS model simulated a region-wide decrease in precipitation of about -3.3% with greater declines in the south (Rosenzweig, 1990). The GFDL model simulated a region-wide decline of only -0.8% with some precipitation increases in the south.

For the crop simulations, no downscaling or bias correction of the GCM results was performed. Daily temperature and precipitation inputs required for the CERES crop models were computed from the ratio of GCM monthly averages to observed monthly averages based on historical observations of daily data obtained from local meteorological stations. Daily solar radiation was estimated from temperature using a weather generation algorithm. A constant wind speed of 2 m/s was assumed in crop models. The effects of changes in humidity were not included in the study.

The CERES crop models were run for 30 year periods to compute both baseline and projected yields. Both dryland (not discussed in this report) and irrigated simulations were performed. Under irrigated conditions, water was automatically applied whenever soil moisture decreased below 80% of field capacity. To simulate the effects of CO₂ at 660 ppm on biomass, increases of 25% and 10% in daily canopy photosynthesis were assumed for wheat and corn respectively. Other assumptions described by Rosenzweig (1990) include:

- Crop parameters developed at temperatures less than those projected by the GCM were used in the simulations.
- Increased canopy temperatures due to increased stomatal resistance were not simulated.
- Overestimate of potential CO₂ yield increases because extreme climatic events, pests and nutrients were not evaluated.

In the baseline simulations, the CERES simulated yields were consistently greater than observed yields for both wheat and corn. However, no additional adjustments to the CERES model parameters were performed. Climate impact simulations were performed both with and without elevated CO₂ effects. In simulations without the physiological effects of increased CO₂, winter wheat yields typically decreased. The larger declines occurred in the southern Plains than in the northern Great Plains where annual temperature remained lower. In the GISS simulations, the projected mean yield decline was -10.9% relative to the baseline simulation with a range from +6.5% to -48.3%. In the approximately 0.5 to 1 °C warmer GFDL simulations without CO₂ effects, the projected mean yield decline was -15.5% with a range from +0.2% to -42.7%. Wheat maturity dates occurred about three weeks earlier throughout the region because the increased temperatures caused the crop to mature more rapidly. However, this shortened growth period also resulted in less biomass production and consequently reduced yields. Including the physiological effects of CO₂, increased mean wheat yields increased by +12% relative to the baseline in the GISS projections. This increase represents approximately a 20% increase relative to the simulations without CO₂ effects (-10.9%). Increasing winter wheat yields were simulated at latitudes greater than 36° north whereas south of this latitude either no change or declines occurred. In the GFDL simulations with CO₂ effects, mean wheat yields increased by +3% relative to the baseline and displayed a south to north trend ranging from -15% in the south to +15% in the north.

Similarly, simulated corn yields declined throughout the region. In the GISS simulations without the physiological effects of CO₂, the projected mean corn yield decline was -16.4% with a range from -8.7% to -22.6%. In the warmer GFDL simulations, the decline in the simulated mean corn yield was -23.8% with a range from -10.9% to -37.3%. Unlike wheat, the crop yield declines were somewhat greater in north than south. In both models, corn maturity dates occurred about 2 and a half to three weeks earlier in the year due to the increased temperatures. However, simulated corn yields do not respond as much as wheat to increased atmospheric CO₂ because corn's C4 photosynthetic pathway is able to accumulate sufficient photosynthetic precursors at lower ambient CO₂ concentrations. Consequently, elevated CO₂ does not increase yields as much as occurs in C3 plants such as wheat.

It is worth noting that Rosenzweig (1990) examined several potential adaptation strategies involving changing planting dates to earlier or later in the year and using cultivars with different vernalization requirements and photoperiod sensitivities and concluded that some improvements could be obtained but not at all locations.

In an international study of the effects of climate change on world food supply, Rosenzweig and Inglesias (1998) reported on the application of the CERES and SOYGRO (Jones et al., 1989b) models at more than 100 locations in 18 countries worldwide. In this study, GCMs including the GISS, GFDL and United Kingdom Meteorological Office (UKMO) described by Mitchell et al. (1987) were applied to simulate equilibrium state climate changes resulting from increased radiative forcing due to a doubling of CO₂ to 660 ppm. The resulting global temperature and precipitation changes ranged from +4.2 – +5.2 °C and +8 - +15%, respectively.

The crop modeling involved calibration and validation using climate data for a baseline period from 1951 to 1980. Unfortunately, location specific results were aggregated to the national scale and only results for wheat were reported for the United States. For the United States, wheat

Plant Physiological Responses to Atmospheric Forcings

yields were reported to decline between -21% to -33% without considering the effects of CO₂ on photosynthesis. Including the effects of CO₂, decreased the yield reduction range to -2% to -14%. The largest declines were associated with the warmest GCM (UKMO). The yield declines were reported to occur because of the combined effects of increased heat stress and a shortened of the growth period.

In the study, there was one transient simulation that explicitly included wheat, corn and soybeans yield changes in the United States. It was performed using the GISS model with results presented for 2010s, 2030s and 2050s assuming CO₂ concentrations of 405, 460, and 530 ppm, respectively. For wheat, yield increases up to about +5% were reported until approximately 2040. For corn, only yield declines (-5% to -15%) occurred. However, soybean yield increases of approximately +15% to +20% occurred throughout the simulation period. Because results for both irrigated and dryland cropping were not explicitly reported, the typically beneficial effects of irrigation cannot be accessed in these results. However, it is clear from these results that significant differences in yield effects occur between C3 (wheat and soybeans) and C4 (corn) crops and that crop specific characteristics are important determinants in the crop's response to the combined effects of temperature and CO₂ changes. Finally, this study demonstrates the importance of transient simulations in order to evaluate when climate change impacts become may be become significant.

Brown and Rosenberg (1999) used the results of GCM simulations to assess climate change impacts to major wheat and corn producing regions throughout the United States. The EPIC crop growth model was calibrated at representative farms using daily weather records from National Weather Service Cooperative Climate Network Stations during the baseline period (1968 – 1989). Climate generators were used to estimate daily values of solar radiation, relative humidity, and wind speed for both the baseline and climate change scenarios. At each representative farm, the EPIC model was calibrated with local yield, soil and management data obtained from variety sources.

The GISS, UK Meteorological Office Transient (Murphy, 1995) and Australian Bureau of Meteorology Research Center (McAveney et al., 1991) GCMs were used to obtain gridded temperature and precipitation over a range of projected global mean temperatures (GMTs) from +1 to +5 °C. Atmospheric CO₂ concentrations of 365, 560, and 750 ppm were used in the EPIC crop simulations.

In most the western United States, wheat was the only crop simulated at the representative farms. In addition, the crop production was simulated only under dryland conditions. In this region under dryland conditions, yields are typically less than under irrigated conditions. However, the GCMs projected generally wetter conditions. At a GMT increase of +1 °C, winter wheat yields declined very slightly at a CO₂ concentrations of 365 ppm but increased by approximately +25% and +50% at CO₂ concentrations of 560 and 750 ppm, respectively. At a GMT increase of +2.5 °C, yield declines averaged about -15% at a CO₂ concentrations of 365 ppm; remained slightly positive at 560 ppm CO₂ and at 750 ppm ranged from about +25% to + 50% for the 3 GCMs. At a GMT increase of +5 °C, yield declines ranged -5% to -75% with the greatest declines at the lowest CO₂ enrichments. The effects on corn yields were similar albeit much less dramatic. The authors attributed the yield declines to early crop maturation caused by elevated temperatures.

As part of the U.S. National Assessment Study, Izaurre et al. (2003) used climate change results from a transient simulation from the HadGM2 (formerly referred to as the UKTR model) that included the entire continental United States. This run assumed a 1% per year increase in atmospheric CO₂ concentrations during the period from 1994 – 2100. In the Pacific, Mountain, Northern and Southern Plains regions, simulated minimum daily temperature increases ranged from +1.1 to +1.9 °C in 2035 and +3.5 to +4.7 °C by 2095 with the smallest increases along the Pacific Coast and the largest increases in the interior Mountain region. Precipitation changes ranged from +1% in the Southern Plains to +21% in the interior Mountain region by 2035 and +12% in the southern Plains to +35% in the interior Mountain region by 2095. Unlike Reclamation's projections, no declines in precipitation were reported anywhere in the western United States during the 21st century.

The EPIC model was used to simulate climate change impacts on several crops including corn and alfalfa at representative farms under both dry land and irrigated growing conditions as well as wheat and soybeans under dry land conditions. CO₂ effects on yield were simulated at 365 and 560 ppm for baseline (1961-1990), 2035 and 2095 climate conditions. Under irrigated conditions without CO₂ effects, alfalfa yields relative to the baseline increased in both 2035 and 2095. The yield increases ranged from +11% to +26% in 2035 and +13% to +28% in 2095 with the largest increases occurring in the Southern Plains region. With CO₂ effects at 560 ppm, yield increases ranged from +32% to 46% in 2035 and +34% to +50% in 2095 with the largest increases occurring in the Southern Plains region.

Under irrigated conditions without CO₂ effects, corn yields increased relative to the baseline in both 2035 and 2095 in all regions except in the Southern Plains in 2095 where yields declined by -6%. The largest yield increase (+27%) occurred in the interior Mountain region in 2095. With CO₂ at 560 ppm in 2095, the yield was increased to +38% in 2095 in the Mountain region and the largest decline decreased to -5% in the Southern Plains. The authors indicated that elevated CO₂ effects were largely derived from reductions in the temperature and water stresses experienced by the crop. Because of the wetter conditions simulated by the HadGM2, decreases in water stress should be anticipated and presumably the decrease in temperature stress is associated with more rapid phenological development due to increased temperatures. However, more rapid crop development is usually associated in decreased rather than increased yields.

For winter wheat which was only simulated under dry land conditions, yields without CO₂ effects increased in both 2035 and 2095 relative to the baseline in all regions except the Southern Plains. With CO₂ effects included, simulated wheat yields increased relative to the baseline without CO₂ in all regions in both 2035 and 2095.

The Sacramento and San Joaquin Basins Study (Reclamation, 2016) also included an assessment of changes in crop yields using the same scenarios described in the preceding section. In total 22 crops were simulated in Central Valley using WEAP-PGM. Table 4.2.1 shows changes in yield for a few selected crops grown in the Central Valley for the three climate scenarios including the warm-wet (WW), central tendency (CEN) and the hot-dry (HD). These scenarios are described in Appendix 4B of Reclamation (2016). The reference scenario is RF.

Table 4.2.1. Selected Crop Yields (Tons/Acre dry weight) in the Central Valley Basins

Period Average Crop Yield Changes by Scenario in Percent of RF scenario

		Alfalfa	Wheat ¹	Corn	Safflower	Citrus	Vine
Year	2025						
	WW	7.37	12.98	-0.47	3.88	-0.32	3.03
	CEN	6.68	13.63	-2.00	4.12	-4.67	0.37
	HD	6.26	14.04	-3.78	4.52	-8.20	-1.82
Year	2055						
	WW	18.48	26.66	-3.45	9.39	0.06	9.12
	CEN	13.48	28.52	-6.62	8.86	-5.81	5.92
	HD	17.88	29.83	-9.40	9.56	-9.79	4.44
Year	2085						
	WW	25.77	36.92	-9.22	11.79	-1.01	12.73
	CEN	27.25	41.71	-15.62	12.38	-6.15	12.17
	HD	24.64	42.24	-24.08	10.91	-14.87	7.12

Note 1. This is a winter wheat crop.

Except for corn, increased CO₂ should benefit all other C3 crops included in Table 4.2.1 by increasing their radiation use efficiency (RUE) and maximum canopy LAI. However, if VPD increases beyond crop specific threshold values, RUE is reduced. Similarly, a decrease in R_s, will result in decreased growth and yield. When temperature increases remain below the crop's optimum temperature, growth and yield are expected to increase whereas if temperature increases beyond a crop's optimum growth temperature, growth and yield are reduced. For corn, a C4 plant, an increase in CO₂ does not result in increased RUE although temperature and VPD effects may affect growth and yield.

From Table 4.1.1 and Figure 4.1.1, it is clear that both temperature and CO₂ are steadily increasing in all scenarios. The early century (2015-2039) increase in R_s was followed by decreases in the mid (2040-2069) and late (2070-2099) time periods. In the HD and HW scenarios, VPD increased steadily throughout the century while in the WD, WW, and CEN scenarios an early century increase was followed by a slight mid-century decrease and a late century increase.

For the winter wheat crop, the simulated yields increased continuously along with the increases in temperature and CO₂ and the increases were greater in the hotter and higher CO₂ HD scenario than in the WW in all time periods. Yield in the CEN scenario were intermediate between these scenarios. Alfalfa and safflower follow a similar pattern of increasing yields throughout the century but differences between the scenarios occur. For alfalfa, there are consistently greater yields in the WW than in the HD scenario. This may be the result of temperature and/or VPD

exceeding optimum threshold values in the HD scenario. For safflower, yields follow a pattern of HD being greater than WW in the early and mid-century periods but a reverse in the late century. Since CO₂ is increasing continuously, this reversal is likely a temperature and VPD threshold effect that does occur until the late century. For citrus, yields tend to decline throughout the century with the decreases in the HD consistently greater than the WW indicating a temperature and/or VPD threshold effects. Yields of vines tend to increase throughout the century with the increases in the WW being greater than the HD indicating temperature and/or VPD effects. Finally, corn yields decline consistently throughout the century with larger declines associated with the hotter HD scenario indicating a temperature and/or VPD effect.

5. Assessment of Plant Physiological Responses to Atmospheric Forcings

5.1 Background

In this study, the technical approach taken to assess plant physiological responses to atmospheric forcings was to select three representative crop groups and evaluate their transpiration, biomass and yield responses. Six climate scenarios based on climate model simulations from the Coupled Model Intercomparison Project Phase 5 (CMIP5) climate model data (Taylor et al., 2012) were used to represent a wide range of potential atmospheric conditions. These scenarios included a reference scenario (RF) similar to historical climate conditions (NoCC) and five ensemble based scenarios warm-dry (WD), hot-dry (HD), hot-wet (HW), warm-wet (WW) and central tendency (CEN) scenarios with names corresponding to their implied differences in temperature and precipitation relative to the NoCC scenario. The methods used to construct these scenarios are described in Appendix 3A of Reclamation (2016).

The atmospheric forcings used in this study were developed from climate model data by methods described in Appendix 4B of Reclamation (2016). The atmospheric forcings included daily maximum and minimum temperature (Tmax & Tmin), dew point temperature (Tdew), incoming short wave solar radiation (Rs), monthly average wind speed (Us) and carbon dioxide (CO₂).

An 89 year daily time step study period starting on 1/1/2011 and ending on 12/31/2099 was used for the simulations of crop responses using the WEAP-PGM crop model described in Section 3.2. The methods used to develop the atmospheric forcings from climate model data are described in more detail in Appendix B. Additional information about the characteristics of the atmospheric scenarios is provide in Section 5.3.

5.2 Selection of Representative Crops

For this study, six crops were selected as representative of plant responses to atmospheric forcings. Alfalfa and winter wheat are important crops that are grown throughout the western United States. In the Central Valley, alfalfa is a perennial crop but its primary growing seasons are spring, summer and fall. In the simulations performed in this study, up to seven fixed cuttings are scheduled to happen during the growing season. Despite the potential for warming to change the growth period, maintaining a fixed cutting schedule is more desirable when making comparison between the scenarios. Furthermore, other practical considerations such excessive soil moisture in fields may preclude harvest earlier or later in the growing season. For the same reasons, winter wheat is planted on fixed date of November 1st and harvested on the following May 31st. This fixed planting date and fixed harvest date approach is accomplished by predetermining the number of heat units in each year and varying the required heats unit from planting to harvest on an annual basis throughout the simulation period. In simulation experiments, it was determined that annual crops like winter wheat started growing earlier in the year with the consequence that their phenological cycles shortened over time with the result that transpiration, biomass and yield declined. By simulating a fixed growth period that occurs

between the same planting and harvest dates, the crop responses are larger whether increased or decreased. This fixed planting date with a fixed harvest date (FIX-FIX) approach also facilitates the comparison of crop responses to different atmospheric forcings amongst the scenarios. It is also more likely to be representative of the kinds of cultivar adaptations that growers will seek to obtain in future.

Corn is another major crop grown extensively in western United States. It was selected to be representative of crops using the C4 photosynthetic pathway. It is an annual crop typically planted on May 1st and harvested on August 15th in the Central Valley. In this study, it was simulated using the FIX-FIX approach. Safflower is an important crop commonly grown in the western United States. It is sometimes planted as an alternative to corn when water supplies are limited. It has a slightly shorter growth period than corn. In the Central Valley, it is planted on April 1st and harvested on July 31st. Like corn, it was simulated using the FIX-FIX approach.

Citrus and vines are important perennial crops grown in the Central Valley. Citrus is representative of non-deciduous tree crop. In this study, oranges are the specific citrus crop being simulated. The type of vines in the study are grapes grown in vineyards. Although perennial, they are representative of deciduous crops and in the Central Valley their growth period is from April 1st to November 1st. In this study, these crops were not simulated using the FIX-FIX approach because they are perennials and have no fixed planting and harvest dates.

5.3 Selection of Representative Atmospheric Forcings

The six atmospheric forcing scenarios used in this study were selected to characterize a wide range of potential, future meteorological conditions that may affect crop transpiration, biomass production and yield. The scenarios were developed from bias corrected and spatially downscaled (BCSD) temperature and precipitation data developed for the Sacramento and San Joaquin Basins Study (Reclamation, 2016). It is important to note that these forcings are outputs from physically based climate models. This preserves the inherent relationships between atmospheric variables which is essential to performing a realistic assessment of plant responses to atmospheric conditions. It also means that a sensitivity analysis in which single variables are perturbed independently of the others would likely produce misleading results.

Details of the methods used to develop these daily time series are described in Appendix 3A of Reclamation (2016). However, these climate data scenarios only represent temperature and precipitation conditions. To simulate the effects of other atmospheric forcings, it is necessary to develop corresponding conditions representing incoming short wave solar radiation, carbon dioxide and atmospheric humidity. In order to develop these additional data sets, several estimation methods using the temperature data were employed to obtain values for these meteorological conditions corresponding to the atmospheric forcing scenarios. As described in more detail in Appendix B, this process requires selecting agricultural meteorological stations with long records of high quality observations including solar radiation, relative humidity, dew point temperature and wind speed. From on these observations, the climate model temperature data can be used to calculate R_s and T_{dew} . These variables along with daily T_{max} and T_{min} are the inputs which WEAP-PGM crop model uses to calculate the daily net radiation (R_n), atmospheric humidity (ea) and vapor pressure deficit (VPD). The CO_2 inputs to the WEAP-PGM

Plant Physiological Responses to Atmospheric Forcings

model were developed by first identifying how many of each of the Representative Concentration Pathways (RCP) are present in each climate scenario and weighting each of the RCP CO₂ concentrations by the total number included to obtain the average concentration. In this study, no inter-annual variations in CO₂ concentration were simulated.

For the Sacramento and San Joaquin Basins Study, Reclamation (2016) prepared six climate scenarios using these methods at four different locations in the Central Valley where long term agricultural meteorological observations were available from California Irrigation Management Information System (CIMIS) stations. For this study, the Firebaugh location was selected because it is intermediate to the northern Sacramento Valley and southern Tulare Lake Basin and not influenced by the meteorological effects of the Sacramento and San Joaquin Delta.

Although wind speed affects ETC, the same monthly average values were used in all the simulations. Therefore, it is not considered in the subsequent discussion of scenario differences. Precipitation did not play a major role in this study because all the simulations were conducted by providing the crops with adequate water to avoid any water stress effects on transpiration, biomass or yield. However, for completeness it is described here.

Figure 5.3.1 presents the total mean annual precipitation and the change from the reference NoCC for each scenario. All values are reported in millimeters (mm).

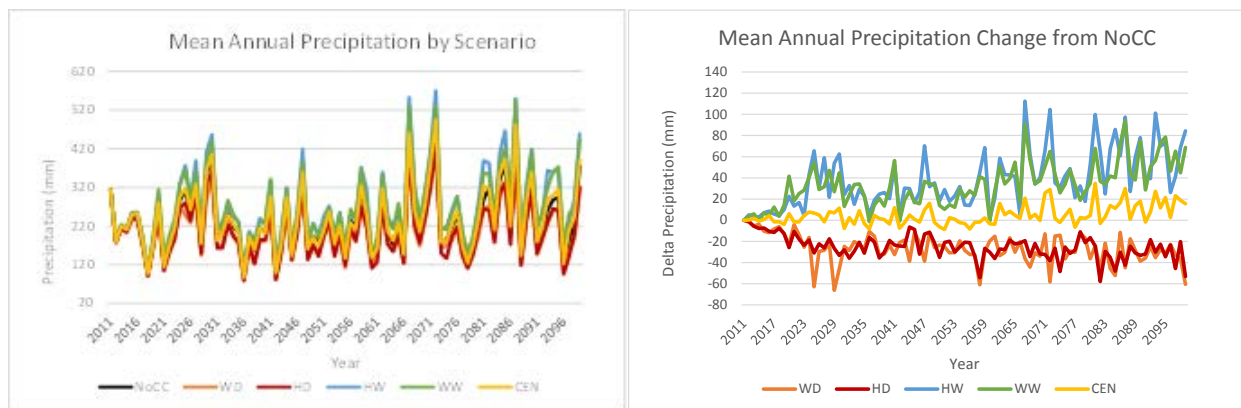


Figure 5.3.1 Total Annual Precipitation and Changes from the NoCC Reference by Scenario during the Study Period (2011 – 2099)

As can be observed, all time series exhibit the same inter-annual variability. This is the result of using the historical climate in the period from 1922-2010 as the basis for these scenarios. Although shown for the annual means, the actual scenarios used in the simulations have daily data. Both the HW and WW scenarios are considerably wetter than the NoCC, while the WD and HD are significantly drier. The CEN scenario does not differ vary significantly from the NoCC.

Figure 5.3.2 shows the study period mean monthly precipitation and changes from the NoCC by month for each scenario. All values are reported in millimeters (mm).

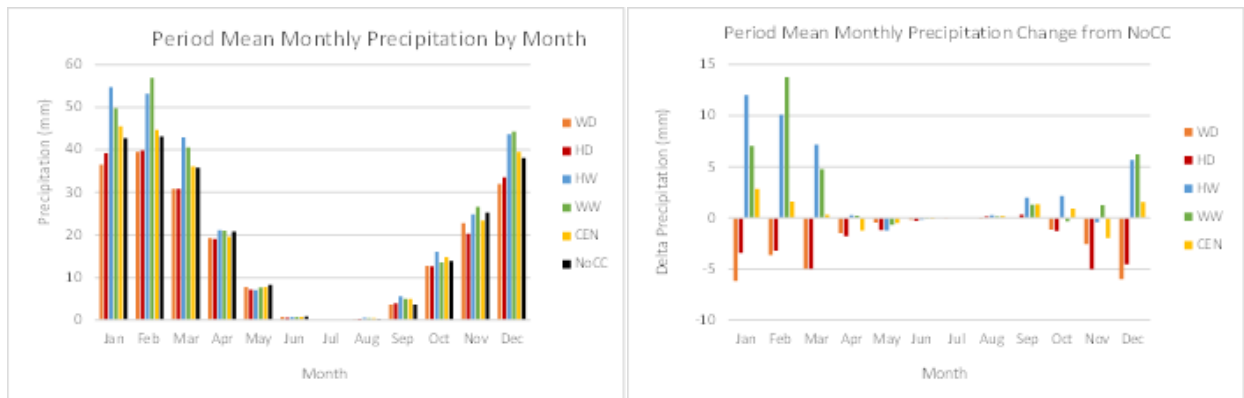


Figure 5.3.2 Period Mean Total Precipitation by Month and Changes from the NoCC Reference by Scenario

Both the largest amounts and the largest changes occur in the fall and winter seasons¹. Figure 5.3.3 presents boxplots of total annual precipitation showing the mean (solid line), median (X), 25th and 75th percentiles (top and bottom) of the boxes, 5th and 95th percentiles shown on the bottom and top whisker lines. Outliers are shown as solid dots. All values are reported in millimeters (mm).

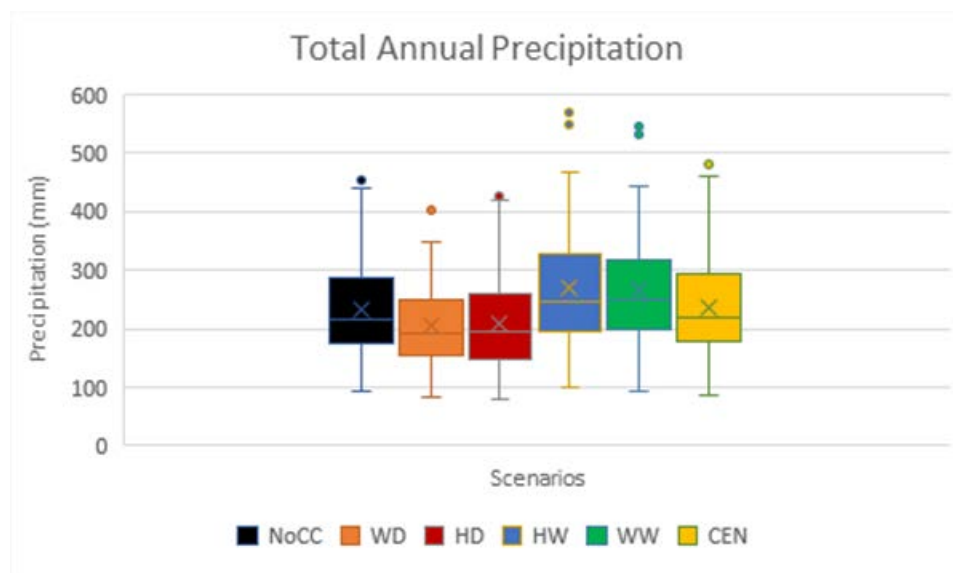


Figure 5.3.3 Boxplots of the Total Annual Precipitation by Scenario

To characterize the effects of temperature, the maximum daily temperature (Tmax) variable was selected. Minimum daily temperature (Tmin) is also an input to WEAP-PGM but because of the way it's calculated using the average daily temperature time series from the climate model data,

¹ In this study, seasons are meteorological seasons. Winter occurs in January (Jan), February (Feb) & March (Mar); Spring is April (Apr), May & June (Jun); Summer is July (Jul), August (Aug) & September (Sep); Fall is October (Oct), November (Nov) & December (Dec).

Plant Physiological Responses to Atmospheric Forcings

it always changes by the same difference from Tmax and therefore separate figures are not shown. Figure 5.3.4 presents a time series for mean annual Tmax during the study period along with changes from the reference NoCC by scenario. All values are reported in degrees centigrade (°C).

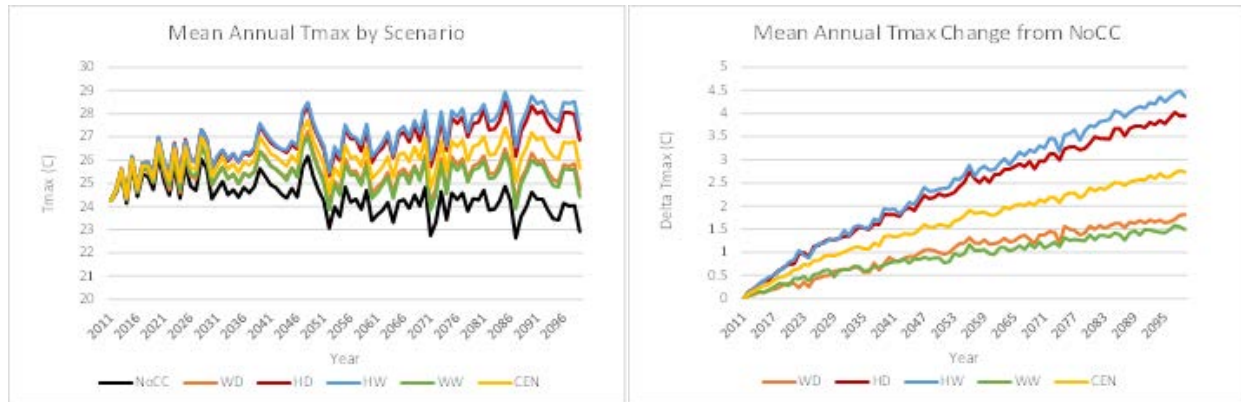


Figure 5.3.4 Mean Annual Tmax and Changes from the NoCC Reference by Scenario during the Study Period (2011 – 2099)

Figure 5.3.5 shows the study period mean monthly Tmax and changes from the NoCC by month for each scenario. All values are reported in degrees C.

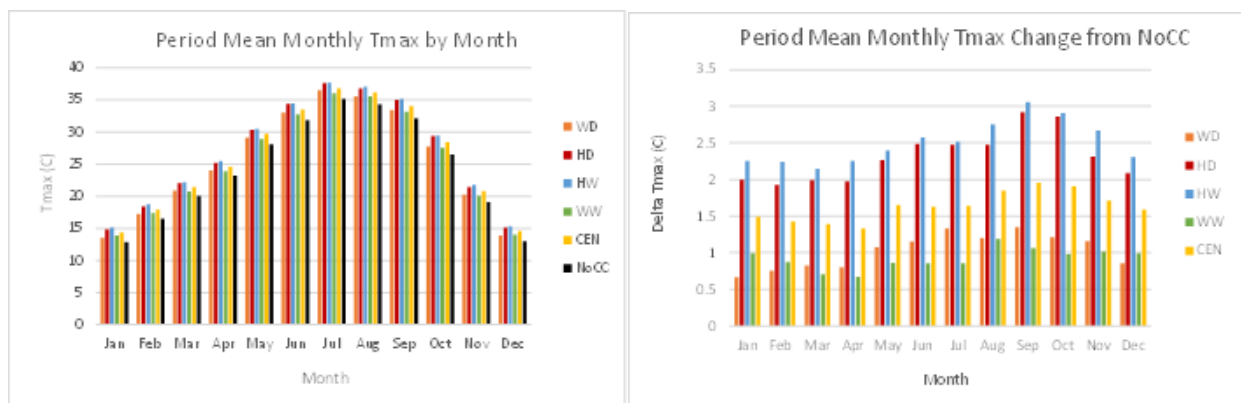


Figure 5.3.5 Period Mean Tmax by Month and Changes from the NoCC Reference by Scenario

As shown, the monthly changes in Tmax are far greater than the differences between the scenarios. However, the largest differences occur in the months from August through September in all the scenarios. The changes from the NoCC reference scenario are largest in the hot HD and HW scenarios and smallest in the WD and WW scenarios. The CEN scenario is intermediate between these groups.

Figure 5.3.6 presents boxplots of mean annual Tmax showing the mean (solid line), median (X), 25th and 75th percentiles (top and bottom) of the boxes, 5th and 95th percentiles shown on the bottom and top whisker lines. Outliers are shown as solid dots. All values are reported in degrees °C.

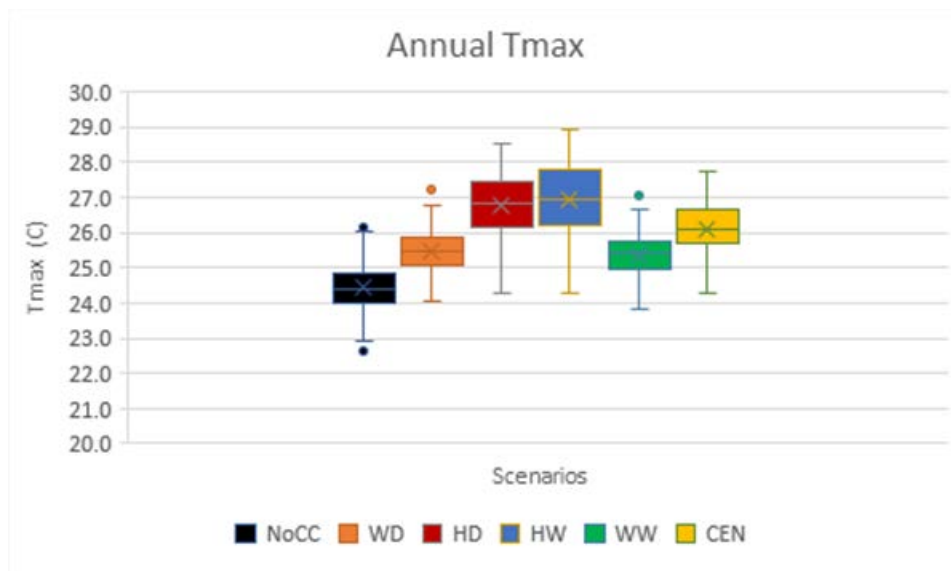


Figure 5.3.6 Boxplots of the Mean Annual Tmax by Scenario

To characterize the effects solar radiation on crop growth and transpiration, the incoming short wave length radiation, R_s is used as an input to WEAP-PGM. Figure 5.3.7 presents a time series for mean annual R_s during the study period along with changes from the reference NoCC by scenario. All values are reported in mega joules per square meter (MJ/m^2).

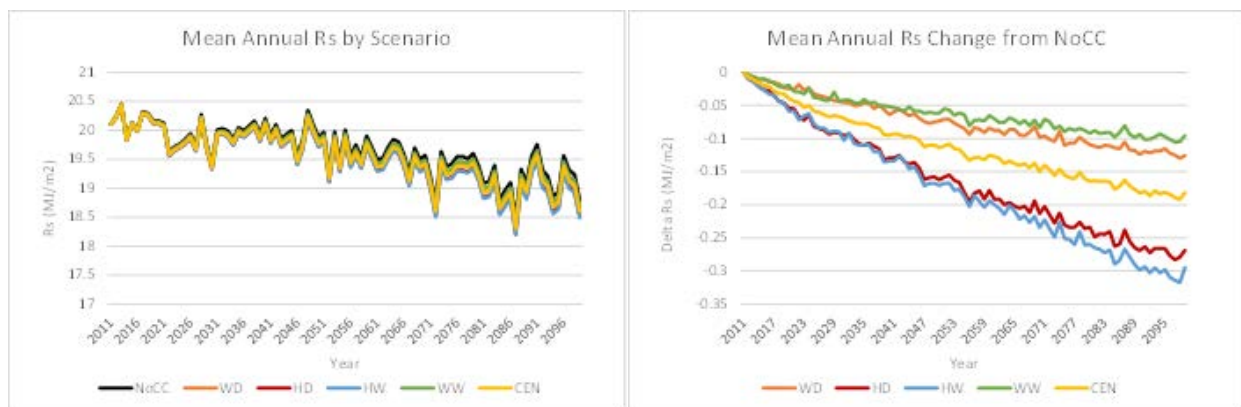


Figure 5.3.7 Mean Annual R_s and Changes from the NoCC Reference by Scenario during the Study Period (2011 – 2099)

As shown on the figure, despite the inter-annual variability, there is an overall decline in R_s during the study period. Although the differences are small between the scenarios, it is clear that the declines are greater in the hot HD and HW scenarios and lesser in the warm WD and WW scenarios. CEN is intermediate between these groups.

Figure 5.3.8 shows the study period mean monthly R_s and changes from the NoCC by month for each scenario. All values are reported in MJ/m^2 .

Plant Physiological Responses to Atmospheric Forcings

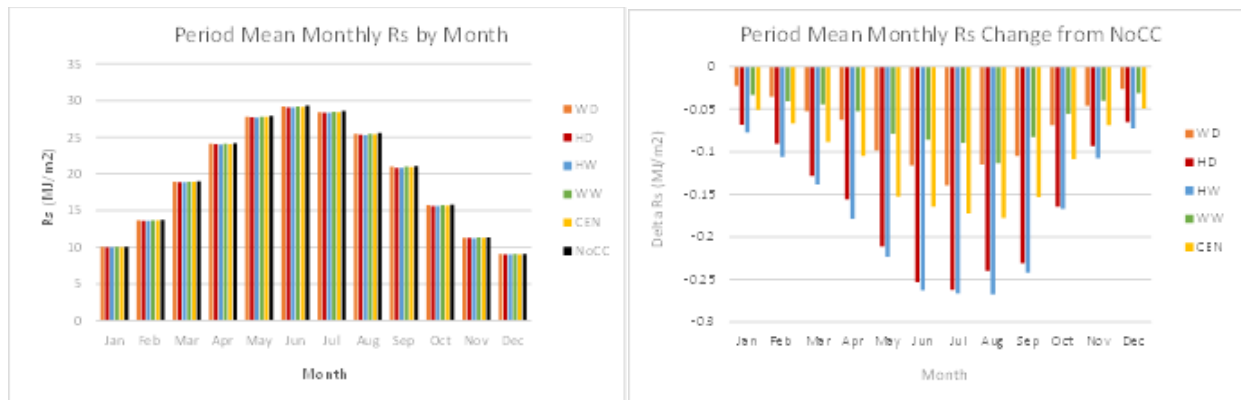


Figure 5.3.8 Period Mean Rs by Month and Changes from the NoCC Reference by Scenario

The seasonal changes in Rs are similar to Tmax and like Tmax. Differences between scenarios are small compared to monthly changes. Despite the small differences there are consistently larger changes in the hot HD and HW scenarios than in the warm WD and WW scenarios. The CEN scenario is intermediate between these groups. Although the month of June has the highest monthly Rs, there are slightly larger changes in the months of July and August.

Figure 5.3.9 presents boxplots of mean annual Rs showing the mean (solid line), median (X), 25th and 75th percentiles (top and bottom) of the boxes, 5th and 95th percentiles shown on the bottom and top whisker lines. Outliers are shown as solid dots. All values are reported in MJ/m².

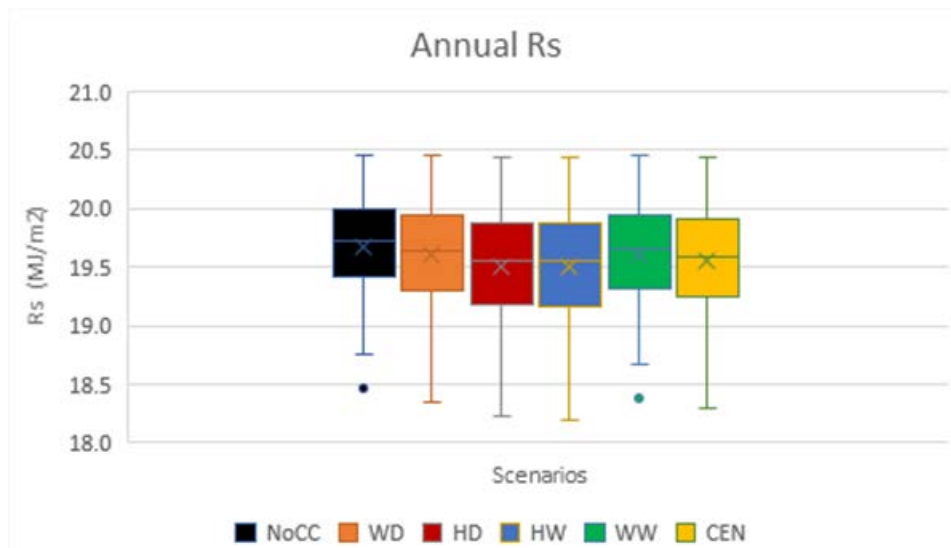


Figure 5.3.9 Boxplots of the Mean Annual Rs by Scenario

To characterize the effects carbon dioxide on crop growth and transpiration, atmospheric CO₂ is used as an input to WEAP-PGM. Figure 5.3.10 presents a time series for mean annual CO₂ during the study period along with changes from the reference NoCC by scenario. All values are reported in parts per million by volume of air (ppm).

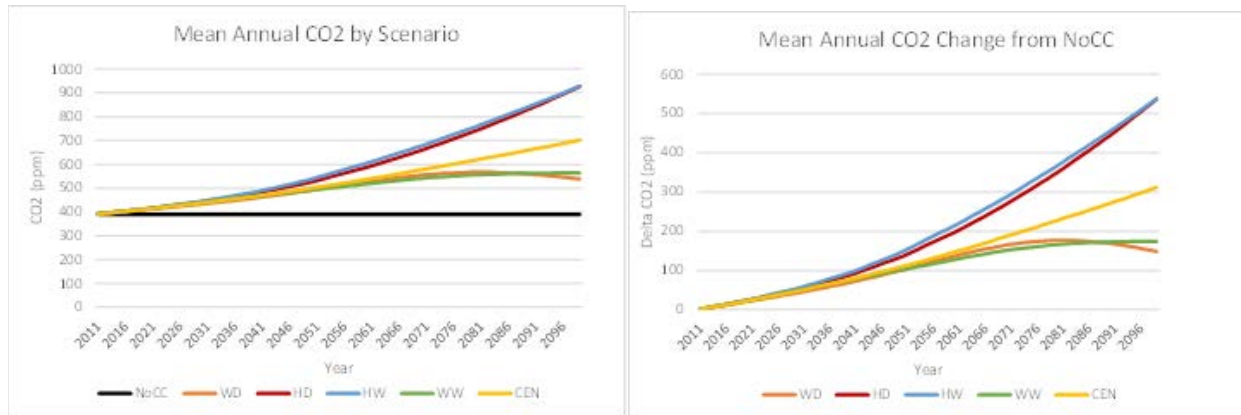


Figure 5.3.10 Mean Annual CO₂ and Changes from the NoCC Reference by Scenario during the Study Period (2011 – 2099)

Except in the NoCC reference scenario, CO₂ concentrations are generally increasing. The NoCC reference scenario has a constant CO₂ concentration on 390 ppm throughout the study period. The largest increases in CO₂ occur on the hot HD and HW scenarios. In the WW scenario, CO₂ concentration increases to about the year 2085 and then remains essentially constant. In the WD scenario, CO₂ concentration increases up to about the year 2085 and subsequently decreases slightly throughout the rest of the study period. In the CEN scenario, CO₂ concentration increases steadily throughout the study period and is intermediate in concentration between the hot and warm groups.

Figure 5.3.11 shows the study period mean monthly CO₂ and changes from the NoCC by month for each scenario. All values are reported in ppm.



Figure 5.3.11 Period Mean CO₂ by Month and Changes from the NoCC Reference by Scenario

There are no monthly variations in CO₂ in this study. The largest CO₂ concentrations occur in the hot HD and HW scenarios while the smallest increases occur in the WD and WW scenarios. The CEN scenario is intermediate to these two groups.

Plant Physiological Responses to Atmospheric Forcings

Figure 5.3.12 presents boxplots of mean annual CO₂ showing the mean (solid line), median (X), 25th and 75th percentiles (top and bottom) of the boxes, 5th and 95th percentiles shown on the bottom and top whisker lines. Any outliers are shown as solid dots. All values are reported in ppm.

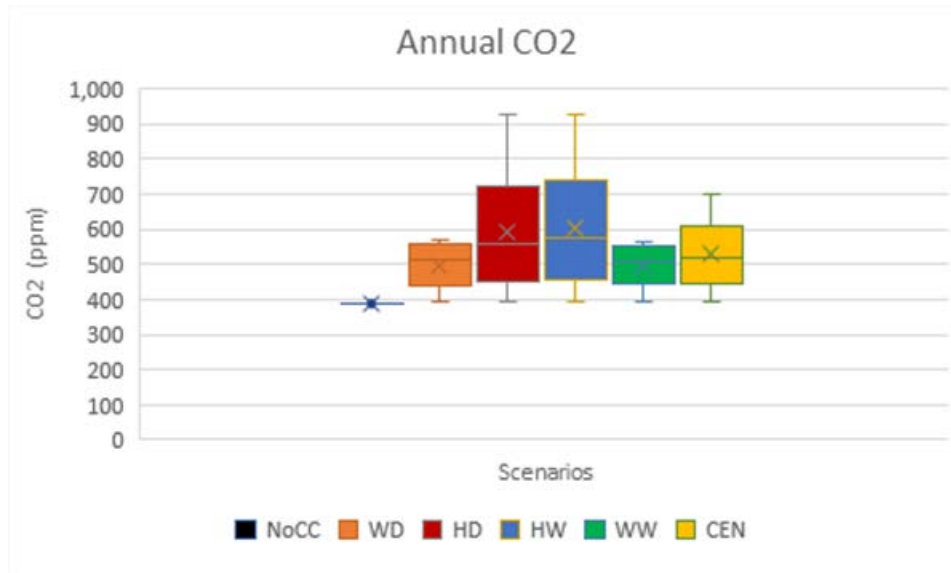


Figure 5.3.12 Boxplots of the Mean Annual CO₂ by Scenario

To characterize the effects the vapor pressure deficit on crop growth and transpiration, VPD is computed by WEAP-PGM from inputs of Tdew or relative humidity (RH) data and mean daily temperature which is computed as the average of input Tmax and Tmin data. In this study, Tdew is used to compute the atmospheric vapor pressure (e_a). Daily average temperature is used to compute the saturation vapor pressure (e_s). VPD is computed as the difference of ($e_s - e_a$). Figure 5.3.13 presents a time series of mean annual VPD during the study period along with changes from the reference NoCC by scenario. All values are reported in kilo Pascals (kPa).

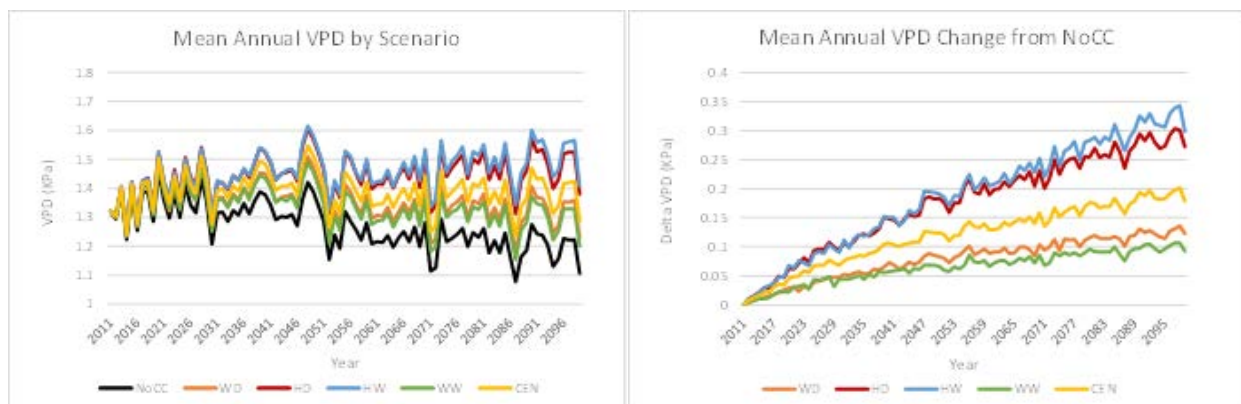


Figure 5.3.13 Mean Annual VPD and Changes from the NoCC Reference by Scenario during the Study Period (2011 – 2099)

As can be observed, the VPD increases steadily in all scenarios during the study period. The largest increases in VPD occur in the hot HD and HW scenarios. The smallest increases occur in the warm scenarios. The CEN scenario is intermediate between these groups.

Figure 5.3.14 shows the study period mean monthly VPD and changes from the NoCC by month for each scenario. All values are reported in kPa.

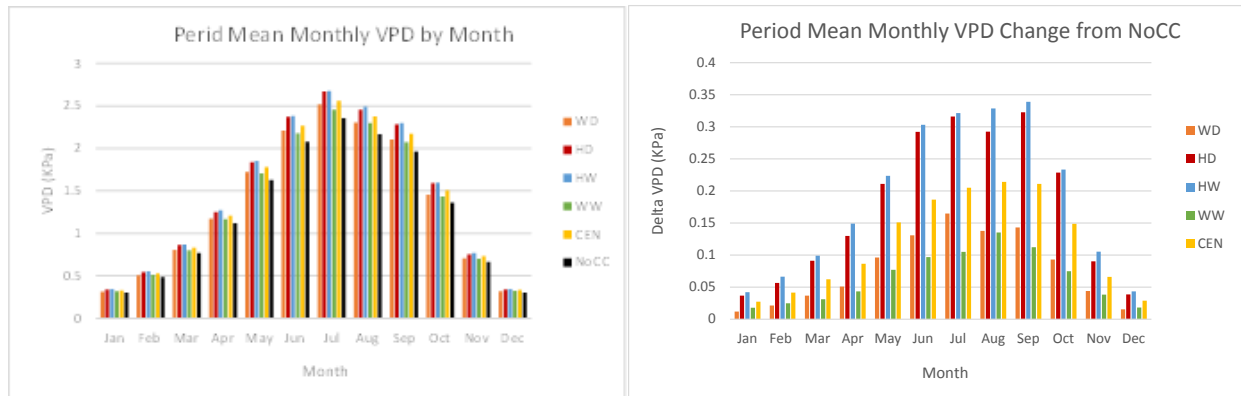


Figure 5.3.14 Period Mean VPD by Month and Changes from the NoCC Reference by Scenario

The monthly changes in VPD are much larger between months than between scenarios. The increases in the summer season are especially large relative to the other seasons especially in the hot HD and HW scenarios. The differences are consistently larger changes in the hot HD and HW scenarios than in the warm WD and WW scenarios. The CEN scenario is intermediate between these groups.

Figure 5.3.15 presents boxplots of mean annual CO₂ showing the mean (solid line), median (X), 25th and 75th percentiles (top and bottom) of the boxes, 5th and 95th percentiles shown on the bottom and top whisker lines. Outliers are shown as solid dots. All values are reported in kPa.

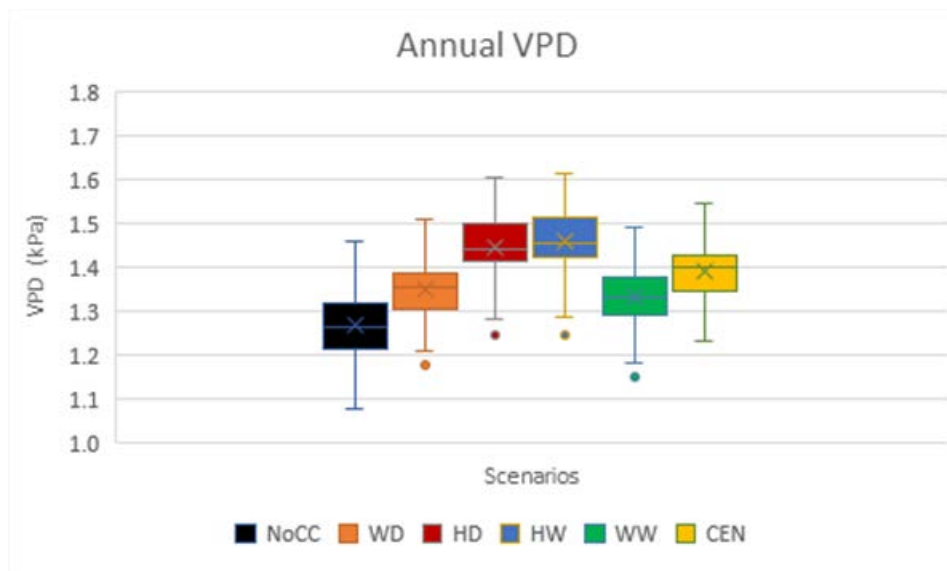


Figure 5.3.15 Boxplots of the Mean Annual VPD by Scenario

An evaluation of the atmospheric forcings was performed to determine what correlations exist in the climate data. Figure 5.3.16 shows the result of a regression between Tmax and CO₂ for both the WD and HW scenarios. In both scenarios, a positive relationship exists between them and this relationship becomes stronger as the CO₂ concentration increases (R^2 in WD = 0.008 & R^2 in HW = 0.572).

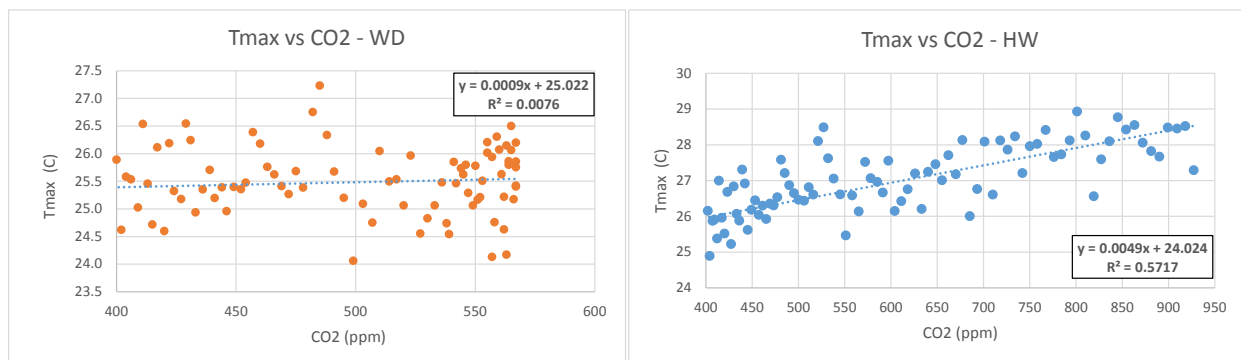


Figure 5.3.16 Correlations between Tmax and CO₂ in the WD and HW Scenarios

From the figure, it is evident that there is little correlation between Tmax and CO₂ in the WD scenario while there is a much stronger relationship between them in the HW scenario. It can also be observed that when CO₂ increases beyond about 600 ppm the correlation increases significantly.

As shown on Figure 5.3.17, an inversely proportional relationship exists between Rs and CO₂.

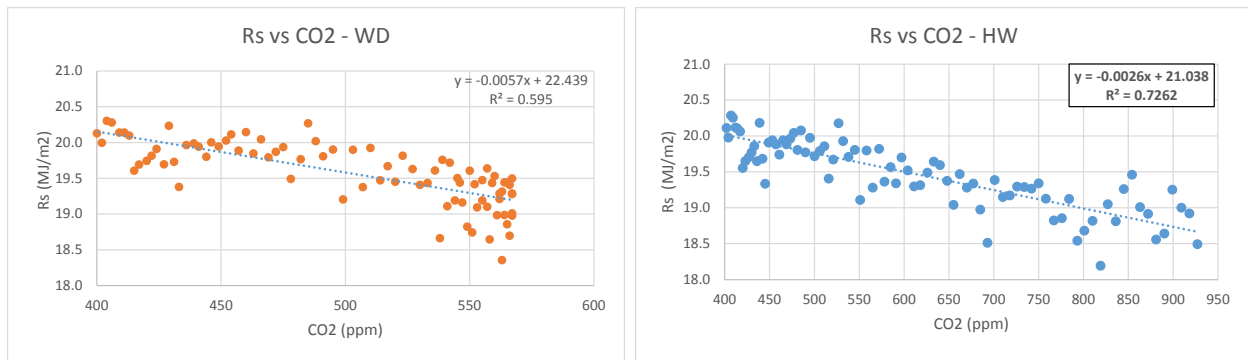


Figure 5.3.17 Correlations between Rs and CO₂ in the WD and HW Scenarios

In this case, there is a reasonable amount of correlation of Rs and CO₂ in both the warm WD and the hot HW. Figure 5.3.18 is a similar graph of VPD and CO₂. In both cases, there is a relatively weak relationship between them in both the WD and HW scenarios. Interestingly, the relationship changes from inversely proportional in the WD to directly proportional in the HD scenario.

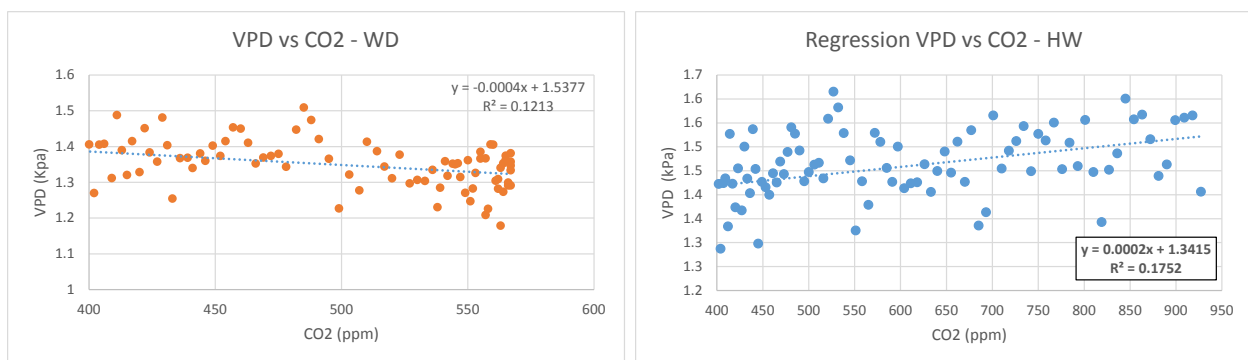


Figure 5.3.18 Correlations between VPD and CO₂ in the WD and HW Scenarios

Table 5.3.1 presents the correlation coefficients between each of the atmospheric variables and CO₂ in all the climate scenarios.

Table 5.3.1. Correlation Coefficients of Atmospheric Forcings with CO₂

Variable	CO ₂ WD	CO ₂ HD	CO ₂ HW	CO ₂ WW	CO ₂ CEN
	Correlation Coefficients				
Tmax (C)	0.087289552	0.680543922	0.756104207	-0.062315635	0.420535142
Rs (MJ/m ²)	-0.771367921	-0.842730855	-0.85219482	-0.785135212	-0.83087414
VPD (kPa)	-0.348333554	0.271614297	0.418515333	-0.45103835	-0.119330422

The strongest correlations between Tmax and CO₂ occur in the hot HD and HW scenarios while there is virtually no correlation in the WD and WW scenarios. CEN is intermediate between these groups. Rs maintains a strong negative correlation in all scenarios with CO₂ while VPD has moderately negative correlations in the warm the WD, WW and CEN scenarios and moderately positive correlations in the hot HD and HW scenarios.

Table 5.3.2 presents results of a similar analysis to evaluate correlations between Rs and VPD and Rs with Tmax in all the scenarios.

Table 5.3.2 Correlation Coefficients of Atmospheric Forcings with Tmax

Variable	<i>Tmax WD</i>	<i>Tmax HD</i>	<i>Tmax HW</i>	<i>Tmax WW</i>	<i>Tmax CEN</i>
	Correlation Coefficients				
Rs (MJ/m ²)	0.187665371	-0.437084838	-0.518935522	0.321078752	-0.125363081
VPD (kPa)	0.801759807	0.832024757	0.86023486	0.829333728	0.770318043

The correlation between Rs and Tmax is moderately negative in the hot HD and HW scenarios while it is weakly positive in the warm WD and WW scenarios. The CEN scenario is weakly negative. The correlation of VPD with Tmax is strongly positive in all the scenarios.

Table 5.3.3 presents results the analysis of the correlations between VPD and Rs.

Table 5.3.3 Correlation Coefficients of Atmospheric Forcings with Rs

Variable	<i>Rs WD</i>	<i>Rs HD</i>	<i>Rs HW</i>	<i>Rs WW</i>	<i>Rs CEN</i>
	Correlation Coefficients				
VPD (kPa)	0.633365384	0.0448188	-0.097182745	0.70062054	0.434419324

In the warm scenarios there is a strong positive correlation between Rs and VPD while in the hot scenarios HD and HW there is virtually no correlation. The CEN scenario is intermediate between these groups.

The correlation coefficients between precipitation and all the other climate variables were also calculated. The only variable which had some correlation with precipitation was Rs. It had a moderately negative correlation in the wet scenarios which is reasonable because the higher atmospheric humidity in these scenarios should decrease the incoming solar radiation.

In summary, the correlation analysis indicates that there are consistently strong negative correlations between Rs and CO₂ and consistently strong positive correlations between VPD and Tmax. Physically both seem reasonable. In the case of VPD, the saturation vapor pressure is a strongly non-linear function of temperature with an increasingly large slope as a function of temperature. Thus, even if the atmospheric humidity increases due to warming, the saturation vapor will increase even more rapidly. The strong negative correlation between Rs and CO₂ is related to increasing atmospheric humidity which increases with temperature and CO₂ which are increasingly correlated as CO₂ and Tmax increase. The low correlations+ between Tmax and CO₂ in the warm WD and WW scenarios is most likely inter-annual variability reducing the correlation between them in these scenarios.

5.4 Calibration of the WEAP-PGM Crop Model

The WEAP-PGM model was calibrated to data set of daily specific ET_c values based on accepted values developed using the Consumptive Use Program (CUP) model. This model and

its input data were originally developed at UC Davis by Snyder et al. (2000) for irrigation scheduling. It was subsequently refined by Orang et al. (2004) and released as the CUP model in collaboration with California Department of Water Resources (DWR). Calibration of PGM crop water use was conducted using ETC values produced by the CUP model as the calibration targets. PGM crop parameters were adjusted until the growing season total crop ET was within 3 percent of the simulated values produced by the CUP model using identical meteorological inputs in both the CUP and PGM models.

Within the PGM model there are several parameters that affect the crop evapotranspiration rate. At the leaf level, the movement of water vapor out of the leaf is regulated by leaf stomatal conductance. The development of the crop canopy is controlled by five parameters which determine its leaf area index (LAI). The development of LAI is a function of the accumulation of heat units, expressed as the Heat Unit Index (HUI). During plant development as the HUI increases the LAI increases. The rate at which LAI increases is defined by two user-specified points (LAI definition points #1 and #2). For each point, there is a corresponding value of HUI that has to be specified. The fifth parameter defines when the canopy LAI begins to decline (Start of LAI Decline). It is the HUI at which senescence begins as the growing season comes to an end. Figure 5.4.1 shows the development of the canopy as a function of the Heat Unit Index (HUI). The HUI represents the fraction of the total heat units (HU) that are required by crop to grow from germination to harvest. HUs are accumulated as the difference between the crop's basal temperature (T_b) and mean daily air temperature.

For calibration, the parameters described above were initially set at values found in the crop database for the SWAT model (Neitsch, et al. 2005). During calibration, adjustments were made to the parameters if the overall shape of the actual daily ET curve from the PGM did not match the curve from CUP. For instance, in some cases the early season ET was less in PGM than in the CUP model. To increase the early season ET the LAI definition points were adjusted to have the canopy develop more rapidly in the early season resulting in more early-season ET.

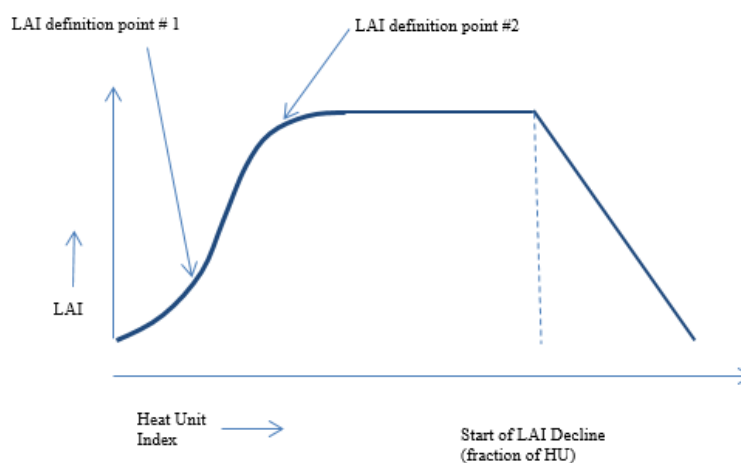


Figure 5.4.1 Illustration of Crop LAI Development as a Function of HUI

Plant Physiological Responses to Atmospheric Forcings

In other cases, the maximum daily ET during the full canopy portion of the season, typically July and August, did not match that computed by the CUP model. In those cases the leaf stomatal conductance was adjusted to bring the two models into agreement. Finally, if there was disagreement between the models in the late-season ET, the “Start of LAI Decline” parameter was adjusted so that the decline matched the CUP model ET. Table 5.4.1 shows a comparison between the CUP model ET_c and WEAP-PGM for the crops selected for this study.

Table 5.4.1 Seasonal ET totals from the CUP and PGM models at Firebaugh

Crop	Period of Comparison	CUP ET _c (mm)	PGM ET _c (mm)	Percent Difference
Alfalfa	Apr 1 – Sep 30	920	946	2.8
Winter Wheat	Nov 1 – May 31	467	456	-2.1
Corn	May 1 – Sep 30	695	698	0.5
Safflower	Apr 1 – Jul 31	533	544	2.1
Citrus	Apr 1 – Sep 30	920	914	-0.6
Vine	Apr 1 – Sep 30	700	709	1.3

Key:

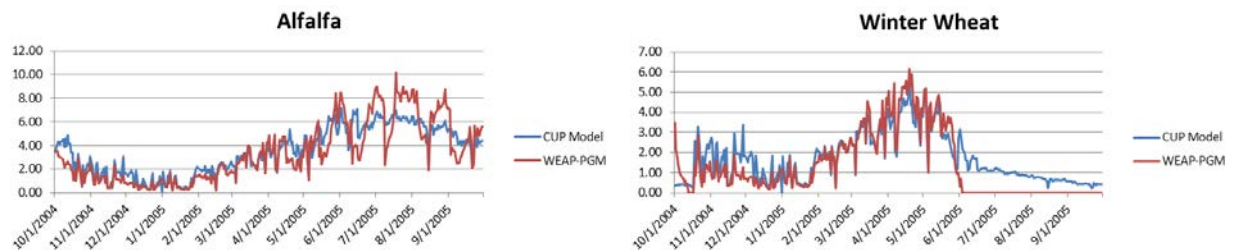
CUP = Consumptive Use Program

ET_c = crop evapotranspiration

mm = millimeters

PGM = Plant Growth Model

Using the approach described above, PGM parameters were adjusted so that daily ET from the WEAP-PGM matched the values produced by the CUP model. The objective of the calibration effort was to obtain a seasonal ET within 3 percent of the CUP model value and to match the shape of daily actual ET curve simulated by CUP.



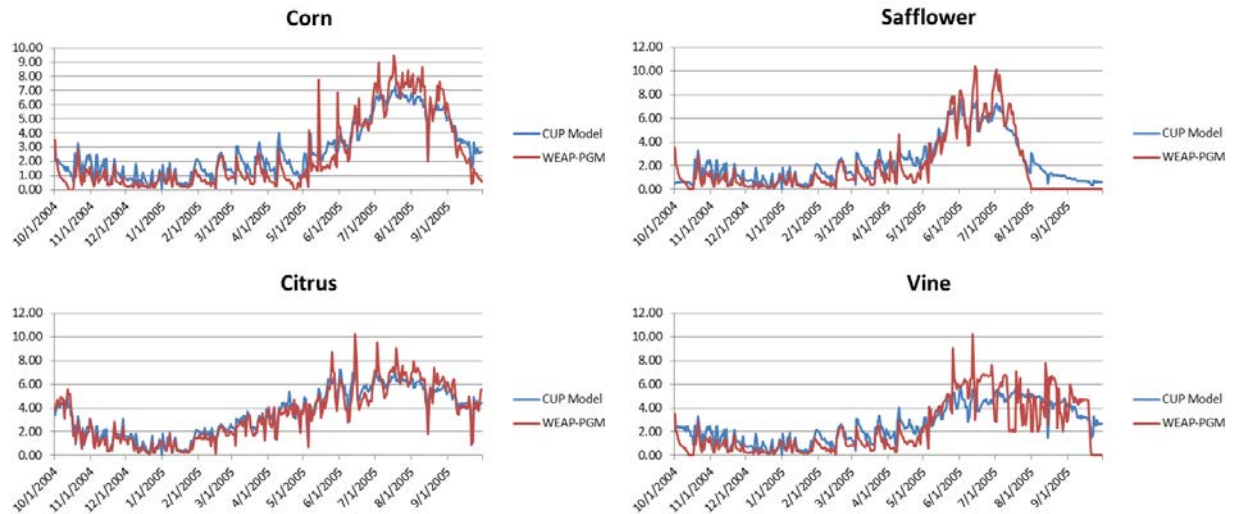


Figure 5.4.2 Comparison of the WEAP-PGM and CUP Simulated ETc

Some reasons for differences between the models include the fact that the WEAP-PGM predicts less winter time bare soil evaporation than the CUP model. Since a significant portion of the winter wheat growing season is during the winter, when crop cover is low and bare soil evaporation dominates the ET, the results are sensitive to these model differences. The CUP model is sensitive to the assumed winter time crop coefficient while the WEAP-PGM is sensitive to assumptions about soil physical parameters and the depth of soil that is subject to bare soil evaporation.

The WEAP-PGM model was calibrated to match crop yields as represented in the Statewide Agricultural Production (SWAP) model. The SWAP model is a regional agricultural production and economic optimization model. It was developed by Professor Richard Howitt, graduate students and other collaborators at U.C. Davis (Howitt et al., 2012). It has been widely used in a range of policy and economic analysis studies. Table 5.4.2 shows the results of the WEAP-PGM calibration.

Table 5.4.2 Crop Yields from the SWAP and WEAP-PGM models at Firebaugh

Crop	WEAP-PGM	SWAP Yield
	Yield (Tons/ha)	Yield (Tons/ha)
Alfalfa	12.47	12.20
Winter Wheat	5.41	5.28
Corn	8.97	8.87
Safflower	0.99	1.00
Citrus	3.75	3.66
Vines	3.41	3.34

Note: All yields reported as dry weight in metric tons per hectare (ha)

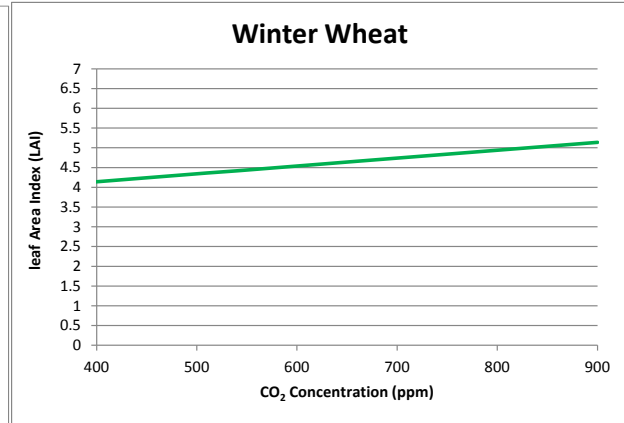
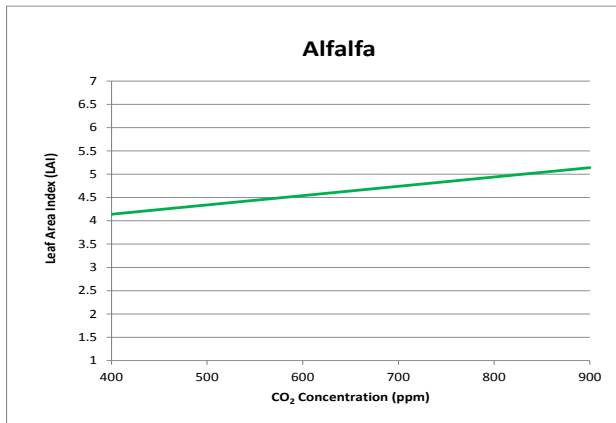
Plant Physiological Responses to Atmospheric Forcings

The differences between the WEAP-PGM and SWAP yields for these crops are less than 3%.

The WEAP-PGM model requires a variety of crop parameters. A complete listing of all the parameters used by the calibrated WEAP-PGM simulations in this study is provided in Appendix 4C of Reclamation (2016). In this section, the focus is on those parameters that affect the transpiration, biomass and yield responses of the selected crop groups.

As described previously, the primary crop parameters used in the calibration of the crops are the canopy development parameters. Figure 5.4.3 shows these crop parameters on the figure along with graphs showing their effects expressed as a function of the HUI on canopy development as well as how CO₂ concentration effects the maximum leaf area index (LAI) for the alfalfa and winter wheat crop group. These parameters are CO₂ effects parameters LAI-330 and LAI-660; canopy development parameters FH1, LA1, FH2, LA2 and Scn.

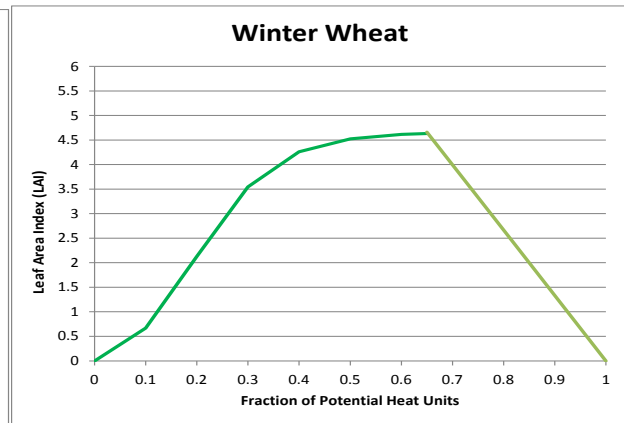
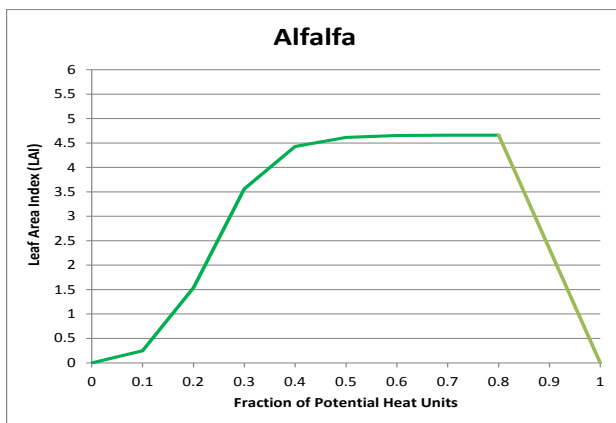
CO2 Effects



LAI-330 = 4.0 LAI-660 = 4.66

LAI-330 = 4.0 LAI-660 = 4.66

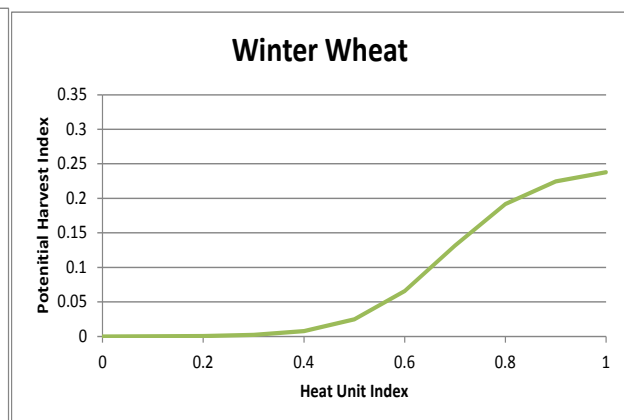
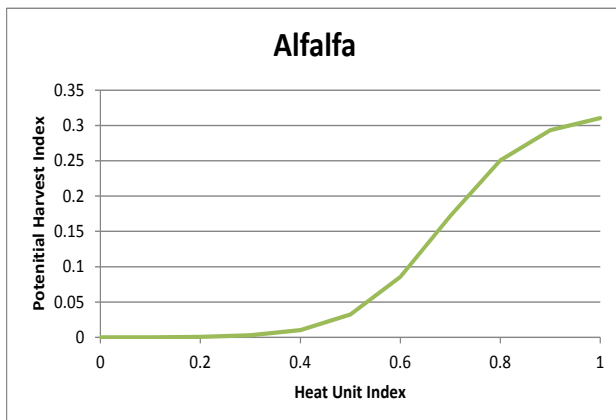
Temperature Effects on Canopy Development



FH1=0.15 LA1=0.15 FH2=0.4 LA2=0.95 Scn=0.80

LA1=0.05 LA2=0.05 LA3=0.45 LA4=0.95 Scn=0.65

Temperature Effects on Harvest



PHRVI = 0.32

PHRVI = 0.245

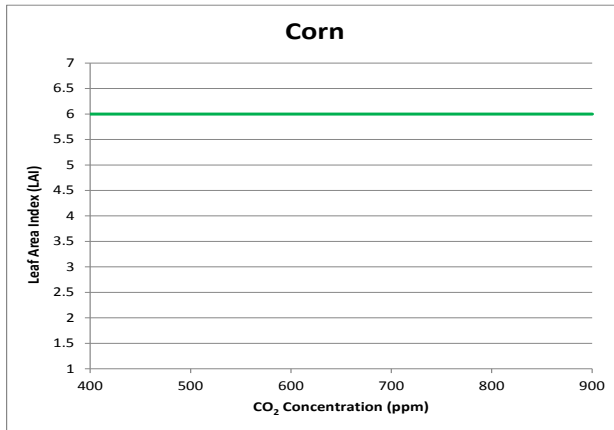
Figure 5.4.3 Plant Growth Parameters – Alfalfa & Winter Wheat - Leaf Area Index (LAI), Canopy Development & Harvest

Plant Physiological Responses to Atmospheric Forcings

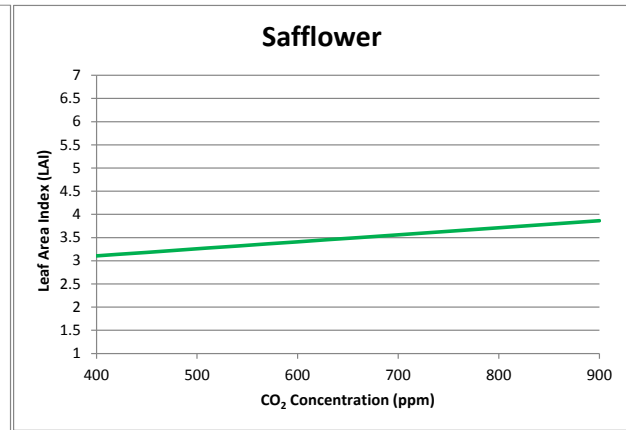
The CO₂ effects on LAI are expressed by the LAI-330 and LAI-660 parameters which represent the maximum LAI at CO₂ concentrations of 330 and 660 ppm respectively. In this study, this linear model is used to represent how CO₂ affects LAI. It is assumed to be valid at higher concentrations. The parameters FH1 and FH2 represent the fraction of the total potential heat units (PHI) required for the crop to reach harvest. The LA1 and LA2 values represent the fraction of the maximum canopy LAI occurring at FH1 and FH2. The Scn parameter represents the fraction of the PHI at which crop senescence begins. In the graphs, the darker green line represents the initiation, rapid growth and crop maturity growth phases. The senescence stage is shown in the lighter green color. The potential harvest index (PHVRI) represents the fraction of the maximum actual biomass which is yield at harvest. It is a function of the HUI. Both alfalfa and winter wheat respond identically to increasing CO₂. Alfalfa reaches maturity at a lower PHI than winter wheat and wheat starts to senescence at a smaller PHI.

The calibrated plant growth parameters for the corn and safflower crop group are presented in Figure 5.4.4.

CO2 Effects

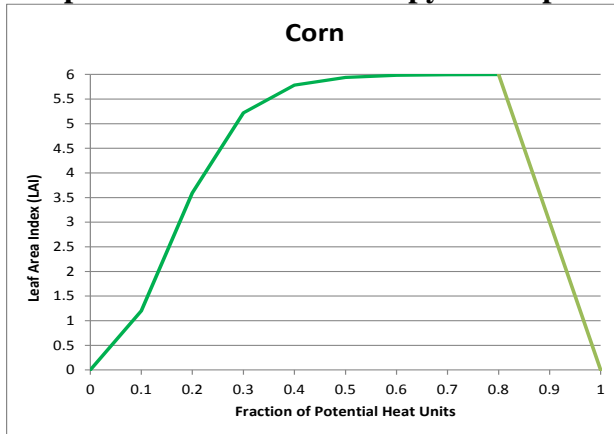


LAI-330 = 6.0 LAI-660 = 6.0

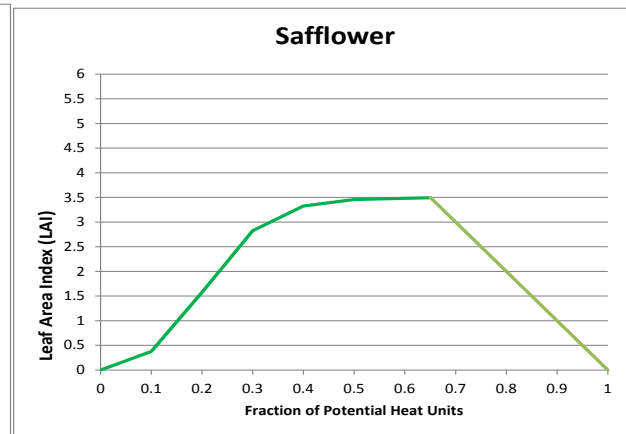


LAI-330 = 3.0 LAI-660 = 3.50

Temperature Effects on Canopy Development

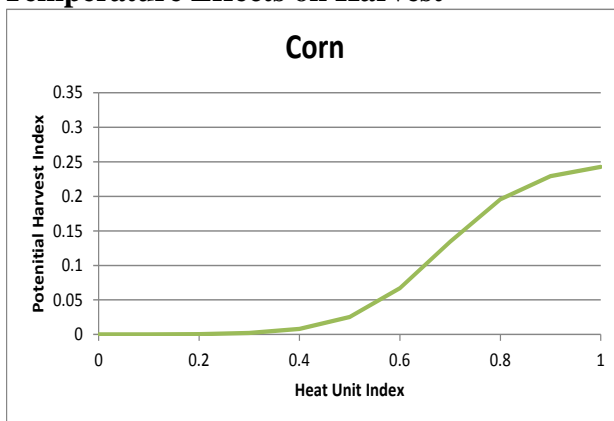


FH1=0.10 LA1=0.20 FH2=0.50 LA2=0.99 Scn=0.80

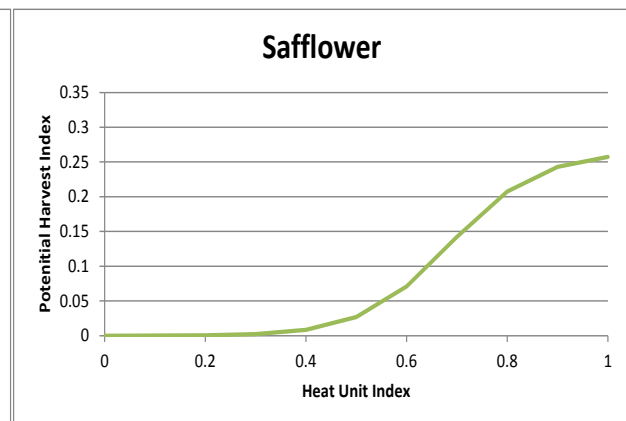


FH1=0.15 LA1=0.25 SH2=0.40 LA2=0.95 Scn=0.65

Temperature Effects on Harvest



PHRVI = 0.250



PHRVI = 0.265

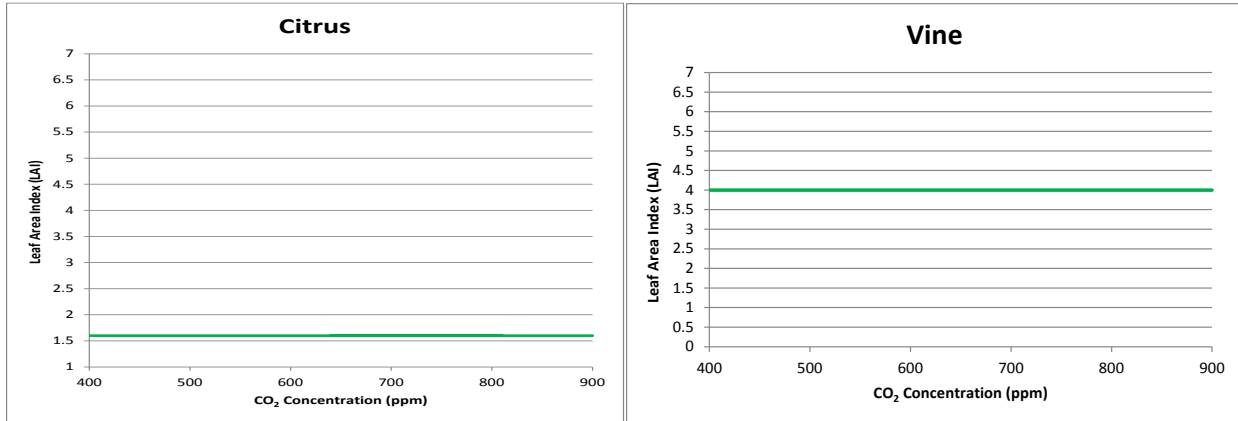
Figure 5.4.4 Plant Growth Parameters – Corn & Safflower - Leaf Area Index (LAI), Canopy Development & Harvest

Plant Physiological Responses to Atmospheric Forcings

Corn being a C4 plant shows no response to CO₂. However, it has a much higher LAI at maturity than safflower. Safflower begins its senescence relatively earlier in its maturity stage. Both crops have similar harvest characteristics.

Figure 5.4.5 shows the plant growth parameters for the citrus and vine crop group.

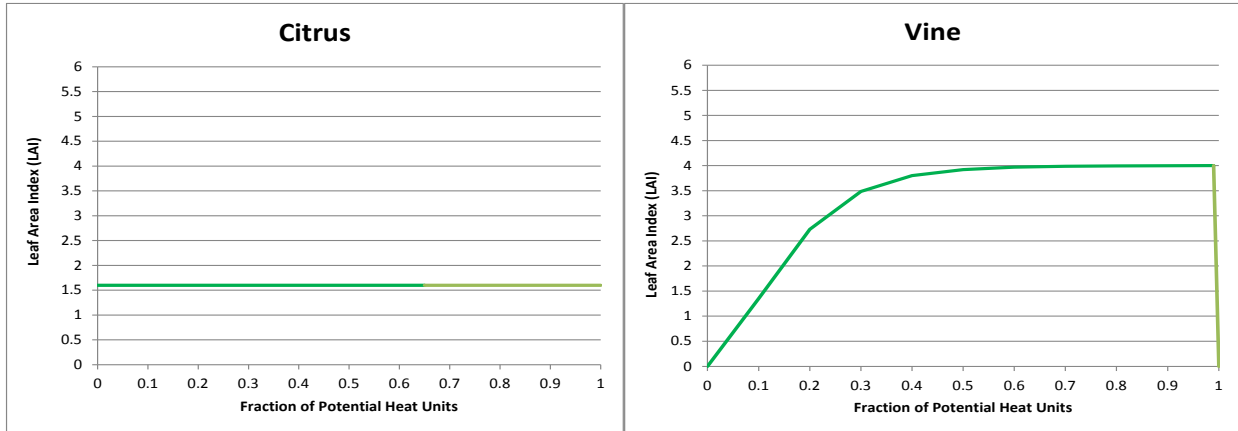
CO2 Effects



LAI-330 = 1.6 LAI-660 = 1.6

LAI-330 = 4.0 LAI-660 = 4.0

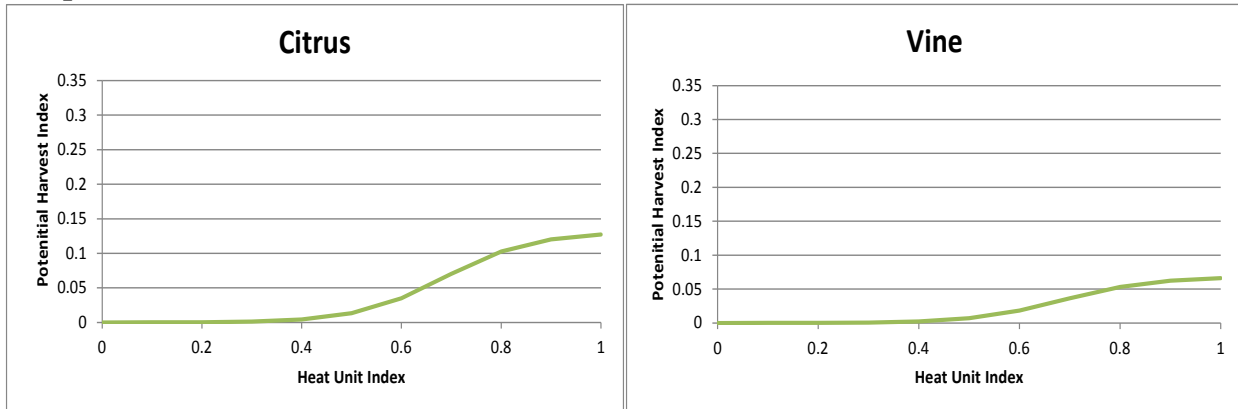
Temperature Effects on Canopy Development



SH1=NA LA1=NA SH2=NA LA2=NA Scn=NA

FH1=0.05 LA1=0.15 SH2=0.40 LA2=0.95 Scn=0.99

Temperature Effects on Harvest



PHVRI = 0.131

PHVRI = 0.068

Figure 5.4.5 Plant Growth Parameters – Citrus & Vine - Leaf Area Index (LAI), Canopy Development & Harvest

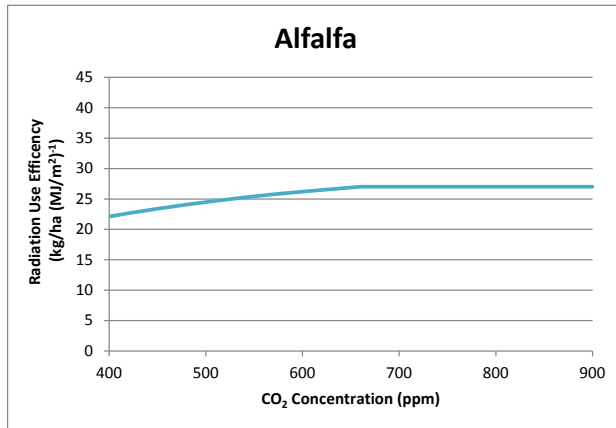
Neither citrus or vine were modeled as responding to changing CO₂ concentrations. However, vines have a much larger canopy LAI than citrus. Citrus being a non-deciduous crop has a constant LAI while vines are modeled as senescing just prior to harvest.

Plant Physiological Responses to Atmospheric Forcings

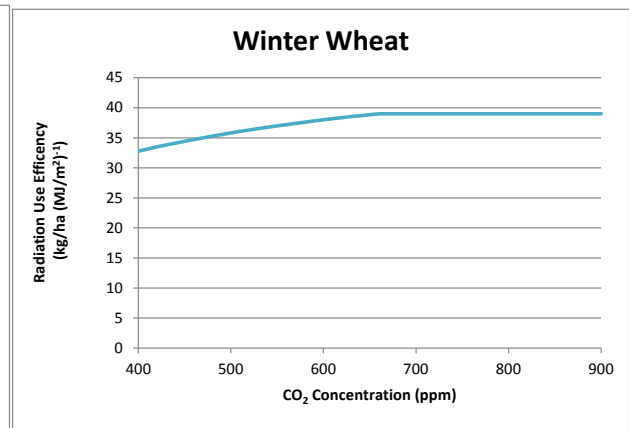
Radiation use efficiency and temperature stress are also parameters which effect crop growth and yield. These parameters include the effects of CO₂ on radiation use efficiency (RUE-330 and RUE-660); effects of VPD on the ambient radiation use efficiency (RUE-Amb), slope of declining RUE curve (RUE-VPD) and the threshold value of VPD above which RUE is reduced (RUE-Thrshld) and the crop growth factor temperature parameters (Tbase and Topt).

Figure 5.4.6 shows these parameter values on the figure for each crop and functional showing how the effects of CO₂, VPD and temperature on RUE and temperature stress growth factor were simulated for the alfalfa and winter wheat crops.

CO2 Effects

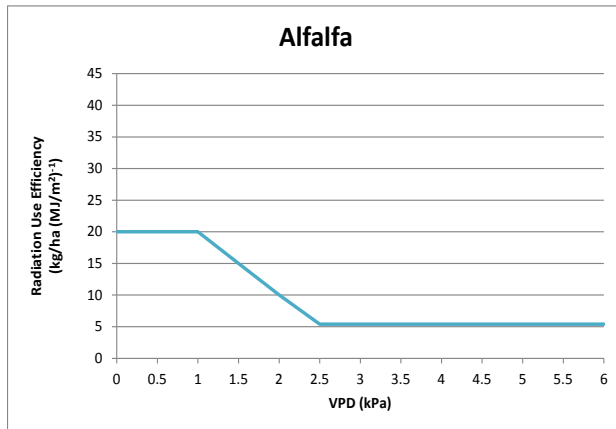


RUE-330 = 20 & RUE-660 = 27

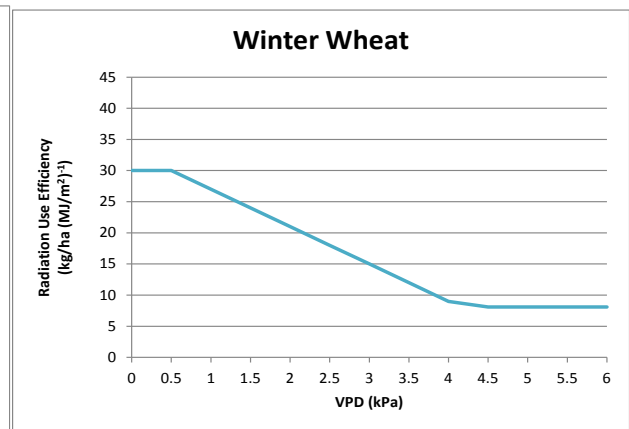


RUE-330 = 30 & RUE-660 = 39

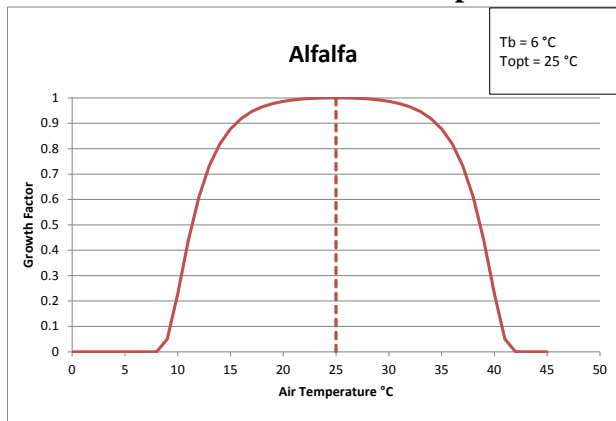
VPD Effects



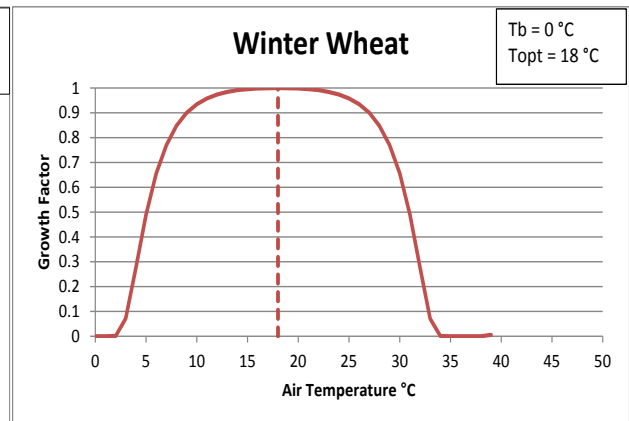
RUE-Amb = 30, RUE-VPD = 6, RUE-Thrshld= 0.5



Plant Growth Parameters – Temperature



Tbase = 6, Topt = 25



Tbase = 0, Topt = 18

Figure 5.4.6 Plant Growth Parameters – Alfalfa & Winter Wheat - Radiation Use Efficiency (RUE) and Temperature Effects on Growth

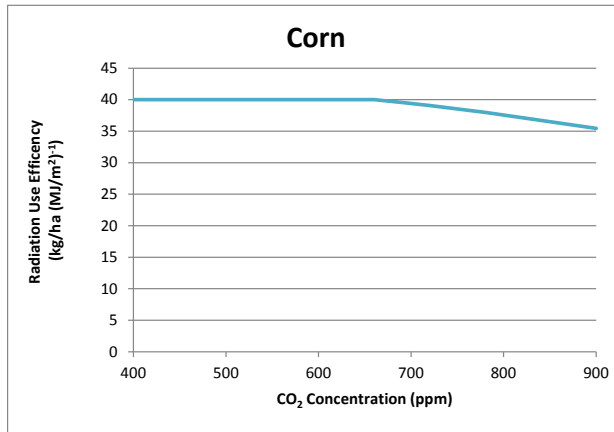
For both crops, increasing CO₂ increases their RUE but slightly more so for winter wheat than for alfalfa. The ambient RUE (RUE-Amb) is also higher in winter wheat than alfalfa. However,

Plant Physiological Responses to Atmospheric Forcings

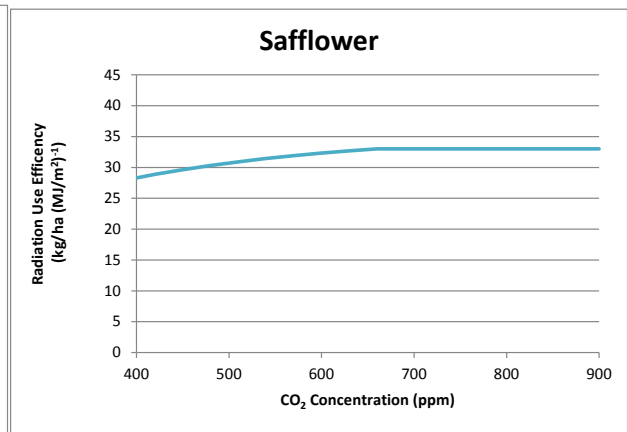
increasing VPD can offset these effects and occurs at a lower VPD threshold (RUE-Thrshld) for winter wheat than for alfalfa but the effect of VPD on decreasing RUE (RUE-VPD) for alfalfa is more significant (10 vs 6). The basal (T_{base}) and optimal temperatures (T_{opt}) and the temperature range for winter wheat are both slightly lower than for alfalfa.

Figure 5.4.7 shows the effects of CO_2 , VPD and temperature on RUE and heat stress for the corn and safflower group.

CO2 Effects

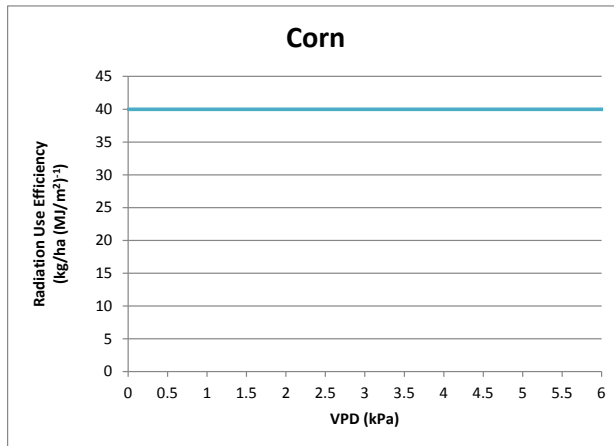


RUE-330 = 40 & RUE-660 = 40

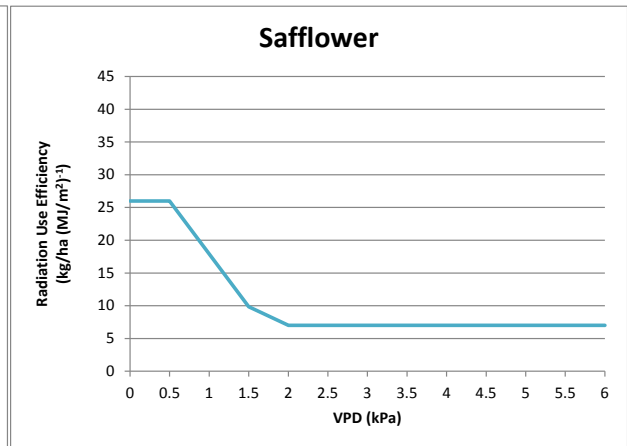


RUE-330 = 26 & RUE-660 = 33

VPD Effects

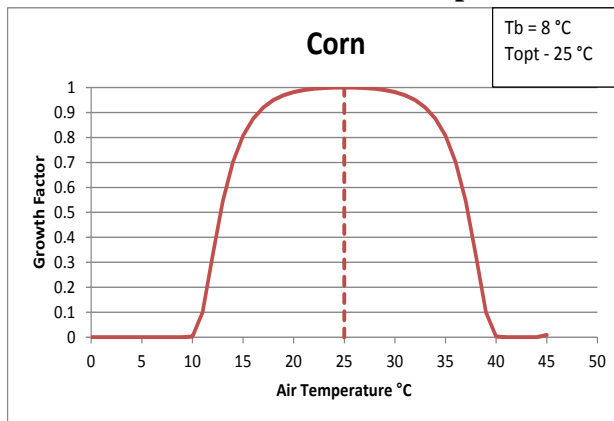


RUE-Amb = 40, RUE-VPD = 8, RUE-Thrshld= 7

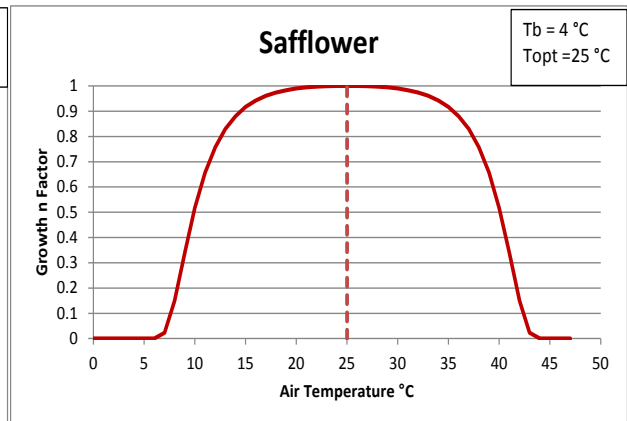


RUE-Amb = 26, RUE-VPD = 32, RUE-Thrshld= 0.5

Plant Growth Parameters – Temperature



Tbase = 8, Topt = 25



Tbase = 4, Topt = 25

Figure 5.4.7 Plant Growth Parameters – Corn & Safflower - Radiation Use Efficiency (RUE) and Temperature Effects on Growth

For corn, there is little effect of CO₂ on RUE except at concentrations above 660 ppm in which case it decreases. This is most likely not representative of actual corn response which should

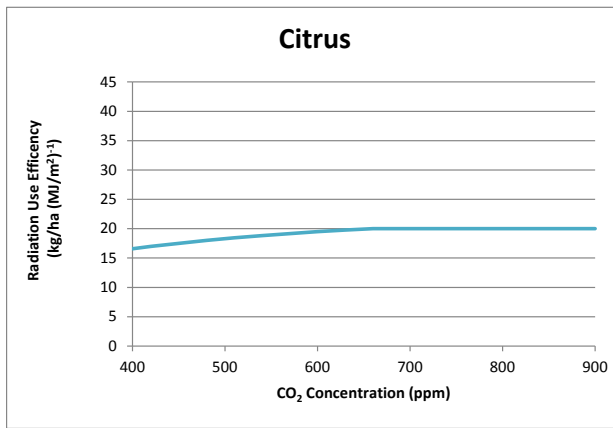
Plant Physiological Responses to Atmospheric Forcings

remain constant. However, given that the purpose of this analysis is not to simulate actual RUE per se but rather to understand how crop responses are affected by atmospheric forcings, this limitation was not addressed in this study. For safflower, RUE increases up 660 ppm and remains constant at higher concentrations.

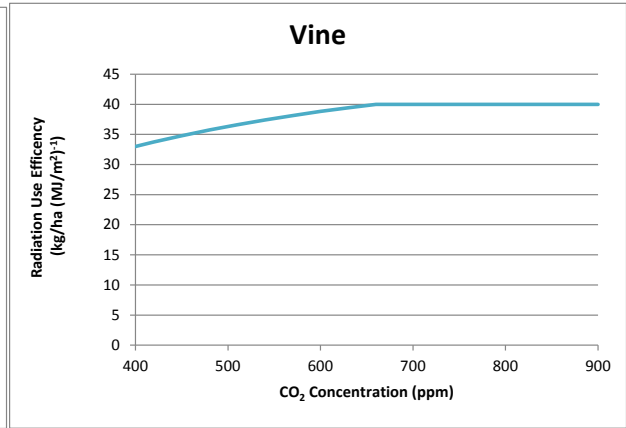
For corn, there is essentially no response to increasing VPD as the RUE-Thrshld of 7 is not reached in the simulations. In contrast, the RUE of safflower decreases significantly above the VPD threshold of 0.5 kPa. Both corn and safflower have the same optimum growth temperature but corn can grow at a lower basal temperature and has a more limited temperature growth range.

Figure 5.4.8 shows the effects of CO₂, VPD and temperature on RUE and heat stress for the citrus and vine crop group.

CO2 Effects

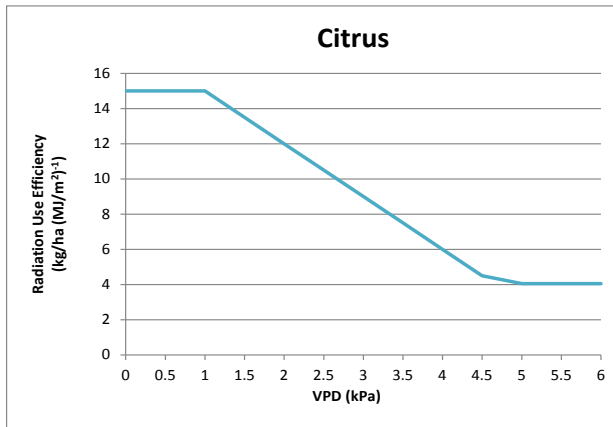


RUE-330 = 15 & RUE-660 = 20

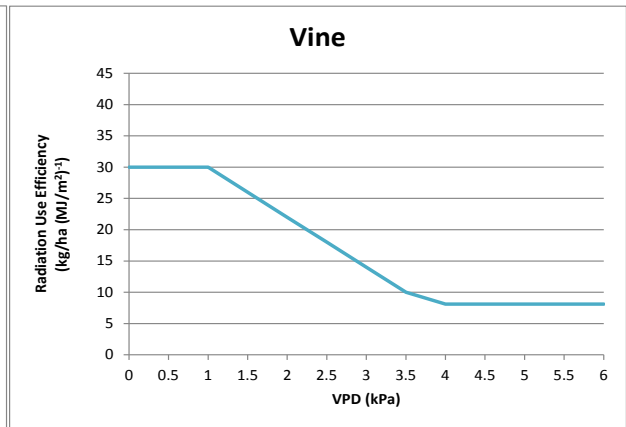


RUE-330 = 30 & RUE-660 = 40

VPD Effects

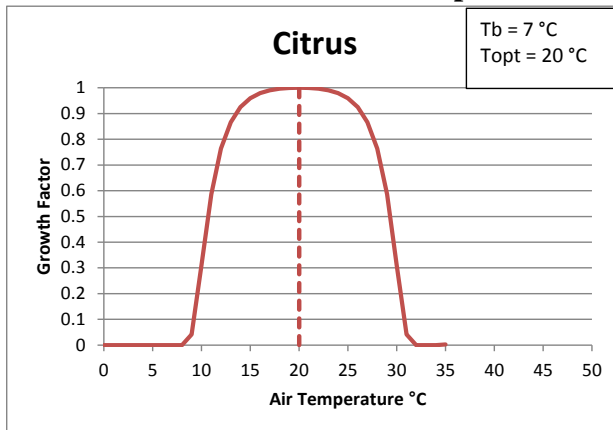


RUE-Amb = 15, RUE-VPD = 3, RUE-Thrshld= 1

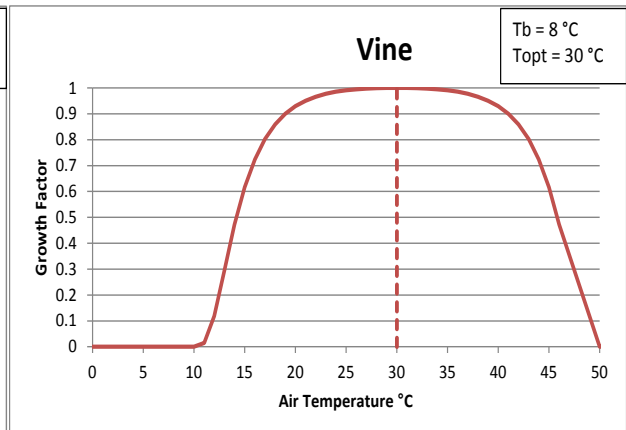


RUE-Amb = 30, RUE-VPD = 8, RUE-Thrshld= 1

Plant Growth Parameters – Temperature



Tbase = 7, Topt = 20



Tbase = 8, Topt = 30

Figure 5.4.8 Plant Growth Parameters – Citrus & Vine - Radiation Use Efficiency (RUE) and Temperature Effects on Growth

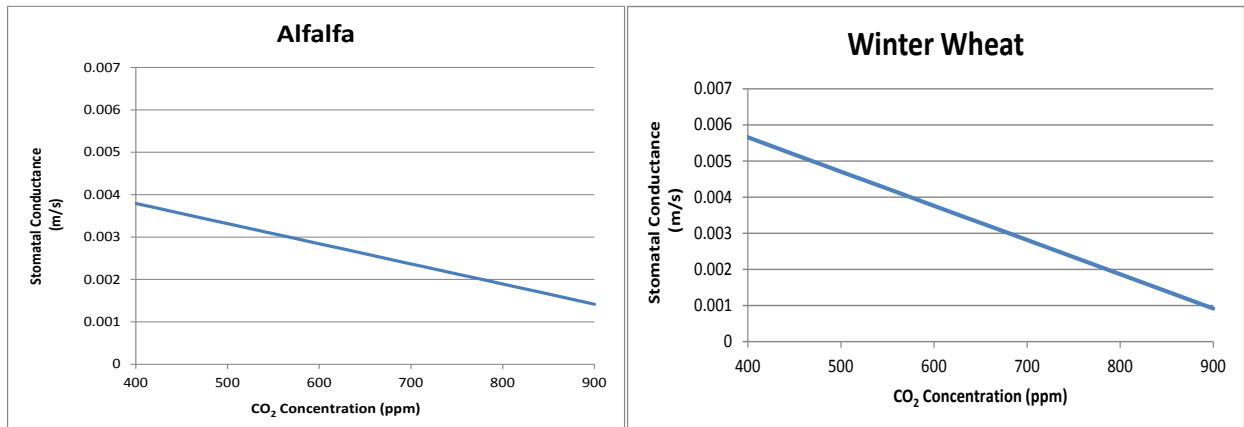
For both crops, RUE increases with CO₂ up to a concentration of 660 ppm and remains constant at higher concentrations. Vine RUE is inherently greater than citrus. However, both crops have

Plant Physiological Responses to Atmospheric Forcings

reduced RUE at VPD above 1 kPa. The effect is greater for vines with an RUE-VPD slope of 8 versus 3 for citrus. The basal and optimal temperatures for citrus are lower than for vines.

The transpiration responses to CO₂ and VPD for the alfalfa and winter wheat crop group are shown on Figure 5.4.9. These parameters include the effects of CO₂ (SC-330 & SC-660); effects of VPD above the VPD threshold (VPD-thrshld) and the stomatal conductance (SC) at a VPD of 4 kPa (VPD-Rdct_4).

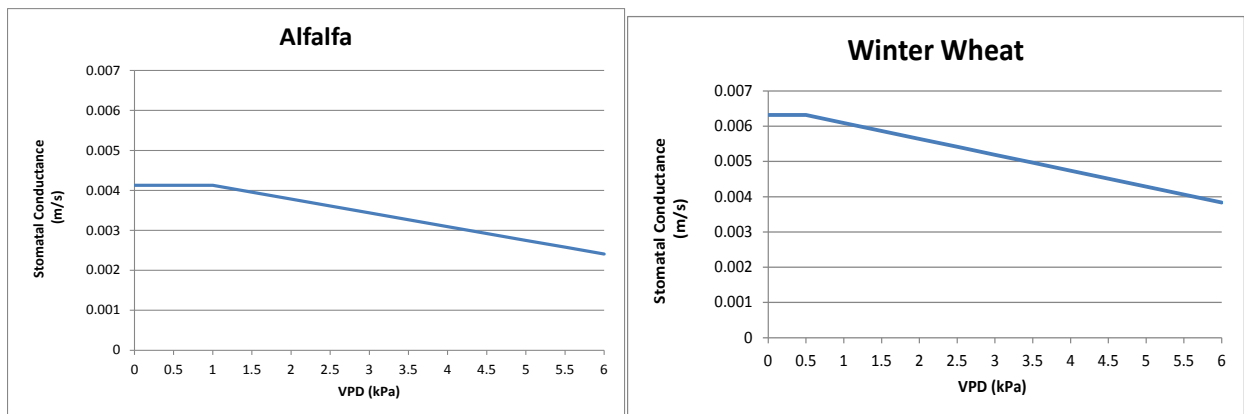
CO₂ Effects



SC-330 = 0.0041 & SC-660 = 0.0026

SC-330 = 0.0063 & SC-660 = 0.0032

VPD Effects



VPD-thrshld = 1 & VPD-Rdct_4 = 0.75

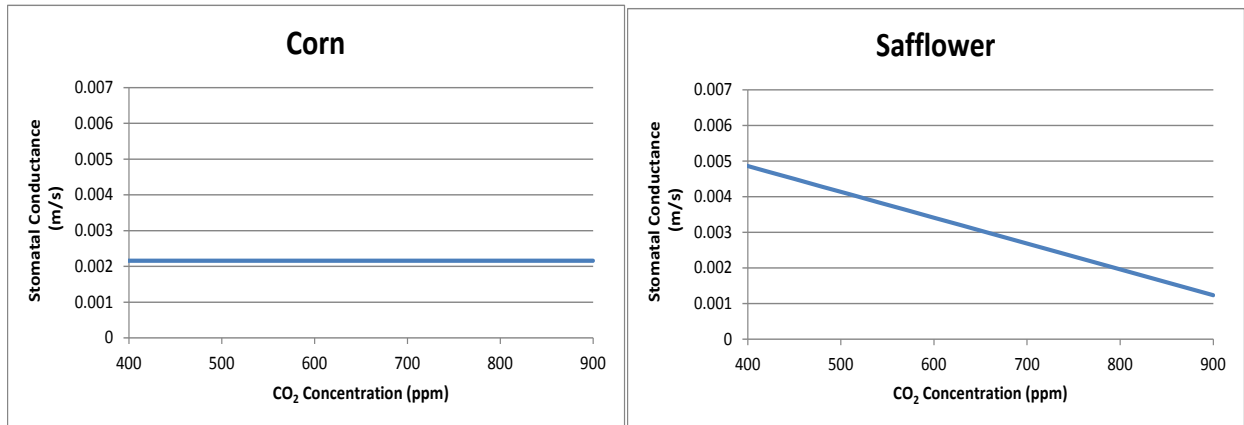
VPD-thrshld = 0.5 & VPD-Rdct_4 = 0.75

Figure 5.4.9 Plant Growth Parameters – Alfalfa & Winter Wheat - Stomatal Conductance Effects on Transpiration

The stomatal conductance (SC) of both crops decreases with increasing CO₂ concentration. In this study, it is assumed that the linear decrease in SC occurs at concentrations greater than 660 ppm. Winter wheat has a higher SC than alfalfa at CO₂ concentrations below 800 ppm. Above this value, it has a slightly lower SC. The SC of winter wheat starts to decrease at lower a VPD than alfalfa (VPD-thrshld – 0.5 vs 1 for alfalfa).

The transpiration responses to CO₂ and VPD for the corn and safflower crop group are shown on Figure 5.4.10.

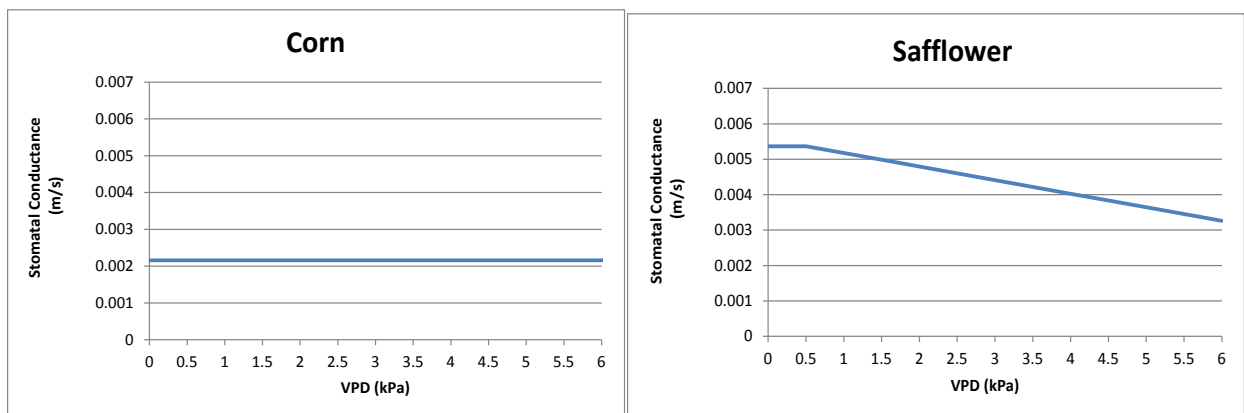
CO₂ Effects



SC-330 = 0.0022 & SC-660 = 0.0022

SC-330 = 0.0053 & SC-660 = 0.0030

VPD Effects



VPD-thrshld = 7 & VPD-Rdct_4 = 0.99

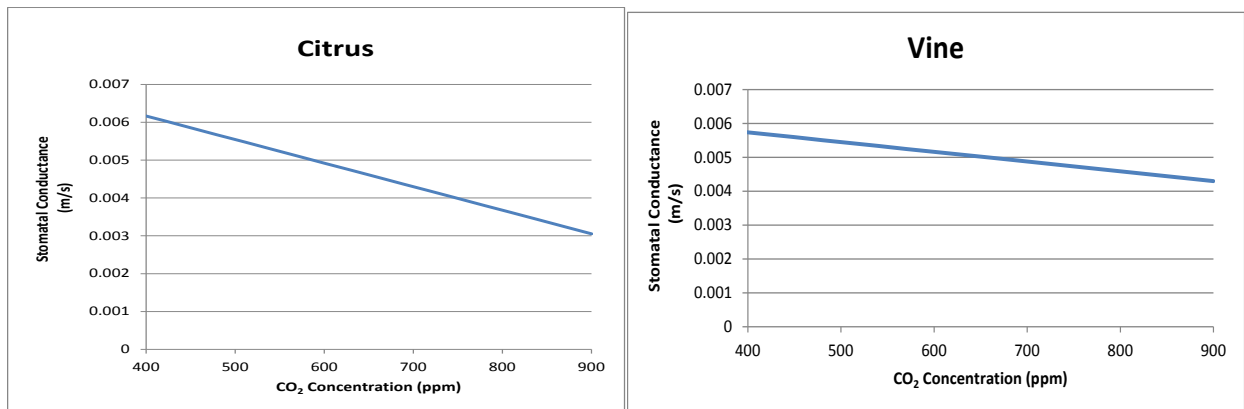
VPD-thrshld = 0.5 & VPD-Rdct_4 = 0.75

Figure 5.4.10 Plant Growth Parameters – Corn & Safflower - Stomatal Conductance Effects on Transpiration

The SC of safflower is greater than that of corn up to a CO₂ concentration of about 800 ppm. Unlike safflower, the C₄ corn crop has a constant SC that does not decrease with either increasing CO₂ or VPD. In contrast, safflower's SC begins to decrease at VPDs above 0.5 kPa.

Figure 5.4.11 shows the transpiration responses of the citrus and vines crop group.

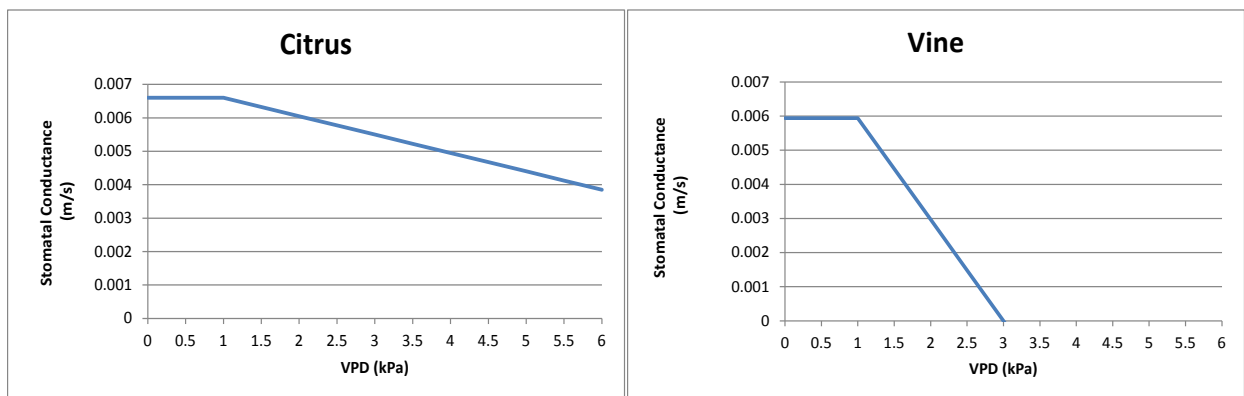
CO2 Effects



SC-330 = 0.0066 & SC-660 = 0.0045

SC-330 = 0.0059 & SC-660 = 0.0050

VPD Effects



VPD-thrshld = 1 & VPD-Rdct₄ = 0.75

VPD-thrshld = 1 & VPD-Rdct_{1.5} = 0.75

Figure 5.4.11 Plant Growth Parameters – Citrus & Vine - Stomatal Conductance Effects on Transpiration

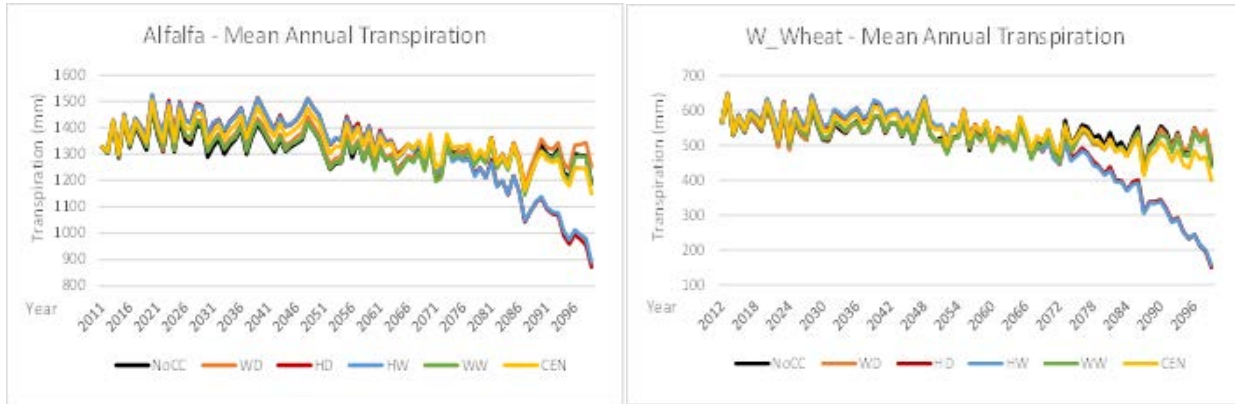
The SC of citrus is slightly greater than that of vines up to a CO₂ concentration of about 700 ppm. The SC of vines begins to decrease rapidly at VPDs above 0.5 kPa reaching a complete cessation of transpiration at a VPD of 3 kPa. This may be physiologically unrealistic over an extended time period but unlikely to affect most of the simulations performed in this study. The SC of citrus remains larger than vines at VPDs above approximately 1.75 kPa.

5.5 Transpiration Responses to Atmospheric Forcings

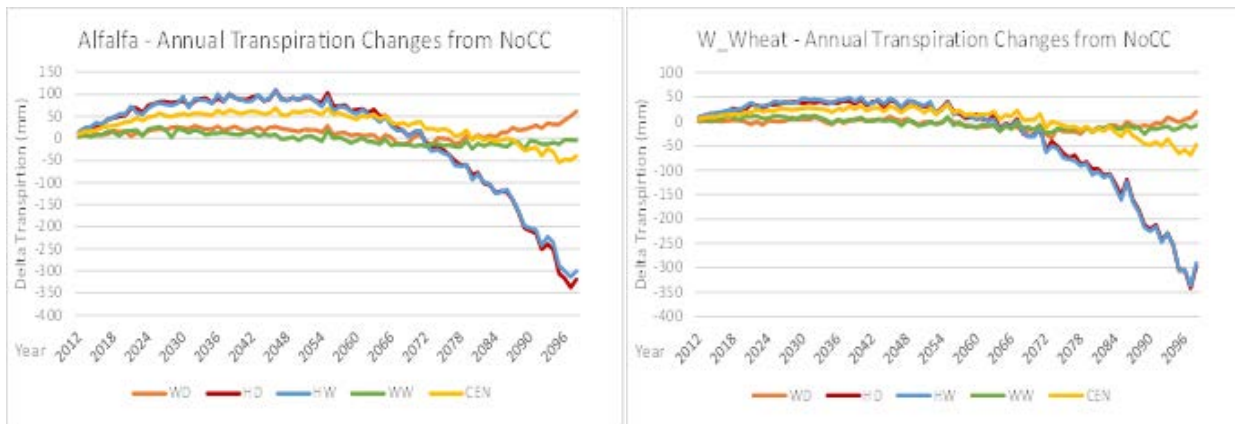
The primary crop parameters affecting transpiration are the stomatal conductance (SC) and the amount and rate of canopy development during the growth period. For the alfalfa and winter wheat crop group, both crops' canopy LAI increases with increasing CO₂ concentration (Figure 5.4.2). However, both respond to increasing CO₂ with decreased stomatal conductance (Figure 5.4.8). The SC threshold VPD for winter wheat is slightly lower than for alfalfa but alfalfa's SC

decreases more rapidly with increasing VPD. Figure 5.5.1 shows mean annual transpiration along with changes in mean annual and period mean monthly transpiration relative to the NoCC reference scenario.

Mean Annual Time Series



Changes from NoCC Scenario



Period Mean Monthly Changes from NoCC Scenario

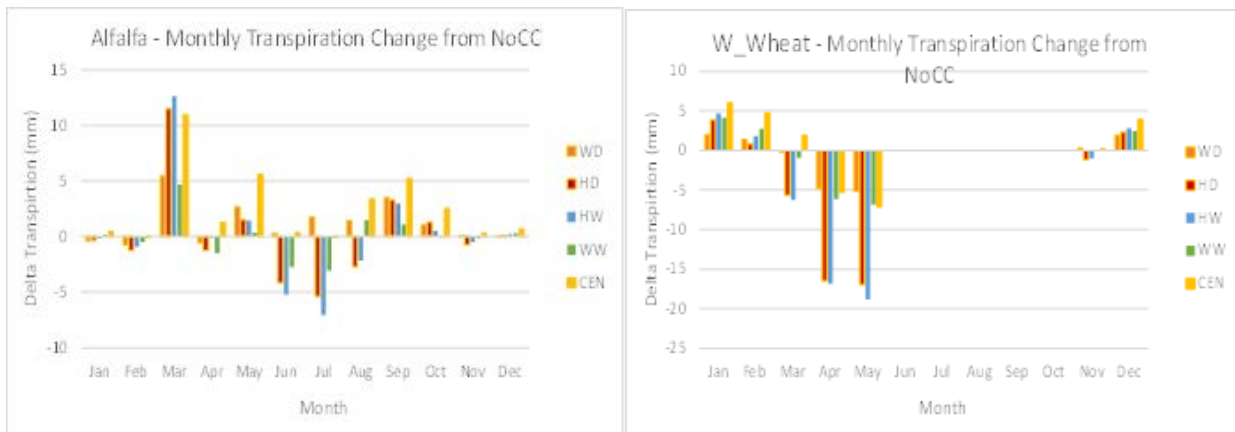


Figure 5.5.1 Transpiration – Alfalfa and Winter Wheat (W_Wheat) by Scenario

During the study period, there is an initial increase in transpiration of both crops. In the hot HD and HW, this increase begins to decline in the mid-century and becomes a strong decrease by the end of the study period relative to the NoCC scenario. Table 5.5.1 provides an analysis of the correlations between the alfalfa and winter wheat transpiration and the atmospheric forcing variables.

Table 5.5.1 Correlations of Alfalfa & Winter Wheat Transpiration with Atmospheric Forcings

Alfalfa	Climate Scenario		
	<i>HD</i>	<i>CEN</i>	<i>WW</i>
Climate Variable	Transpiration - Correlation Coefficients		
CO ₂ (ppm)	-0.89	-0.75	-0.68
T _{max} (C)	-0.35	0.21	0.68
R _s (MJ/m ²)	0.78	0.77	0.74
VPD (kPa)	0.07	0.67	0.90
Winter Wheat	Climate Scenario		
	<i>HD</i>	<i>CEN</i>	<i>WW</i>
Climate Variable	Transpiration - Correlation Coefficients		
CO ₂ (ppm)	-0.79	-0.42	-0.25
T _{max} (C)	-0.29	0.27	0.53
R _s (MJ/m ²)	0.69	0.50	0.41
VPD (kPa)	0.04	0.46	0.50

The highest correlations are the negative correlations with CO₂ and the positive correlations with R_s both of which increase in magnitude from WW to HD scenario. However, as shown in Table 5.3.1, R_s is also strongly correlated with CO₂ and it declines steadily throughout the study period as CO₂ increases. Both the T_{max} and VPD have high positive correlations that decrease from WW to HD scenario. The relationship between changes in transpiration, CO₂ and VPD are shown in Figure 5.5.2.

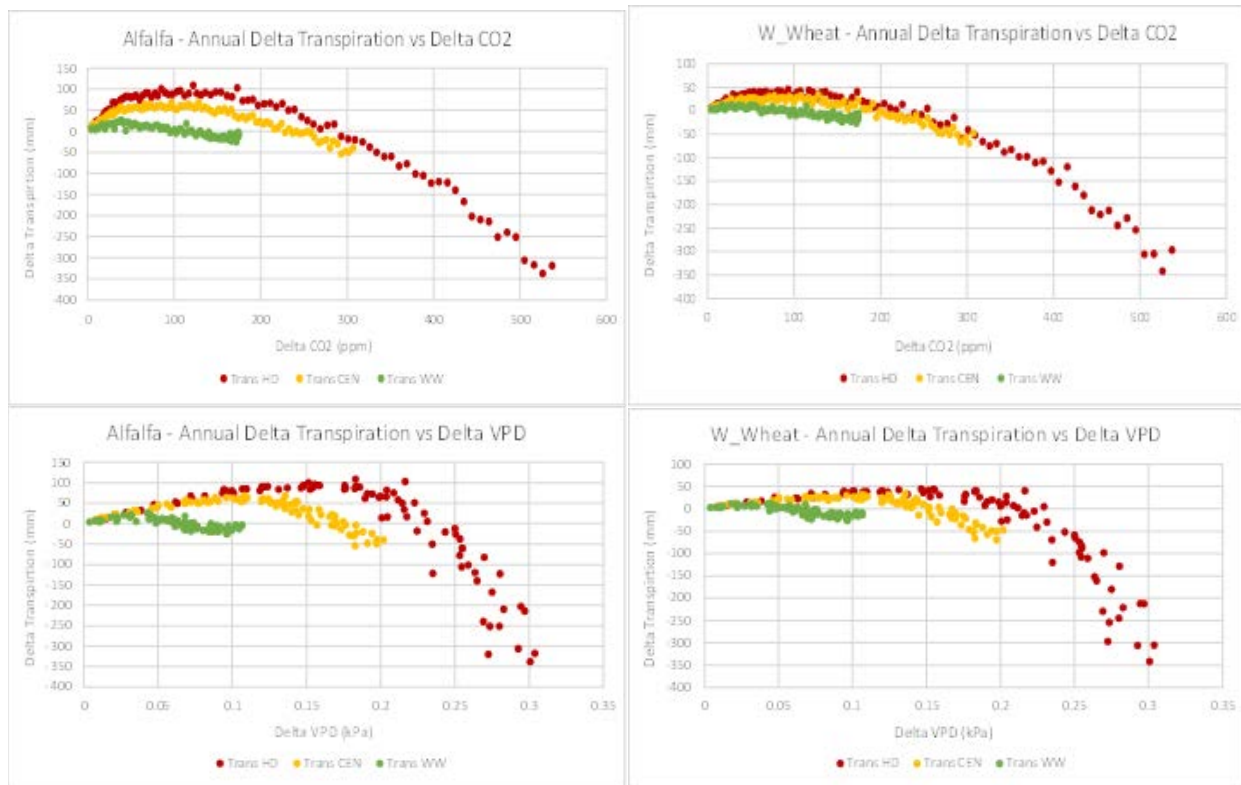


Figure 5.5.2 Changes in Transpiration - Alfalfa & Winter Wheat with Changes in CO₂ and VPD by Scenario

For these crops, transpiration would not be expected to increase with increasing CO₂ and decreasing Rs. These forcings do not account for the early period increases in transpiration. More likely, the early increases in transpiration are driven by increases in temperature (Figure 4.3.3) that increase the canopy's rate of development as well as increases in CO₂ that increase the canopy LAI (Figure 5.4.2). Subsequently, the continuing increases in VPD and CO₂ eventually become large enough to counter act these effects and drive down the transpiration of both crops (Figure 5.4.8).

Interestingly, there are increases in transpiration during the winter months which become decreases in summer months with the largest decreases in the hot HD scenario. Since CO₂ concentration is only changing on an annual basis, these effects must be related to seasonal changes in temperature and VPD. As noted in Table 5.3.2, there is a very strong correlation between VPD and Tmax in all the climate scenarios. Figure 5.5.3 shows the alfalfa and winter wheat monthly transpiration for the HD, CEN, and WW scenarios.

Plant Physiological Responses to Atmospheric Forcings

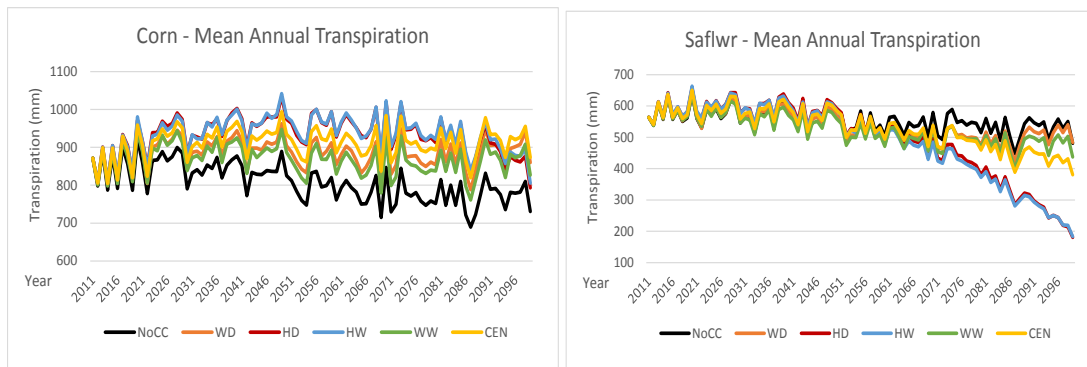


Figure 5.5.3 Period Mean Monthly Changes in Transpiration and VPD by Scenario

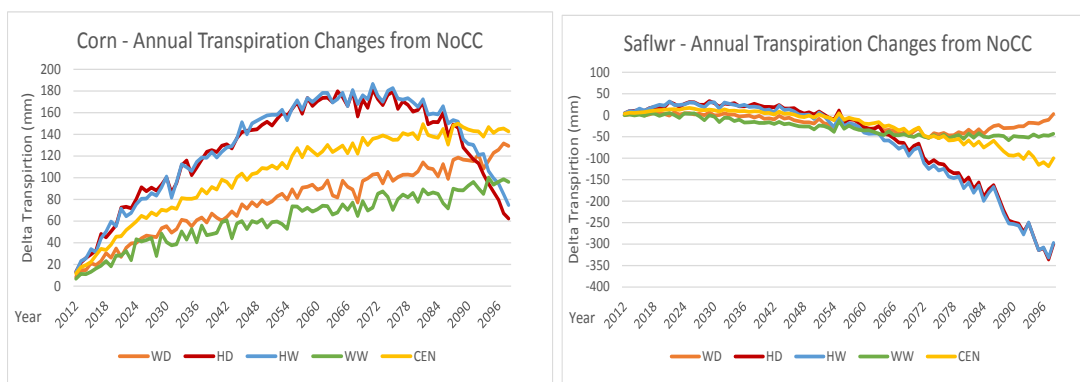
In this case, alfalfa with its higher VPD threshold (Figure 5.4.5) and higher basal and optimal growth temperature responds with increased canopy growth (Figure 5.4.2) without any VPD reduction in SC during the winter and even some of the fall months. These responses correspond with the months of November through March which have period average VPD less than 1 kPa (alfalfa threshold). In contrast, winter wheat with its greater sensitivity to VPD only has increased transpiration in the months December, January and February and which have period average VPDs of less than 0.5 kPa (winter wheat threshold).

For the corn and safflower crop group, only safflower has increased canopy LAI with increasing CO₂ concentration (Figure 5.4.3). Because corn is a C₄ crop, it's maximum LAI is unresponsive to increasing CO₂. However, the maximum canopy LAI of corn is greater than safflower and the onset of senescence is significantly greater than safflower. Similarly, only safflower responds to increasing CO₂ and VPD above its threshold value (0.5 kPa) with decreased stomatal conductance (Figure 5.4.9). Figure 5.5.4 shows mean annual transpiration along with changes in mean annual and period mean monthly transpiration relative to the NoCC reference scenario for both crops.

Mean Annual Time Series



Changes from NoCC Scenario



Period Mean Monthly Changes from NoCC Scenario

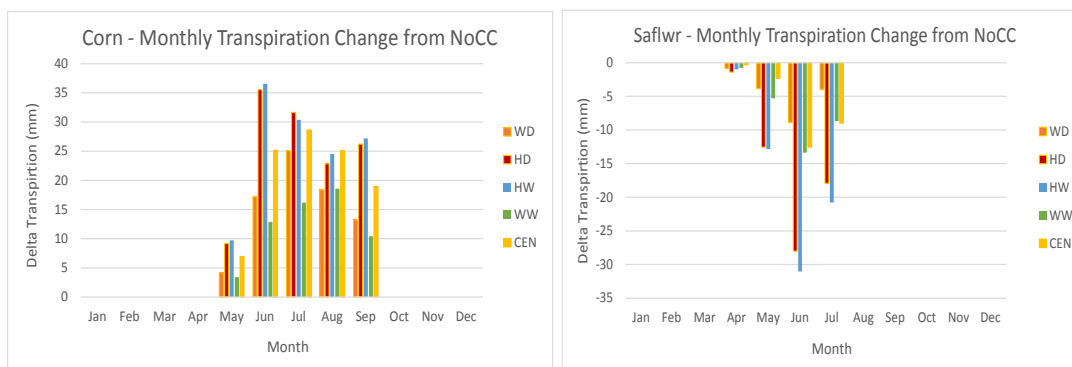


Figure 5.5.3 Transpiration – Corn and Safflower (Safldr) by Scenario

For corn, there is an increase in transpiration in all scenarios through the mid-century. However, in the hot HD and HW scenarios, this large increase starts reversing in mid-century and becomes a large decline by the end of the study period. In contrast, transpiration in scenarios with less warming continues to increase except that the CEN begins to reach its maximum near the end of the study period. For safflower, the mid to late study period changes in transpiration closely correspond to the changes in CO₂ (Figure 5.3.10) and VPD (Figure 5.3.13). Based on the sensitivities of safflower to these atmospheric forcings (Figures 5.4.9), this correspondence is

reasonable. Table 5.5.2 shows the correlations of corn and safflower transpiration with the atmospheric forcings.

Table 5.5.2 Correlations of Corn and Safflower Transpiration with Atmospheric Forcings

Corn	Climate Scenario		
	<i>HD</i>	<i>CEN</i>	<i>WW</i>
Climate Variable	Transpiration - Correlation Coefficients		
CO ₂ (ppm)	-0.23	0.09	-0.23
Tmax (C)	0.35	0.65	0.66
Rs (MJ/m ²)	0.25	0.12	0.40
VPD (kPa)	0.64	0.79	0.80
Safflower	Climate Scenario		
	<i>HD</i>	<i>CEN</i>	<i>WW</i>
Climate Variable	Transpiration - Correlation Coefficients		
CO ₂ (ppm)	-0.95	-0.88	-0.79
Tmax (C)	-0.50	-0.08	0.47
Rs (MJ/m ²)	0.82	0.84	0.78
VPD (kPa)	-0.07	0.46	0.78

For corn, the highest correlations are strongly positive with VPD and to lesser degree with Tmax. However from Table 5.3.2, it is clear that there is a very high correlation between Tmax and VPD. Because corn is not modeled as responding to VPD in this study, these changes in corn transpiration are most likely attributable to changes in temperature which increases growth until the optimal growth temperature is exceeded. Since a decrease in Rs would not cause an increase in transpiration, Rs does not play a significant role until late in the century when both declining Rs and increasing temperature combine to cause corn transpiration to decrease very rapidly. Figure 5.5.4 shows changes in corn and safflower transpiration as a function of changes in Tmax.

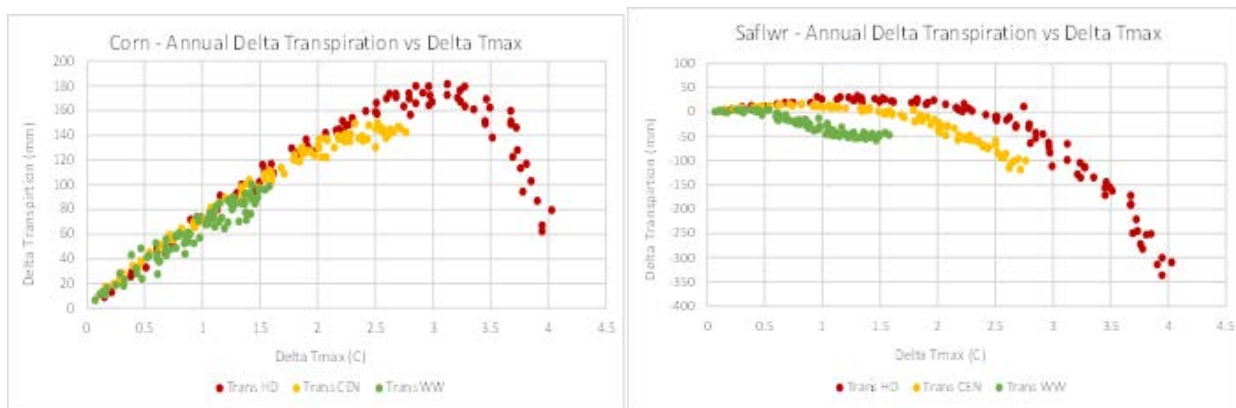


Figure 5.5.4 Changes in Corn and Safflower Transpiration and Changes in Tmax by Scenario

For safflower, the highest correlations are with CO₂ and R_s. However, CO₂ and R_s have a strong inverse correlation. Safflower transpiration decreases with both rising CO₂ and VPD once the threshold is exceeded which explains why the early century increase is due to increased canopy LAI and more rapid growth but becomes a mid to late century decline as CO₂ and VPD increase. Figure 5.5.5 shows the period mean monthly changes in corn and safflower transpiration as a function of T_{max}.



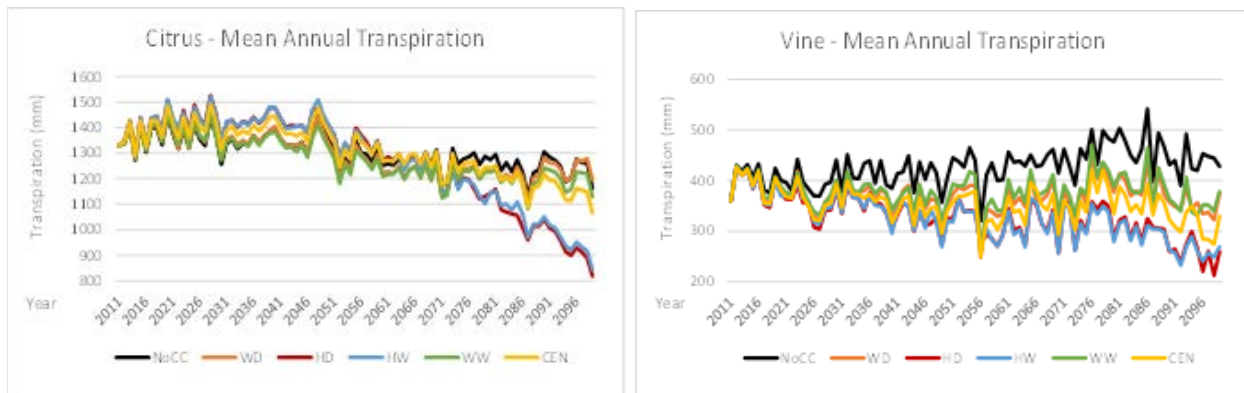
Figure 5.5.5 Period Mean Monthly Changes in Transpiration and Tmax by Scenario

For corn, the largest monthly increases in transpiration occur in the early spring in the HD scenario. In the summer, it declines slightly in the warmer months. The CEN scenario shows lesser increase in transpiration but continuing to increase into the early summer while the less warming WW scenario shows rising transpiration through most of the summer. Clearly, these seasonal changes are reflective of temperature effects on the rate of canopy development and the optimal growth temperature. For safflower, there are declines in transpiration that correspond to increases in CO₂ as well as increases in temperature beyond the optimal growth temperature (25 °C) in the warm season months (Figure 5.3.5). The period average T_{max} exceeds 25 °C in months from May through October which corresponds closely the decreases in monthly decreases in transpiration. From Figure 5.3.5, it is clear that the increases in T_{max} correspond closely with the decreases in transpiration.

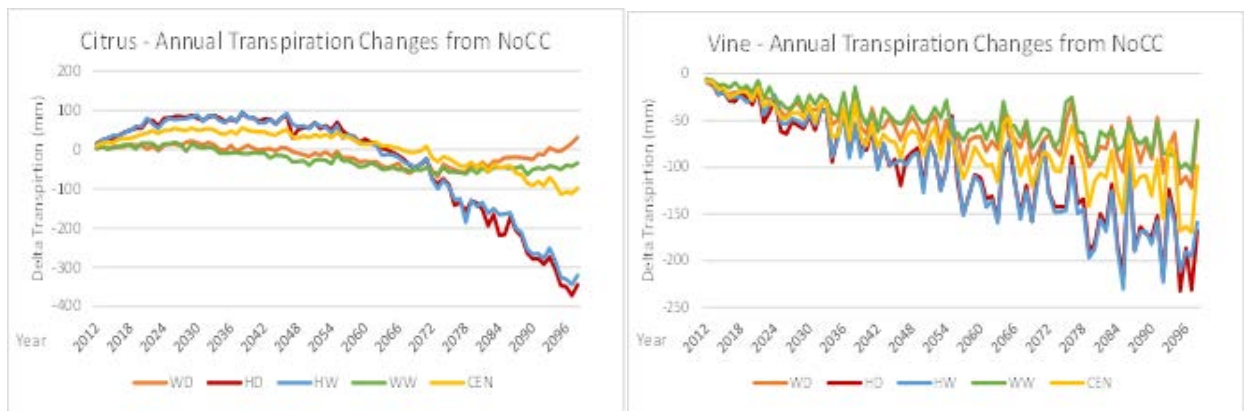
The citrus and vine crop group is representative of perennial crops. Unlike citrus, vine is a deciduous crop whose canopy increases rapidly during the spring, reaches maturity in the summer and senesces in the fall (Figure 5.4.4). In contrast, citrus is a non-deciduous crop which has constant canopy LAI. Neither of these crop's canopy LAI is responsive to increasing CO₂ but the stomatal conductance of both decrease with increasing CO₂ and VPD. Citrus has a lower optimal growth temperature and narrower growth range than vine (Figure 5.4.7). Figure 5.5.6 shows the changes in mean annual transpiration during the study period along with changes relative to the NoCC for the mean annual transpiration and study period monthly means.

Plant Physiological Responses to Atmospheric Forcings

Mean Annual Time Series



Changes from NoCC Scenario



Period Mean Monthly Changes from NoCC Scenario

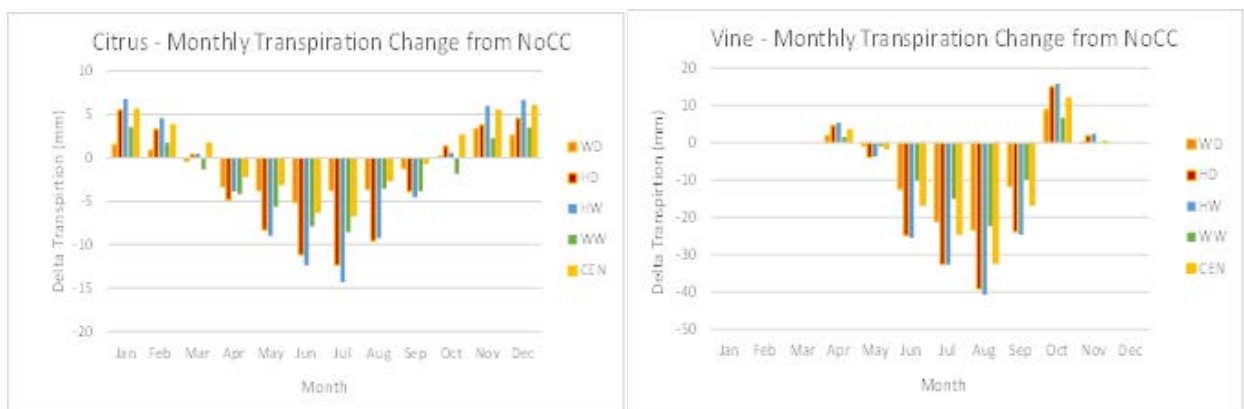


Figure 5.5.6 Transpiration – Citrus and Vine by Scenario

In the early study period, citrus transpiration increases all scenarios but in the hot HD and HW scenarios there is a significant decline in mid to late century period. Furthermore, in the warm WD and WW scenarios there is some slight increased transpiration near the end of the century. This increase corresponds closely with the decrease in CO₂ that occurs during this period in these scenarios (Figure 5.3.10). For vines, transpiration declines steadily throughout the study period

with largest declines in the hot HD and HW which is reasonable given its sensitivity to both increased CO₂ and VPD.

Despite the overall declines in transpiration, both crops show a tendency toward some increased transpiration in the cooler winter and fall months along with large declines in the hotter summer months. These seasonal differences are indicative of temperature sensitivity during the months of increased transpiration being closer to the optimal growth temperature (Figure 5.4.7). For citrus, its optimal growth temperature is exceeded in all months from April through October while vines optimal growth temperature is exceeded only in the months from June through September. These effects can be clearly seen in Figure 5.5.6.

Additionally, during the months of increased transpiration, the hot scenarios which have higher CO₂ and VPD show the most increase in transpiration. However, in the warmer summer months, the hotter scenarios have the most reduction in transpiration revealing a combined effect of unfavorable temperatures limiting growth along with CO₂ and VPD reducing stomatal conductance. Table 5.5.3 shows the correlations of corn and safflower transpiration with the atmospheric forcings.

Table 5.5.3 Correlations of Citrus and Vine Transpiration with Atmospheric Forcings

Citrus	Climate Scenario		
	<i>HD</i>	<i>CEN</i>	<i>WW</i>
Climate Variable	Transpiration - Correlation Coefficients		
CO ₂ (ppm)	-0.95	-0.88	-0.84
Tmax (C)	-0.45	0.03	0.56
Rs (MJ/m ²)	0.85	0.88	0.87
VPD (kPa)	0.00	0.56	0.86
Vine	Climate Scenario		
	<i>HD</i>	<i>CEN</i>	<i>WW</i>
Climate Variable	Transpiration - Correlation Coefficients		
CO ₂ (ppm)	-0.70	-0.39	-0.04
Tmax (C)	-0.65	-0.33	-0.11
Rs (MJ/m ²)	0.50	0.24	0.01
VPD (kPa)	-0.53	-0.29	-0.23

For citrus, there are large negative and positive correlations associated with CO₂ and Rs. As discussed previously, Rs has a strong negative correlation with CO₂. Both decreasing Rs and increasing CO₂ are causative factors explaining the decrease in transpiration. There is also a high correlation of citrus transpiration with VPD and to a lesser degree with Tmax in the WW scenario. Tmax is highly correlated with VPD in all scenarios (Table 5.3.2). However, the Tmax correlation decreases and becomes negative in the HD scenario. This pattern indicates that as temperature increases in the early study period, growth initially increased transpiration before increases in CO₂ and VPD offset these increases. For vines, there are weak CO₂ and Rs correlations in the WW scenario which become strong in the HD scenario indicating the

dominant effect of CO₂ as vines have relatively large temperature range. Figure 5.5.7 shows the relationships between transpiration, CO₂ and VPD for these crops.

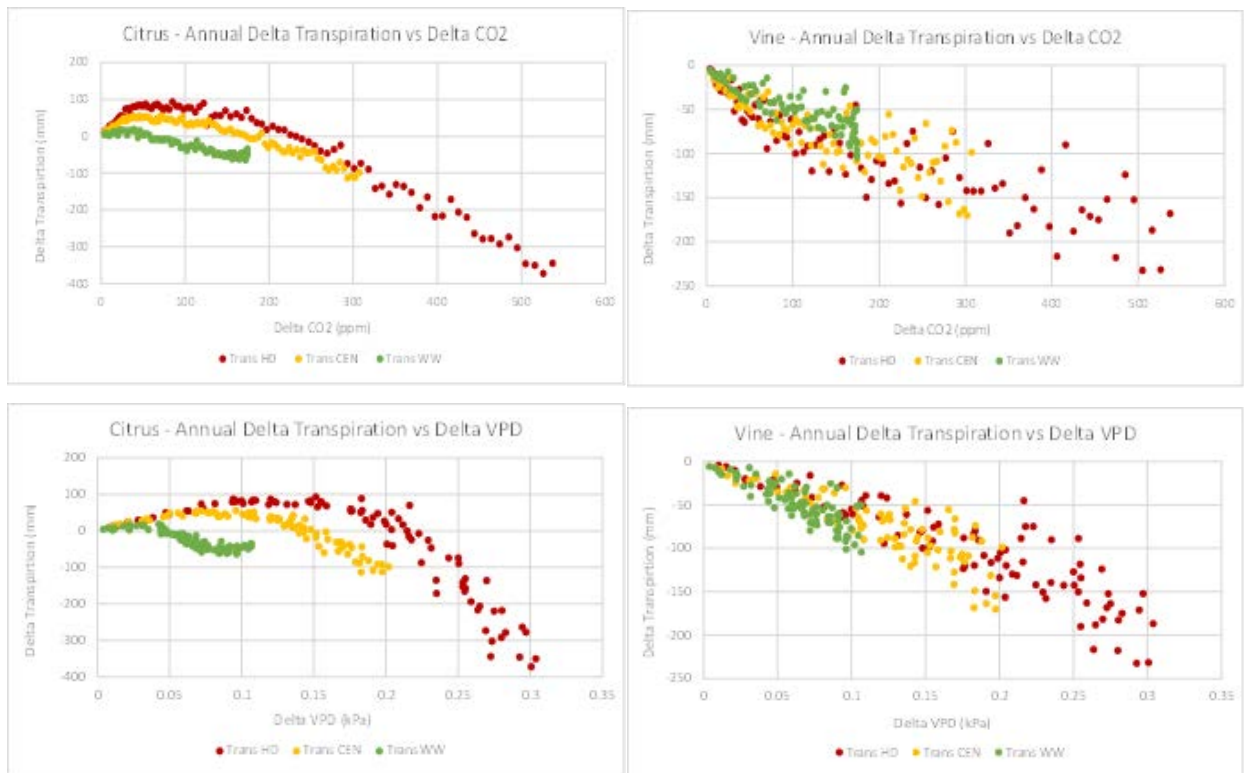


Figure 5.5.7 Changes in Citrus and Vine Transpiration and Changes in CO₂ and VPD by Scenario

For citrus, the hot HD scenario has higher transpiration than the NoCC scenario until CO₂ increases by about 200 ppm and/or VPD increases by about 0.2 kPa. Since any increase in CO₂ relative the NoCC scenario reduces transpiration in citrus, this increase is clearly related to improved growing conditions in fall and winter seasons (Figure 5.5.6). Although there are some slight increases in the cooler early spring and fall seasons when its VPD threshold is not exceeded, annual vine transpiration declines constantly throughout the study period. This decline in annual transpiration is well correlated with increasing CO₂ in all the scenarios.

5.6 Biomass and Yield Responses to Atmospheric Forcings

In the WEAP-PGM model crop yield is computed as tons per acre on a dry weight basis (Tons/acre) directly from accumulated biomass after the crop has accumulated sufficient heat units to complete its growth period. However, yield can be reduced by such factors as heat stress and water stress. In this study, all crops were simulated in such a way as to avoid the occurrence any water related stress. Furthermore, WEAP-PGM does not account for any nutrient related limitations on growth. In the crop yield simulations, it is also assumed that crop management practices including irrigation and fertilization are identical to those resulting in the simulated yields from the SWAP model.

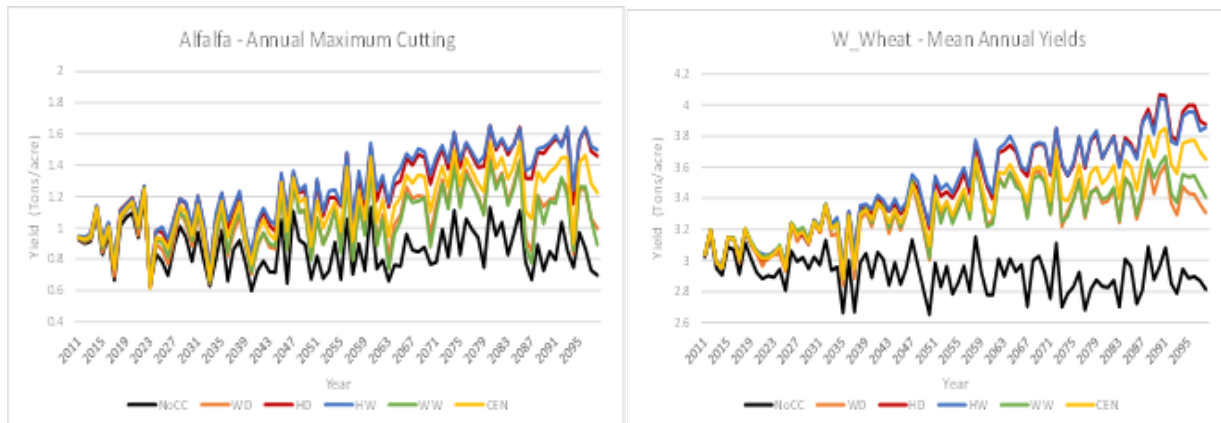
The primary crop parameters affecting crop biomass and yield are the radiation use efficiency (RUE), the amount and rate of canopy development along with growth limitations due to unfavorable temperatures during the growth period. As previously discussed, increased CO₂ can increase the maximum canopy LAI of some crops. It can also increase the crop's RUE which in turn increases the amount of biomass produced per unit of Rs received which potentially increases both biomass and crop yield. Increases in temperature up to the optimal temperature (Topt) increase the growth factor (GF) which increases biomass and yield. However, temperature increases above Topt reduce the GF resulting in reduced biomass and yield.

For the alfalfa and winter wheat crop group, both crops have increased canopy LAI (Figure 5.4.2) and increased RUE (Figure 5.4.5) with increasing CO₂ concentration. However, increases in VPD beyond the threshold VPD reduces the RUE of winter wheat at a slightly lower VPD threshold (0.5kPa) than for alfalfa (Figure 5.4.5) but the rate of decline per unit increase in VPD is greater for alfalfa than winter wheat. Alfalfa has higher basal growth temperature (Tb) and Topt than winter wheat. In WEAP-PGM, alfalfa is harvested on fixed schedule. In this study, its annual yield is reported as the maximum cutting yield. All yields are reported in units of dry weight tons/acre and reported biomass is considered actual biomass without partitioning into above and below ground portions.

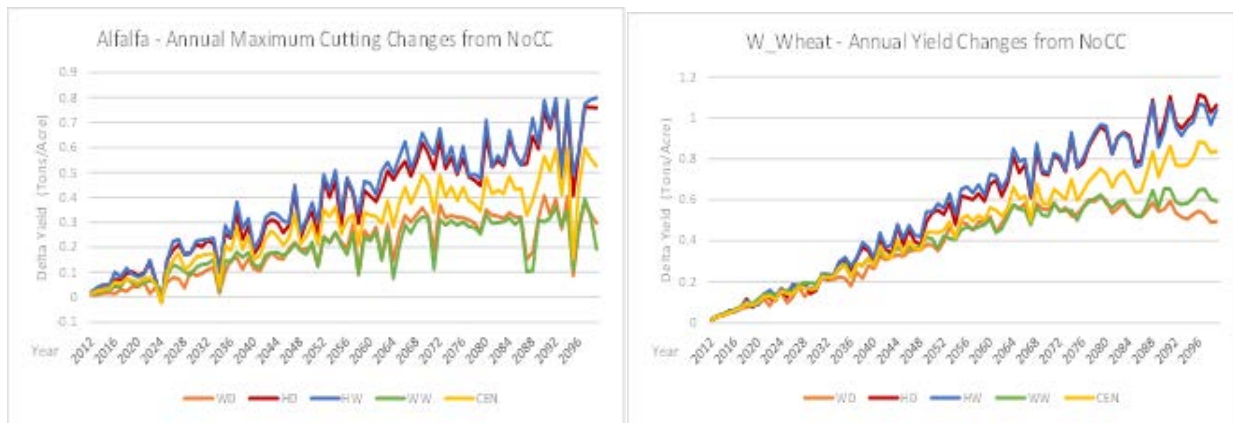
Figure 5.6.1 shows annual maximum alfalfa cuttings and mean annual wheat yields along with their changes relative to the NoCC reference scenario over the study period. Period mean monthly changes in biomass are also reported.

Plant Physiological Responses to Atmospheric Forcings

Mean Annual Time Series



Changes from NoCC Scenario



Period Mean Monthly Changes from NoCC Scenario

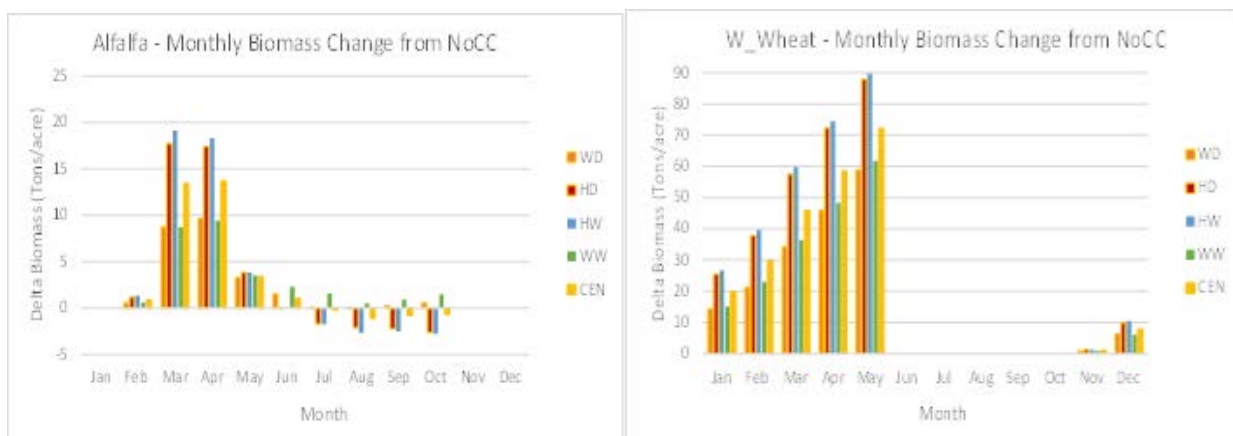


Figure 5.6.1 Biomass and Yield – Alfalfa and Winter Wheat (W_Wheat) by Scenario

For both alfalfa and winter wheat, yields increase steadily in all scenarios with the largest increases in the hot HD and HW scenarios. Wheat with its higher RUE and CO₂ responses (Figure 5.4.5) has a larger yield increases relative to the NoCC scenario than alfalfa. For both

crops there is definite change in the rate of yield increase in the warm WD and WW scenarios at the end of the study period. This change in rate of increase clearly corresponds with the leveling off and even slight declines in CO₂ at the end of the study period in the warm scenarios (Figure 5.3.10). In the hot HD and HW scenarios, in which CO₂ continues to increase, yields continue to rise. It is also clear from Figure 5.6.1 that the increases in biomass are primarily occurring in the cooler winter and spring months. For alfalfa, its VPD threshold is exceeded in the months of May through October. These months generally correspond with reduced biomass production. In contrast, despite its VPD threshold and optimal growth temperature being exceeded in the winter and spring months, winter wheat's biomass increases in proportion to the increasing CO₂ increasing its canopy LAI and increasing temperature within its optimal growth range (Figure 5.4.5).

Table 5.6.1 presents the crop yield correlations with the atmospheric forcings for these crops.

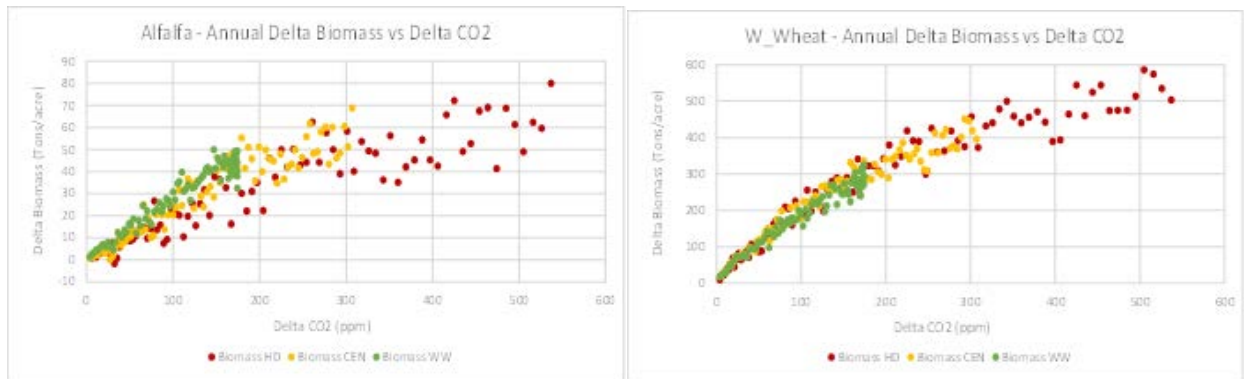
Table 5.6.1 Correlations of Alfalfa and Winter Wheat (W_Wheat) Yield with Atmospheric Forcings by Scenario

Alfalfa	Climate Scenario		
	<i>HD</i>	<i>CEN</i>	<i>WW</i>
Climate Variable	Yield - Correlation Coefficients		
CO ₂ (ppm)	0.79	0.68	0.45
Tmax (C)	0.72	0.54	0.35
Rs (MJ/m ²)	-0.70	-0.56	-0.33
VPD (kPa)	0.34	0.08	0.01
W_Wheat	Climate Scenario		
	<i>HD</i>	<i>CEN</i>	<i>WW</i>
Climate Variable	Yield - Correlation Coefficients		
CO ₂ (ppm)	0.68	0.61	0.53
Tmax (C)	0.64	0.46	0.20
Rs (MJ/m ²)	-0.55	-0.45	-0.33
VPD (kPa)	0.34	0.07	-0.10

For both crops, the highest positive yield correlations are with CO₂ in all scenarios. These correlations become stronger as CO₂ concentrations increase. As previously discussed, there is a strong correlation between Tmax and VDP in all scenarios as well as between Tmax and CO₂ in the hot scenarios. The steady decline in Rs is highly correlated with CO₂ concentrations increase. A decline in Rs would tend to produce a decline in biomass and yield. However, this does not happen with these crops indicating simulative effects of CO₂ and warmer spring temperature are more than compensating for the declining Rs. Similar correlation coefficient patterns exist in the biomass correlation coefficients (not shown).

Figure 5.6.2 shows the changes in biomass and yield and changes in CO₂ relative to the NoCC reference by scenario for both crops.

Changes in Biomass and Changes in CO₂ by Scenario



Changes in Yield and Changes in CO₂ by Scenario

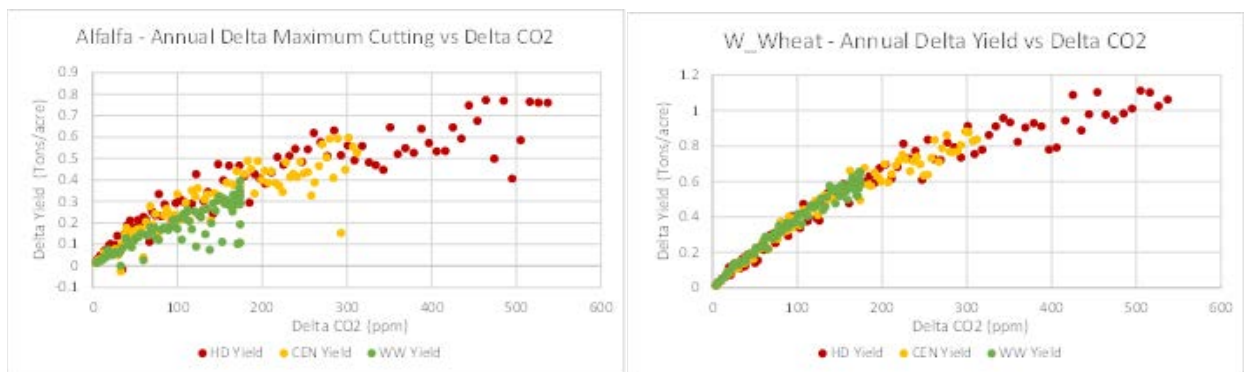


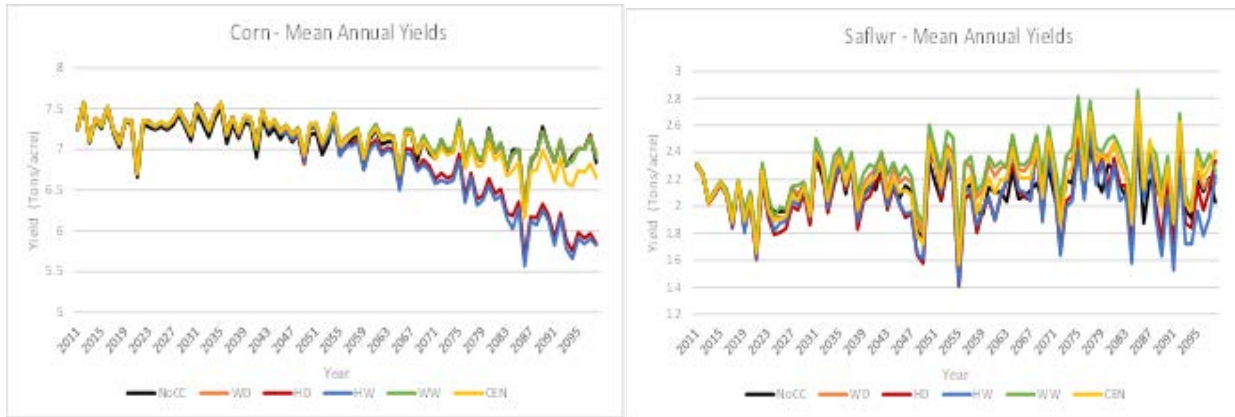
Figure 5.6.2 Changes in Biomass and Yield - Alfalfa and Winter Wheat (W_Wheat) and Changes in CO₂ by Scenario

For both crops, the increases in biomass and yield correspond closely with changes in CO₂.

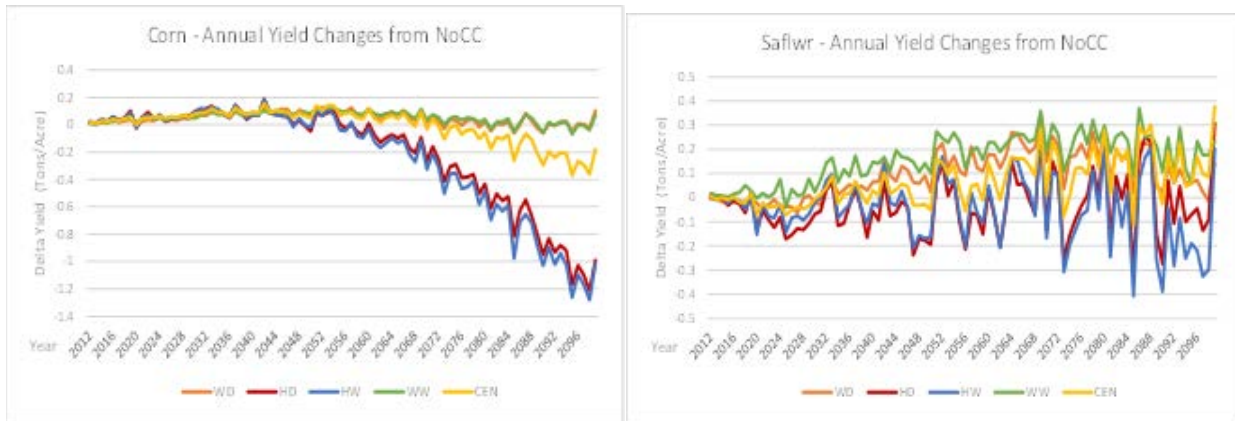
For the corn and safflower crop group, corn being a C₄ annual crop is simulated as having no RUE response to increasing CO₂ until its concentration exceeds 700 ppm (Figure 5.4.6). Above 700 ppm, its RUE declines slightly as concentration increases. This decrease is a result of the function used in WEAP-PGM and is probably not realistic. However, as this study is more focused on crop responses than actual values, this parameterization was not changed. As previously described corn does not have either an increase in maximum canopy LAI with increasing CO₂. In contrast, safflower a C₃ crop responds to increasing CO₂ with increased canopy LAI and increased RUE. However as VPD increases beyond its threshold value (0.5 kPa), its RUE declines rapidly (Figure 5.4.6). Both corn and safflower have similar T_b and T_{opt} temperature characteristics.

Figure 5.6.3 shows mean annual corn and safflower yields along with their changes relative to the NoCC reference scenario over the study period. Period mean monthly changes in biomass are also reported.

Mean Annual Time Series



Changes from NoCC Scenario



Period Mean Monthly Changes from NoCC Scenario

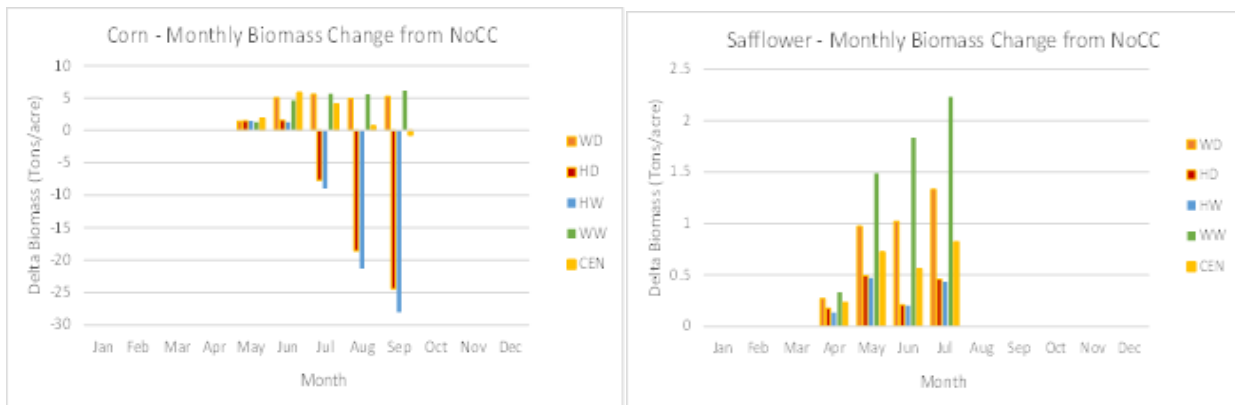


Figure 5.6.3 Biomass and Yield – Corn and Safflower (Safldr) by Scenario

For corn, yield changes are closely associated with differences in temperature between scenarios. In the hot HD and HW scenarios, the slight increases in the early part of the study period become significant and steady declines in the mid to late period. However in the warm WD and WW scenarios, corn maintains a slight yield increase. The CEN scenario has yield changes that are intermediate. The differences in biomass are consistent with the changes in yield. All scenarios

show increases in biomass production in the spring months but the increases become declines in the summer months in the hot scenarios. Corn has a fairly large optimal growth range from approximately 20 °C to 30 °C which is only exceeded in the months between June to September. Clearly, increasing temperature combined with decreasing solar radiation are the causative forcings.

For safflower, there are overall study period increases in yield for the warm WD and WW scenarios. In contrast, yield declines in the hot HD and HW start early and continue throughout the study period. These declines occur despite the large increases in CO₂ concentrations in these scenarios. There is also a notably high degree of variability in yields especially towards the end of the study period. These peaks and troughs appear to correspond with inter-annual variations in temperature (Figure 5.3.4). In cooler years of the hot scenarios which have high CO₂ concentrations, safflower growth is less constrained by temperature and can utilize the high CO₂ advantageously. For safflower, biomass production also corresponds closely with the degree of warming in each scenario. The WD and WW scenarios consistently produce more biomass than the hot HD and HW scenarios. The CEN is intermediate between these groups.

Table 5.6.2 presents the crop yield correlations with the atmospheric forcings for these crops.

Table 5.6.2 Correlations of Corn and Safflower Yield with Atmospheric Forcings by Scenario

Corn	Climate Scenario		
	<i>HD</i>	<i>CEN</i>	<i>WW</i>
Climate Variable	Yield - Correlation Coefficients		
CO ₂ (ppm)	-0.93	-0.78	-0.59
Tmax (C)	-0.55	-0.15	0.29
Rs (MJ/m ²)	0.82	0.77	0.67
VPD (kPa)	-0.14	0.31	0.55
Safflower	Climate Scenario		
	<i>HD</i>	<i>CEN</i>	<i>WW</i>
Climate Variable	Yield - Correlation Coefficients		
CO ₂ (ppm)	0.17	0.36	0.44
Tmax (C)	-0.09	-0.01	-0.12
Rs (MJ/m ²)	-0.14	-0.26	-0.24
VPD (kPa)	-0.32	-0.31	-0.32

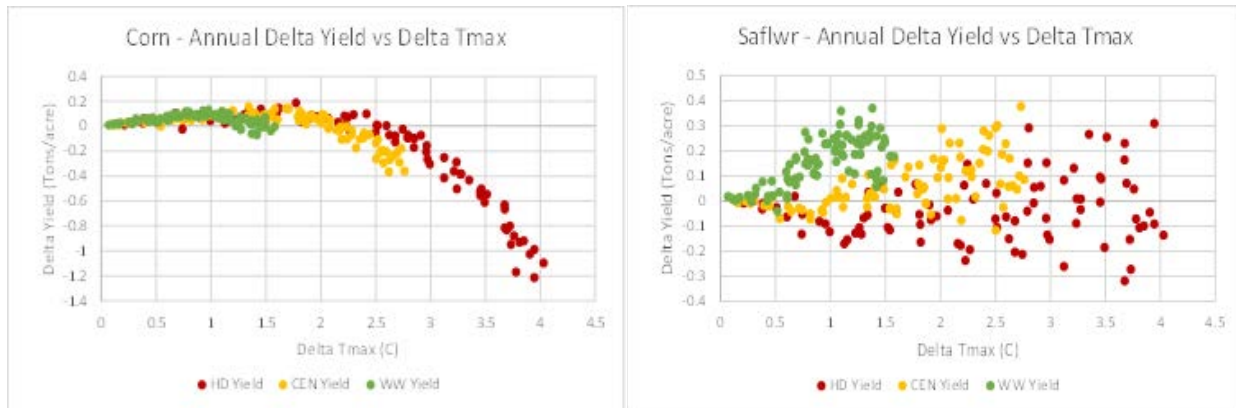
For corn, the highest correlations in all scenarios occur with Rs and these correlations increase from the WW to the HD scenario. This corresponds with the direct effect of decreasing Rs causing decreasing yield. In the WW, both Tmax and VPD are positively correlated with corn yield. However, these correlations become negative as yield declines significantly in the HD with increasing temperature and decreasing Rs. The negative correlations of CO₂ which does not directly affect corn yield occurs because of its high correlation with Rs in all scenarios.

For safflower, none of the atmospheric forcings have particularly strong correlations with yield. This is likely the result of the high degree of yield variability in all scenarios. The highest

positive correlation is with CO₂ which increases yield by increasing RUE. This correlation weakens in the CEN and HD scenarios corresponding with the decreasing yields. The strongest negative correlation occurs with VPD which when it increases above the crops threshold (0.5 kPa) results in a reduction in RUE and therefore yield.

Figure 5.6.4 shows the changes in yield and changes in Tmax and Rs relative to the NoCC reference by scenario.

Changes in Yield and Changes in Tmax by Scenario



Changes in Yield and Changes in Rs by Scenario

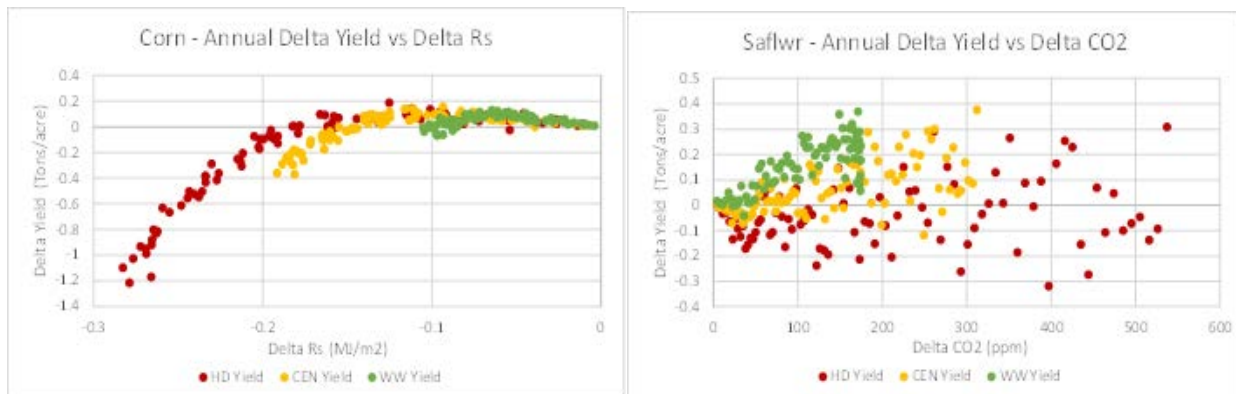


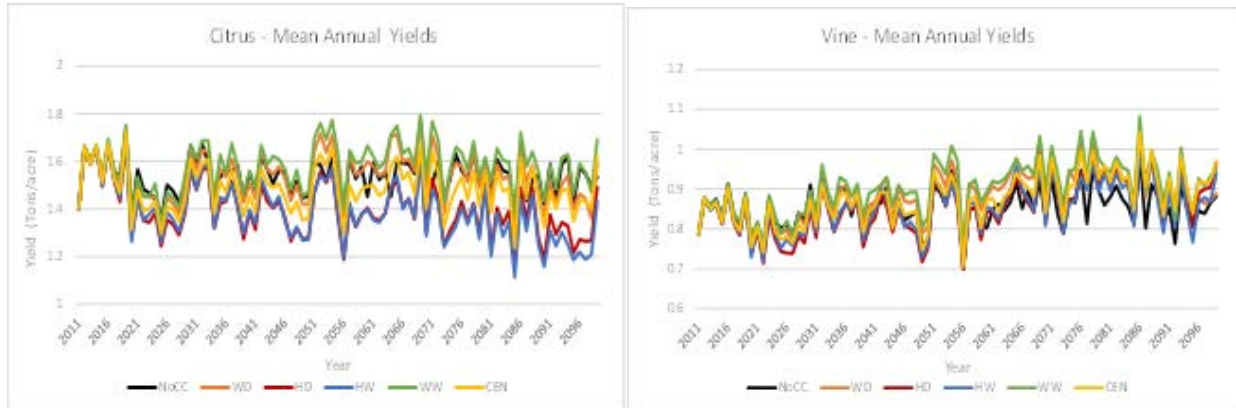
Figure 5.6.4 Changes in Yield – Corn and Safflower (Safflwr) and Changes in Tmax, Rs and CO₂ by Scenario

For the citrus and vine crop group, both of these perennial crops respond to increases in CO₂ with increasing RUE. With its inherently higher RUE, the vine response is more significant (Figure 5.4.7). However, the increase in RUE can be reduced by increases in the VPD in excess of threshold values. In this case, rate of decline per unit increase in VPD is greater for vines. Citrus has a slightly lower basal growth temperature and considerable smaller temperature growth range. Being non-deciduous, citrus is simulated as having a constant canopy LAI whereas the vine canopy has an increasing canopy LAI which develops in response to temperature from initial growth through maturity to senescence (Figure 5.4.7). The maximum canopy LAI of these crops does not change in response to increasing CO₂.

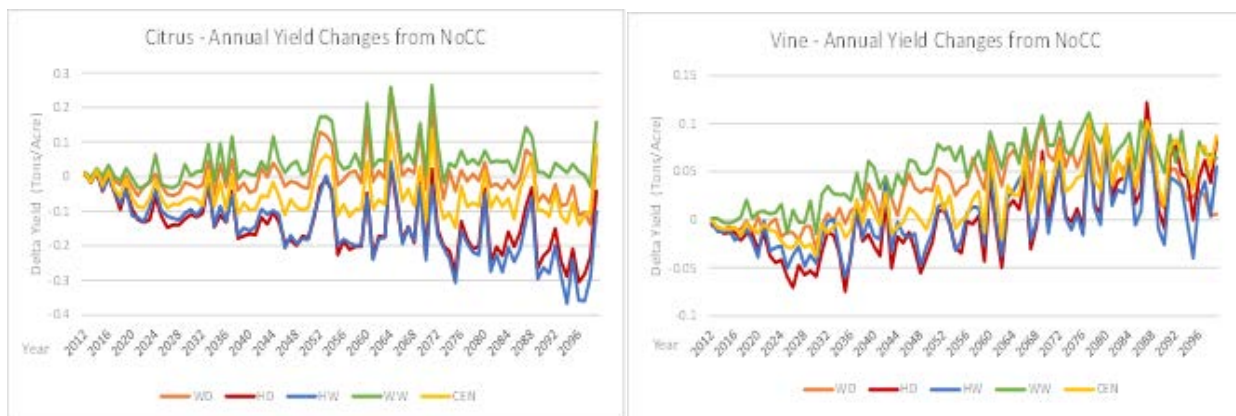
Plant Physiological Responses to Atmospheric Forcings

Figure 5.6.5 shows mean annual citrus and vine yields along with their changes relative to the NoCC reference scenario over the study period. Period mean monthly changes in biomass are also reported.

Mean Annual Time Series



Changes from NoCC Scenario



Period Mean Monthly Changes from NoCC Scenario

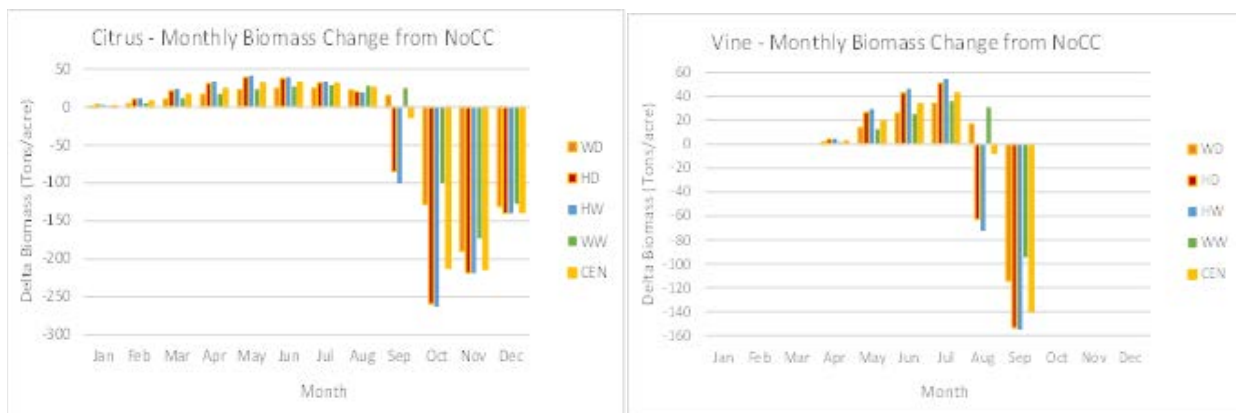


Figure 5.6.5 Biomass and Yield – Citrus and Vine by Scenario

For citrus, yield changes are closely associated with temperature differences between scenarios. In the hot HD and HW scenarios, there is a consistent downward trend over the study period. In the WD, WW and CEN, there are also declines in yield but they are more moderate in magnitude. There is also a considerable amount of inter-annual variability in all scenarios which appears to be inversely correlated with changes in Tmax. This variability is larger for the HD and HW scenarios. Slight increases in biomass production relative to the NoCC scenario occur in the winter, spring and early summer seasons followed by large declines in late summer and fall.

For vines, there is a general increase in yields during early and mid-study periods with the larger increases occurring in the warm WD and WW scenarios. In the late period, there appears to be somewhat of a decline in the WD yields that correlates well with the decrease in CO₂ associated with this scenario (Figure 5.3.10). Similar to citrus, the increase vine biomass production in the spring and early summer months is followed by decreases in the mid and late summer. This corresponds reasonably well with Tmax being in the optimum growth range of 20 °C to 35 °C in the months from October through June.

Like citrus, there is also a considerable amount of increased variability in yields especially in the hot HD and HW scenarios at the end of the study period. This effect can also be reasonably explained by the combined effects of inter-annual variability in temperature at high CO₂ concentrations.

Table 5.6.3 presents the crop yield correlations with the atmospheric forcings for these crops.

Table 5.6.3 Correlations of Citrus and Vine Yield with Atmospheric Forcings by Scenario

Citrus	Climate Scenario		
	<i>HD</i>	<i>CEN</i>	<i>WW</i>
Climate Variable	Yield - Correlation Coefficients		
CO ₂ (ppm)	-0.37	-0.11	0.18
Tmax (C)	-0.64	-0.54	-0.54
Rs (MJ/m ²)	0.30	0.06	-0.12
VPD (kPa)	-0.72	-0.65	-0.62
Vine	Climate Scenario		
	<i>HD</i>	<i>CEN</i>	<i>WW</i>
Climate Variable	Yield - Correlation Coefficients		
CO ₂ (ppm)	0.57	0.59	0.59
Tmax (C)	0.16	0.02	-0.25
Rs (MJ/m ²)	-0.51	-0.50	-0.41
VPD (kPa)	-0.24	-0.42	-0.51

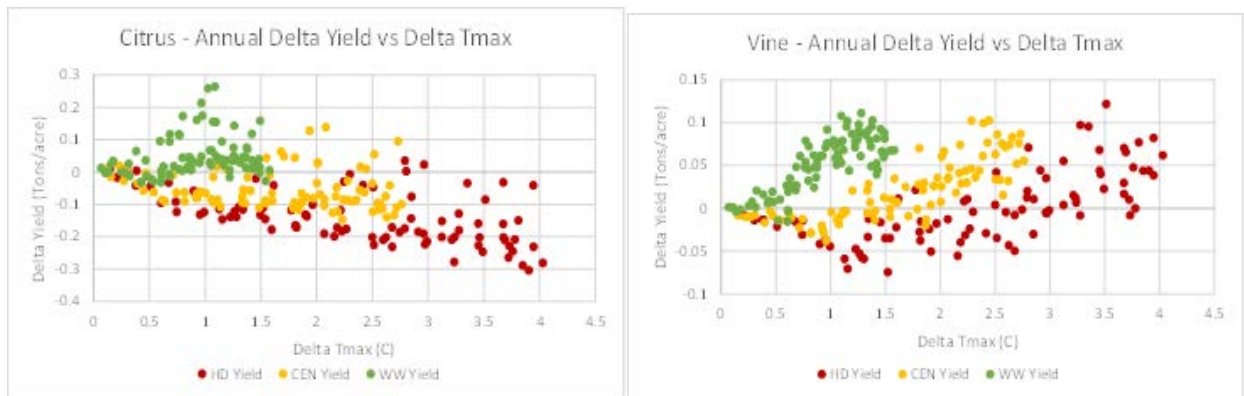
For citrus, the highest correlations are the negative correlations with Tmax and VPD. However, VPD and Tmax are highly correlated in all scenarios. Thus, increasing temperature is the primary forcing factor causing declines in citrus yields. The increasing positive correlation with Rs in the CEN and HD scenarios also indicates that it has an increasing role in the yield declines with rising CO₂.

Plant Physiological Responses to Atmospheric Forcings

For vines, the highest correlations are the positive correlation with CO₂ and negative correlation with Rs. Since these forcings have opposite effects on yield, it is clear that the positive effect of CO₂ on yield is partially offset by decreases in Rs. This makes sense in light of the fact that largest yield increases occur in the WW scenario where the positive effects of CO₂ are not as strongly affected by the slight declines in Rs.

Figure 5.6.6 shows the changes in yield and changes in Tmax and Rs relative to the NoCC reference by scenario.

Changes in Yield and Changes in Tmax by Scenario



Changes in Yield and Changes in Rs and CO₂ by Scenario

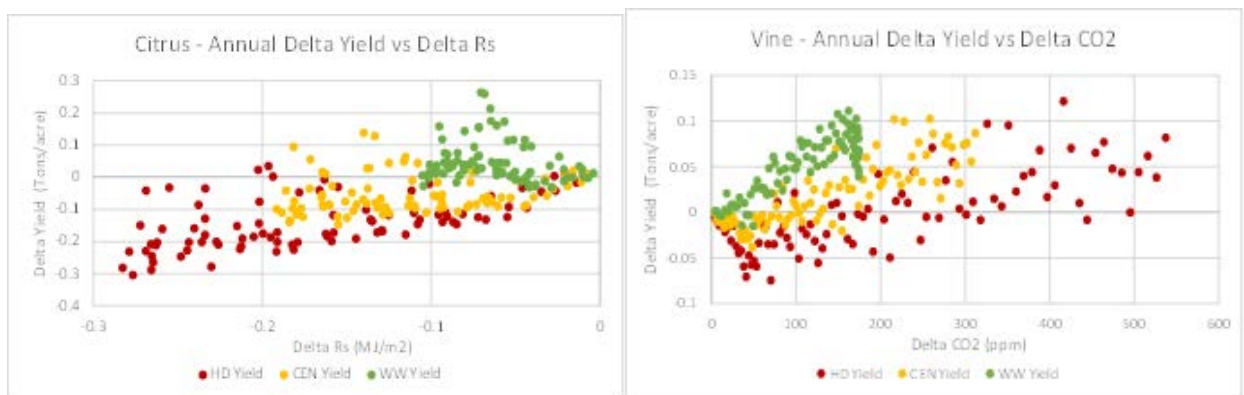


Figure 5.6.6 Changes in Yield – Citrus and Vine and Changes in Tmax, Rs and CO₂ by Scenario

6. Summary of Results

6.1 Atmospheric Forcings

The assessment of plant responses to atmospheric forcings involved examining the effects of temperature (Tmax), incoming short wave radiation (Rs), atmospheric CO₂ and the vapor pressure deficit (VPD) on transpiration, actual biomass and yield of six crops widely grown in the western United States including alfalfa, winter wheat, corn, safflower, citrus and vines.

The atmospheric forcings used in the assessment are based climate scenarios developed by Reclamation for the Sacramento and San Joaquin Basins Study (Reclamation, 2016). These forcings were based on global climate models (GCM) simulations which had been bias corrected and spatially downscaled by Reclamation (2011). These GCM results only include temperature and precipitation. Therefore, there was a need to use GCM results in conjunction agro-meteorological stations observations to develop the necessary atmospheric forcings to simulate crop responses. This was accomplished by using observations of the variables at the Firebaugh CIMIS station and applying estimation methods described in Appendix B to compute the dew point temperature, solar radiation and wind speed. The CO₂ concentrations were calculated by weighting the number of GCM projections included each scenario.

Six climate scenarios were selected to characterize a wide range of potential atmospheric forcings occurring over an 89 year study period. All scenarios have the same inter-annual variability. The selected scenarios included a reference scenario (NoCC) with daily temperature and precipitation based on historic climate conditions. The other scenarios fall into 3 groups including a central tendency scenario (CEN), scenarios hotter than the CEN scenario including hot-dry (HD) and hot-wet (HW) scenarios and scenarios with less warming than CEN including warm-dry (WD) and warm-wet (WW) scenarios.

All scenarios were warmer than the NoCC scenario. In all scenarios, Tmax steadily increased throughout the study period with largest increases in the hot scenarios and the least increase in the warm ones. The CEN was intermediate to these groups (Figure 5.3.4). The other atmospheric forcings had similarly consistent differences between the hot, warm and CEN groups. In all groups, solar radiation steadily decreased throughout the study period with the largest declines in the hot scenarios and the smallest in the warm group. The CEN scenario was intermediate (Figure 5.3.7). The CO₂ concentration increased in all scenarios except NoCC with most increase in the hot and least in the warm group and the CEN being intermediate (Figure 5.3.10). The VPD atmospheric forcing increased steadily in all scenarios with the greatest increases in the hot group and smallest in the warm with the CEN being intermediate (Figure 5.3.13).

In order to assess relationships between plant responses and atmospheric forcings, a correlation coefficient analysis was performed to evaluate the relationships between the atmospheric variables. While the correlation between CO₂ and Tmax in the warm scenarios is low, it increases significantly in hot scenarios. The low correlation in the warm group is likely the result of the inter-annual variability in Tmax in these scenarios being relative large compared to the relatively smaller changes in CO₂ concentration. However, as CO₂ concentrations increase, its

effect on T_{max} becomes clearly correlated (Table 5.3.1). The other highly correlated atmospheric forcing with CO_2 is R_s . In this case, there is a high negative correlation that is consistent across all the scenarios. Like CO_2 , T_{max} has a stronger but negative correlation with R_s in the hot scenarios. On a physical basis, the increasing correlations between T_{max} with CO_2 and R_s in the hot scenarios are reasonable because as CO_2 increases temperature increases which in turn increases atmospheric humidity which decreases R_s .

There is a strongly positive correlation between T_{max} and VPD in all scenarios (Table 5.3.2). This correlation is also physically reasonable given that increasing VPD is primarily a function of the saturation vapor pressure which increases more rapidly as a function of temperature than does the atmospheric humidity.

There also exists strong positive correlations between VPD and R_s in the warm scenarios. These correlations weaken significantly in the hot scenarios. Given the consistently high correlations between T_{max} and VPD in all scenarios, these changes in correlation likely reflect the direct effects of T_{max} on VPD affecting the correlations between VPD and R_s (Table 5.3.3).

6.2 Transpiration Responses to Atmospheric Forcings

For this study, six crops were selected to assess transpiration, biomass and yield responses to the atmospheric forcings. The primary crop parameters affecting transpiration are stomatal conductance, the amount and rate of canopy development along with growth limitations due to unfavorable temperatures during the growth period. In the Central Valley, alfalfa is a perennial crop with its primary growing seasons occurring spring, summer and fall while winter wheat is annual crop whose growth period starts in the fall and extends through the following spring. The transpiration of both of these crops is sensitive to CO_2 and VPD (Figure 5.4.7). With rising temperature, the transpiration of both crops initially increased but subsequently declined especially in the hot scenarios. The greatest increases during the early century occurred in the hot scenarios. This can be attributed to increased canopy LAI due to rising CO_2 along with VPD beneath the threshold values. With continued warming, rising CO_2 concentrations and higher VPD, reductions in stomatal conductance eventually overwhelm the increase in canopy LAI (Figure 5.5.2). Seasonal differences in transpiration also occur. The greatest transpiration reductions occur in the hot summer months when VPD is highest while in the cooler fall and winter months when VPD is lower both crops have increased transpiration. These responses are also evident in the correlations of transpiration with the atmospheric forcings. For CO_2 , there is an increasingly strong negative correlation from the warm to the hot scenarios indicating its growing effect on reduced stomatal conductance. The opposite is true for T_{max} and VPD. Their positive correlations in the warm scenarios decrease in hot scenarios as transpiration increases become decreases. The strengthening positive correlation between transpiration and R_s from the warm to hot scenarios reflects its strong negative correlations with CO_2 .

Corn and safflower are both annual crops planted in spring and harvested in summer. Unlike safflower, corn is a C4 crop that does not have reduced stomatal conductance with rising CO_2 or VPD. In contrast, safflower responds to increasing CO_2 with increased canopy LAI and reduced stomatal conductance. Its stomatal conductance is also sensitive to VPD above its threshold. For corn, there is an increase in transpiration in all scenarios through the mid-century. Except for

the hot scenarios, these increases continue steadily upward throughout the study period (Figure 5.5.3). The decreases in corn transpiration in the hot scenarios are related to its optimal growth range of approximately 20 °C to 30 °C being exceeded more frequently. Additionally, these scenarios also have the largest reductions in solar radiation which is a contributing factor.

For safflower, transpiration initially increases in the early century but declines in all scenarios by the end of the study period (Figure 5.5.4). The largest declines are in the hot scenarios with high CO₂ concentrations. The initial increase is characteristic of effects of increased CO₂ on canopy LAI combined with temperature still in the optimal growth range. With continued warming, rising CO₂ concentrations and higher VPD, reductions in stomatal conductance eventually overwhelm the increase in canopy LAI (Figure 5.5.2). Monthly differences in transpiration also correspond closely with changes in VPD with the largest decreases at the highest VPDs.

These responses are also evident in the correlations of transpiration with the atmospheric forcings. For corn, there are strong correlations between transpiration and T_{max}. These positive correlations are strongest in the warm scenarios and decrease somewhat in hot scenarios as corn transpiration strongly reduces in the late study period. As expected, there is basically no correlation with CO₂. For safflower, there are very high correlations of transpiration with CO₂ in all scenarios and a high correlation with VPD in the warm scenarios which weakens in the hot scenarios. This is the same pattern of changes that occurred with the alfalfa and winter wheat crops.

The citrus and vine crops are both perennial crops. Vines are deciduous and drop their leaves during senescence while citrus has a constant canopy LAI. Neither is responsive to increasing CO₂ increasing canopy LAI. However both are responsive to the effects of CO₂ and VPD on stomatal conductance. Citrus also has a lower optimal temperature and growth range than vines. In the early study period, citrus transpiration increases in all scenarios but in the hot scenarios there is a significant decline in mid to late century period (Figure 5.5.6). For vines, transpiration declines steadily throughout the study period with largest declines in the hot scenarios. Despite the overall declines in transpiration, both crops had some increased transpiration in the winter and fall months accompanied by large declines in the summer months. For citrus, its optimal growth temperature is exceeded in all months from April through October while vines optimal growth temperature is exceeded only in the months from June through September. In the summer, the hot scenarios which have higher CO₂ and VPD have greater reductions in transpiration than the warm scenarios. These effects are reflected in the correlations between transpiration and CO₂ and VPD. For citrus there is a negative correlation with CO₂ in all scenarios. In the warm scenarios, there is also a strong positive correlation with T_{max} and VPD. These correlation decrease significantly in the hot scenarios reflecting the change from early period increases to late period declines. For vines, there are increasing negative correlations with CO₂, T_{max} and VPD occurring from the warm to hot scenarios reflecting the steady decrease in transpiration. The increasing correlation with R_s reflects the effect decreasing R_s corresponding with decreasing transpiration.

From the discussion presented here, it is also possible to assess how applicable the use of the standardized reference evapotranspiration method may be for use in long term planning studies. Figure 6.2.1 shows a comparison of mean annual transpiration of alfalfa and corn during the study period.

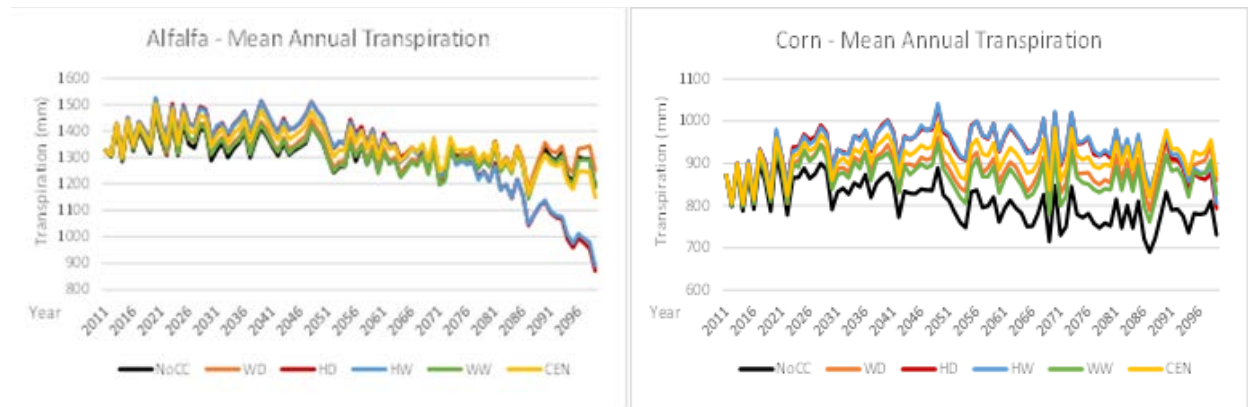


Figure 6.2.1 Comparison of Alfalfa and Corn Transpiration by Scenario

As can be seen clearly, the transpiration response of alfalfa which is sometimes used a reference crop differs considerably from that of the corn over the course of the study period. However, the standardized reference method depends on maintaining a constant ratio between corn evapotranspiration and the reference for the empirically determined coefficients to remain valid. By inspection, this assumption does not apply for long term planning studies in which atmospheric forcings and crop responses may be considerably different than those used to determine the original crop coefficients.

6.3 Biomass and Yield Responses to Atmospheric Forcings

The primary crop parameters affecting crop biomass and yield are the radiation use efficiency (RUE), the amount and rate of canopy development along with growth limitations due to unfavorable temperatures during the growth period. For both alfalfa and winter wheat, yields increase steadily in all scenarios with the largest increases in the hot scenarios (Figure 5.6.1). The largest increases in biomass occur in the winter and spring months. For alfalfa, its VPD threshold is exceeded in the months of May through October. In these months, there is slight reduction relative to the NoCC biomass production. In contrast, winter wheat's biomass increases steady through its growth period with larger increases occurring in hot, high CO₂ concentration scenarios. For both crops, the highest positive yield correlations are with CO₂ and Tmax in all scenarios. These correlations become stronger as CO₂ concentrations and Tmax increase from the warm to hot scenarios indicating their positive effects on yield. This occurs despite the fact that Rs is declining more in the hot scenarios than in the warm ones indicating simulative effects of CO₂ and warmer spring temperature are more than compensating for the declining Rs.

Being a C₄ annual crop, corn is simulated as having no RUE response to increasing CO₂ while safflower, a C₃ crop, responds to increasing CO₂ with increased canopy LAI and increased RUE. For corn, yield changes are closely associated with differences in temperature between scenarios. In the hot scenarios, the slight increases in the early part of the study period become significant and steady declines in the mid to late period. In the warm scenarios, corn maintains a slight yield increase relative to the NoCC scenario. For safflower, changes in yield are closely related to changes in temperature. In the hot scenarios, there is an overall trend toward declining yields

throughout the study period (Figure 5.6.3). However, in the warm scenarios, yields increase through the mid-late century when they decline slightly. It is also notable that there are very large inter-annual changes in yield especially toward the end of the century. This is especially true for the hot scenarios. These yield changes correspond with changes in temperature. In relatively cooler years, yield increases.

For corn, the highest correlations in all scenarios occur with R_s and these correlations increase from the warm to the hot scenarios. This corresponds with the direct effect of decreasing R_s causing decreasing yield in the all scenarios. For safflower, none of the atmospheric forcings have particularly strong correlations with yield. This is likely the result of the high degree of yield variability in all scenarios. The correlation with CO_2 is highest in the warm scenarios which have increased yield and lowest in the hot ones with yield decreases. Unlike corn, it has negative correlations with R_s indicating that the simulative effects of CO_2 are overwhelming the yield decreasing effects of R_s . VPD has a steady but moderate correlation with safflower yield reflecting its role in decreasing RUE.

For the citrus and vine crops, both of these perennial crops respond to increases in CO_2 with increasing RUE. However, the potential benefits can be counteracted by increasing VPD and decreasing R_s associated with the increasing CO_2 . For citrus, yield changes are closely associated with temperature differences between scenarios. In the hot scenarios, there is a consistent downward trend over the study period (Figure 5.6.5). In the warm scenarios, there are some erratic increases in yield which typically correspond with cooler years but overall there is only a slight decrease relative to the NoCC scenario. Both crops have strong declines in biomass production in hot, late summer and fall months. Citrus and vines both have slight increases in biomass production prior to late summer. For citrus, the highest correlations are the negative correlations with T_{max} and VPD which increase from the warm to hot scenarios indicating the combined effects increasing temperature being outside of the optimal growth range along with increasing VPD reducing the RUE. For vines, the highest correlations are the positive correlation with CO_2 and negative correlation with R_s . In light of the fact that largest yield increases occur in the warm scenarios, this is another indication of the positive effects of CO_2 overcoming the negative effects of decreasing R_s on biomass and yield reductions.

References

In addition to these references, an on-line Mendeley bibliography containing more than 500 journal articles relevant to the subject of plant and atmospheric interactions was developed during this study. If you wish to have access to this library, please contact the author of this report.

Addington, R.N., R.J. Mitchell, R. Oren, & L.A. Donovan. 2004. *Tree Physiology*. 24,561-569.

Adejuwon, J. 2005. Assessing the suitability of the EPIC crop model for use in the study of impacts of climate variability and climate change in West Africa. Singapore. *Trop. Geog.* 26(1): 44-60.

Ainsworth, E.A. and S.P. Long. 2005. What we have learned from 15 years of free-air CO₂ enrichment (FACE)? A meta-analytic review of the responses of photosynthesis, canopy properties and plant production to rising CO₂. *New Phytologist*, 154(351-372).

Allen, R. G., Walter, I. A., Elliott, R., Itenfisu, D., Brown, P., M. Jensen, and R.L. Snyder. 2005. ASCE Standardized Reference Evapotranspiration Equation. American Society of Civil Engineers. p. 58.

Allen, R.G., L.S. Pereira, D. Raes, M. Smith. 1998. *Crop Evapotranspiration – Guidelines for computing crop water requirements – FAO Irrigation and Drainage Paper 56*. United Nations FAO, Rome, Italy, 330 p.

Allen, R.G., F.N. Gichuki & C. Rosenzweig 1991. CO₂-Induced Climatic Changes and Irrigation Water Requirements. *Journal of Water Resources Planning and Management*. Vol. 117, No. 2 pp. 157-178.

Borg, H. and D.V. Grimes. 1986. Depth development of roots with time: An empirical description. *Trans. ASAE* 29:194-197.

Bloom, A.J. 2010. *Global Climate Change: Convergence of Disciplines*. Sinauer Assoc., Sunderland, MA, 420 pp.

_____. 2009 Responses of crop plants to rising atmospheric carbon dioxide concentrations. *California Agriculture* 63:67-72.

Brown, R.A. and N.J. Rosenberg. 1999. Climate change impacts on the potential productivity of corn and winter wheat in their primary United States growing regions. *Climate Change* 41:73-107.

Bureau of Reclamation (Reclamation). 2016. *Sacramento and San Joaquin Rivers Basin Study*. Prepared by U.S. Department of the Interior, Bureau of Reclamation, Mid Pacific Region, Sacramento, California.

_____. 2015. West-Wide Climate Risk Assessments: Irrigation Demand and Reservoir Evaporation Projections. Technical Memorandum No. 86-68210-2014-01. Technical Services Center, Denver, Colorado.

_____. 2014. Sacramento and San Joaquin Basins Climate Risk Assessment. Prepared by U.S. Department of the Interior, Bureau of Reclamation, Mid Pacific Region, Sacramento, California.

_____. 2013. Summary Report Central Valley Project Integrated Resource Plan. Prepared by U.S. Department of the Interior, Bureau of Reclamation, Mid Pacific Region, Sacramento, California.

_____. 2011. SECURE Water Act Section 9503(c) – Reclamation Climate Change and Water 2011. Prepared by U.S. Department of the Interior, Bureau of Reclamation, Technical Services Center, Denver, Colorado.

California Department of Water Resources (DWR). 2007. Land Use Survey Data.

Hansen, J., G. Russell, D. Rind, P. Stone, A. Lacia, S. Lebedeff, R. Ruedy & L. Travis. 1988. Global climate changes as forecast by the GISS 3-D model. *Journal of Geophysical Research* 93:9341-9364.

Doorenbos, J. and A.H. Kassam. 1979. Yield response to water. *Irrigation and Drainage Paper 33*. Food Agric. Org. United Nations, Rome.

Eckhardt, K. N. Fohrer & H.G. Frede. 2002. SWAT-G, a version of SWAT99.2 modified for application to low mountain range catchments. *Phys. Chem. Earth*. 27:641-644.

Ficklin, D.L., Y. Luo, E. Luedeling & M. Zhang. 2009. Climate change assessment of a highly agricultural watershed using SWAT. *Journal of Hydrology*. 374:16-29.

Gassman, P.W., M.R. Reyes, C.H. Green, and J.G. Arnold. 2007. The Soil and Water Assessment Tool: historical development, applications, and future research directions. *Transactions of the ASABE*. 50 4:1211-1250

Hatfield, J.L. 2008. The effects of climate change on agriculture, land resources, water resources and biodiversity. U.S. Climate Change Science Program: Synthesis and Assessment Product 4.3.

Howitt R.E., J. Medellín-Azuara, D. MacEwan, and J.R. Lund. 2012. Calibrating disaggregate economic models of agricultural production and water management. *Environmental Modelling & Software* 38: 244-258.

Huntington, T.G. 2004. Climate change, growing season length, and transpiration: Plant response could alter hydrologic regime. *Plant Biology*, 6(651-653).

Izaurrealde, R.C., N.J. Rosenberg, R.A. Brown,, & A.M. Thomson. 2003. Integrated assessment of Hadley Center (HadCM2) climate-change impacts on agricultural

- productivity and irrigation water supply in the conterminous United States Part II. Regional agricultural production in 2030 and 2095. *Agricultural and Forest Meteorology*. 117:97-122.
- Jensen, M.E., R.D. Burman, and R.G. Allen (ed.). 1990. Evapotranspiration and irrigation water requirements. ASCE Manuals and Reports on Engineering Practice No. 70. ASCE, N.Y. 332 pp.
- Jones, J.W. and Kinery, J.R. 1986. CERES-Maize: a simulation model of maize growth and development. Texas A&M Press, College Station, Texas.
- Jones, J.W., G. Hoogenboom, C.H. Porter, K.J. Boote, W.D. Batchelor, L.A. Hunt, P.W. Wilkens, U. Singh, A.J. Gijsman, & J.T. Ritchie. 2003. The DSSAT cropping system model. *Europ. J. Agronomy*. 18:235-265.
- Jones, J.W., G.Y. Tsuji, G. Hoogenboom, L.A. Hunt, P.K. Thornton, P.W. Wilkens, D.T. Imamura, W.T. Bowen & U. Singh. 1989a. Decision support system for agrotechnology transfer; DSSAT v3. In: G.Y. Tsuji, G. Hoogenboom, & P.K. Thornton (Eds.). *Understanding Options for Agricultural Production*. Kluwer Academic, Dordrecht, the Netherlands, pp 157-177.
- Jones, J.W, K.J. Boote, G. Hoogenboom, S. Jagtap & G. Wilkerson. 1998b. SOYGRO v5.42: soybean crop growth simulation model. User's Guide. Dept. of Agr. Eng. & Agro., University of Florida, Gainesville, Fl.
- Keating, B.A., P.S. Carberry, G.L. Hammer, M.E. Probert, M.J. Robertson, D. Holzworth, N.I. Huth, J.N.G. Hargreaves, H. Meinke, Z. Hochman, G. McLean, K. Verburg, V. Snow, J.P. Dimes, M. Silburn, E. Wang, S. Brown, K.L. Bristow, S. Asseng, S. Chapman, R.L. McCown, D.M. Frebairn, & C.J. Smith. *Europ. J. Agronomy*. 18:267-288.
- Kimball, B.A. 2010. Lessons from FACE: CO₂ effects and interactions with water, nitrogen and temperature. Chapter 5 in "Handbook of Climate Change and Agroecosystems." Daniel Hillel and Cynthia Rosenzweig eds.
- _____. 2007. Global Change and Water Resources. In: *Irrigation of Crops*, 2nd ed., Agronomy Monograph no. 30, American Society of Agronomy, Madison, WI.
- _____. 1983. Carbon dioxide and agricultural yield: An assemblage and analysis of 770 prior observations. Water Conservation Laboratory, Report No. 14. USDA/ARS Phoenix, AZ.
- Kimball, B.A. and S.B. Idso. 1983. Increasing CO₂: Effects on crop yield, water use and climate. *Agricultural Water Mangement*. 7:55-72.
- Kimball, B.A., K. Kobayashi, and M. Bindi. 2002. Responses of agricultural crops to Free-Air CO₂ Enrichment. *Advances in Agronomy*, 77(293-368).

- Long, S.P., E.A. Ainsworth, A.D.B. Leakey, J. Nosberger, and D.R. Ort. 2006. Food for thought: Lower-than-expected crop yield stimulation with rising CO₂ concentrations. *Science*, 312:1918 – 1921.
- Manabe, S. and R. Wetherald. 1987. Large-scale changes in soil wetness induced by increase in atmospheric carbon dioxide. *Journal of Atmospheric Science*, 44:1211-1236.
- McAveney, B.J., R. Coleman, J.F. Fraser & R.R. Dhani. 1991. The Response of the BMRC AGCM to a Doubling of CO₂. BMRC Technical Memorandum N. 3. Melbourne, Australia.
- Mearns, L.O., T. Mavromatis, E. Tsvetsinskaya, C. Hays, and W. Easterling. 1999. Comparative response of EPIC and CERES crop models to high and low resolution climate change scenarios. *J. Geophys. Res.* 104: 6623-6646.
- Mitchell J.F.B, C.A. Wilson, and W. M. Cunningham. 1987. On CO₂ climate sensitivity and model dependence of results. *Quarterly Journal of the Royal Meteorology Society*, <https://doi.org/10.1002/qj.49711347517>
- Monteith, J.L., 1981. Evaporation and Surface Temperature. *Quarterly Journal Royal Meteorological Society*, 107, 1-27.
- Murphy, J.M. 1995. Transient Response of the Hadley Center Coupled Ocean-Atmosphere Model to Increasing Carbon Dioxide. Part I. Control; Climate and Flux Correction. *J. Clim.* 8:35-56.
- National Assessment Synthesis Team. 2001. Climate Change Impacts on the United States. U.S. Global Change Research Program. Report for the US Global Change Research Program, Cambridge University Press, Cambridge UK, pp. 620
- Neitsch, S.L., J.G. Arnold, J.R. Kiniry, and J.R. Williams. (2005) Soil and Water Assessment Tool Theoretical Documentation: Version 2005.
- Ocheltree, T.W., J.B. Nippert, & P.V.V. Prasad. 2014. Stomatal responses to changes in vapor pressure deficit reflect tissue-specific differences in hydraulic conductance. *Plant, Cell and Environment*. Vol. 37, Issue 1, p. 132–139.
- Orang, M.N., S.J. Matyac, and R.L.Snyder. 2004. Consumptive Use Program (CUP) Model. *Acta Horticulturae*. International Society for Horticultural Science. 664:461-468.
- Penman, H.L. 1956. Evaporation: An introductory survey. *Netherlands Journal of Agriculture Science* 4:7-29.
- Ritchie, J. T. (1972). Model for predicting evaporation from a row crop with incomplete cover. *Water Resources Research*, 8(5), 1204–1213.
- Rivington, M. and Koo J. 2010. Report on the meta-analysis of crop modelling for climate change and food security survey. Copenhagen, Denmark: CCAFS, pp 73.

- Rosenberg, N.J., B.A. Kimball, P. Martin, & C.F. Cooper. 1990. Climate change, CO₂ Enrichment and evapotranspiration. In: P.E. Waggoner (Ed), Climate Change and US Water Resources. Wiley, New York, p. 151-175.
- Rosenzweig, C. 1990. Crop Response to Climate Change in the Southern Great Plains: A Case Study. *Professional Geographer*. 41 1:20-37.
- Rosenzweig, C. and A. Inglesias. 1998. The use of crop models for international climate change impact assessment. In: *Understanding Options for Agricultural Production*. G.Y. Tsuji et al. (eds). pp.267-292. Kluwer Academic Publishers. Great Britain.
- Snow, V. and N. Huth. 2004. The APSIM – MICROMET module. Hort Research Internal Report No. 2004/12848. Auckland, New Zealand.
- Snyder, R.L, K. Bali, F. Ventura, and H. Gomez-MacPherson. 2000. Estimating Evaporation from Bare or Nearly Bare Soil. *Journal of Irrigation and Drainage Engineering*. ASCE, 126(6): 399-403.
- Stockle, C.O., M. Donatelli & R. Nelson. 2003. CropSyst, a cropping systems simulation model. *Europ. J. Agronomy*. 18:289-3007.
- Stockle, C.O., J.R. Williams, N.J. Rosenberg, and C.A. Jones. 1992. A method for estimating the direct and climatic effects of rising atmospheric carbon dioxide on growth and yield of crops: Part I--Modification of the EPIC model for climate change analysis. *Agric. Systems* 38:225-238.
- Streck, N. A. 2003. Stomatal Response to Water Vapor Pressure Deficit: An Unsolved Insolved Issue. *Revista Brasileira Agrociencia*. Vol. 9, No.4. p. 317-322.
- Taylor K.E., R.J. Stouffer, and G.A. Meehl, 2012: An Overview of CMIP5 and the Experiment Design. *Bull. Amer. Meteor. Soc.*, 93, 485–498.
- Thornthwaite, C. W. 1948. An approach toward a rational classification of climate. *Geographical Review* 38:55-94.
- Tubiello, F.N. and F. Ewert. 2002. Simulating the effects of elevated CO₂ on crops: approaches and applications for climate change. *European Journal of Agronomy*. 18:57-74
- Uchijima, Z., T. Udagawa, T. Horie, and K. Kobayashi. 1968. The penetration of direct solar radiation into corn canopy and the intensity of direct radiation on the foliage surface. *J. Agron. Meteorol.* Tokyo 3:141-151.
- United States Department of Agriculture (USDA). Soil Survey Staff, Natural Resources Conservation Service, United States Department of Agriculture. Web Soil Survey.

U.S. Global Change Research Program, USGCRP. Scientific Assessment of the Effects of Global Change on the United States. A Report of the Committee on Environment and Natural Resources National Science and Technology Council. May 2008.

Wang, E., M.J. Robertson, G.L. Hammer, P.S. Carberry, D. Holzwoorth, H. Meinke, S.C. Chapman, J.N.G. Hargreaves, N.I. Hith & G. McLean. *Europ. J. Agronomy*. 18:121-140.

White, J.W., G. Hoogenboom, B.A. Kimball, & G.W. Wall. 2011. Methodologies for simulating impacts of climate change on crop production. *Field Crops Research*. 124: 357-368.

Williams, J.W., R.C. Izaurralde, and E.M. Steglich. 2008. Agricultural Policy/Environmental Extender Model: Theoretical Documentation, Version 0604. Blackland Research and Extension Center, Temple, Texas.

Williams, J.R., C.A. Jones, J.R. Kiniry, and D.A. Spanel. 1989. The EPIC crop growth model. *Trans. ASAE* 32(2): 497-511.

Ziska, L.H., and J.A. Bunce. 2007. Predicting the impact of changing CO₂ on crop yields: some thoughts on food. *New Phytologist* 175:607-618.

Appendix A – WEAP-PGM Algorithms

In order to simulate the effects of climate on crop water use and yield, algorithms simulate the following processes were selected for inclusion in the PGM.

- Increase in soil evaporation and plant transpiration caused by increased temperature.
- Increase or decrease in temperature stress caused by increased temperature.
- Increase in radiation use efficiency caused by elevated CO₂ (fertilization effect).
- Increase in leaf area caused by elevated CO₂.
- Reduction in stomatal conductance caused by elevated CO₂.
- Reduction in stomatal conductance and radiation use efficiency caused by increases in vapor pressure deficit.
- Initiation, senescence, and termination of the growth period based on accumulated heat units.
- Plant growth rate and harvest yield driven by accumulation of degree day heat units.

These processes are discussed in more detail in several publications (Kimball et al., 2002; Huntington, 2004; Neitsch, et al., 2005; Long et al., 2006; Ainsworth and Long, 2005; Hatfield et al., 2008; Kimball, 2010; Bloom, 2009; Streck, 2003; Addington et al., 2004; and Ocheltree et al., 2014). At this time, there are no algorithms for the interactions between plants and nutrients in the PGM.

A.1 Potential Evapotranspiration

In WEAP-CV PGM, a tall grass (alfalfa) reference, as described in Allen et al. (2005) is used as the reference crop. In the description of the evapotranspiration (ET) algorithm that follows, the source of each equation is provided. Equations were taken from the ASCE EWRI standardized reference evapotranspiration document (Allen et al., 2005) and SWAT documentation (Neitsch, et al., 2005, Eckhardt et al 2002).

The model estimates potential evapotranspiration (PET) for each daily time step using the approach found in SWAT:

1. The potential evapotranspiration is initially estimated for the alfalfa reference crop (PETDAY) using the Penman-Monteith method.
2. The maximum plant evapotranspiration (EPMAX) is estimated using the Penman-Monteith method for specific crops such as annuals, and deciduous and non-deciduous perennial crops.
3. Evaporation from the crop canopy is calculated as a function of the size of the crop canopy and available moisture.
4. Potential bare soil evaporation is calculated as a function of canopy cover and crop residues.

5. The sum of canopy evaporation, crop transpiration, and bare soil evaporation is compared to PETDAY. If the sum exceeds PETDAY, then potential bare soil evaporation and maximum plant transpiration (EPMAX) are reduced, in that order.

A.1.1 Potential Evapotranspiration for the Alfalfa Reference Crop (PETDay)

$$PET_{Day} = \frac{DLT * RN + \rho * c_p * 86400 * VPD / AR}{HV * (DLT + GMA * [1 + CR / AR])} \quad \text{Eq. 1}$$

Where

PETDay: potential plant transpiration in mm d⁻¹ [Eq. 2:2.2.1 in SWAT 2005]

DLT: slope of the saturation vapor pressure curve in kPa °C⁻¹

RN: net radiation in MJ m⁻² d⁻¹

rho: air density in kg m⁻³

cp: specific heat of moist air at constant pressure in MJ kg⁻¹ °C⁻¹

VPD: vapor pressure deficit in kPa

AR: aerodynamic resistance for heat and vapor transfer in s m⁻¹

HV: latent heat of vaporization in MJ kg⁻¹

GMA: psychrometer constant in kPa °C⁻¹

CR: canopy resistance for vapor transfer in s m⁻¹

To calculate potential evapotranspiration, the Penman-Monteith method must be solved for a reference crop. The model uses alfalfa at a height of 40 cm with a minimal leaf resistance of 100 s m⁻¹. The terms necessary to solve the Penman-Monteith equation for the alfalfa reference crop are as follows:

- a) The slope of saturation vapor pressure curve is calculated using the following equation:

$$DLT = \frac{4098 \exp\left(\frac{17.27 * T}{T + 237.3}\right)}{(T + 237.3)^2} \quad \text{Eq. 2}$$

Where

DLT: slope of saturation vapor pressure curve in kPa °C⁻¹ [Eq. 5 in ASCE EWRI]

T : daily mean air temperature ($[T_{\min} + T_{\max}] / 2$) in °C

b) The net radiation for PET is calculated using the following equation:

$$\mathbf{RN_PET = ralb + rout} \quad \mathbf{Eq. 3}$$

Where

RN_PET : net radiation for PET in MJ m⁻² d⁻¹ [Eq. 15 in ASCE EWRI]

$ralb$: net short-wave radiation for PET in MJ m⁻² d⁻¹

$rout$: net outgoing long-wave radiation in MJ m⁻² d⁻¹

$$\mathbf{ralb = ra * (1.0 - 0.23)} \quad \mathbf{Eq. 4}$$

Where

$ralb$: [Eq. 16 in ASCE EWRI]

ra : extraterrestrial radiation in ASCE EWRI or daily mean short-wave radiation in MJ m⁻² d⁻¹

Note: Surface albedo is assumed to be a constant value of 0.23 characteristic of a standardized short or tall reference crop.

$$rout = rbo * rto * 4.9E - 9 * \left[\frac{T_{K \max}^4 + T_{K \min}^4}{2} \right] \quad \mathbf{Eq. 5}$$

Where

$rout$: [Eq. 17 in ASCE EWRI]

$T_{K \max}$: maximum absolute temperature during the 24-hour period [K]
(K=°C+273.16)

$T_{K \min}$: minimum absolute temperature during the 24-hour period [K]
(K=°C+273.16)

Note: 4.9E-9 is the Stefan-Boltzman constant

$$\mathbf{rbo = -(0.34 - 0.139 * \sqrt{ED})} \quad \mathbf{Eq. 6}$$

Where

rbo: net emissivity [Eq. 17 in ASCE EWRI]

ED: actual vapor pressure [kPa]

There are two options for calculating the actual vapor pressure. One takes into consideration the min and max relative humidity, the second option determines the vapor pressure using dew point temperature. If the dew point temperature data are available, it is the preferred method (Allen et al., 2005).

Option 1. Min and Max Relative Humidity approach for determining vapor pressure

$$ED = \frac{svpmin * maxRH/100 + svpmax * minRH/100}{2} \quad \text{Eq.7}$$

Where

ED: [Eq. 11 in ASCE EWRI]

svpmin: minimum saturation vapor pressure using the ASCE EWRI approach in kPa

svpmax: maximum saturation vapor pressure using the ASCE EWRI approach in kPa

maxRH: maximum relative humidity in percent

minRH: minimum relative humidity in percent

$$svpmin = 0.6108 * e^{\frac{17.27 * MinTemp}{237.3 + MinTemp}} \quad \text{Eq.8}$$

$$svpmax = 0.6108 * e^{\frac{17.27 * MaxTemp}{237.3 + MaxTemp}} \quad \text{Eq.9}$$

$$SVP = \frac{svpmin + svpmax}{2} \quad \text{Eq. 10}$$

Where:

svpmin: [Eq. 7 in ASCE EWRI]

svpmax: [Eq. 7 in ASCE EWRI]

SVP: saturation vapor pressure in kPa [Eq. 6 in ASCE EWRI]

MinTemp: minimum temperature in °C

MaxTemp: maximum temperature in °C

Option 2. Dew Point Temperature approach for determining actual vapor pressure

ED: Actual vapor pressure using dew point temperature in kPa

$$\mathbf{ED = 0.6108 * e^{\frac{17.27 * Dew\ Point\ Temp}{237.3 + Dew\ Point\ Temp}}} \quad \mathbf{Eq.11}$$

Where:

ED: [Eq. 8 in ASCE EWRI]

Dew Point Temp: dew point temperature in °C

Note: Dew point temperature can be measured directly or computed from relative humidity and air temperature

The cloudiness function is estimated as follows:

$$\mathbf{rto = 1.35 * \left(\frac{Rs}{RMx} \right) - 0.35} \quad \mathbf{Eq. 12}$$

Where

rto: Cloudiness function [dimensionless] (limited to $0.05 \leq rto \leq 1.0$)
[Eq. 18 in ASCE EWRI]

Rs/RMx: relative solar radiation (limited to $0.3 \leq Rs/Rso \leq 1.0$)

Rs: measured or calculated solar radiation for the day in MJ m⁻² d⁻¹

RMx: calculated clear-sky radiation in MJ m⁻² d⁻¹

The ratio *Rs/RMx* in Eq. 12 represents relative cloudiness and is limited to $0.3 < Rs/RMx \leq 1.0$ so that *rto* has limits of $0.05 \leq rto \leq 1.0$. It is used in Eq. 5 to calculate outgoing long wave radiation.

To calculate the maximum possible radiation for the day, the solar declination, the relative distance of the earth from the sun, the sine and cosine of the site's latitude, and the corresponding Julian day have to be known.

Solar declination:

$$\mathbf{sd = 0.409 * \sin \left(\frac{JulianDay}{58.09} - 1.39 \right)} \quad \mathbf{Eq. 13}$$

Where

sd: solar declination in radians [Eq. 24 in ASCE EWRI]

The eccentricity of the orbit is calculated as:

$$\mathbf{dd} = 1 + 0.033 * \mathbf{Cos} \left(\frac{\mathbf{JulianDay}}{58.09} \right) \quad \text{Eq. 14}$$

Where

dd: inverse relative distance factor (squared) for the earth-sun [unitless]

[Eq. 23 in ASCE EWRI]

Sine and Cosine of the site's latitude (Lat):

$$\mathbf{latsin} = \mathbf{Sin} (\mathbf{Lat} * 2\pi/360) \quad \text{Eq. 15}$$

$$\mathbf{latcos} = \mathbf{Cos} (\mathbf{Lat} * 2\pi/360) \quad \text{Eq. 16}$$

The sunset hour angle, *h*, is given by:

$$\mathbf{h} = \mathbf{ArcCos}[-\mathbf{tan} (\mathbf{lat}) \mathbf{tan}(\mathbf{sd})] \quad \text{Eq. 17}$$

$$\mathbf{ys} = \mathbf{latsin} * \mathbf{Sin} (\mathbf{sd}) \quad \text{Eq. 18}$$

$$\mathbf{yc} = \mathbf{latcos} * \mathbf{Cos} (\mathbf{sd}) \quad \text{Eq. 19}$$

Where

h: [Eq. 27 in ASCE EWRI]

Extraterrestrial radiation, *ra*, is defined as short-wave solar radiation in the absence of an atmosphere. It is a well-behaved function of the Julian Day of the year and latitude. It is needed for calculating *RMx*, which is in turn used in calculating *Rn*. For daily (24-hour) periods, *ra* can be estimated from the solar constant, the solar declination and the julian day of the year as follows:

$$\mathbf{ra} = 37.586 * \mathbf{dd} * (\mathbf{h} * \mathbf{ys} + \mathbf{yc} * \mathbf{Sin} (\mathbf{h})) \quad \text{Eq. 20}$$

Where

ra: [Eq. 24 in ASCE EWRI]

When a dependable, locally calibrated procedure for determining *RMx* is not available, *RMx*, for purposes of calculating *Rn*, can be computed as:

$$\mathbf{RMx} = (0.75 + 2 * 10^{-5} \mathbf{Elev}) \mathbf{ra} \quad \text{Eq. 21}$$

Where

RMx: [Eq. 19 in ASCE EWRI]

Elev: station elevation above sea level in m

The net radiation for maximum plant evapotranspiration (ET) is calculated by the following equation:

$$\mathbf{RN_ET} = \mathbf{ralb1} + \mathbf{rout} \quad \text{Eq. 22}$$

Where:

RN_ET: net radiation for maximum plant ET in MJ m⁻² d⁻¹ [Eq. 42 in ASCE EWRI]

ralb1: net short-wave radiation for maximum plant ET in MJ m⁻² d⁻¹

$$\mathbf{ralb1} = \mathbf{ra} * (\mathbf{1.0} - \mathbf{albday}) \quad \text{Eq. 23}$$

Where:

ralb1: [Eq. 43 in ASCE EWRI]

albday: surface albedo for the day

To calculate the albedo for the day, the residue on soil surface for current day has to be determined.

$$\mathbf{SolCov} = \mathbf{Max} (\mathbf{0.8} * [\mathbf{PBio} + \mathbf{Residue}], \mathbf{0.0}) \quad \text{Eq. 24}$$

$$\mathbf{eaj} = \mathbf{Exp} (\mathbf{cej} * [\mathbf{SolCov} + \mathbf{0.1}]) \quad \text{Eq. 25}$$

$$\mathbf{albday} = \mathbf{0.23} * (\mathbf{1.0} - \mathbf{eaj}) + \mathbf{salb} * \mathbf{eaj} \quad \text{Eq. 26}$$

If the crop type is non-deciduous and completely covers the soil, albedo is constant:

$$\mathbf{albday} = \mathbf{0.23} \quad \text{Eq. 27}$$

Where:

SolCov: aboveground biomass and residue for current day in Tons/ha
[SWAT 2005]

PBio: potential biomass production for current day in Tons/ha (Computed in PGM)

Residue: crop residue on soil surface after harvest in Tons/ha

Plant Physiological Responses to Atmospheric Forcings

eaj: soil cover index [Eq. 1:1.2.16 in SWAT 2005]

cej: constant (-5×10^{-5})

salb: soil albedo for wet bare soil (0.08)

albday: [Eq. 1:1.2.15 in SWAT 2005]

The psychrometric constant is calculated by the following equation:

$$\mathbf{GMA} = \frac{\mathbf{1.013E - 3 * PB}}{\mathbf{0.622 * HV}} \quad \text{Eq. 28}$$

Where:

GMA: [Eq. B.12 in ASCE EWRI]

Specific capacity of moist air = $1.013E-3$

Ratio of molecular weight of water vapor to dry air = 0.622

The atmospheric pressure is calculated by the following equation:

$$\mathbf{PB} = \mathbf{101.3 (1.0 - 2.21E - 5 * ELEV)^{5.257}} \quad \text{Eq. 29}$$

Assuming reference temperature of 293K – see ASCE EWRI Eq. 3

PB: atmospheric pressure in kPa [Eq. 3 in ASCE EWRI]

ELEV: elevation of the site in meters [m] above mean sea level

$$\mathbf{HV} = \mathbf{2.501 - 2.361E - 3 * TX} \quad \text{Eq. 30}$$

HV: latent heat of vaporization in MJ/kg [Eq. B.7 in ASCE EWRI]

TX: average daily air temperature in °C

The specific heat of moist air at constant pressure is as follows in MJ kg⁻¹ °C⁻¹:

$$\mathbf{cp} = \mathbf{1.013E - 3} \quad \text{Eq. 31}$$

The air density, rho, (kg/m³) is calculated by the following equation:

$$\mathbf{rho} = \mathbf{3.486 * PB / Tkv} \quad \text{Eq. 32}$$

Where:

rho: [Eq. B.10 in ASCE EWRI]

$$T_{kv} = \frac{TX + 273.16}{1.0 - 0.378 * \left(\frac{ED}{PB}\right)} \quad \text{Eq. 33}$$

T_{kv}: virtual temperature (°K) [Eq. B.11 in ASCE EWRI]

Vapor pressure deficit (kPa) is calculated by the following equation:

$$VPD = SVP - ED \quad \text{Eq. 34}$$

Where:

VPD: vapor pressure deficit in kPa [Eq. 1:2.3.5 in SWAT 2005]

SVP: saturation vapor pressure at mean air temperature in kPa

ED: actual vapor pressure at mean air temperature in kPa

The aerodynamic resistance is calculated by the following equation:

$$AR = \frac{109.6}{U2} \quad \text{Eq. 35}$$

Where

AR: aerodynamic resistance in s/m [Constant 109.6 is derived from ASCE EWRI Eq. B.2 for 0.5 m alfalfa reference crop and 2 m shelter height]

U2: mean daily wind speed at 2 m height in m s⁻¹

Note: This equation is similar to Eq. B.2 in ASCE EWRI when the measurement height is 2 m and the reference crop height is 0.5 m as assumed for the tall reference crop (alfalfa). When equation B.2 is used the value in the numerator is 109.6.

The canopy resistance is calculated by the following equation:

$$CR = \frac{45}{1.4 - 0.4 * (CO2 / 330)} \quad \text{Eq. 36}$$

Where:

CR: canopy resistance in s/m [Constant 45 based on alfalfa reference crop in ASCE EWRI Table 2]

CO₂: atmospheric carbon dioxide concentration in ppm

Note: This equation is similar to Eqs. B.3 to B.6 in ASCE EWRI. In the ASCE standardized reference eqn., the tall crop (alfalfa) canopy resistance is assumed to be 45 s m⁻¹.

A.1.2 Maximum Plant Evapotranspiration (EPMax)

To calculate the maximum plant evapotranspiration (EPMax) for a specific crop, the Penman-Monteith method is solved as follows:

$$EP_{Max} = \frac{DLT * RN_{ET} + \rho * c_p * 86400 * VPD / ARM_{xET}}{HV * (DLT + GMA * (1 + CRM_{xET} / ARM_{xET}))} \quad \text{Eq. 37}$$

Where

EPMax: maximum plant evapotranspiration for a specific crop in mm d⁻¹
[Eq. 2:2.2.1 in SWAT 2005]

DLT: slope of the saturation vapor pressure curve in kPa °C⁻¹

RN_{ET}: net radiation for maximum plant ET in MJ m⁻² d⁻¹ [Eq. 42 in ASCE EWRI]

rho: air density in kg m⁻³

c_p: specific heat of moist air at constant pressure in MJ kg⁻¹ °C⁻¹

VPD: vapor pressure deficit in kPa

ARM_{xET}: aerodynamic resistance for maximum plant ET in s m⁻¹

HV: latent heat of vaporization in MJ kg⁻¹

GMA: psychrometric constant in kPa °C⁻¹

CRM_{xET}: Canopy resistance for maximum plant ET in s m⁻¹

To make sure maximum ET is not greater than potential ET (reference crop: Alfalfa)

$$EP_{Max} = \text{Min} (EP_{Max}, PET_{Day}) \quad \text{Eq. 38}$$

Where:

EPMax: Maximum evapotranspiration for a specific crop in mm d⁻¹ [SWAT 2005 Code]

The wind speed and height of wind speed measurement is calculated by the following equations based on the approach taken in SWAT.

If the crop height is less than 1.0 m (CPHT<1.0) in height, the wind speed is adjusted as follows:

$$UZZMxET = U2 \quad \text{Eq. 39}$$

$$ZZMxET = 200 \quad \text{Eq. 40}$$

$$ZOM = 0.123 * CHZ \quad \text{Eq. 41}$$

If the crop height is greater than 1.0 m and less than or equal to 2.5 m (1.0<CPHT≤2.5) in height, the wind speed is adjusted as follows:

$$ZZMxET = CPHT * 100 + 100 \quad \text{Eq. 42}$$

$$ZOM = 0.123 * CHZ \quad \text{Eq. 43}$$

$$UZZMxET = U2 * \left(\frac{\text{Log}\left(\frac{ZZMxET-D}{ZOM}\right)}{\text{Log}\left(\frac{200-D}{ZOM}\right)} \right) \quad \text{Eq. 44}$$

If the crop height is greater than 2.5 m (CPHT>2.5) in height, the wind speed is adjusted as follows:

$$ZZMxET = CPHT * 100 + 100 \quad \text{Eq. 45}$$

$$UZZMxET = U2 * (ZZMxET/200)^{0.2} \quad \text{Eq. 46}$$

$$ZOM = 0.058 * CHZ^{1.19} \quad \text{Eq. 47}$$

Where:

UZZMxET: wind speed (m s⁻¹) at height ZZ (cm) [Eq. B.14 in ASCE EWRI]

ZZMxET: height at which wind is determined in cm [Eq. B.14 in ASCE EWRI]

CPHT: canopy height in m

ZOM: roughness length for momentum transfer in cm [Eq. B.14 in ASCE EWRI]

CHZ: canopy height in cm

The canopy height is calculated by the following equation. If crop height is less than 0.01 m, canopy height is as follows:

$$CHZ = 1.0 \quad \text{Eq. 48}$$

Otherwise

$$CHZ = CPHT * 100 \quad \text{Eq. 49}$$

Where

CHZ: [SWAT 2005 Code]

The roughness length for vapor transfer is calculated by the following equation.

$$\mathbf{ZOV} = \mathbf{0.1} * \mathbf{ZOM} \quad \text{Eq. 50}$$

Where:

ZOV: roughness length for vapor transfer in cm [Eq. 2:2.2.6 in SWAT 2005]

The zero-plane displacement of wind profile is calculated by the following equation.

$$\mathbf{D} = \mathbf{0.667} * \mathbf{CHZ} \quad \text{Eq. 51}$$

Where:

D: displacement height for plant type in cm [Eq. 2:2.2.7 in SWAT 2005]

The aerodynamic resistance for maximum plant ET is calculated by the following equation.

$$\mathbf{ARMxET} = \frac{\ln\left[\frac{\mathbf{ZZMxET}-\mathbf{D}}{\mathbf{ZOM}}\right] * \ln\left[\frac{\mathbf{ZZMxET}-\mathbf{D}}{\mathbf{ZOV}}\right]}{(\mathbf{0.41}^{\wedge}2) * \mathbf{UZZMxET}} \quad \text{Eq. 52}$$

Where:

ARMxET: aerodynamic resistance for maximum plant ET in s m⁻¹

[Eq. 2:2.2.3 in SWAT 2005]

The stomatal conductivity is adjusted for high vapor pressure according to Figure 1 and it is calculated by the following equations.

$$\mathbf{FvpdMxET} = \mathbf{Max}(\mathbf{0.1}, \mathbf{1.0} - \mathbf{bx} * \mathbf{XX}) \quad \text{if} \quad \mathbf{XX} > \mathbf{0} \quad \text{Eq. 53}$$

$$\mathbf{FvpdMxET} = \mathbf{1.0} \quad \text{if} \quad \mathbf{XX} < \mathbf{0}$$

$$\mathbf{gsi_adj} = \mathbf{gsi} * \mathbf{FvpdMxET} \quad \text{Eq. 54}$$

Where:

$$\mathbf{XX: VPD} - \mathbf{vpth} \quad \text{Eq. 55}$$

$$bx = (1 - vpd2) / (vpdabth - vpth)$$

Eq. 56

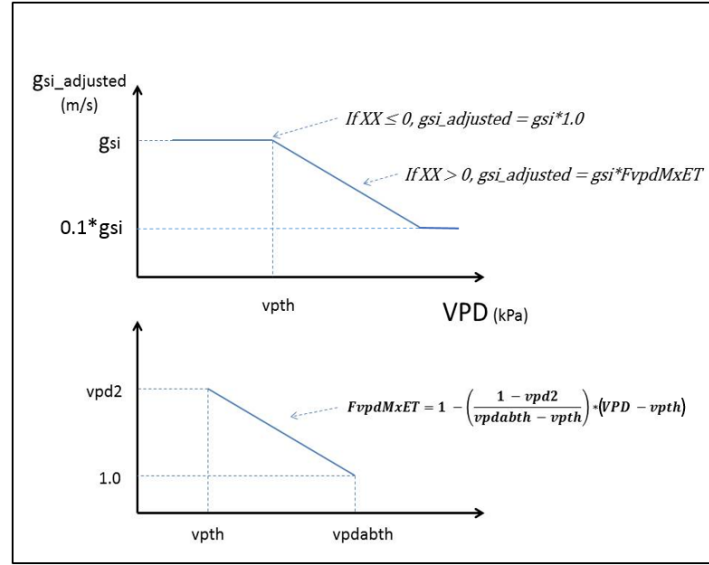


Figure A.1.1. Stomatal Conductivity Adjustment for High Vapor Pressure

FvpdMxET: [SWAT 2005 Code]

gsi_adj: adjusted stomatal conductivity for high vapor pressure in $m s^{-1}$

[SWAT 2005 Code]

gsi: maximum stomatal conductance in $m s^{-1}$

bx: rate of decline in leaf conductance per unit increase in VPD ($m s^{-1} kPa^{-1}$)

[Eq. 2:2.2.16 in SWAT 2005]

vpd2: corresponding fraction of the maximum stomatal conductance at the value of VPD

vpdabth: value of VPD above *vpth*

vpth: threshold VPD above which the stomatal conductivity is adjusted in kPa

The canopy resistance for maximum plant ET is calculated by the following equation.

$$CRM_{xET} = \frac{1.0}{gsi_adj} \frac{1}{(0.5 * LAI) * (StomResp1 - StomResp2 * \frac{CO2}{330})}$$

Eq. 57

Where:

CRM_xET: Canopy resistance for maximum plant ET in s m⁻¹

[Eq. 2:2.2.15 in SWAT 2005]

LAI: Leaf area index of canopy

StomResp1: Stomatal response value 1 at elevated CO₂ concentration (C3/C4 crop parameter dimensionless)

StomResp2: Stomatal response value 2 at elevated CO₂ concentration (C3/C4 crop parameter dimensionless)

CO₂: Carbon dioxide concentration in the atmosphere (ppm)

A.1.3 Canopy Interception

Canopy interception is the portion of rainfall that remains in the canopy and does not contribute to surface runoff or infiltration. PGM allows the maximum amount of water that can be held in canopy storage to vary from day to day as a function of the leaf area index as follows:

$$CanMxl = CanMx * \frac{LAI}{XLAI330} \quad \text{Eq. 58}$$

Where:

CanMxl: maximum amount of water that can be trapped in the canopy on a given day in mm of H₂O [Eq. 2:2.2.1 in SWAT 2005]

CanMx: maximum amount of water that can be trapped in the canopy when the canopy is fully developed in mm of H₂O

LAI: leaf area index for a given day (dimensionless)

XLAI330: maximum leaf area index for the plant at 330 ppm of CO₂ (dimensionless)

When precipitation falls on any given day, the canopy storage is filled before any water is allowed to reach the ground and infiltrate or become surface runoff.

When rainfall is less than the difference between *CanMxl* and *CanStor*:

$$CanStor = CanStor + RF \quad \text{Eq. 59}$$

$$RF = 0 \quad \text{Eq. 60}$$

Otherwise

$$\mathbf{CanStor} = \mathbf{CanMxl} \quad \mathbf{Eq. 61}$$

$$\mathbf{RF} = \mathbf{RF} - (\mathbf{CanMxl} - \mathbf{CanStor})$$

Where

CanStor: amount of free water held in the canopy on a given day in mm

[Eq. 2:2.1.2 in SWAT 2005]

RF: rainfall reaching the ground on a given day in mm [Eq. 2:2.1.3 in SWAT 2005]

Once the potential evapotranspiration is determined, the actual evaporation is calculated. This model first evaporates any rainfall intercepted by the canopy. Next, the model calculates the maximum amount of transpiration and the maximum amount of soil evaporation.

The model removes as much water as possible from canopy storage when calculating actual evaporation. If potential evapotranspiration, PETDAY, is less than the amount of free water held in the canopy, CanStor, then

$$\mathbf{CanStor} = (\mathbf{CanStor} - \mathbf{PETDAY}) \quad \mathbf{Eq. 62}$$

$$\mathbf{CanET} = \mathbf{PETDAY} \quad \mathbf{Eq. 63}$$

$$\mathbf{EPMax} = 0 \quad \mathbf{Eq. 64}$$

$$\mathbf{ESMax} = 0 \quad \mathbf{Eq. 65}$$

Otherwise

$$\mathbf{CanET} = \mathbf{CanStor} \quad \mathbf{Eq. 66}$$

$$\mathbf{CanStor} = 0 \quad \mathbf{Eq. 67}$$

Where:

CanET: Plant canopy evapotranspiration in mm

A.2 Potential Soil Evaporation

To calculate the potential soil evaporation (ESMax), PETDay from the Penman-Monteith method is used as follows:

$$\text{ESMax} = \text{PETDay} * \text{eaj} \quad \text{Eq. 68}$$

$$\text{Eos1} = \text{PETDay} / (\text{ESMax} + \text{EPMax}) \quad \text{Eq. 69}$$

$$\text{Eos1} = \text{ESMax} * \text{Eos1} \quad \text{Eq. 70}$$

$$\text{ESMax} = \text{Min} (\text{ESMax}, \text{Eos1}) \quad \text{Eq. 71}$$

Where:

eaj: soil cover index. See Eqn 25.

To be sure that maximum plant and soil evapotranspiration do not exceed potential ET, the following equations and conditions are used.

$$\text{IF PETday} - \text{CanET} < \text{EPMax} + \text{ESMax} \text{ THEN} \quad \text{Eq. 72}$$

$$\text{ESMax} = \text{PETDay} * \text{ESMax} / (\text{ESMax} + \text{EPMax}) \quad \text{Eq. 73}$$

$$\text{EPMax} = \text{PETDay} * \text{EPMax} / (\text{ESMax} + \text{EPMax})$$

ELSE

$$\text{ESMAX} = \text{ESMAX}$$

$$\text{EPMAX} = \text{EPMAX} \quad \text{Eq. 74}$$

A.3 Soil Water Balance & Actual Evapotranspiration

A.3.1 Soil Water Movement

Precipitation that is not intercepted by the canopy can become either surface runoff or infiltrates into the soil. Water in the soil exits the model domain through either transpiration, evaporation, or deep percolation out the bottom of the root zone.

Of these different pathways, plant uptake of water removes the majority of water that enters the soil profile. The potential plant uptake as a function of depth is calculated using:

$$\mathbf{UXLayers(i)} = \frac{\mathbf{EPMax}}{\mathbf{1-Exp(-bw)}} * \left(\mathbf{1 - Exp} \left(-\mathbf{bw} * \frac{\mathbf{TotLayDepth(i)}}{\mathbf{RDepth}} \right) \right) \quad \mathbf{Eq. 75}$$

Where:

UXLayers(i): potential transpiration from soil layer between the ground surface and the bottom of layer (i) in mm d⁻¹ [Eq. 5:2.2.1 in SWAT 2005]

bw: water-use distribution parameter (10 by default), dimensionless

TotLayDepth(i): distance from the soil surface to the bottom of layer (i) in mm

RDepth: depth of root development in the soil in mm

The potential water uptake from a particular soil layer can be calculated by solving the previous equation for the depth at the top and bottom of the soil layer and taking the difference between the values. Since root density is greatest near the soil surface and decreases with depth, the water uptake from the upper layer is assumed to be much greater than that in the lower layers. The water-use distribution parameter, *bw*, is set to 10 in PGM. With this value, 50% of the water uptake will occur in the upper 6% of the root zone.

As the water content of the soil decreases, the water in the soil is held more and more tightly by the soil particles. To reflect the effect this has on a plant's ability to extract water the following equation is used:

IF $\mathbf{SWLayer(i)} < (\mathbf{AWCLayer(i)} / 4)$ **THEN**

$$\mathbf{F(i)} = \mathbf{Exp} \left(5 * \frac{4 * \mathbf{SWLayer(i)}}{\mathbf{AWCLayer(i)}} - 1 \right) \quad \mathbf{Eq. 76}$$

ELSE

$$\mathbf{F(i)} = \mathbf{1.0} \quad \mathbf{Eq. 77}$$

Where:

F(i): water availability factor (dimensionless) for layer (i) [Eq. 5:2.2.4 in SWAT 2005]

SWLayer (i): amount of water in the soil layer on a given day in mm

AWCLayer(i): available water capacity for layer (i) in mm

$$AWCLayer(i) = SWCFC(i) - SWCWP(i) \text{ [Eq. 5:2.2.6 in SWAT 2005]}$$

$SWCFC(i)$: soil water content at field capacity for layer (i) (fraction)

$SWCWP(i)$: soil water content at wilting point for layer (i) (fraction)

The soil layers' thickness and the number of layers defined in the model are shown in Figure 2. In PGM, there are 13 layers in total ($i = 13$). The top layer, which is the evaporation layer ($Z[1]$), is the only layer that is defined by the user in the interface.

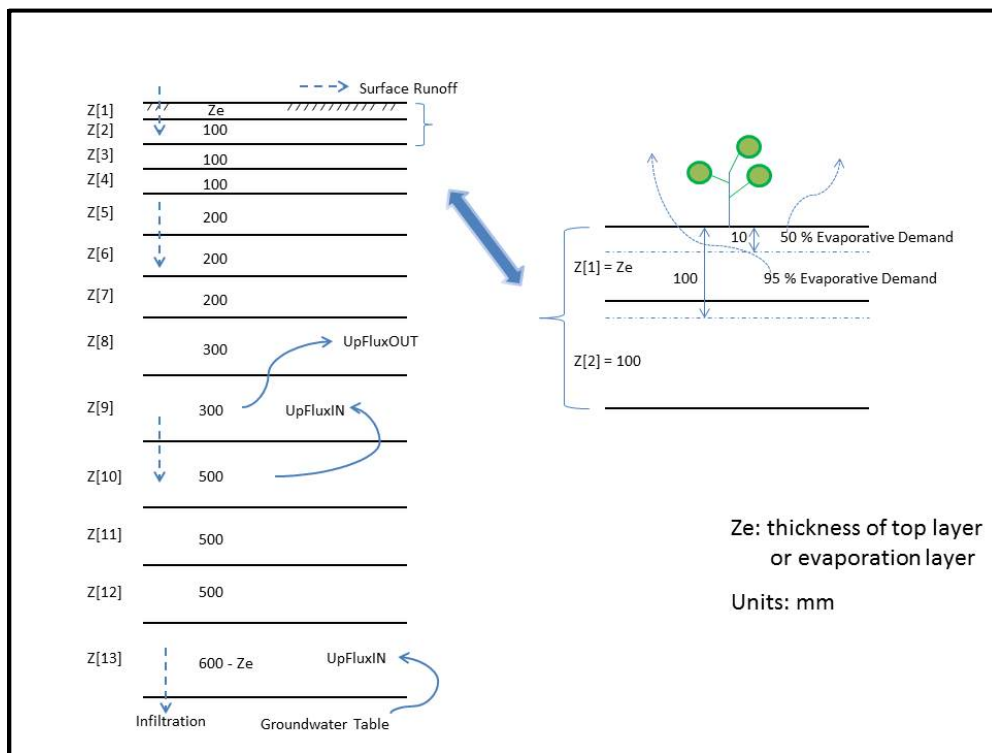


Figure A.3.1. Soil Layer Profile

Once the potential water uptake and water availability factor have been obtained for soil water conditions, the actual amount of water uptake from the soil layer is calculated.

$$TALayer(i) = (UXLayer(i) + TRemain * epco) * F(i) \tag{Eq. 78}$$

$$TRemain = UX - TA \tag{Eq. 79}$$

Where:

$TALayer(i)$: actual water uptake from soil layer in mm [Eq. 5:2.2.3 in SWAT 2005]

$TRemain$: water uptake remaining in mm

epco: plant uptake compensation factor: 0 to 1.0 (dimensionless)

UX: potential water use rate for the whole soil profile in mm d⁻¹

TA: actual water uptake from the whole soil profile in mm d⁻¹

The plant uptake compensation factor (*epco*) allows plants to compensate for water deficiencies in dry layers by using water from other layers for soils with good rooting environments (*epco* near 1.0). However, compensation is reduced and finally is not allowed as *epco* approaches 0.0.

The total sum of the actual water uptake from all soil layers is the actual plant transpiration for the day. Once total actual plant transpiration is calculated, actual soil evaporation must be calculated. When an evaporation demand for soil exists, the model must first partition the evaporative demand between the different layers. The depth distribution used to determine the maximum amount of water allowed to be evaporated is:

$$EPlayer(i) = ESMax * \frac{TotLayDepth(i)}{TotLayDepth(i) + \text{Exp}(2.374 - 0.00713 * TotLayDepth(i))} \quad \text{Eq. 80}$$

Where:

EPlayer(i): potential evaporation demand for the soil between the soil surface and the bottom of layer (i) [Eq. 2:2.3.16 in SWAT 2005]

ESMax: potential soil evaporation in mm

TotLayDepth(i): total depth from the soil surface to bottom of layer (i) in mm

The coefficients in equation (80) were selected so that 50% of the evaporative demand is extracted from the top 10 mm of the soil and 95% of the evaporative demand is extracted from the top 100 mm of soil (Figure 2). The amount of evaporative demand for a particular soil layer is determined by taking the difference between the evaporative demands calculated at the upper and lower boundaries of the soil layer.

To reflect the decrease in soil water content in the evaporative water demand from drier soils, an evaporative water demand factor is determined based on the soil physical properties and estimated with the function:

$$EFactor(i) = \text{Min} \left(1.0, \text{Exp} \left(2.5 * \frac{SWLayer(i) - SWCFC(i)}{AWCLayer(i)} \right) \right) \quad \text{Eq. 81}$$

Where:

EFactor(i): evaporative water factor for layer (i) (dimensionless) [Eq. 2:2.3.18 in SWAT 2005]

$SWLayer(i)$: amount of water in the soil layer on a given day in mm

$SWCFC(i)$: soil water content at field capacity for layer (i) in mm

$AWCLayer(i)$: available water capacity for layer (i) in mm

Once the potential evaporative soil demand has been obtained for soil water conditions, the actual amount of soil evaporation from the soil layer is calculated.

$$EALayer(i) = EPLayer(i) * EFactor(i) \quad \text{Eq. 82}$$

Where:

$EALayer(i)$: actual amount of soil evaporation from the layer (i) in mm [Eq. 2:2.3.18 in SWAT 2005]

In addition to limiting the amount of water removed by evaporation in dry conditions, the model defines a maximum value of water that can be removed at any time. This maximum value is 80% of the plant available water on a given day where the plant available water is defined as the total water content of the soil layer minus the water content of the soil layer at wilting point.

$$EALayer'(i) = \text{Min}(EALayer(i), 0.8 * (SWLayer(i) - SWCWP(i))) \quad \text{Eq. 83}$$

Where:

$EALayer'(i)$: amount of water removed from layer (i) by evaporation in mm [Eq. 2:2.3.20 in SWAT 2005]

The amount of water removed from soil layers is determined by taking the difference between the actual evaporative demands calculated at the upper and lower boundaries of the soil layers. Even further the model limits soil evaporation to some specific soil depth. The maximum soil depth from which evaporation is allowed to occur is set to 0.5 m.

A.3.2 Infiltration

Infiltration is determined using the Philip Equation. The root zone sorptivity is calculated if irrigation, rainfall or water ponding is greater than 0.0.

$$\text{CapDrive} = \frac{0.46*m+2.07*m^2+ 19.5* m^3}{1+4.7*m+16* m^2* 1/\alpha} \quad \text{Eq. 84}$$

$$\beta = 1.3 \quad \text{Eq. 85}$$

$$\text{RZSorp} = (2 * (\text{SWCS} - \text{ThRZ}) * \text{Ksat} * \frac{\text{CapDrive}}{\beta})^{1/2} \quad \text{Eq. 86}$$

MaxInfil =

$$(\text{RZSorp} * \sqrt{\text{InfilEnd}} + \text{Ksat} * \text{InfilEnd}) - (\text{RZSorp} * \sqrt{\text{InfilStart}} + \text{Ksat} * \text{InfilStart}) \quad \text{Eq. 87}$$

Where:

CapDrive: capillary drive

$$m = 1 - 1/n$$

n: van Genuchten parameter

α : inverse of the air-entry value (bubbling pressure)

β : assumed to be 1.3

SWCS: soil water content at saturation, dimensionless

ThRZ: soil water content in root zone, dimensionless

Ksat: saturated hydraulic conductivity in length/time

RZSorp: The root zone sorptivity in length/time

MaxInfil: maximum infiltration rate in length/time [PGM Internal Code]

InfilEnd: time of infiltration end

InfilStart: time of infiltration start

Upflux coming into layer (i) from underneath layer (see **Figure D-4** above) is calculated with the function:

$$\text{UpFlux}(i) = \text{KUpFlux}(i) * \frac{(\psi_{A+\text{CLayDepth}(i-1)} - \psi_{B+\text{CLayDepth}(i)})}{\text{CLayDepth}(i-1) - \text{CLayDepth}(i)} \quad \text{Eq. 88}$$

Where:

$UpFlux(i)$: Upflux coming into layer (i) in mm

$KUpFlux(i)$: upflux hydraulic conductivity in $mm\ s^{-1}$

ψ_A : Pressure head at point A

ψ_B : Pressure head at point B

$CLayDepth(i)$: center layer depth point for layer (i) in mm

The main assumption is that ψ_B is greater than ψ_A for upflux to happen.

If the depth of the center of layer (i) is below the groundwater table depth, the soil water content is adjusted to saturation.

if $CLayDepth(i) > WTDepth$

$$\mathbf{Th(i) = SWCS(i)} \quad \text{Eq. 89}$$

Where:

$WTDepth$: water table depth in mm [PGM Internal Code]

The ponded water mass balance is computed only for the top layer when there is water ponding ($DSP > 0$).

If the potential soil evaporation ($ESMax$) is greater or equal than total depth of applied water and ponded surface water:

$$\mathbf{Infilt(i) = 0.0} \quad \text{Eq. 90}$$

$$\mathbf{EvapRemain = ESMax - DSP + TWDAL} \quad \text{Eq. 91}$$

$$\mathbf{SurfEvap = DSP + TWDAL} \quad \text{Eq. 92}$$

$$\mathbf{DSP = 0.0} \quad \text{Eq. 93}$$

$$\mathbf{SWRO = 0.0} \quad \text{Eq. 94}$$

If the potential soil evaporation ($ESMax$) is smaller than total applied water and depth of ponded water:

$$\mathbf{Infilt(i) = Min(DSP + TWDAL - ESMax, MaxInfil)} \quad \text{Eq. 95}$$

$$\mathbf{EvapRemain = 0.0} \quad \text{Eq. 96}$$

$$\mathbf{SurfEvap = ESMax} \quad \text{Eq. 97}$$

$$\mathbf{DSP = \text{Min}(\text{MaxPond}, \text{DSP} + \text{TWDAL} - \text{ESMax} - \text{Infil}(i))} \quad \mathbf{Eq. 98}$$

$$\mathbf{SWRO = DSP + TWDAL - ESMax - Infil(i) - MaxPond} \quad \mathbf{Eq. 99}$$

Where:

Infil(i): infiltration into soil layer (i) in mm

EvapRemain: evaporation remain in mm

SurfEvap: surface evaporation in mm

DSP: depth of surface ponding in mm

SWRO: surface water runoff in mm

MaxPond: maximum depth of surface ponding in mm

TWDAL: total water depth applied to land in mm

If surface ponding is not present, runoff may still occur. In this case the model first determines if the total applied water depth is greater than the maximum infiltration and the maximum ponding depth. If so,

$$\mathbf{SWRO = TWDAL - (\text{MaxInfil} + \text{MaxPond})} \quad \mathbf{Eq. 100}$$

$$\mathbf{DSP = \text{MaxPond}} \quad \mathbf{Eq. 101}$$

$$\mathbf{\text{Infil}(i) = \text{MaxInfil}} \quad \mathbf{Eq. 102}$$

$$\mathbf{\text{EvapRemain} = \text{EA} + \text{TA}} \quad \mathbf{Eq. 103}$$

$$\mathbf{\text{SurfEvap} = 0.0} \quad \mathbf{Eq. 104}$$

If the opposite condition is reached, the model uses the following relationships.

$$\mathbf{SWRO = 0.0} \quad \mathbf{Eq. 105}$$

$$\mathbf{DSP = TWDAL - \text{MaxInfil}} \quad \mathbf{Eq. 106}$$

$$\mathbf{\text{Infil}(i) = \text{MaxInfil}} \quad \mathbf{Eq. 107}$$

$$\mathbf{\text{EvapRemain} = \text{EA} + \text{TA}} \quad \mathbf{Eq. 108}$$

$$\mathbf{\text{SurfEvap} = 0.0} \quad \mathbf{Eq. 109}$$

Where:

MaxPond: maximum ponding depth in mm

EA: actual soil evaporation in mm

TA: actual plant transpiration in mm

When the total applied water depth is less than the maximum infiltration rate, the model determines the following:

$$\mathbf{SWRO = 0.0} \qquad \mathbf{Eq. 110}$$

$$\mathbf{DSP = 0.0} \qquad \mathbf{Eq. 111}$$

$$\mathbf{Infilt(i) = TWDAL} \qquad \mathbf{Eq. 112}$$

$$\mathbf{EvapRemain = EA} \qquad \mathbf{Eq. 113}$$

$$\mathbf{SurfEvap = 0.0} \qquad \mathbf{Eq. 114}$$

And finally when there is no water applied at all, PGM determines the following:

$$\mathbf{SWRO = 0.0} \qquad \mathbf{Eq. 115}$$

$$\mathbf{DSP = 0.0} \qquad \mathbf{Eq. 116}$$

$$\mathbf{Infilt(i) = 0.0} \qquad \mathbf{Eq. 117}$$

$$\mathbf{EvapRemain = EA} \qquad \mathbf{Eq. 118}$$

$$\mathbf{SurfEvap = 0.0} \qquad \mathbf{Eq. 119}$$

The following steps are used to compute the soil layer water mass balance. There are two potential conditions.

1. **The first condition is when there is infiltration at the soil surface.**

For soil layers below the groundwater table:

If CLayDepth(i) is greater than WTDepth:

$$\mathbf{Infilt(i) = \text{Min} (Ksat, infilt(i) - UpFluxOut(i))} \qquad \mathbf{Eq. 120}$$

For cases in which there is infiltration:

For the case where infiltration fills the soil in excess of saturation:

$$\mathbf{Infilt(i) = (Infilt(i - 1) + UpFluxIn(i - 1) - UpFluxOut(i - 1) + Th(i - 1) - evap - TAlayer(i - 1) - SWCS(i - 1))} \quad \mathbf{Eq. 121}$$

For the case in which infiltration fills soil between field capacity and saturation:

$$\mathbf{Infilt(i) = (Infilt(i - 1) + UpFluxIn(i - 1) - UpFluxOut(i - 1) + Th(i - 1) - evap - TAlayer(i - 1) - SWCFC(i - 1)) * (1 - DCF)} \quad \mathbf{Eq. 122}$$

For the case in which infiltration fills soil to less than field capacity:

$$\mathbf{Infilt(i) = 0.0} \quad \mathbf{Eq. 123}$$

2. The second condition is for when there is no infiltration at the ground surface:

For the case when the soil water content is in excess of saturation:

$$\mathbf{Infilt(i) = Min(Ksat, (SWCS(i - 1) - SWCFC(i - 1)) * (1 - DCF))} \quad \mathbf{Eq. 124}$$

For the case in which the soil water content is between field capacity and saturation:

$$\mathbf{Infilt(i) = Min(Ksat, (Infilt(i - 1) + UpFluxIn(i - 1) - UpFluxOut(i - 1) + Th(i - 1) - evap - TAlayer(i - 1) - SWCFC(i - 1)) * (1 - DCF))}$$

Eq. 125

For the case in which irrigation fills soil to less than field capacity:

$$\mathbf{Infilt(i) = 0.0} \quad \mathbf{Eq. 126}$$

Where:

Infilt(i): infiltration into soil layer (i) in mm

UpFluxIn(i): upflux going in to layer (i) in mm

UpFluxOut(i): upflux going out from layer (i) in mm

Th(i): soil water content for layer (i) in mm

evap: soil evaporation in mm

TAlayer(i): actual plant water uptake from soil layer (i) in mm

SWCS: soil water content at saturation in mm

SWCFC: soil water content at field capacity in mm

DCF: soil water content decline factor (dimensionless) [Eq. 2:3.2.3 in *SWAT 2005*]

Where:

$$\mathbf{DCF} = \mathbf{1} - \mathbf{Exp}\left(-\frac{\mathbf{1}}{\mathbf{TT}}\right) \quad \text{Eq. 127}$$

and

$$\mathbf{TT} = \frac{\mathbf{SWCS} - \mathbf{SWCFC}}{\mathbf{Ksat}} \quad \text{Eq. 128}$$

$$\mathbf{evap} = \mathbf{Min}(\mathbf{EALayer}(i), \mathbf{EvapRemain}) \quad \text{Eq. 129}$$

Where:

TT: travel time for percolation (hrs) [Eq. 2:3.2.4 in *SWAT 2005*]

evap: evaporation in mm

The model checks that plant transpiration and soil evaporation won't reduce the soil water content below wilting point. If the soil water available for transpiration and evaporation is less than what is demanded, both evaporation and transpiration are reduced using relative weights as follows:

$$\mathbf{EFrac} = \frac{\mathbf{evap}}{\mathbf{evap} + \mathbf{TALayer}(i)} \quad \text{Eq. 130}$$

$$\mathbf{TFrac} = \frac{\mathbf{TALayer}(i)}{\mathbf{TALayer}(i) + \mathbf{evap}} \quad \text{Eq. 131}$$

$$\mathbf{TALayer}(i) = \mathbf{TFrac} * \left(\left(\mathbf{Th}(i) - \mathbf{SWCWP}(i) \right) + \mathbf{Infilt}(i) + \mathbf{UpFluxIN}(i) - \mathbf{UpFluxOUT}(i) \right) \quad \text{Eq. 132}$$

$$\mathbf{EALayer}(i) = \mathbf{EFrac} * \left(\left(\mathbf{Th}(i) - \mathbf{SWCWP}(i) \right) + \mathbf{Infilt}(i) + \mathbf{UpFluxIN}(i) - \mathbf{UpFluxOUT}(i) \right) \quad \text{Eq. 133}$$

The model may allow evaporation to decrease the soil water content below wilting point.

$$\mathbf{EALayer}(i) = \mathbf{EALayer}(i) + \mathbf{Min}(\mathbf{EvapLeft}, \mathbf{P5} * \mathbf{SWCWP}(i)) \quad \text{Eq. 134}$$

Where:

EFrac: fraction of evaporation to evaporate (dimensionless) [PGM Internal Code]

TFrac: fraction of transpiration to transpire (dimensionless) [PGM Internal Code]

EvapLeft: evaporation that was not met in mm [PGM Internal Code]

P5: maximum water content that can be removed below wilting point ($0.0 \leq P5 \leq 1$) in the top 0.5 m of soil and it is set to 1.0 below 0.5 m (dimensionless)

Thus, model can be adjusted to allow the top 0.5 m of soil to dry down to any fraction of wilting point.

Finally the model recalculates the new soil water content by doing a soil water mass balance for each soil layer.

$$\mathbf{Th(i - 1)} = \mathbf{Th(i - 1)} + \mathbf{Infilt(i - 1)} + \mathbf{UpFluxIn(i - 1)} - \mathbf{UpFluxOut(i - 1)} + \mathbf{EALayer(i - 1)} - \mathbf{TALayer(i - 1)} - \mathbf{Infilt(i)} \quad \mathbf{Eq. 135}$$

Also the model checks that no layer has a water content greater than saturation. If such a condition exists, then the water in excess of saturation is transferred to the layer above.

$$\mathbf{Transfer(i)} = \mathbf{Th(i)} - \mathbf{SWCS(i)} \quad \mathbf{if} \quad \mathbf{Th(i)} > \mathbf{SWCS(i)} \quad \mathbf{Eq. 136}$$

$$\mathbf{Th(i)} = \mathbf{SWCS(i)} \quad \mathbf{if} \quad \mathbf{Th(i)} > \mathbf{SWCS(i)} \quad \mathbf{Eq. 137}$$

$$\mathbf{Transfer(i)} = \mathbf{0.0} \quad \mathbf{if} \quad \mathbf{Th(i)} \leq \mathbf{SWCS(i)} \quad \mathbf{Eq. 138}$$

If there is a correction for excess water in the top layer, the surface runoff is adjusted.

$$\mathbf{SWRO} = \mathbf{SWRO} + \mathbf{Transfer(i)} \quad \mathbf{Eq. 139}$$

Where:

Transfer(i): excess water transfer to layer (i) in mm

SWCS(i): soil water content at saturation in layer (i) in mm

SWRO: surface runoff in mm

A.4 Crop Growth and Yield

Crop growth is simulated with a single model using different parameters for different crop types. Due to the similarities with the APEX and SWAT models, the model can be parameterized using the databases provided with those models. The growth period for annual crops can be initiated at a user specified planting date or once a user specified number of heat units has accumulated. Leaf senescence occurs when a crop specific fraction of the heat units required to reach maturity (PHU) is reached. Harvest can be

specified as a date or as a function of heat unit accumulation. Perennial crops initiate growth once the daily average air temperature exceeds the crop specific base temperature.

Phenological development of the crop is based on daily heat unit accumulation. It is computed using the equation:

$$\mathbf{HU = 0.5 * (TMX + TMN) - TBSC} \quad \mathbf{HU > 0} \quad \mathbf{Eq. 140}$$

Where:

HU: number of heat units accumulated during a day [Eq. 5:1.1.1 in SWAT 2005]

TMX: maximum temperatures for the day in °C

TMN: minimum temperatures for the day in °C

TBSC: crop-specific base temperature of all variables in °C (no growth occurs at or below TBSC)

A heat unit index is calculated by dividing the accumulated heat units by the total HU required to reach maturity ($HUI = \sum HU / \text{Potential HU}$). The HUI ranges from 0.0 at germination to 1.0 at harvest. The timing of harvest, leaf area growth and senescence, and partitioning of dry matter among roots, shoots, and economic yield are affected by HUI.

A.4.1 Potential Growth

Potential growth is calculated using the following formula. Potential growth is the growth that can occur if there is no temperature, water, or nutrient stress. In this version model, only temperature and water stress are simulated.

$$\mathbf{Bio = 0.001 * PAR * (RUE - WAVP * X1)} \quad \mathbf{Eq. 141}$$

Where:

Bio: daily potential increase in biomass in $t \text{ ha}^{-1} \text{ d}^{-1}$ [Eq. 275 in APEX 2008]

PAR: intercepted photosynthetic active radiation in $\text{MJ m}^{-2} \text{ d}^{-1}$

RUE: radiation-use efficiency factor for converting energy to biomass ($\text{kg ha}^{-1} / (\text{MJ m}^{-2})$)

WAVP: crop specific parameter relating RUE and VPD ($\text{kg ha}^{-1} / (\text{MJ m}^{-2} / \text{kPa})$). It is the slope of the RUE/VPD curve specific to each crop.

X1: See Eq. 144 (kPa)

$$\mathbf{PAR = 0.5 * RA * (1.0 - \exp(-0.65 * LAI))} \quad \mathbf{Eq. 142}$$

Where:

PAR: [Eq. 5:2.1.1 in SWAT 2005]

RA: solar radiation in MJ m⁻² d⁻¹

LAI: leaf area index (dimensionless)

Constant 0.5: used to convert solar radiation to photosynthetically active radiation

Constant 0.65: light extinction coefficient (dimensionless)

$$\text{RUE} = \frac{100 * \text{CO}_2}{\text{CO}_2 + \exp(\text{bc1} - \text{bc2} * \text{CO}_2)} \quad \text{Eq. 143}$$

Where:

RUE: [Eq. 5:2.1.4 in SWAT 2005]

CO₂: atmospheric CO₂ concentration in ppm

bc1, *bc2*: crop specific parameters obtained from two known values on the RUE-CO₂ curve

Note: The calculation of the parameters *bc1* and *bc2* from two known values on the RUE-CO₂ curve is described in the SWAT documentation (Neitsch, et al., 2005).

$$X1 = \max(0.0, \text{VPD} - \text{VPD}_{th}) \quad \text{Eq. 144}$$

Where:

X1: [Eq. 275b in APEX 2008]

VPD: vapor pressure deficit in kPa

VPD_{th}: threshold vpd (default = 1.0)

LAI is simulated as a function of heat units, crop stress, and crop development stage. During the crop growth stages from emergence to leaf senescence, LAI is estimated with the following equations:

$$\text{LAI} = \text{LAI}_0 + \text{dHUF} * \text{XLAI} * (1.0 - \text{Exp}(5.0 * \text{LAI}_0 - \text{XLAI}) * \text{sqrt}(\text{REG}))$$

Eq. 145

$$\mathbf{HUF} = \frac{\mathbf{HUI}}{\mathbf{HUI} + \exp(\ell(1) - \ell(2) * \mathbf{HUI})} \quad \text{Eq. 146}$$

Where:

LAI: leaf area index value of the crop at the end of the day, dimensionless
[Eq. 5:2.1.16 in SWAT 2005]

LAI₀: leaf area index value of the crop at the beginning day, dimensionless

dHUF: daily change in HUF, dimensionless

HUF: heat unit factor, dimensionless [Eq. 5:2.1.10 in SWAT 2005]

XLAI: maximum leaf area index of the crop, dimensionless

REG: value of the minimum crop stress factor, dimensionless

HUI: heat unit index (0 at planting to 1 at physiological maturity) of the crop, dimensionless

ℓ1 and ℓ2 coefficients: crop parameters relating HUF and HUI for crop

$$\mathbf{HUI} = \frac{\mathbf{Acc\ daily\ HU}}{\mathbf{Potential\ HU}} \quad \text{Eq. 147}$$

Where:

HUI: [Eq. 5:2.1.11 in SWAT 2005]

Acc Daily HU: Cumulative heat units

Potential HU: Number of heat units required to reach maturity

From leaf senescence to the end of the growing season, LAI is estimated with the equation:

$$\mathbf{LAI} = \mathbf{XLAI} * \left[\frac{\mathbf{1.0 - HUI}}{\mathbf{(1.0 - HUI}_d)} \right] \quad \text{Eq. 148}$$

Where:

LAI: [Eq. 5:2.1.19 in SWAT 2005]

HUI_D : value of HUI when LAI starts declining

A.4.2 Crop Height

Crop height is estimated with the relationship:

$$CPHT = HMX * \text{sqrt}(HUF) \quad \text{Eq. 149}$$

Where:

CHT : crop height in m [Eq. 5:2.1.14 in SWAT 2005]

HMX : maximum height for crop

HUF : heat unit factor (see Eq. 146)

A.4.3 Root Growth

In the PGM, it is assumed that the portion of total biomass production allocated to the roots declines from a value of 0.4 at germination to 0.2 at maturity. The root allocation fraction is computed with the equation:

$$Fr_{\text{root}} = 0.40 - 0.20 * HUI \quad \text{Eq. 150}$$

Where:

Fr_{root} : Fraction of total biomass partitioned to roots on a given day in the growing season, [Eq. 5:2.1.21 in SWAT 2005]

HUI : Fraction of potential heat units accumulated for the plant by a given day in the growing season

A.4.4 Above-ground Biomass

The potential above-ground biomass is estimated as a fraction of the total crop biomass production that considers the fraction of biomass partitioned to the root system.

$$Bio_{\text{above}} = (1.0 - Fr_{\text{root}}) * Bio \quad \text{Eq. 151}$$

Where:

Bio_{above} : potential aboveground biomass on a given day in $t \text{ ha}^{-1}$, [Eq. 5:2.4.4 in SWAT 2005]

A.4.5 Root Depth

Rooting depth is simulated as a function of heat units and potential root zone depth:

$$RD = \min(2.5 * RDMX * HUI, RDMX, RZ) \quad \text{Eq. 152}$$

Where:

RD : root depth in m for crop [Eq. 5:2.1.23 in SWAT 2005]

RDMX: maximum root depth in m for crop

HUI: heat unit index of the crop

RZ: soil profile depth in m

A.5 Growth Constraints

In the PGM, plant growth can be limited by water and/or temperature stresses.

A.5.1 Water Stress Factor

The water stress factor is computed by considering the potential transpiration which is a function of the leaf area, stomatal conductance, and atmospheric conditions (*EPMax*). This value is compared to the moisture constrained transpiration (*TALayers*) that accounts for the moisture status of the soil.

$$WS = \frac{TALayers}{EPMax} \quad \text{Eq. 153}$$

Where:

WS: water stress factor for a specific crop (dimensionless) [Eq. 5:3.1.1 in SWAT 2005]

TALayers: actual plant water uptake from soil layers in mm d⁻¹ (See Eq. 78)

EPMax: maximum plant transpiration in mm d⁻¹ (See Eq.38)

A.5.2 Temperature Stress Factor

The plant temperature stress is computed with the following constraints and equations:

$$TS = \text{Exp}(-0.1054 * RTO) \quad RTO \leq 200 \text{ and } TGX > 0.0 \quad \text{Eq. 154}$$

$$TS = 0.0 \quad RTO > 200 \text{ or } TGX \leq 0.0 \quad \text{Eq. 155}$$

Where:

$$RTO = \frac{TOPC - TX}{2 * TGX} \quad \text{Eq. 156}$$

$$TGX = TX - TBSC \quad TX \leq TOPC \quad \text{Eq. 157}$$

Where:

TS: plant temperature stress factor (dimensionless) [Eq. 5:3.1.2 to Eq. 5:3.1.5 in SWAT 2005]

TX: average daily air temperature in °C

TBSC: base temperature for corresponding crop in °C

TOPC: optimal temperature for corresponding crop in °C

Finally, the plant stress factor is determined as the lowest value of the WS and TS stress factors.

$$\mathbf{REG = Min (TS, WS)} \quad \mathbf{Eq. 158}$$

Where:

REG: plant stress factor due to either *TS* and *WS*, dimensionless

A.6 Actual Growth

Actual growth is calculated as a function of the potential growth and the plant stress factor:

$$\mathbf{ActBio = Bio * REG} \quad \mathbf{Eq. 159}$$

Where:

ActBio: actual plant biomass on a given day in t ha⁻¹ [Eq. 5:3.2.1 in SWAT 2005]

Bio: potential increase in biomass in t ha⁻¹ d⁻¹ (See Eq. 141)

REG: plant stress factor due to *TS* and *WS*, dimensionless

For the above-ground biomass the following equation is used.

$$\mathbf{ActBio_{above} = Bio_{above} * REG} \quad \mathbf{Eq. 160}$$

Where:

ActBio_{above}: actual above-ground biomass on a given day in t ha⁻¹ [Eq. 5:3.2.1 in SWAT 2005]

Bio_{above}: potential increase in above-ground biomass in t ha⁻¹ d⁻¹ (See Eq. 151)

A.7 Economic Yield

In PGM, economic yield is calculated using a harvest index. The harvest index specifies the portion of the plant mass that is harvested. This value is relatively stable for a range of plant types (SWAT 2005):

Harvest Index is calculated for each day of the plant's growing season using the relationship:

$$HI = HI_{opt} * \frac{100 * HUI}{(100 * HUI + \exp(11.11 - 10 * HUD))} \quad \text{Eq. 161}$$

Where:

HI: Potential harvest index on the day of harvest, dimensionless [Eq. 5:2.4.1 in SWAT 2005]

HI_{opt}: potential harvest index for the plant at maturity given ideal growing conditions

HUI: heat unit index (fraction of potential heat units accumulated for the plant on a given day in the growing season)

The potential crop yield is calculated using the following equations and constraints:

$$yld = Bio_{above} * HI \quad \text{when } HI \leq 1.00 \quad \text{Eq. 162}$$

$$yld = Bio * \left(1 - \frac{1}{(1 + HI)}\right) \quad \text{when } HI \geq 1.00 \quad \text{Eq. 163}$$

Where:

yld: crop yield in t ha⁻¹ [Eq. 5:2.4.2 & Eq. 5:2.4.3 in SWAT 2005]

Bio_{above}: above-ground biomass on the day of harvest t ha⁻¹

HI: harvest index on the day of harvest

A.8 Actual Crop Yield

In this model an actual harvest index is calculated during the second half of the crop growth season. The actual harvest index accounts for the potential impact of cumulative water stress on crop yield.

$$YLD_{Actual} = HI_{Actual} * ActBio_{Above} \quad \text{Eq. 164}$$

$$HI_{Actual} = (HI - HI_{Min}) \frac{WS}{WS + \exp(6.13 - 0.0883 * WS)} + HI_{Min} \quad \text{Eq. 165}$$

where:

YLD_{Actual} : actual crop yield in t ha⁻¹ [Eq. 281 in APEX 2008]

HI_{Actual} : actual harvest index used to compute crop yield, dimensionless [Eq. 5:3.3.1 in SWAT 2005]

HI : potential harvest index on the day of harvest, dimensionless

HI_{Min} : minimum harvest index for a specific crop, dimensionless

A.9 Rice Specific Algorithms

Accurately reproducing water management practices can be one of the most complicated portions of modeling. Because water management affects the hydrologic balance, it is critical that the model is able to accommodate management practices like those used in rice production. In this section the rice ponding algorithm is described starting with pond evaporation.

The volume of water lost to evaporation from the pond is calculated using a factor, n (0.875), for free surface evaporation. The factor 0.875 is the ratio of the crop coefficient found in FAO56 for open water less than 2 m deep (1.05) and the conversion from the alfalfa reference (PETDay) to the short grass reference (1.2) (Allen et al., 2005). The total potential evaporation is then further reduced by the transpiration (EPMax) which accounts for the growth of the rice crop:

$$EPond = n * PETDay - EPMax \quad \text{Eq. 166}$$

where:

$EPond$: evaporation from water surface in mm

n : evaporation coefficient (0.875), dimensionless

$EPMax$: Maximum plant evapotranspiration in mm (See Eq. 38)

The volume of water lost to transpiration from a rice field:

$$TaRice = EPMax + CanET \quad \text{Eq. 167}$$

where:

$TaRice$: transpiration from rice in mm

A.9.1 Rice Ponding

Rice ponding is controlled by parameters that specify the depth of ponding required during various growth stages of rice crop development. The timing of ponding depth requirements is specified either using heat units or calendar dates. If using heat units to determine planting date and crop stage development (HU-HU), the following equations and constraints are employed:

$$\text{MaxPondD} = \text{MaxPondD}_1 \quad \text{if } \text{accHU} < \text{Pre}_1 \quad \text{Eq. 168}$$

$$\text{MaxPondD} = \text{MaxPondD}_2 \quad \text{if } \text{Pre}_1 \leq \text{accHU} < \text{Pre}_2 \quad \text{Eq. 169}$$

$$\text{MaxPondD} = \text{MaxPondD}_3 \quad \text{if } \text{Pre}_2 \leq \text{accHU} < \text{Initial} \quad \text{Eq. 170}$$

$$\text{MaxPondD} = ((\text{MaxPondD}_4 - (\text{MaxPondD}_3 + 0.0833)) * \left(\frac{\text{CropHU}}{\text{Develop}}\right)) + \text{MaxPondD}_3 + 0.0833$$

$$\text{If } \text{JulianDay} \geq \text{Initial} \text{ and } \text{CropHU} < \text{Develop} \quad \text{Eq. 171}$$

$$\text{MaxPondD} = ((\text{MaxPondD}_5 - \text{MaxPondD}_4) * \left(\frac{\text{CropHU} - \text{Develop}}{\text{Mid} - \text{Develop}}\right) + \text{MaxPondD}_4$$

$$\text{If } \text{Develop} \leq \text{CropHU} < \text{Mid} \quad \text{Eq. 172}$$

$$\text{MaxPondD} = ((\text{MaxPondD}_6 - \text{MaxPondD}_5) * \left(\frac{\text{CropHU} - \text{Mid}}{\text{Late} - \text{Mid}}\right) + \text{MaxPondD}_5$$

$$\text{If } \text{Mid} \leq \text{CropHU} < \text{Late} \quad \text{Eq. 173}$$

$$\text{MaxPondD} = ((\text{MaxPondD}_7 - \text{MaxPondD}_6) * \left(\frac{\text{CropHU} - \text{Late}}{\text{EndLate} - \text{Late}}\right) + \text{MaxPondD}_6$$

$$\text{If } \text{Late} \leq \text{CropHU} < \text{EndLate} \quad \text{Eq. 174}$$

where:

MaxPondD : maximum ponding depth in mm [PGM Internal Code]

MaxPondD_1 : maximum ponding depth before pre-flooding stage in ft

MaxPondD_2 : maximum ponding depth during pre-flooding stage in ft

MaxPondD_3 : maximum ponding depth during non-flooding stage in ft

MaxPondD₄: maximum ponding depth during Initial stage in ft

MaxPondD₅: maximum ponding depth during Develop stage in ft

MaxPondD₆: maximum ponding depth during Mid-stage in ft

MaxPondD₇: maximum ponding depth during Late stage in ft

MaxPondD₈: maximum ponding depth for EndLate stage in ft

Pre_1: heat units required for pre-stage_1 of flooding since January 1,
dimensionless

Pre_2: heat units required for pre-stage_2 of non-flooding since January 1,
dimensionless

Initial: heat units required for initial growing stage or planting date heat units
threshold since January 1, dimensionless

Develop: heat units required for development growing stage since planting day,
dimensionless

Mid: heat units required for mid growing stage since planting day, dimensionless

Late: heat units required for late growing stage since planting day, dimensionless

EndLate: heat units required for end growing stage since planting day,
dimensionless

CropHU: accumulated heat units since rice planting ⁰C

accHU: accumulated heat units since January 1 using a base temperature of 0 ⁰C.

If using FIX-HU approach (User specified planting date with accHU determining growth stages) is employed, then the previous algorithms from Eq. 168 to Eq. 174 apply as well. The only difference is how the timing of the initial stages is determined. In the FIX-HU approach the stages prior to planting are fixed and determined based on Julian Days and then heat units are the driver for the developmental stages. The way that these stages are determined for the FIX-HU approach is described below:

Pre_1: julian day for pre-stage_1 of flooding, dimensionless (Eq. 168)

Pre_2: julian day for pre-stage_2 of non-flooding, dimensionless (Eq. 169)

Initial: julian day for initial growing stage or planting date, dimensionless (Eq. 170)

Develop : heat units required as a fraction of PHU (heat units required to reach maturity) for development growing stage since planting day, dimensionless (Eq. 171)

Mid : heat units required as a fraction of PHU for mid growing stage since planting day, dimensionless (Eq. 172)

Late : heat units required as a fraction of PHU for late growing stage since planting day, dimensionless (Eq. 173)

EndLate : heat units required as a fraction of PHU for end growing stage since planting day, dimensionless (Eq. 174)

To better understand the different ponding depths and growing stages for the complete rice growing season a scheme of them is shown in **Figure D-5**. As observed in the figure, the different stages can be determined based on heat units (HU-HU approach) or a combination of Julian days and heat units (Fix-HU approach). Both approaches determine when a specific stage starts and ends.

1. Initially there is a five-day flood-up stage (Pre_1) where a ponding depth of 3 inches is reached.
2. A non-ponding period of 10-days follows the flood-up stage (Pre_2).
3. Seeding occurs at the beginning of the Initial stage (May 1) with a gradually flood-up period until 5 inches of ponding is reached by the beginning of the Develop stage.
4. Flood-up continues up to 8 inches of ponding at the beginning of Mid stage.
5. Pond depth remains constant at 8 inches until the Late stage is reached.
6. From Late stage to the EndLate stage the pond depth is gradually reduced down to zero pond depth. During this stage there are no more irrigation applications. Harvest may occur any time after the EndLate stage.

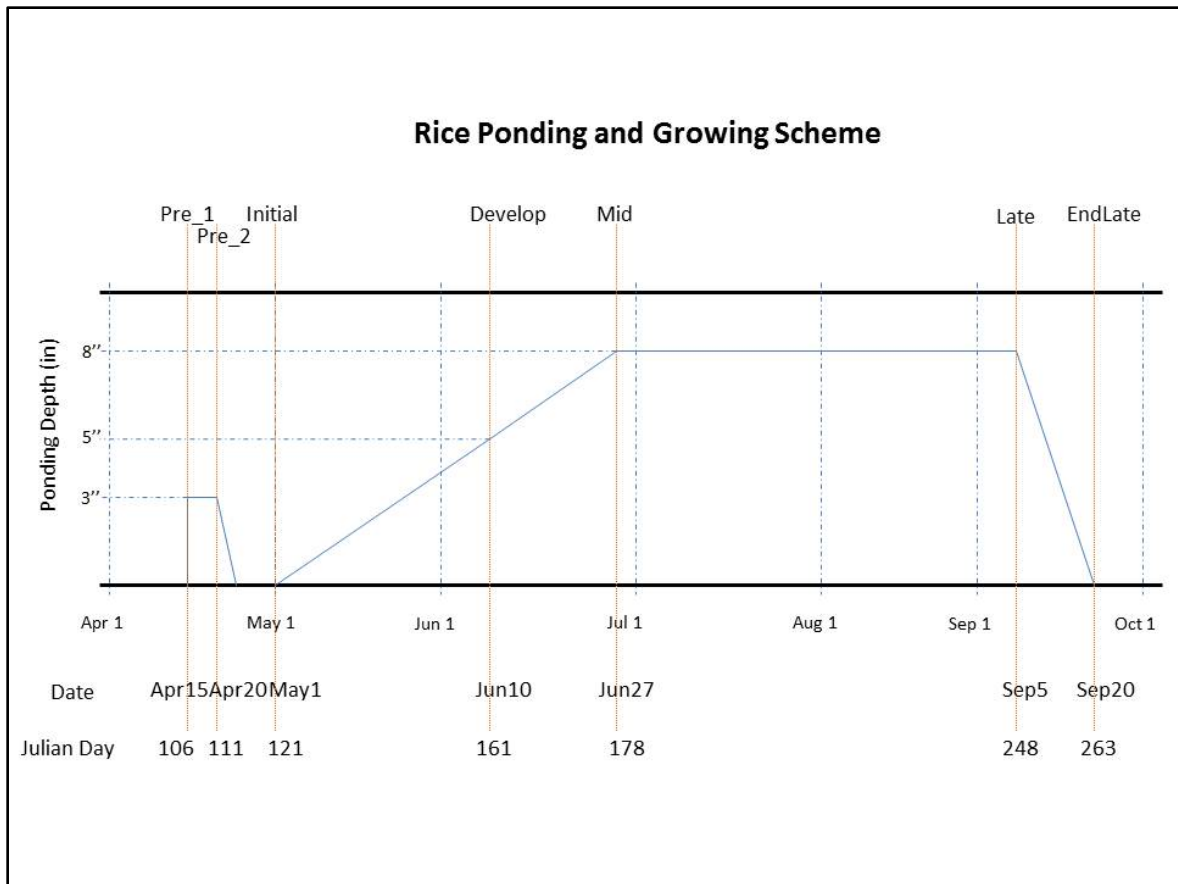


Figure A.9.1. Schematic Representation of Rice Ponding Depth during Growing Season

A.10 Deciduous Crop Algorithms

In the fall, deciduous crops lose all their leaves and become dormant for a period of time. Almonds, apples and vineyards are examples of these types of crops. For such deciduous crops some specific crop management practices must be specified including the time when irrigation ceases and the time when leaves start to fall. Specifying when irrigation ceases is necessary because after harvest occurs, deciduous crops are typically given reduced amounts of irrigation water which eventually ceases completely as the weather cools. To determine the exact day when irrigation should be stopped for each year, a temperature threshold is used. In PGM, several conditions may be applied. These conditions include temperature and Julian day of the year conditions. Finally the Julian Days may vary depending on the crop to be modeled. In PGM, the **JulianDay** and **NumDaysTempOct1** variables are hardwired into the code.

If $MinTemp < StopIrrMinTemp$

Eq. 175

$JulianDay > 274$ (Oct 1)

$$\text{NumDaysTempOct1} > 3$$

Then

$$\text{StopDecidIrrig} = \text{true} \quad \text{Eq. 176}$$

Where:

MinTemp: minimum temperature on a specific day in °C

StopIrrMinTemp: temperature threshold for which irrigation stops in °C

NumDaysTempOct1: number of days with minimum temperature is lower than the temperature threshold, dimensionless

StopDecidIrrig: flag that indicates that irrigation must be stopped

A similar approach is used to determine the day when the “fall” starts. When this occurs, it means that the deciduous trees lose their leaves and the transpiration ceases.

$$\text{If } \text{MinTemp} < \text{FallLeavesMinTemp} \quad \text{Eq. 177}$$

$$\text{JulianDay} > 305 \text{ (Nov 1)}$$

$$\text{NumDaysTempNov1} > 3$$

Then

$$\text{StartFall} = \text{true} \quad \text{Eq. 178}$$

Where:

FallLeavesMinTemp: temperature threshold for which fall starts in °C

NumDaysTempNov1: number of days with minimum temperatures lower than the temperature threshold, dimensionless

StartFall: flag that indicates that fall starts and leaves fall [PGM Internal Code]

A.11 Perennials Crop Algorithms

Simulation of non-deciduous perennial crop management also may require some additional conditions . Examples of some non-deciduous perennial crop include alfalfa, pasture and urban lawns. For these plant types, a specific number of cuttings can be defined. For alfalfa , up to 7 fixed cuttings are defined, and they are scheduled to happen each year based on a regular defined schedule and using Julian Days as shown below.

$$\text{Cutting 1: Julian Day 105 (Apr 15)} \quad \text{Eq. 179}$$

Cutting 2: Julian Day 133 (May 13)

Cutting 3: Julian Day 161 (Jun 10)

Cutting 4: Julian Day 189 (Jul 8)

Cutting 5: Julian Day 217 (Aug 5)

Cutting 6: Julian Day 245 (Sep 2)

Cutting 7: Julian Day 288 (Oct 15)

For pasture and urban lawn plant types, a slightly different approach can be used. For these crops the regularly scheduled intervals between cuttings can be employed to simulate cattle grazing and lawn mowing.

A.12 Winter Wheat Specific Algorithms

For annual crop types, winter wheat is the only crop that is treated differently than the rest. The reason for this treatment is because winter wheat is planted in the late fall and is harvested in the late spring or early summer. To simulate these conditions, PGM only starts accumulating heat units for winter wheat beginning on June 1 of each year and continues accumulating them until May 31 of the following year. If winter wheat starts growing on December 15 as it is set up by default, it continues growing until it accumulates sufficient heat units to be harvested. On May 31, all PGM variables related to winter wheat are set up back to zero in order to start another crop cycle. Consequently during the 1st year for a model simulation run, there is not a winter wheat crop growing until the 2nd year.

Appendix B – Development of Atmospheric Forcings for WEAP-PGM

The analysis of the effects of potential future climate changes on agricultural water demands and productivity requires meteorological information beyond projections of future temperature and precipitation conditions. Crop growth, yield and evapotranspiration (ET) are also sensitive to solar radiation, atmospheric humidity, wind speed and carbon dioxide. In order to provide these additional data sets, several estimation methods using the projected temperature and precipitation projections were employed to obtain values for these meteorological conditions corresponding to the future climate scenarios. These methods with the exception of including CO₂ were also employed in the West-Wide Climate Risk Assessments: Irrigation Demand and Reservoir Evaporation Projections report (Reclamation 2015).

In order to represent a reasonable range of spatial variability in these meteorological conditions, four locations were selected to characterize representative conditions in the Central Valley. These locations are shown on **Figure B-1**.

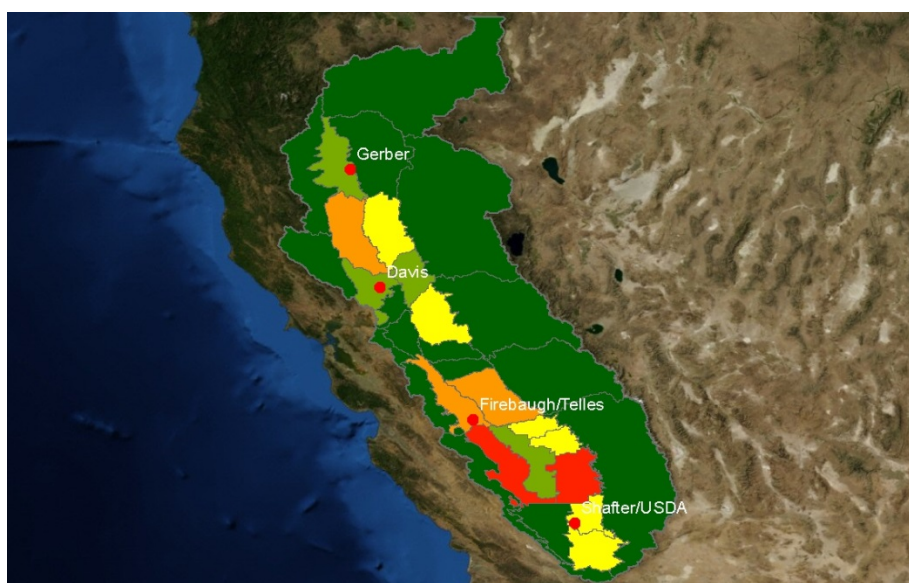


Figure B-1. Locations of the CIMIS station used in estimating meteorological conditions for Agricultural Demand and Productivity Analyses

The selected locations include existing California Irrigation Management Information System (CIMIS) stations located at Gerber, Davis, Firebaugh, and Shafter. These CIMIS stations were chosen because long term observations of daily maximum and minimum temperature (T_{max}, T_{min}), solar radiation (R_s), dew point temperature (T_{dew}), relative humidity (RH), and wind speed were available. All the historical data from the stations were also carefully checked for erroneous values prior to preparing the subsequent projections. In **Figure B-2**, an example of solar radiation (R_s) data from the CIMIS station located at Davis is presented. The top panel shows the observations prior to the elimination of values in excess of the daily clear sky radiation, R_{so} maximum. The middle panel shows the same data with the extreme outliers

eliminated. From this data, the ratio of daily R_s/R_{so} was calculated and the average ratio of the top 20% of values on a monthly basis was computed. The daily data were then adjusted by dividing by this adjustment factor to obtain the results shown in the bottom panel.

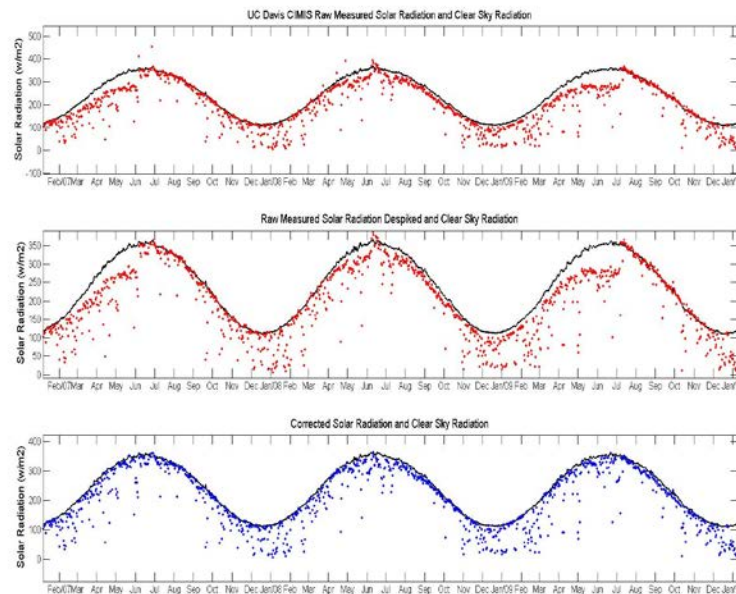


Figure B-2. Adjustment of CIMIS daily solar radiation, R_s , values. Top panel shows raw data; Middle Panel shows data after elimination of extreme values; Bottom panel shows the adjusted data.

A similar analysis was performed on the relative humidity (RH) data. The top panel of **Figure B-3** shows the raw hourly RH data from the CIMIS located at Davis. As can be observed, the maximum RH values decline slowly over an extended period of time. This sensor drift was corrected by adjusting the values so that some of the values approach 100% RH during each year. The adjusted RH values are shown in the bottom panel of **Figure B-3**. After adjustment, any missing data values were estimated using methods described by Annaandale et al. (2002).

Plant Physiological Responses to Atmospheric Forcings

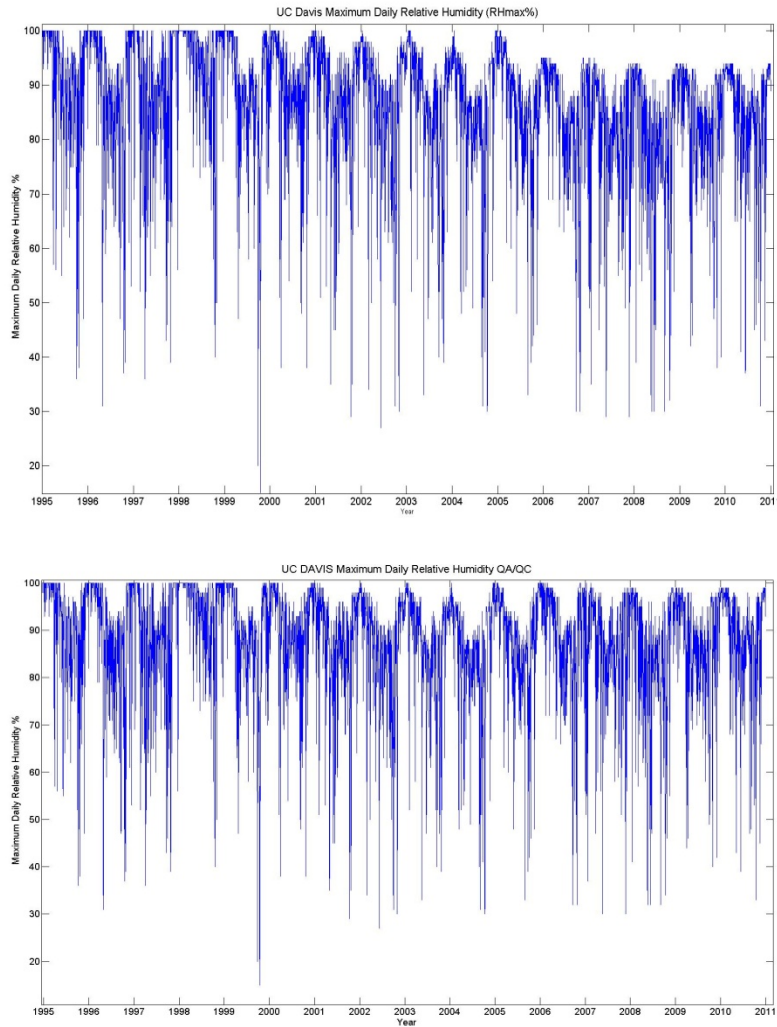


Figure B-3. Adjustment of CIMIS hourly relative humidity, RH, values. Top panel shows raw data; Bottom panel shows the adjusted data.

Solar radiation is one of the factors affecting crop ET. It can be estimated from the Tmax and Tmin using the clear radiation (Ro) which only depends on latitude, day of the year and a site specific parameter (B). For this study, an alternative method computing Ro was employed. This method which accounts for the effect of atmospheric humidity on Ro is described in Allen et al. (2005) in Appendix D.

The CIMIS station historical records were used to calibrate B parameters and the climate projections of Tmax and Tmin were then used to compute Rs based on the Thornton and Running (1999) method for each of the EI climate projections.

Table B-1 shows the calibrated monthly B parameters at each of the four CIMIS stations. These values were computed from the following equation.

$$B=0.031+0.201*\exp(-0.185*(Tmax - Tmin)) \quad \text{Eqn. 1}$$

where Tmax and Tmin are the daily maximum and minimum temperatures respectively.

Table B-1. Average Monthly B parameters for the Central Valley CIMIS Stations

Station Name	Month											
	Jan	Feb	Mar	Apr	May	Jun	Jul	Aug	Sep	Oct	Nov	Dec
Davis	0.072	0.061	0.052	0.046	0.043	0.040	0.038	0.037	0.039	0.043	0.055	0.071
Firebaugh/Telles	0.067	0.056	0.049	0.045	0.042	0.040	0.039	0.039	0.040	0.043	0.051	0.065
Gerber	0.066	0.059	0.052	0.047	0.046	0.044	0.041	0.039	0.040	0.044	0.054	0.067
Shafter/USDA	0.060	0.051	0.046	0.042	0.040	0.039	0.039	0.038	0.038	0.039	0.045	0.056

Figure B-4 shows a comparison of the observed and estimated Rs at the CIMIS station located at U. C. Davis.

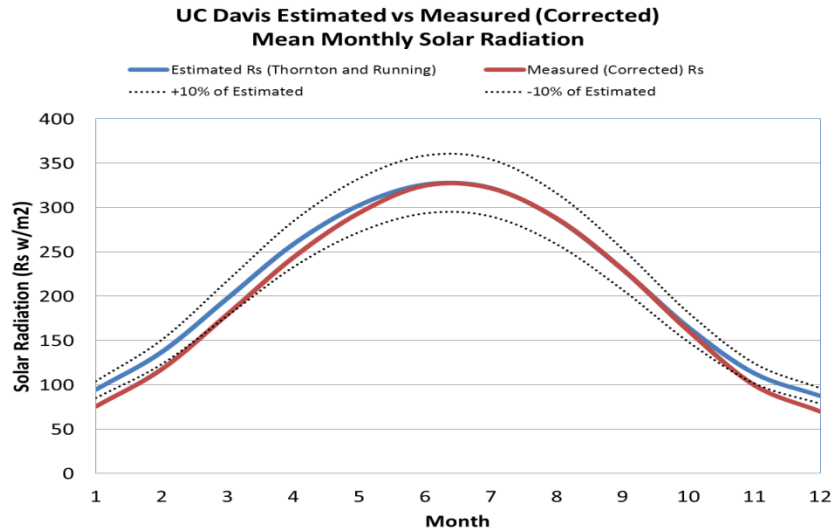


Figure B-4. Comparison of observed CIMIS and estimated Rs results at the U.C. Davis CIMIS station.

The average Tmax, Tmin, Tmax-Tmin, and Rs results for the Baseline and each of the EI5 climate scenarios during the 2011-2040 (2025), 2041-2070 (2055), and 2070-2099 (2084) periods are presented in **Figure B-5** through **Figure B-8** respectively for the U.C. Davis CIMIS station.

Plant Physiological Responses to Atmospheric Forcings

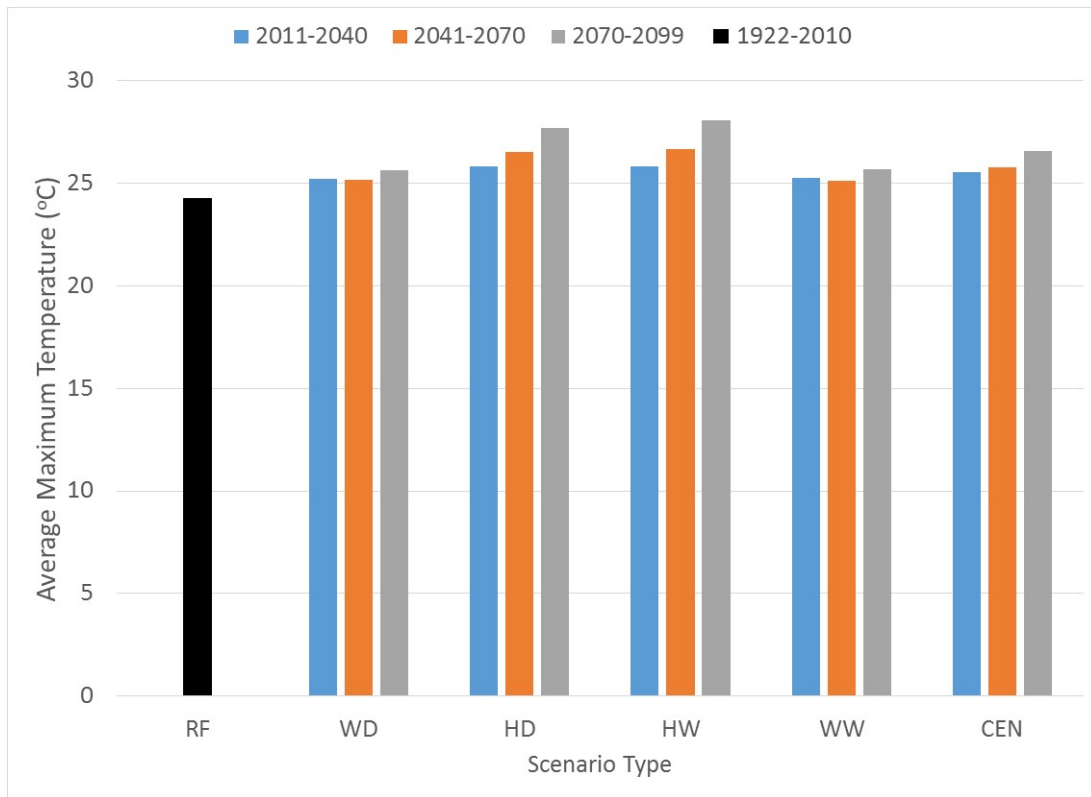


Figure B-5. Period average of daily maximum temperatures in degrees centigrade (°C) for each climate scenario for 2011-2040 (2025), 2041-2070 (2055) and 2070-2099 (2084)

Note: RF scenario was averaged over historical climate sequence for 1922-2010

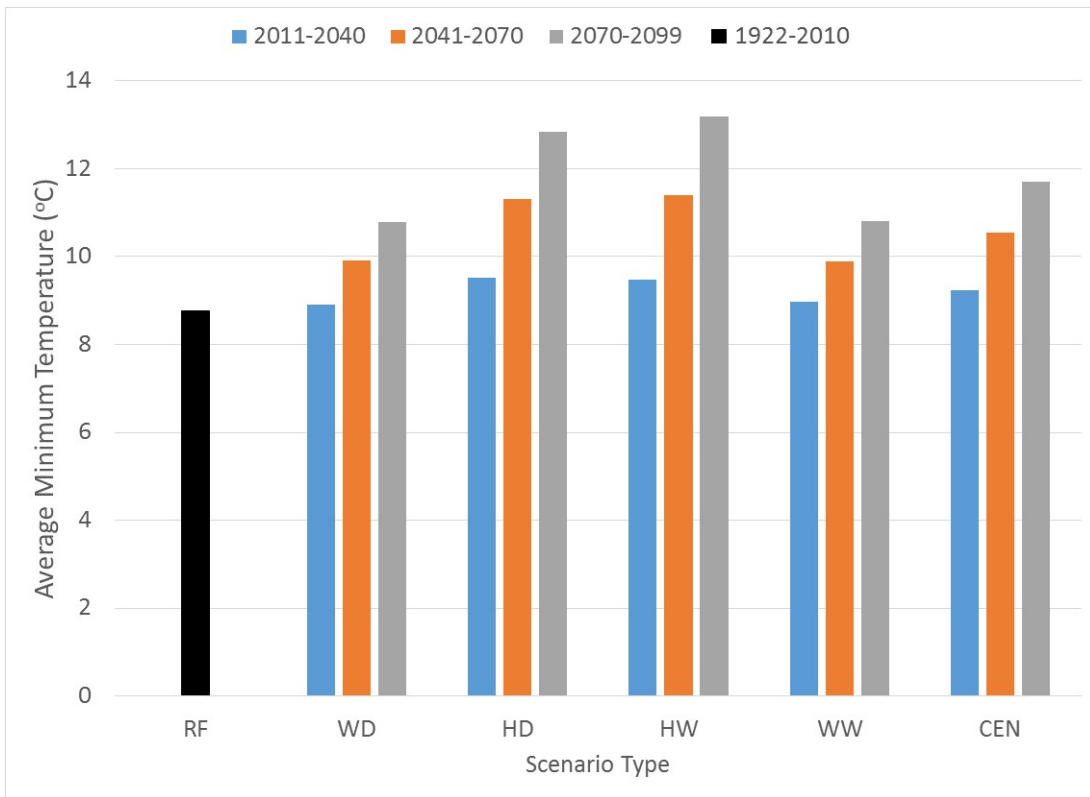


Figure B-6. Period average of daily minimum temperatures in degrees centigrade (°C) for each climate scenario for 2011-2040 (2025), 2041-2070 (2055) and 2070-2099 (2084)

Notes: RF scenario was averaged over historical climate sequence for 1922-2010

Plant Physiological Responses to Atmospheric Forcings

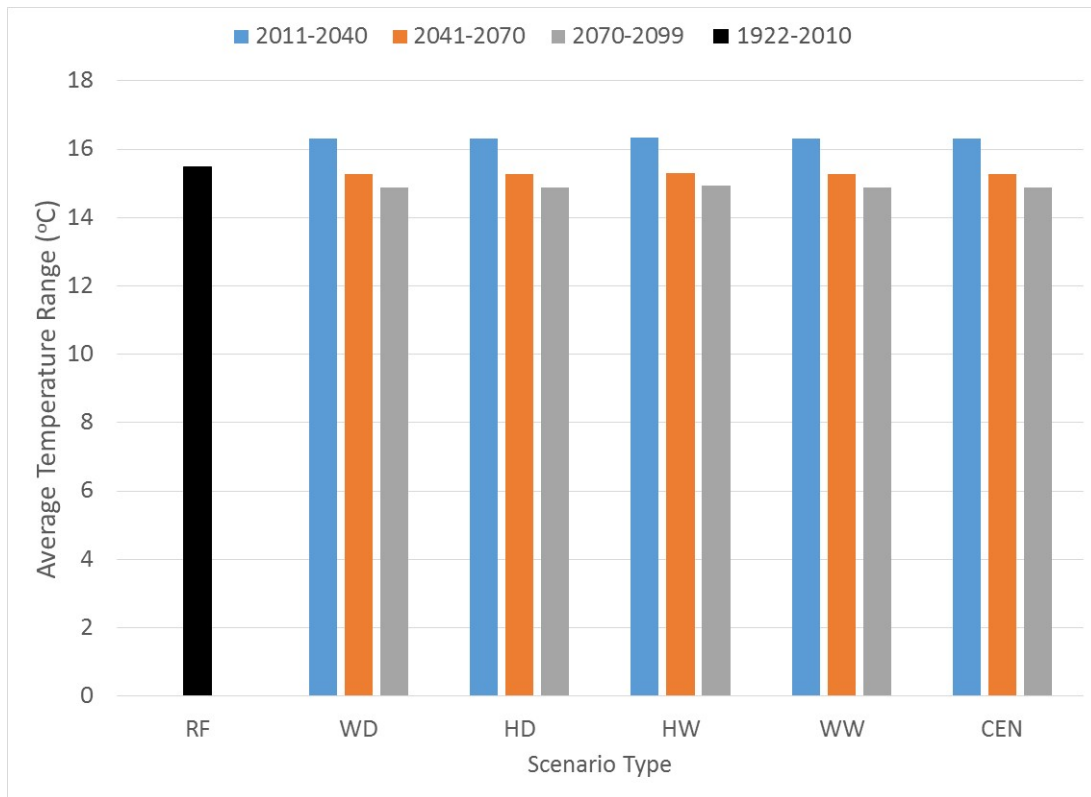


Figure B-7. Period average of daily temperature range (Tmax-Tmin) in degrees centigrade (°C) for each climate scenario for 2011-2040 (2025), 2041-2070 (2055) and 2070-2099 (2084)

Notes: RF scenario was averaged over historical climate sequence for 1922-2010

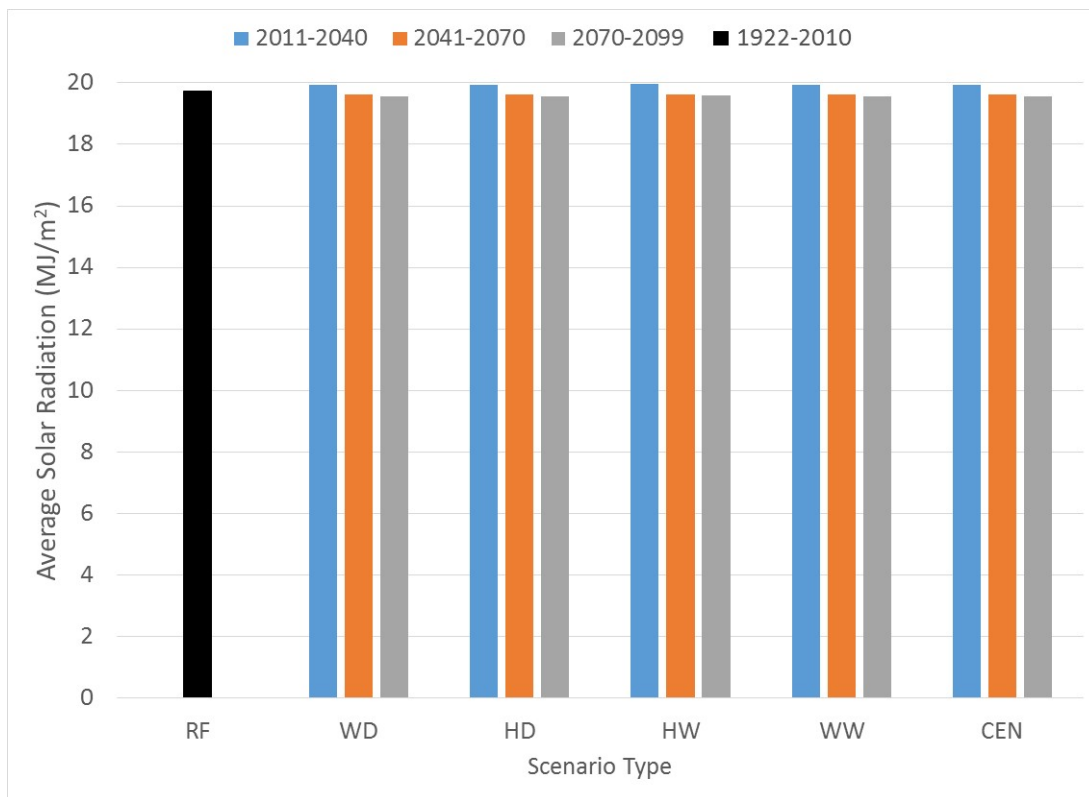


Figure B-8. Period average of daily solar radiation in mega-joules per square meter (MJ/m²) for each climate scenario for 2011-2040 (2025), 2041-2070 (2055) and 2070-2099 (2084)

Notes: RF scenario was averaged over historical climate sequence for 1922-2010

Atmospheric humidity also has a significant effect of crop ET. As the air becomes drier, ET generally increases. The dew point temperature (T_{dew}) is an indicator of the moisture content of the air. As the atmospheric humidity increases, T_{dew} also increases. The daily minimum temperature is a good indicator of T_{dew}. Cloudiness and high humidity reduce the amount of heat loss from the surface to the atmosphere which is generally reflected in higher T_{min} values. To estimate projected changes in atmospheric humidity, an analysis of the CIMIS station records was performed to determine the monthly average differences between the observed T_{min} and T_{dew} values. This difference is referred to as the dew point depression (K_o). Average monthly K_o values computed for each of the four CIMIS stations are presented in **Table B—2** below.

Table B-2. Average monthly Ko values for each Central Valley CIMIS station

Station Name	Month											
	Jan	Feb	Mar	Apr	May	Jun	Jul	Aug	Sep	Oct	Nov	Dec
Davis	-1.91	-1.56	-0.40	0.85	2.25	2.48	1.34	1.79	3.19	2.34	-0.51	-1.72
Firebaugh/Telles	-1.23	-0.51	0.86	2.81	4.40	5.13	3.89	2.99	3.40	2.69	-0.11	-1.40
Gerber	-0.46	1.06	1.52	2.27	2.61	4.06	4.07	3.51	3.96	3.37	0.56	-0.20
Shafter/USDA	-1.38	-0.46	0.40	2.07	3.63	3.91	3.14	2.92	3.18	1.61	-1.09	-1.56

To estimate projected changes in Tdew, these monthly average observed Ko values were subtracted for the projected Tmin values. The average Tdew results for the Baseline and each of the EI5 climate scenarios for 2011-2040 (2025), 2041-2070 (2055) and 2070-2099 (2084) are presented in **Figure B-9**.

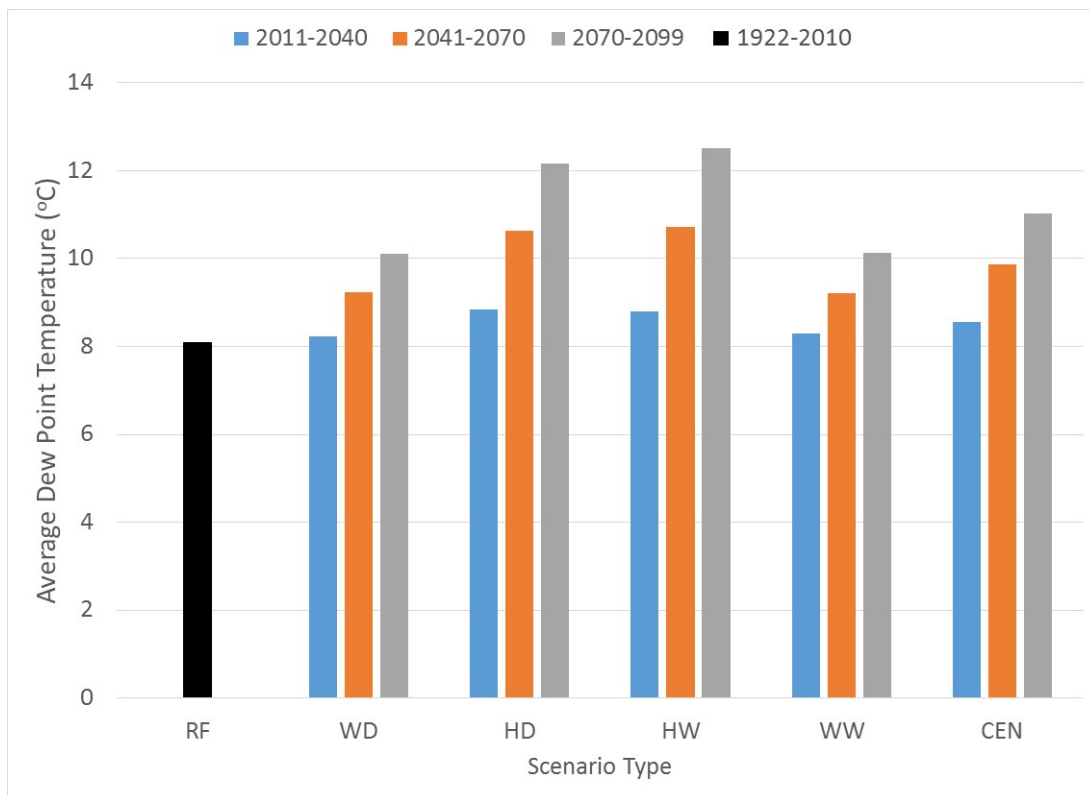


Figure B-9. Period average of daily dew point temperatures in degrees centigrade (°C) for each climate scenario for 2011-2040 (2025), 2041-2070 (2055) and 2070-2099 (2084)

Notes: RF scenario was averaged over historical climate sequence for 1922-2010

The effects of atmospheric humidity are reflected in ET calculations by the difference between the saturated vapor pressure (es) in the moist plant leaves and the typically drier surrounding atmosphere (ea). Projected changes in es and ea are presented on **Figure B-10** and **Figure B-11**

respectively. This difference is referred to as the vapor pressure deficit (VPD). As the VPD increases, crop ET generally increases. Because the saturation vapor pressure is a function of temperature, projections of VPD can be computed from the projections of daily Tmax, Tmin and Tdew using methods described by Walter et al. (2005). **Figure B-12** shows the projected VPD results for the RF and each of the EI5 climate scenarios during the 2011-2040 (2025), 2041-2070 (2055) and 2070-2099 (2084).

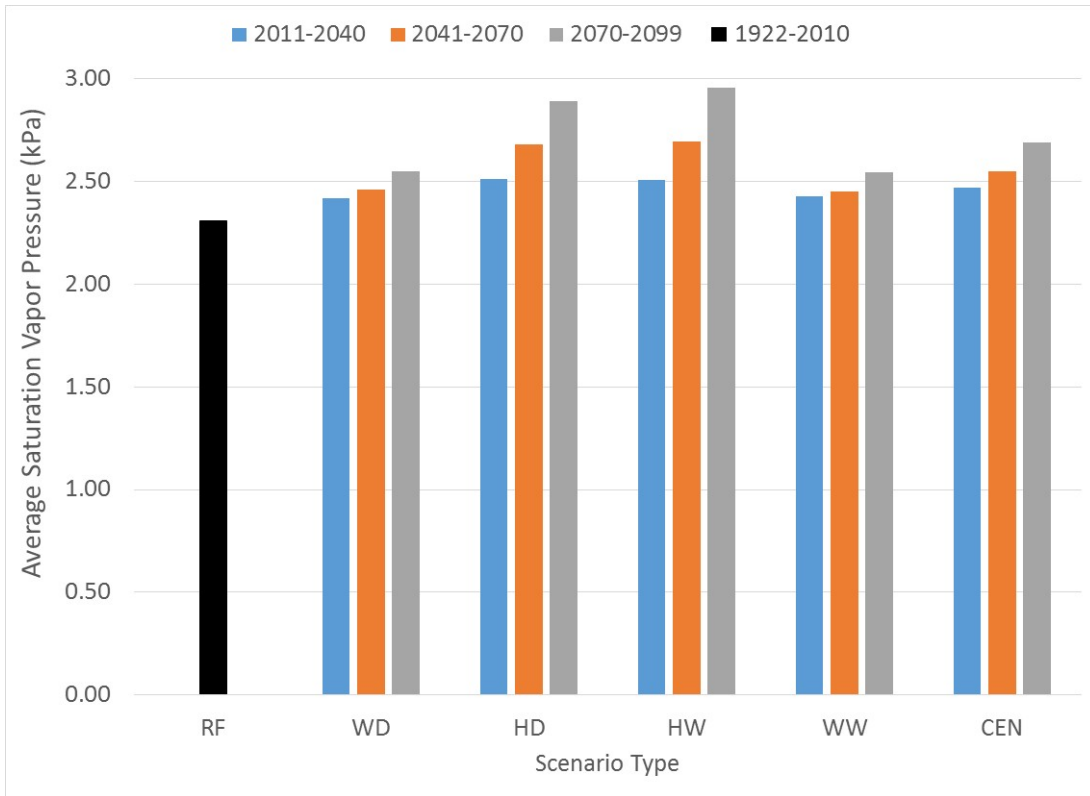


Figure B-10. Period average of daily saturation vapor pressure (kPa) for each climate scenario for 2011-2040 (2025), 2041-2070 (2055) and 2070-2099 (2084)

Notes: RF scenario was averaged over historical climate sequence for 1922-2010

Plant Physiological Responses to Atmospheric Forcings

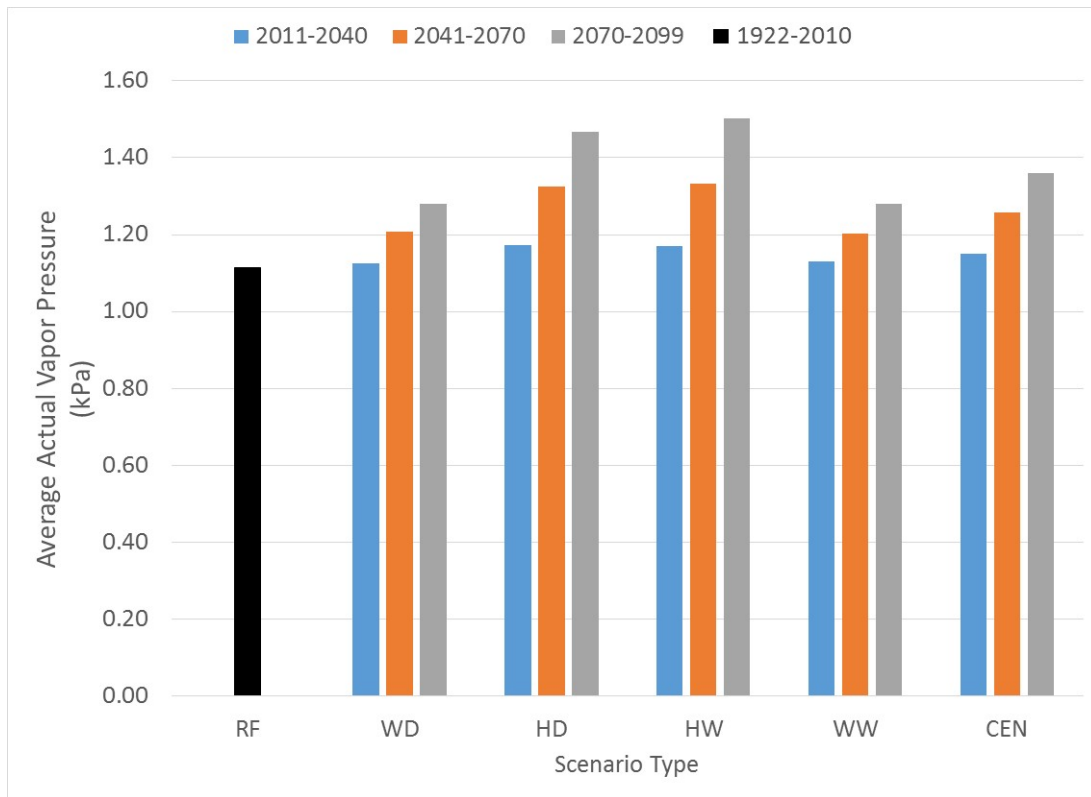


Figure B-11. Period average of daily actual vapor pressure (kPa) for each climate scenario for 2011-2040 (2025), 2041-2070 (2055) and 2070-2099 (2084)

Notes: RF scenario was averaged over historical climate sequence for 1922-2010

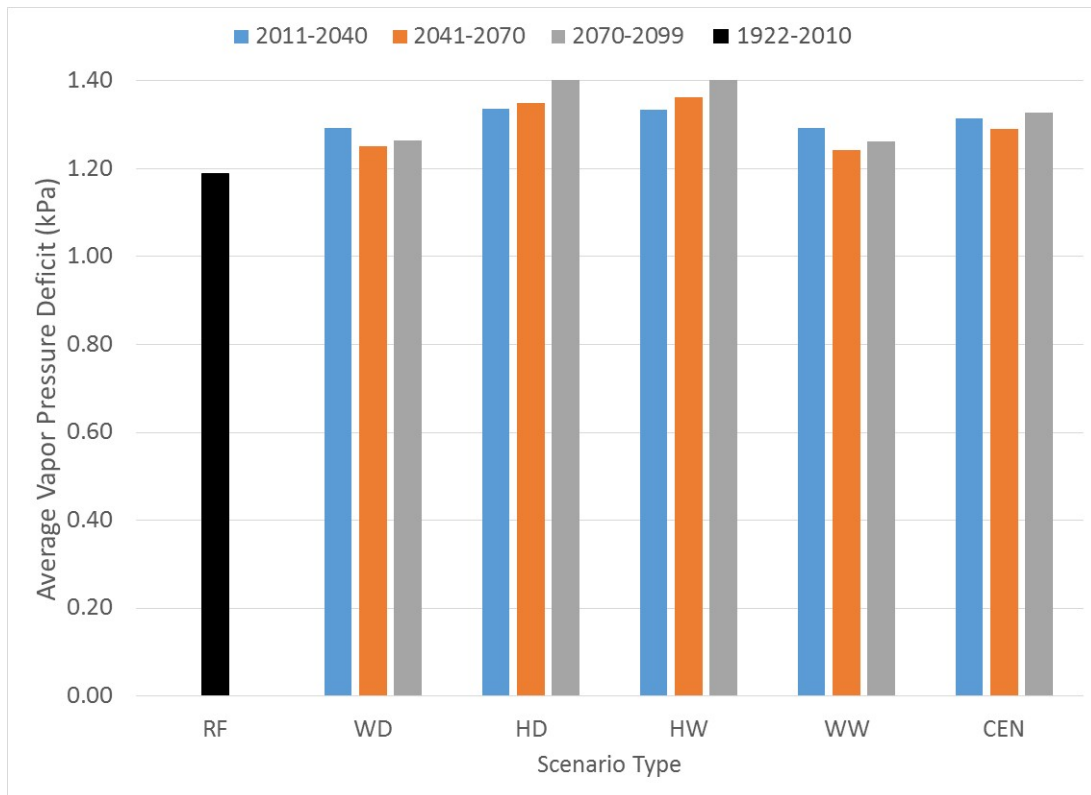


Figure B-12. Period average of daily Vapor Pressure Deficit in kilo Pascals (kPa) for each climate scenario for 2011-2040 (2025), 2041-2070 (2055) and 2070-2099 (2084)

Notes: RF scenario was averaged over historical climate sequence for 1922-2010

Carbon dioxide (CO₂) has also been observed to exert a strong effect on crop ET. As CO₂ concentrations increase, many crops have been observed to exhibit reductions ET. The representative concentration pathways (RCP) have associated CO₂ concentrations (see Appendix A for details). **Figure B-13** presents these values.

Plant Physiological Responses to Atmospheric Forcings

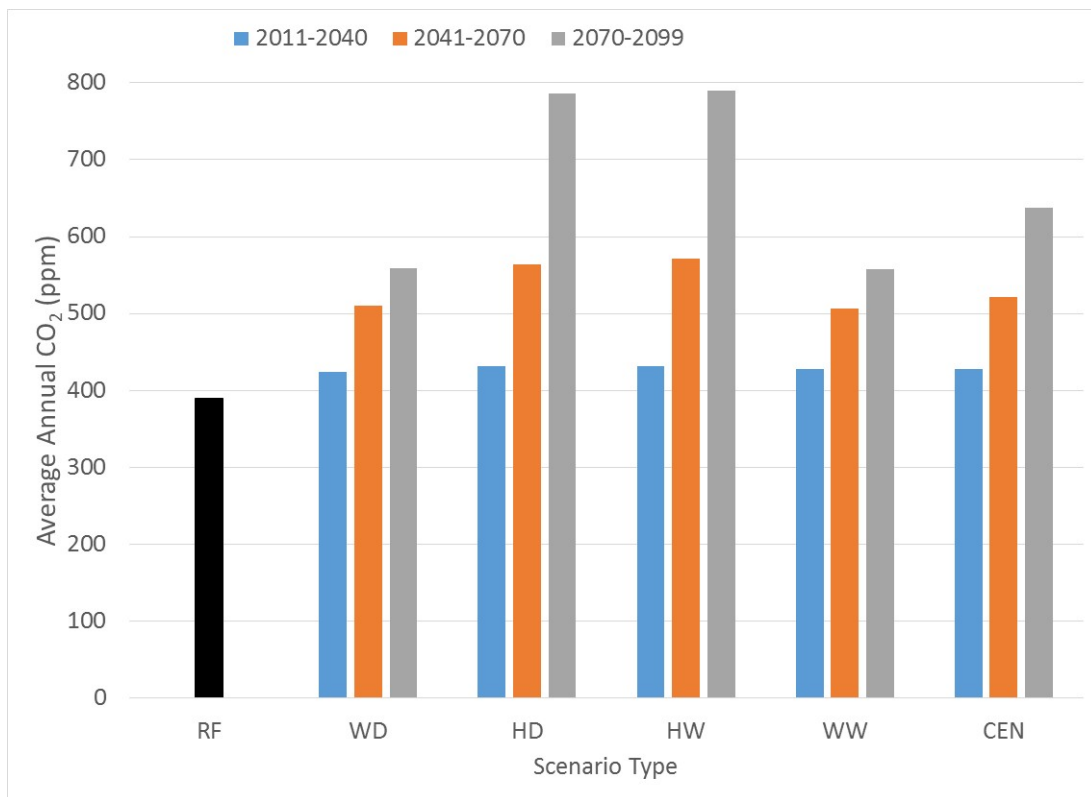


Figure B-13. Period average of annual carbon dioxide concentrations (parts per million (ppm) of CO₂ by volume of air) for each climate scenario during for 2011-2040 (2025), 2041-2070 (2055) and 2070-2099 (2084)

Notes: RF scenario was averaged over historical climate sequence for 1922-2010

References

Allen, R. G., Walter, I. A., Elliott, R., Itenfisu, D., Brown, P., M. Jensen, and R.L. Snyder. 2005. ASCE Standardized Reference Evapotranspiration Equation. American Society of Civil Engineers. p. 58.

Annandale, J.G., Jovanovic, N.Z., Benade, N. and Allen, R.G. 2002. Software for missing data error analysis of Penman-Monteith reference evapotranspiration, *Irrigation Science*, 21, 57-67.

Bureau of Reclamation (Reclamation). 2015. West-Wide Climate Risk Assessments: Irrigation Demand and Reservoir Evaporation Projections. Technical Memorandum No. 86-68210-2014-01. Technical Services Center, Denver, Colorado.

Thornton, P.E. and S.W. Running. 1999. An improved algorithm for estimating incident daily solar radiation from measurements of temperature, humidity, and precipitation. *Agricultural and Forest Meteorology* (93) 211 -228.

